



**HAL**  
open science

# Phosphorus sequestration by magnetotactic bacteria in the stratified water column of Lake Pavin

Cécile Bidaud

► **To cite this version:**

Cécile Bidaud. Phosphorus sequestration by magnetotactic bacteria in the stratified water column of Lake Pavin. Earth Sciences. Université Paris Cité, 2021. English. NNT: 2021UNIP5144. tel-04513735

**HAL Id: tel-04513735**

**<https://theses.hal.science/tel-04513735>**

Submitted on 20 Mar 2024

**HAL** is a multi-disciplinary open access archive for the deposit and dissemination of scientific research documents, whether they are published or not. The documents may come from teaching and research institutions in France or abroad, or from public or private research centers.

L'archive ouverte pluridisciplinaire **HAL**, est destinée au dépôt et à la diffusion de documents scientifiques de niveau recherche, publiés ou non, émanant des établissements d'enseignement et de recherche français ou étrangers, des laboratoires publics ou privés.

Université de Paris

PhD Program Frontières de l'Innovation en Recherche et Éducation - ED N° 474

Institut de Mineralogie, de Physique des Matériaux et de Cosmochimie - Sorbonne Université

---

## Phosphorus sequestration by magnetotactic bacteria in the stratified water column of Lake Pavin

---

by

Cécile BIDAUD

Science of the earth system - Interdisciplinary PhD thesis  
supervised by Nicolas MENGUY and Christopher LEFEVRE  
and co-supervised by Élodie DUPRAT

presented and publicly defended the  
October 21 2021

in front of a jury composed of:

<b>Valérie MICHOTÉY</b>	Rapporteur
Professor (Aix Marseille Université)	
<b>Heide SCHULZ-VOGT</b>	Rapporteur
Professor (Leibniz Institute for Baltic Sea Research, Warnemünde (IOW))	
<b>Bénédicte MÉNEZ</b>	Examiner
Professor (Université de Paris)	
<b>Dirk SCHÜLER</b>	Examiner
Professor (University of Bayreuth)	
<b>Nicolas MENGUY</b>	PhD advisor
Professor (Sorbonne Université)	
<b>Christopher LEFEVRE</b>	PhD co-advisor
CNRS Researcher (Aix Marseille Université)	
<b>Élodie DUPRAT</b>	PhD co-advisor
Associate professor (Sorbonne Université)	



Université de Paris

PhD Programme Frontières de l'Innovation en Recherche et Éducation - ED N° 474

Institut de Mineralogie, de Physique des Matériaux et de Cosmochimie - Sorbonne Université

---

## Séquestration du phosphore par les bactéries magnétotactiques de la colonne d'eau stratifiée du Lac Pavin

---

par

Cécile BIDAUD

Sciences du système terrestre - Thèse Interdisciplinaire  
dirigée par Nicolas MENGUY et Christopher LEFEVRE  
et co-encadré par Élodie DUPRAT

présentée and publiquement défendue le  
21 Octobre 2021

devant un jury composé de:

<b>Valérie MICHOTÉY</b>	Rapportrice
Professeure (Aix Marseille Université)	
<b>Heide SCHULZ-VOGT</b>	Rapportrice
Professeure (Institut Leibniz pour la recherche sur la Mer Baltique, Warnemünde (IOW))	
<b>Bénédicte MÉNEZ</b>	Examinatrice
Professeure (Université de Paris)	
<b>Dirk SCHÜLER</b>	Examineur
Professeur (Université de Bayreuth)	
<b>Nicolas MENGUY</b>	Directeur
Professeur (Sorbonne Université)	
<b>Christopher LEFEVRE</b>	Co-directeur
Chercheur CNRS (Aix Marseille Université)	
<b>Élodie DUPRAT</b>	Co-encadrante
Maîtresse de conférence (Sorbonne Université)	



*“Joy does not happen to us. We have to choose joy and keep choosing it every day.”*

Henri Nouwen (1932-1996)

*”La franchise ne consiste pas à dire ce qu’on pense, mais à penser ce qu’on dit.”*

Coluche (1944-1986)

*”You get in life what you have the courage to ask for.”*

Oprah Winfrey



---

## Remerciements (Acknowledgments)

J'aimerais commencer par remercier mes trois tuteurs de thèse, Élodie Duprat, Nicolas Menguy et Christopher Lefevre, avec qui j'ai passé trois incroyables années. Chacun de mes tuteurs ayant une spécialité différente, j'ai pu profiter de leur différentes expertises et acquérir diverses connaissances.

Je tiens tout d'abord à remercier Élodie pour son infaillible disponibilité, que ce soit pour les moments épineux ou pour les moments plus positifs et excitants, durant lesquels je pouvais débarquer de manière improvisée dans son bureau. Merci Élodie, pour ta pédagogie, ta patience, ta gentillesse, mais aussi pour ta grande participation dans mes travaux lorsque j'en avais besoin. Je n'aurais pu demander meilleure tutrice...

Je veux aussi remercier mon second tuteur Nicolas. Nicolas, je te remercie pour ton grand enthousiasme dans mon travail de thèse, ta disponibilité, mais aussi pour ta patience et le temps que tu as consacré à m'apprendre le fonctionnement du microscope électronique à transmission. Tu as su satisfaire ma curiosité et répondre à mes innombrables questions. Finalement, je te remercie pour m'avoir tant encouragée, et pour m'avoir aidée à surmonter les divers moments de doutes !

Je voudrais finir par remercier Christopher. Christopher tu m'as fait découvrir le monde de la microbiologie et des bactéries, et notamment les bactéries magnétotactiques. Merci à tes supers accueils au centre de Cadarache, à ton enseignement et à ton temps passé à m'apprendre toutes les expériences sur les bactéries magnétotactiques. Merci pour ta bonne humeur et à tes grands sourires. Sans toi notre collaboration à quatre n'aurait pas existé !

Notre temps passé ensemble est représentatif des conditions de travail que je chercherais à l'avenir. Merci à vous trois, vous allez me manquer...

J'aimerais remercier Caroline Monteil pour tout son travail en lien avec ma thèse et sans qui mes résultats auraient sûrement été beaucoup moins glamour ou complets. Merci Caroline pour ta persévérance et la réitération des calculs encore et encore ! Et merci aussi pour ton accueil à Cadarache !

J'aimerais remercier mes collègues de travail, notamment Fériel Skouri-Panet, qui m'a énormément aidée dans le laboratoire avec mes expériences quelque fois un peu longues et pas forcément aisées à faire seule. Fériel, merci pour tes innombrables conseils et idées, et à tout le temps que tu as passé avec moi. Je ne compte pas le nombre de fois où j'ai pu entendre dans le laboratoire: "Tu sais où est Fériel?", tout le monde à besoin de toi, et tu es sans aucun doute irremplaçable...

J'aimerais ensuite remercier Cynthia Travert et le plus beau sourire de l'équipe. Cynthia, ton



---

enthousiasme pour les projets du laboratoire et le mien à travailler en groupe ont fait de nous un super et récurrent binôme. Tu m'as beaucoup aidé lors d'expériences nécessitant plusieurs paires de mains, j'ai adoré ta compagnie, tout nos fou rires et conversations. Merci beaucoup, surtout ne change pas et garde ta joie de vivre!

Merci Jean-Michel Guigner pour ton aide lors de mes multiples journées au microscope électronique, pour m'avoir tenue compagnie de temps en temps, et pour être venu systématiquement vérifier que tout allait bien pour moi!

Merci Karim pour nos multiples discussions sur mon travail de thèse, mais aussi pour tes conseils et pour m'avoir formé au microscope électronique à balayage et au confocal!

Merci à Anne-Catherine Lehours, Hermine Billard et Jonathan Colombet pour leur aide à l'Université Clermont-Ferrand et en mission au Lac Pavin. Merci à toute votre aide pour l'élaboration de la technique de Cytométrie en flux et à votre super accueil dans vos locaux.

Je veux aussi remercier mes co-bureaux, Laura Galezowski et Apolline Bruley, pour toutes nos conversations durant nos pauses cafés ou thés, mais aussi pour leur patience lorsque je revenais frustrée ou agacée d'une expérience. Sans vous, le travail aurait peut être été plus efficace, mais aussi beaucoup moins agréable! Vous m'avez accompagnée, ainsi que Juliette Debie (aussi dans le laboratoire), à mon enterrement de vie de jeune fille! Je vous aime les filles!

À Laura, Apolline et Juliette, je veux rajouter Dania Zuniga, Baptiste Truffet, Léon Andriambariarijaona, Jaysen Sawmynaden, et tous les autres doctorants de l'IMPMC avec qui j'ai pu aussi partager mes pauses cafés, mes déjeuners et des inoubliables moments au bar.

J'aimerais aussi remercier mes amis en dehors du laboratoire qui ont été là pour moi tout au long de ma thèse, et même avant...: Thaïs, Binj, Marie, Océane, Morgane, Gert-Jan, Louis,... Vous avez pu m'apporter un soutien constant que ce soit au bar, au café, chez les uns ou les autres, ou en vidéo.

À mon meilleur colocataire, passé et futur, François Giovanetti... Je n'oublierais pas nos très long moments passés à discuter de tout et de rien, de mes soucis, de tes soucis, ou du repas du soir. Je serais toujours nostalgique de notre vie commune à Paris. Merci beaucoup pour cette partie de ma vie à laquelle je tiens particulièrement!

J'aimerais attribuer des remerciements particuliers à Benjamin Wheeler qui, sans aucun conteste a été l'ami le plus présent, et sans qui cette thèse se serait sans doute passée bien différemment! Benjamin, merci pour ces longs moments de télétravail, mais aussi il ne faut pas mentir... pour tous ces repas, apéros, jeux vidéos (Zelda, Tetris, Overcooked, Unravel two,...etc.) et séries télévisées (The Expanse, New Girl,...etc.)! Grâce à toi, l'écriture de mon manuscrit s'est mieux déroulée! Merci à cette superbe organisation de mon enterrement de vie de jeune fille, à mes chevilles gonflées et à cette belle chasse au trésor! Tu es un ami en or et j'ai hâte de découvrir

---

la suite de notre amitié dans le futur !

Je veux aussi remercier ma famille, mon père, ma mère et mon frère jumeau, pour leur soutien. Merci de m'avoir rappelée que j'étais capable de réussir et de finir cette thèse. Je rajoute aussi un grand merci à votre soutien financier qui m'a permis de finir ma thèse dans les meilleures conditions possibles. Merci pour votre aide régulière avec Rusty, vous avez été parfait pendant les moments difficiles.

Je veux finir par remercier Tanner, mon compagnon. Merci à ton soutien sans faille, tes conseils, tes encouragements, ta patience, ton calme et à ton sourire. Merci de m'avoir, oh combien de fois, redonné confiance et rassuré, et d'avoir encore et encore écouté mes répétitions d'oral... Malgré la distance New York/Paris qui pouvait nous séparer, tu as constamment et sans faillir été présent pour moi. Sans toi, cette thèse aurait été incroyablement moins belle.





Université de Paris  
**Phosphorus sequestration by magnetotactic bacteria in the stratified  
water column of Lake Pavin**

Short Summary

Phosphorus (P) is essential for life but limited or pollutant in some environments. Few microorganisms known to accumulate P as polyphosphates (PolyP) in oxic conditions, at marine water-sediment interface or in wastewater treatment plants, provide a promising strategy for P resource management.

This thesis stems on the recent discovery of a group of magnetotactic bacteria (MTB) affiliated to the Magnetococcaceae family (MTBc), sequestering PolyP in the anoxic layer of the water column of Lake Pavin. Both biological and environmental drivers of this process remain unknown. First, this thesis aimed at describing the vertical distributions of MTB populations along chemical gradients of the lake water column and the relative abundance of MTBc. By combining *in situ* monitoring of physicochemical parameters, bulk geochemistry, optical and electron microscopies and multivariate statistics, my work contributed to (i) describe a unique morphotype capable to form intracellular calcium carbonates, (ii) develop a water sampling strategy with high vertical resolution and (iii) identify the biogeochemical niche of MTBc whose parameters were further used to design a promising isolation medium.

The second part of this thesis focused on MTBc heterogeneity according to their P sequestration capabilities. My work contributed to (i) develop a cell classification scheme based on ultrastructural description of their inclusions, (ii) identify a stratification of MTBc along the chemical gradients of the water column confirming the relationship between P and S metabolisms and (iii) optimize sample preparation and staining for specific sorting of PolyP-sequestering cells by flow cytometry.

Keywords: magnetotactic bacteria, polyphosphates, Lake Pavin, biogeochemical niches, chemical gradients, electron microscopy, intracellular inclusions, biomineralization, flow cytometry.



Université de Paris  
**Séquestration du phosphore par les bactéries magnétotactiques de la  
colonne d'eau stratifiée du Lac Pavin**

Résumé Court

Le phosphore (P) est essentiel à la vie mais limité ou polluant dans certains environnements. Quelques microorganismes connus pour accumuler le P sous forme de polyphosphates (PolyP) en oxyde, à l'interface marine eau-sédiments ou en stations d'épuration, offrent une stratégie prometteuse pour la gestion des ressources de P.

Cette thèse fait suite à la récente découverte de bactéries magnétotactiques (MTB) affiliées à la famille Magnetococcaceae (MTBc) séquestrant des PolyP en zone anoxique de la colonne d'eau du Lac Pavin. Les facteurs biologiques et environnementaux de ces processus restent inconnus. Cette thèse a eu pour objectif de décrire les distributions verticales des MTB le long des gradients chimiques de la colonne d'eau et l'abondance relative des MTBc. En alliant les mesures *in situ* des paramètres physicochimiques, la géochimie des eaux, la microscopie optique et électronique et des statistiques multivariées, mon travail a permis de (i) décrire un morphotype formant des carbonates de calcium intracellulaires, (ii) développer une méthode d'échantillonnage à haute résolution et (iii) identifier la niche biogéochimique des MTBc dont les données ont servi à créer un milieu d'isolement prometteur.

La thèse s'est aussi centrée sur l'hétérogénéité de séquestration du P des MTBc. Mon travail a permis de (i) créer une classification cellulaire basée sur la description ultrastructurale des inclusions, (ii) identifier une stratification des MTBc le long des gradients chimiques de la colonne d'eau confirmant la relation entre les métabolismes du P et du S et (iii) optimiser la préparation et le marquage des échantillons pour le tri de cellules séquestrant du P par cytométrie en flux.

Mots-clés: bactéries magnétotactiques, polyphosphates, Lac Pavin, niches biogéochimiques, gradients chimiques, microscopie électronique, inclusions intracellulaires, biominéralisation, cytométrie de flux.





# Table of contents

<b>Acknowledgments</b>	<b>7</b>
<b>Small Summary/Résumé court (English/Français)</b>	<b>11</b>
<b>List of Figures</b>	<b>21</b>
<b>List of Acronyms</b>	<b>24</b>
<b>Résumé du Manuscrit (en Français)</b>	<b>27</b>
<b>Chapter 1. Introduction</b>	<b>35</b>
1.1 <b>Scientific context</b> . . . . .	36
1.1.1 Management of phosphorus resources: a current environmental issue . . . . .	36
1.1.1.1 Phosphorus is a limited resource for life . . . . .	36
1.1.1.2 Anthropogenic pollution of phosphorus . . . . .	36
1.1.2 Life as a dynamic reservoir of phosphorus . . . . .	38
1.1.2.1 Biotic and abiotic reservoirs of P . . . . .	39
1.1.2.2 Transformation of P reservoirs induced by microbial activities . . . . .	41
1.1.3 The <i>Magnetococcaceae</i> family as a new model for polyphosphate sequestration . . . . .	44
1.1.4 Lake Pavin as a model site for the identification of geochemical drivers of polyphosphate sequestration by magnetotactic cocci . . . . .	46
1.1.4.1 General presentation . . . . .	46
1.1.4.2 Chemical gradients . . . . .	47
1.1.4.3 Potential relationships between microbial activities and phosphogenesis . . . . .	49
1.2 <b>Thesis objectives and strategy</b> . . . . .	51
<b>Chapter 2. Vertical structure of magnetotactic bacteria populations in the water column of Lake Pavin</b>	<b>55</b>
2.1 <b>Introduction</b> . . . . .	57
2.1.1 Known diversity and biogeography of magnetotactic bacteria . . . . .	57



## Table of contents

---

2.1.2	Magnetosomes diversity can be a proxy of environments, taxonomy or metabolism . . . . .	58
2.1.3	Magnetotactic bacteria: a life at the interfaces . . . . .	59
2.1.4	Magnetotactic bacteria sorting, isolation and methods of study . . . . .	61
2.1.5	Objectives and strategy of the chapter . . . . .	63
2.2	<b>Discovery of a magnetotactic bacteria group capable of sequestering intracellularly amorphous calcium carbonate in the water column of Lake Pavin - Monteil et al. (2021)</b> . . . . .	65
2.3	<b>Improvement of the magnetotactic bacteria collection with a higher vertical resolution sampling and a proxy to detect their abundance - Busigny et al. (2021)</b> . . . . .	85
2.4	<b>Thin description of the magnetotactic bacteria profile as a function of the depth and varying chemical parameters in the water column of Lake Pavin</b>	103
2.4.1	Material and methods . . . . .	103
2.4.1.1	Site description and water sampling strategy . . . . .	103
2.4.1.2	<i>In situ</i> measurements of physicochemical parameters . . . . .	104
2.4.1.3	Chemical analyses of dissolved and particulate fractions in the water column . . . . .	104
2.4.1.4	Estimation of the magnetotactic bacteria population sizes and analysis of morphotypes diversity . . . . .	104
2.4.1.5	Statistical analyses . . . . .	105
2.4.2	Results . . . . .	107
2.4.2.1	Magnetotactic bacteria communities are localized just below the oxic-anoxic transition zone (OATZ) in a zone spatially structured in discrete geochemical niches . . . . .	107
2.4.2.2	Magnetotactic bacteria are diverse and predominantly composed of Magnetotactic bacteria cocci (MTBc) . . . . .	109
2.4.2.3	The abundance of MTBc is correlated to the concentration of dissolved sulfates, mass percentage of organic N and C, particulate magnesium and phosphorus . . . . .	111
2.4.3	Discussion . . . . .	112
2.5	<b>Design of culture media for the isolation of the Lake Pavin MTBc and preliminary results</b> . . . . .	114
2.5.1	Materials and methods . . . . .	114
2.5.1.1	Design of double gradient media . . . . .	114
2.5.1.2	Media oxygen profile - oxygen microsensor . . . . .	115
2.5.1.3	Magnetotactic bacteria sampling and isolation protocol . . . . .	116
2.5.2	Results . . . . .	118

2.5.2.1	Four double gradient media presenting different redox gradients	118
2.5.2.2	The resazurin is a redox indicator allowing the visualization of oxygen gradients . . . . .	119
2.5.2.3	Culture of magnetospirillum-like magnetotactic bacteria . . . . .	120
2.5.3	Discussion . . . . .	121
2.6	<b>Conclusions and perspectives</b> . . . . .	125
<b>Chapter 3.</b>	<b>Magnetotactic cocci in the water column of Lake Pavin: morphotype classification and sorting of P-sequestering cells</b>	<b>129</b>
3.1	<b>Introduction</b> . . . . .	131
3.1.1	Detection, quantification and characterization of PolyP in the cell fraction: state of the art . . . . .	133
3.1.1.1	Bulk analyses . . . . .	134
3.1.1.2	Localization of polyphosphates (PolyP) at cell scale . . . . .	135
3.1.1.3	Combination of techniques . . . . .	139
3.1.2	Questions and strategy of the chapter . . . . .	140
3.2	<b>Diversity and distribution of P-sequestering MTBc along the chemical gradients in the water column of Lake Pavin</b> . . . . .	141
3.2.1	Material and methods . . . . .	141
3.2.1.1	Water sampling strategy . . . . .	141
3.2.1.2	transmission electron microscopy (TEM) grid deposition (optimization) . . . . .	141
3.2.1.3	Classification of the magnetotactic cocci according to the magnetosome organization and the relative size of PolyP granules	143
3.2.1.4	Statistical analyses . . . . .	146
3.2.2	Results . . . . .	146
3.2.2.1	The proportion of MTBc sequestering PolyP differs with depth in the water column . . . . .	146
3.2.3	Discussion . . . . .	150
3.3	<b>Cell sorting of MTBc with large PolyP inclusions using flow cytometry: methodological developments and preliminary results</b> . . . . .	155
3.3.1	Methodological strategy: samples and parameters . . . . .	155
3.3.2	Material and methods . . . . .	156
3.3.2.1	Staining protocols . . . . .	156
3.3.2.2	Flow Cytometry set up . . . . .	157
3.3.3	Bacterial models: choice and conditions to obtain negative and positive controls . . . . .	159
3.3.4	Dual staining on the positive control . . . . .	160

## Table of contents

---

3.3.5	Cell sorting on the bacterial models . . . . .	161
3.3.6	Sample preparation optimization for flow cytometry analyses - M2 Internship - Clémentin Bouquet . . . . .	165
3.3.6.1	Optimization of the dual staining protocol . . . . .	165
3.3.6.2	Cell sorting as a function of polyphosphate detection for a mix of both control cultures and for an environmental sample . . .	166
3.4	<b>Conclusions and Perspectives</b> . . . . .	169
<b>Chapter 4.</b>	<b>Conclusions and perspectives</b>	<b>175</b>
4.1	<b>Conclusions</b> . . . . .	175
4.2	<b>General perspectives</b> . . . . .	178
	<b>Bibliography</b>	<b>183</b>
	<b>Appendices</b>	<b>209</b>

# List of Figures

1.1	Schematic representation of the natural and anthropogenic phosphorus cycles. . . . .	37
1.2	Schematic representation of the reservoirs of P and the cell interactions between these reservoirs . . . . .	38
1.3	Monomeric and polymeric forms of orthophosphate constitute the intracellular inorganic P molecules (particulate inorganic phosphorus (PIP)) . . . . .	39
1.4	Schematic representation of the PolyP PPK and PPX enzymes functions for the PolyP synthesis and hydrolysis . . . . .	43
1.5	Scanning transmission electron microscopy (STEM)-high-angle annular dark-field (HAADF) and STEM-X-ray energy-dispersive spectrometry (XEDS) images of a MTBc accumulating P under the form of PolyP in Lake Pavin . . . . .	45
1.6	Geographical map of France locating Lake Pavin (red dot), in addition to an aerial view of the lake (right) . . . . .	47
1.7	Concentration profiles of dissolved $O_2$ , $SO_4^{2-}$ , $Mn^{2+}$ , $H_2S$ , $Fe^{2+}$ and soluble reactive phosphorus (SRP) chemical species (a and b) in Lake Pavin water samples and collected in July 2007 . . . . .	49
2.1	Physicochemical depth profiles in the water column of Lake Pavin measured <i>in situ</i> in October, the 30 <sup>th</sup> . . . . .	107
2.2	Environmental structuring of depths according to their geochemical features . . . . .	108
2.3	Relationships between the Magnetotactic bacteria (MTB) population structure and abundance and the environmental features in the water column . . . . .	110
2.4	Scanning transmission electronic microscopy images of magnetotactic bacteria with different morphology found in Lake Pavin water column . . . . .	111
2.5	Schematic of the different inverse gradient media (oxygen versus a sulfur compound) tested for the MTBc growth . . . . .	115
2.6	Photo of the microelectrode-micromanipulator setup for $O_2$ measurement in Lake Pavin growth media . . . . .	116
2.7	MTB sampling and purification setup for inoculation in the MTBc growth media . . . . .	117
2.8	MTB culture medium showing a band of MTB growing at the oxic-anoxic interface in a tube of MTB culture . . . . .	118
2.9	Different inverse gradient media tested for the Lake Pavin MTBc . . . . .	119

## List of Figures

---

2.10	Oxygen micro profiles comparison of the media with a Na <sub>2</sub> S solid bottom plug with or without cysteine . . . . .	120
2.11	Image of the tube which isolated the magnetospirillum-like cells . . . . .	121
2.12	Different ideas of media to test in the future for the isolation of the MTBc of Lake Pavin. . . . .	127
3.1	Table of the techniques specificities for the detection and quantification of PolyP	132
3.2	Schematic view of the different methods for the detection of PolyP and PolyP accumulators . . . . .	133
3.3	Confocal analysis of cells stained with 4',6-diamidino-2-phenylindole (DAPI) whose emission spectra are associated with DNA (blue) or PolyP (green) . . . .	137
3.4	Schematic view of the set up used for TEM grids preparation . . . . .	141
3.5	TEM-bright-field (BF) observations of MTBc on a TEM grid prepared with the "ring technique" showing the segregation of the MTBc as a function of their PolyP accumulation capabilities . . . . .	142
3.6	Schematic view of the optimized TEM grid preparation with poly-L-lysine coating	143
3.7	STEM-HAADF observations of PolyP-accumulating MTBc and intracellular calcium carbonate (iACC)-rods and their analyses on the TEM for statistical analysis . . . . .	144
3.8	Elemental mapping of MTB sequestering granules of PolyP, S or iACC . . . . .	146
3.9	STEM-HAADF images showing different magnetosomes organizations and PolyP accumulation capacities of MTBc and PolyP accumulating rod-shaped MTB . . .	147
3.10	Morphological analysis of prismatic magnetosomes in cocci with three different magnetosomes organizations . . . . .	148
3.11	Distribution of MTBc in the water column according to their ability to form different types of magnetosome chains and PolyP inclusions . . . . .	149
3.12	Schematic illustration of the main MTBc morphotypes inhabiting the anoxic layer of the water column of Lake Pavin . . . . .	154
3.13	Schematic representation of the experiments and analytical approaches used during the flow cytometry study . . . . .	156
3.14	Schematic representation of the flow cytometry (FC) cells sorting of an environmental sample . . . . .	159
3.15	Dual DAPI-SYTO <sup>®</sup> 62 staining order comparison on the positive model control <i>Tetrasphaera elongata</i> . . . . .	161
3.16	Cytograms of the three culture models: RX culture, <i>Acinetobacter junii</i> , <i>Tetrasphaera elongata</i> and mixed of the three as a function of the fluorescence intensity of the PolyP DAPI and DNA SYTO <sup>®</sup> 62 . . . . .	162

3.17 scanning electron microscopy (SEM) analyses coupled with XEDS of the three independent model cultures before sorting on the flow cytometer . . . . .	163
3.18 SEM analyses coupled with XEDS of the P1, P2 and P4 populations after sorting of the model culture mix on the flow cytometer . . . . .	164
3.19 Physico-chemical profiles in the water column of Lake Pavin (0-62 m) and TEM images of the samples retrieved from the OATZ for FC analyses . . . . .	166
3.20 PolyP+ cell proportions (%) for the culture mix <i>T. elongata</i> and <i>RX</i> and the environmental sample before sorting and in the PolyP- and PolyP+ collected fractions . . . . .	167
3.21 Schematic of the methodology for the infraspecific diversity description of the MTBc as a function of their PolyP accumulation capabilities and the depth . . . .	172



## List of Acronyms

**BF** bright-field

**CEMOVIS** cryo-electron microscopy of vitreous sections

**DAPI** 4',6-diamidino-2-phenylindole

**DOP** dissolved organic phosphorus

**DIP** dissolved inorganic phosphorus

**EM** Electron microscopy

**FACS** fluorescence-activated cell sorting

**FC** flow cytometry

**FISH** fluorescence *in situ* hybridization

**FSC** forward scatter

**HAADF** high-angle annular dark-field

**HEPES** 4-(2-hydroxyethyl)-1-piperazineethanesulfonic acid

**iACC** intracellular calcium carbonate

**ICP-OES** Inductively Coupled Plasma-Optical Emission Spectroscopy

**MMPs** multicellular magnetotactic prokaryotes

**MTB** Magnetotactic bacteria

**MTBc** Magnetotactic bacteria cocci

**OATZ** oxic-anoxic transition zone

**OAI** oxic-anoxic interface

**PAO** polyphosphates accumulating organisms

**PBS** phosphate-buffer saline

**PolyP** polyphosphates

**POP** particulate organic phosphorus



## List of Acronyms

---

<b>PPX</b>	exopolyphosphatase
<b>PPK</b>	polyphosphate kinase
<b>PIP</b>	particulate inorganic phosphorus
<b>RT</b>	room temperature
<b>Tc</b>	Tetracycline
<b>TEM</b>	transmission electron microscopy
<b>TDP</b>	total dissolved phosphorus
<b>TPP</b>	total particulate phosphorus
<b>SEM</b>	scanning electron microscopy
<b>SOB</b>	sulfur oxidizing bacteria
<b>SRB</b>	sulfate reducing bacteria
<b>SRP</b>	soluble reactive phosphorus
<b>SSC</b>	side scatter
<b>STEM</b>	Scanning transmission electron microscopy
<b>STXM</b>	synchrotron-based scanning transmission X-ray microscopy
<b>TE</b>	Tris-EDTA (Tris hydrogen chloride and Ethylenediaminetetraacetic acid)
<b>WWTP</b>	wastewater treatment plants
<b>XEDS</b>	X-ray energy-dispersive spectrometry
<b>XRF</b>	X-ray fluorescence





# Séquestration du phosphore par les bactéries magnétotactiques de la colonne d'eau stratifiée du Lac Pavin

## Résumé

### Introduction

Le phosphore (P) est un élément essentiel pour le vivant mais également limitant dans de nombreux écosystèmes. Cette limitation est due à l'absence de réservoir atmosphérique et aux processus relativement lents d'altération des roches phosphatées. Ces roches, les phosphorites, constituent le puits principal de P minéral mais aussi une ressource non renouvelable extrêmement utilisée par l'Homme en tant qu'engrais, dont l'épuisement est prévu avant la fin du siècle par différents modèles. Cette exploitation crée un flux unidirectionnel de P depuis ces roches jusqu'aux systèmes aquatiques conduisant dans certaines zones à un excès de P. Cet excès est susceptible d'induire la croissance incontrôlée de microorganismes conduisant à la mise en place de conditions hypoxiques voire anoxiques délétères pour la vie locale. Ce phénomène, appelé eutrophication, donne lieu à l'apparition de « zones mortes ». Il existe par ailleurs un réservoir éolien de P dont la taille et le dépôt sont influencés par la combustion d'énergies fossiles et de biomasse ainsi que par la présence d'engrais et de bétail. La taille de ce réservoir est amplifiée avec l'industrialisation ce qui favorise d'autant plus l'apport excessif de P dans les écosystèmes naturels. Ce déséquilibre dans le cycle du P met en avant la nécessité de développer des stratégies durables pour la gestion des ressources.

Afin de préserver la biodiversité impactée par l'utilisation intensive du P, les microorganismes constituent des solutions prometteuses de bioremédiation. En effet, ceux-ci peuvent agir, d'une part, en tant que réservoir du P, notamment en séquestrant le P sous la forme de polyphosphates intracellulaires (PolyP) et, d'autre part, en tant qu'acteurs de processus transformant ces réservoirs. Ils peuvent (i) reminéraliser les espèces organiques de P, leur permettant une incorporation dans la biomasse sous la forme de nouvelles molécules et (ii) immobiliser le P en induisant sa précipitation sous forme de phases minérales phosphatées (par biominéralisation) ou en rentrant en concurrence avec les phases minérales pour l'adsorption du P.

Les PolyP sont des polymères d'orthophosphates synthétisés par toutes les formes de vie. Ces polymères accomplissent une multitude de fonctions au sein de la cellule et notamment en tant que source d'énergie ou de phosphates. Leur métabolisme est particulièrement dynamique et sous influence de paramètres environnementaux. Le paradigme actuel de formation des PolyP repose sur quelques modèles microbiens environnementaux identifiés principalement en milieu marin, à l'interface eau-sédiment au niveau des marges continentales où se forment les phosphorites

actuelles (e.g. *Thiomargarita* et *Beggiatoa*), ou enrichis dans les boues de stations d'épuration (e.g. *Accumulibacter* spp.) et permettant une dépollution du P dans les eaux usées. Pour ces différents micro-organismes, il a été mis en évidence que la présence d'oxygène est nécessaire à la formation de PolyP tandis que l'anoxie constitue un facteur de leur hydrolyse.

Cette présente thèse fait suite à la découverte de bactéries magnétotactiques (MTB) de forme sphérique, i.e. cocci magnétotactiques (MTBc), appartenant à la famille *Magnetococcaceae* au sein de l'embranchement des Proteobacteria, séquestrant des PolyP en anoxie dans la colonne d'eau du Lac Pavin. Cette découverte ainsi que celle de deux autres modèles possédant des PolyP en conditions anoxiques dans la Mer Noire et dans la Mer Baltique remet en question le paradigme précédemment décrit. L'affiliation des bactéries de la Mer Noire aux *Magnetococcaceae* suggère un impact plus global de cette famille dans le cycle biogéochimique du P. Les modèles réagissent différemment à des conditions riches en soufre. Dans de telles conditions, les MTBc de la Mer Noire hydrolysent leur PolyP à l'instar des *Thiomargarita* et *Beggiatoa*, tandis que les *Sulfurimonas* de la Mer Baltique accumulent des PolyP intracellulaires. Ces données contradictoires mettent en lumière la nécessité d'étudier de nouveaux modèles d'accumulation du P et notamment dans des environnements d'eaux douces pour lesquels il manque des données. Dans la colonne d'eau du Lac Pavin, les facteurs biologiques et environnementaux d'accumulation ou d'hydrolyse des PolyP par les MTBc restent inconnus. Pour cette thèse, la présence de forts gradients chimiques ( $\text{Fe}^{2+}$ ,  $\text{SO}_4^{2-}$ ,  $\text{PO}_4^{3-}$ ,  $\text{H}_2\text{S}$ ...) et ce, sur plusieurs mètres, dans la zone d'habitat des MTB nous ont permis d'étudier l'influence de ces paramètres sur la structuration des populations de MTB et la capacité des MTBc à séquestrer du P sous forme de PolyP.

Cette thèse a eu pour objectif de décrire les distributions verticales des MTB le long des gradients chimiques de la colonne d'eau et l'abondance relative des MTBc. Alliant les mesures *in situ* des paramètres physicochimiques, la géochimie des eaux, la microscopie optique et électronique et des statistiques multivariées, mon travail a permis de (i) décrire un morphotype formant des carbonates de calcium intracellulaires, (ii) développer une méthode d'échantillonnage à haute résolution et (iii) identifier la niche biogéochimique des MTBc dont les données ont servi à créer un milieu d'isolement prometteur.

La thèse s'est aussi centrée sur l'hétérogénéité de séquestration du P des MTBc. Mon travail a permis de (i) créer une classification cellulaire basée sur la description des inclusions, (ii) identifier une stratification des MTBc le long des gradients chimiques de la colonne d'eau confirmant la relation entre les métabolismes du P et du S et (iii) optimiser la préparation et le marquage des échantillons pour le tri de cellules séquestrant le P par cytométrie en flux.

### Structure vertical des populations de bactéries magnétotactiques dans la colonne d'eau du lac Pavin.

Les bactéries magnétotactiques (MTB) constituent un groupe de microorganismes non monophylétique, également divers d'un point de vue de leur morphologie et de leur physiologie. Les

MTB vivent en milieu aquatique. La plupart de ces bactéries sont microaérophiles ou anérobies et vivent principalement à proximité des interfaces oxique-anoxiques. Les MTB ont toutes la capacité de former des magnétosomes, organites intracellulaires composés de vésicules lipidiques enfermant des nanocristaux magnétiques biominéralisés par les bactéries elles-mêmes. Il s'agit de l'un des rares exemples de biominéralisation contrôlée chez les procaryotes. Selon les espèces de MTB, ces structures varient en composition, taille, forme, nombre et organisation. Les propriétés magnétiques de ces cristaux permettent aux MTB de s'aligner parallèlement aux lignes de champ magnétique et de s'orienter de façon active dans leur environnement. Les MTB présentes dans la colonne d'eau du lac Pavin sont diverses, et incluent les MTBc hyperaccumulant des PolyP. Ce chapitre vise à (i) décrire les différentes populations de MTB (définies en fonction de leur diversité morphotypique) et leurs abondances relatives en fonction de leur habitat et (ii) à caractériser les conditions environnementales caractérisant leurs habitats. Pour cela, l'utilisation de techniques de microscopie, de chimie analytique et de statistiques multivariées a été mise en œuvre.

Ces travaux ont permis la caractérisation d'un nouveau type de MTB biominéralisant de larges granules de carbonate de calcium intracellulaires (nommée iACC MTB) au sein de la colonne d'eau et des sédiments du Lac Pavin. Ces MTB sont très abondantes et leur distribution peut donc être statistiquement comparée à celle des MTBc. En parallèle, une nouvelle technique d'échantillonnage à haute résolution verticale de la colonne d'eau a été développée, combinée à des mesures physico-chimiques in situ. Nous avons ainsi découvert que la conductivité constitue un proxy du maximum d'abondance des MTB. Cette nouvelle technique de prélèvement a également permis d'établir un profil précis de la distribution des différentes MTB de la colonne d'eau et de différents paramètres environnementaux (géochimiques et physico-chimiques). Les observations en microscopie optique et électronique ont permis de distinguer et de caractériser sept morphotypes différents de MTB, classés en fonction de leur ultrastructure ainsi que la forme, l'organisation, la taille et le nombre de leurs magnétosomes. La microscopie optique a permis de mettre en évidence la stratification des deux morphotypes de MTB les plus abondants, les MTBc et les iACC MTB. Les statistiques multivariées ont permis de révéler l'appartenance des MTBc à une niche biogéochimique et d'identifier les paramètres géochimiques correspondants. Nous avons ainsi mis en évidence la corrélation des pourcentages massiques du carbone et de l'azote, des concentrations du phosphore et magnésium particulaires et des sulfates dissous à l'abondance des MTBc. Ces résultats suggèrent la co-localisation des MTBc avec la biomasse locale et consolide l'hypothèse que les MTBc sont des microorganismes dont le métabolisme est lié au cycle du soufre. Dans le but de pouvoir étudier ces MTBc en laboratoire, des milieux de cultures ont été conçus sur la base de l'hypothèse d'un métabolisme d'oxydation du soufre des MTBc. Les milieux de culture présentant un double gradient d'oxygène et de thiosulfate ou de sulfure d'hydrogène se sont avérés prometteurs, permettant le maintien de cellules ressemblant aux MTBc de par leur forme après trois semaines d'incubation. De plus, un des tubes de culture

## Résumé du Manuscrit (en Français)

---

a favorisé la croissance de MTB ressemblant aux bactéries du genre *Magnetospirillum*.  
De future analyses de métagénomique permettront de révéler l'identité des MTB de la colonne d'eau, leur diversité fonctionnelle et potentiel métabolique. De nouvelles conditions de croissance pourront ainsi être testées pour la culture des MTBc.

### Les cocci magnétotactiques dans la colonne d'eau du lac Pavin: classification morphotypique et tri des cellules séquestrant le P.

Il a été suggéré que les MTBc du Lac Pavin représenteraient un nouveau modèle de séquestration du P sous forme de PolyP (Rivas-Lamelo et al., 2017). Dans cette étude, les MTBc observées présentaient des organisations différentes de leurs magnétosomes et des accumulations variables de PolyP intracellulaires. Les paramètres biologiques ou environnementaux régissant cette hétérogénéité sont pour l'instant inconnus. Dans ce contexte, ce chapitre vise à (i) classer les différentes sous-populations de MTBc de la colonne d'eau du lac Pavin en fonction de leur morphotype et de leur capacité à séquestrer des PolyP, (ii) estimer leur abondance relative en fonction de la profondeur dans la colonne d'eau, (iii) caractériser les conditions environnementales spécifiques de leur habitat. Pour ce faire, les données de géochimie des solutions et de la matière en suspension présentées dans le précédent chapitre ont été complétées par des observations des communautés de MTB en microscopies optique et électronique. L'ensemble de ces données biogéochimiques a été exploité par des analyses statistiques multivariées.

La microscopie électronique a permis de révéler la présence de plusieurs morphotypes de MTBc et de les classer en fonction, d'une part, de l'organisation de leurs magnétosomes (doubles chaînes ou magnétosomes désorganisés - critère n°1) et, d'autre part, de leur capacité ou non à séquestrer des PolyP (critère n°2). Le maximum d'abondance de chaque catégorie de MTBc définie selon le critère n°1 est observé à deux profondeurs distinctes, correspondant respectivement au maximum d'abondance des MTB (51.3 m) pour les doubles chaînes et à celui des iACC MTB (52 m) pour les magnétosomes désorganisés. Pour chacune de ces deux catégories, il apparaît que la proportion de cellules séquestrant des PolyP (critère n°2) est maximale à 52 m. Les conditions environnementales observées à cette profondeur (en particulier la concentration minimale en sulfates dissous) semblent donc être optimales pour la séquestration de PolyP par les MTBc indépendamment de leur morphotype. Il est cependant à noter que des MTBc à doubles chaînes avec des PolyP sont observées à toutes les profondeurs échantillonnées.

Dans le but d'identifier les MTBc séquestrant des PolyP et de caractériser leur métabolisme par une approche génomique, un développement méthodologique permettant de trier spécifiquement cette sous-population de cellules a été réalisé par cytométrie en flux. Cette approche permet, en combinaison du marquage fluorescent des PolyP, la détection et un tri cellulaire à haut débit des hyperaccumulateurs de PolyP à partir d'un échantillon hétérogène. L'approche a été validée par l'utilisation de modèles bactériens représentant des contrôles négatifs et positifs d'accumulation de PolyP puis appliquée à des échantillons de la colonne d'eau du lac Pavin. Les résultats préliminaires obtenus indiquent que le tri sur ces échantillons naturels complexes est moins efficace que sur des systèmes modèles mais semble néanmoins prometteur.



### Conclusions et perspectives

Cette thèse a permis d'identifier des paramètres environnementaux structurant les communautés de MTB dans la colonne d'eau du lac Pavin, tel que (i) les pourcentages massiques de C et N liés à la biomasse locale, (ii) les concentrations particulières de P et Mg liées au pic de phosphatogénèse mais aussi éventuellement aux PolyP des MTBc et (iii) la concentration en sulfates dissous suggérant un lien avec un métabolisme du soufre chez les MTBc.

La capacité de séquestration de PolyP par les MTBc ne semble pas dépendante de facteurs biologiques (telle que l'espèce, dont le type de magnétosomes a été considéré comme un proxy) mais favorisée par des paramètres environnementaux spécifiques (tel que la concentration en sulfates dissous). Le couplage entre capacité de séquestration de PolyP et métabolisme du S, suggéré par la littérature et confirmé lors de cette thèse, reste à préciser et ce pour chaque espèce de MTBc résidant dans la colonne d'eau du lac Pavin. Leur identification taxonomique et la description de leur potentiel fonctionnel (génomique) fourniront des informations essentielles pour cela. La quantité d'ADN extraite d'échantillons naturels est souvent critique et limitante, en particulier pour des microorganismes peu abondants comme les MTB (de l'ordre de  $10^3$  cellules par mL). Nos avancées permettant d'une part de concentrer les MTB de façon efficace (Busigny et al., 2021) et d'autre part de trier la fraction cellulaire enrichie en PolyP (cytométrie en flux) nous permettront de lever ce verrou.

La dynamique de ce réservoir biotique de P et l'impact de cette dynamique sur la phosphatogénèse de la colonne d'eau du Lac Pavin restent à explorer. Parmi les composantes potentielles de cette dynamique, la migration verticale des MTBc et l'expression des gènes associés au métabolisme du P et du S seraient à envisager. L'isolement des souches de MTBc et leur mise en culture en conditions contrôlées est actuellement un verrou méthodologique. Les milieux testés au cours de cette thèse pourraient être améliorés, selon les corrélations observées durant cette thèse (notamment avec le soufre) ou les paramètres importants pour les MTB décrits dans la littérature, en augmentant ou en diminuant par exemple la concentration en soufre du gradient inverse  $O_2$  versus  $H_2S$  ou en formant des gradients inverse en anoxie de nitrate ou fer versus  $H_2S$ .

Le suivi de cultures de ces MTBc dans des conditions mimant les conditions observées dans la colonne d'eau du Lac Pavin permettrait, en utilisant des techniques de transcriptomique, microscopies et quantification de phosphore dissous et particulaire, d'évaluer (i) leur métabolisme, (ii) les conditions dans lesquelles celles-ci accumulent ou hydrolysent leurs PolyP et (iii) leur impact sur le cycle biogéochimique du P dans le Lac Pavin. Ces conditions contrôlées pourraient notamment mimer les conditions des deux profondeurs où les MTBc accumulent le moins ou le plus les PolyP. L'étude d'autres modèles d'hyperaccumulation de PolyP, à l'aide des mêmes techniques utilisées pendant cette thèse et d'analyses génomiques, permettraient de comparer leurs conditions environnementales de croissance, leurs métabolismes et leur potentiel fonctionnel. Cette comparaison aiderait à confirmer ou infirmer chez les *Magnetococcaceae* un lien

entre le métabolisme du S et du P mais aussi la présence de gènes spécifiques à l'hyperaccumulation de PolyP. L'étude des MTB en forme de bâtonnet, de la famille des *Magnetococcaceae*, observées dans la colonne d'eau du Lac Pavin pourrait fournir un premier élément de réponse. La recherche et l'étude de nouveaux sites modèles, tels que d'autres lacs méromictiques, en utilisant toutes les méthodes mises en place durant cette thèse pourrait enrichir nos connaissances sur l'impact des conditions environnementales sur la capacité de séquestration PolyP par les microorganismes.



---

# Chapter 1. Introduction

---

## Contents

---

1.1	<b>Scientific context</b> . . . . .	<b>36</b>
1.1.1	Management of phosphorus resources: a current environmental issue . . . . .	36
1.1.1.1	Phosphorus is a limited resource for life . . . . .	36
1.1.1.2	Anthropogenic pollution of phosphorus . . . . .	36
1.1.2	Life as a dynamic reservoir of phosphorus . . . . .	38
1.1.2.1	Biotic and abiotic reservoirs of P . . . . .	39
1.1.2.2	Transformation of P reservoirs induced by microbial activities . . . . .	41
1.1.3	The <i>Magnetococcaceae</i> family as a new model for polyphosphate sequestration . . . . .	44
1.1.4	Lake Pavin as a model site for the identification of geochemical drivers of polyphosphate sequestration by magnetotactic cocci . . . . .	46
1.1.4.1	General presentation . . . . .	46
1.1.4.2	Chemical gradients . . . . .	47
1.1.4.3	Potential relationships between microbial activities and phosphogenesis . . . . .	49
1.2	<b>Thesis objectives and strategy</b> . . . . .	<b>51</b>

---

### 1.1 Scientific context

#### 1.1.1 Management of phosphorus resources: a current environmental issue

##### 1.1.1.1 Phosphorus is a limited resource for life

Phosphorus (P) is essential for all living organisms. However, this element (Ruttenberg, 2003) is also limiting in many ecosystems (Paytan and McLaughlin, 2007; Pasek, 2008; Moore et al., 2013). Indeed, the availability of the major form of P incorporated in the biomass without transformation, i.e. inorganic orthophosphates  $\text{PO}_4^{3-}$  also called  $P_i$ ), can be limited due to the phosphate-binding capacities of several type of soils or minerals (Zapata and Roy, 2004; Syers et al., 2008). Moreover, no atmospheric reservoir of P exists and the abiotic input of P in aquatic natural environments only comes from two slow processes: terrestrial weathering and/or erosion (Tyrrell, 1999).

Rock phosphate is often used as a fertilizer to overcome the P limitation for crop yields. However, the mined phosphate rocks constitute a non-renewable resource with >75 % of known remaining reserves only located in Morocco (Schoumans et al., 2015). As human population and demand for food increased in the latter half of the 20<sup>th</sup> century, current models predict that the P demand will exceed the available resources by the end of the century (Gilbert, 2009; Ruttenberg, 2019).

##### 1.1.1.2 Anthropogenic pollution of phosphorus

Despite the frequent limitation of bioavailable P in natural ecosystems, local excesses of P are also observed. This excess mostly comes from human activities and is deleterious for living ecosystems.

The increased use of P fertilizers can trigger toxicity in some lakes and coastal areas by discharging a surplus of P (Stramma et al., 2008). Such excess of P induces algal blooms and mass growth of toxic cyanobacteria (Wetzel, 2001), leading to an increase in the consumption of oxygen and the promotion of hypoxic and anoxic conditions harmful to the local life. This phenomenon, called eutrophication, corresponds with the formation of "dead zones" (Diaz and Rosenberg, 2008).

Eutrophication has been accentuated by deforestation, over-cultivation, and urban and industrial waste disposal. Overall, the human use of P has increased the riverine phosphorus flux to the oceans by 50 to 300% (Ruttenberg, 2019) starting in the latter half of the 20<sup>th</sup> century and doubled the total number of dead zones every decade since the 1960s (Diaz and Rosenberg, 2008). In freshwater habitats, the concentration of P is estimated to have increased more than 75% since

the pre-industrial period, and the fluxes of P toward the oceans to have increased from 8 to 22 million tons per year in the same time span (Bennett et al., 2001).

The eolian reservoir of P (Pan et al., 2021) is heterogeneously composed of coal combustion particles (Weinberger et al., 2016), dust particles (Gross et al., 2013; 2016), ashes of burning biomass (Bigio and Angert, 2019; Barkley et al., 2019), and tree pollen (Bigio and Angert, 2018). This eolian P can afterward be deposited via dry or wet processes (e.g., dust and rainfall deposition of particles) (Tipping et al., 2014). With the increasing human population, the use of livestock, crops with fertilizers and combustion of fossil fuels increases as well. Thus, the anthropogenic release of P into the atmosphere has become significant (Du et al., 2016).

As phosphorus limitation or excess leads to a disequilibrium in the P cycle (Elser and Bennett (2011); Fig. 1.1), the elaboration of strategies for a sustainable management of P become mandatory and urgent.

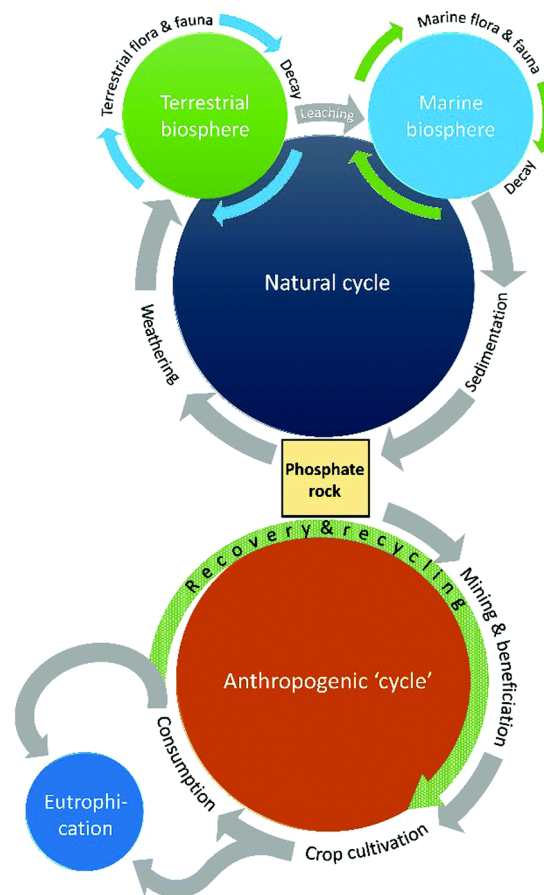


**Figure 1.1: Schematic representation of the natural and anthropogenic phosphorus cycles.** The current anthropogenic use of P is represented by an unidirectional flow of P between the natural cycle of P and the non renewable phosphate rocks, resources, and crops. The green arrow for "recovery & recycling" shows how important the development of P management strategies is. Figure from Jupp et al. (2021).

### 1.1.2 Life as a dynamic reservoir of phosphorus

Microorganisms have been shown to be major actors in the modern and past geochemical cycle of P (Froelich et al., 1982; Gächter and Meyer, 1993) due to their significant contribution to the reservoirs and fluxes of P (see Fig. 1.2).

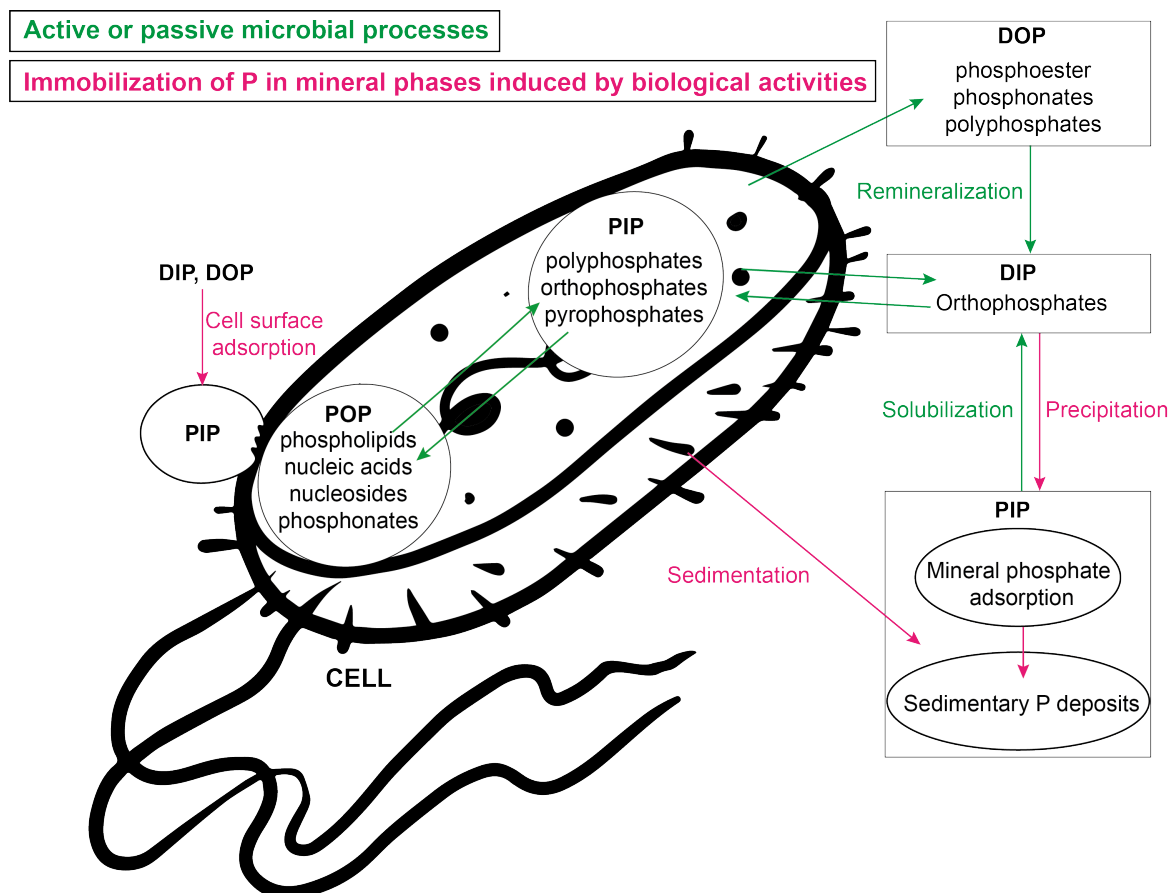


**Figure 1.2: Schematic representation of the reservoirs of P and the cell interactions between these reservoirs.** TDP (Total Dissolved Phosphorus) = DOP (Dissolved Organic Phosphorus) + DIP (Dissolved Inorganic Phosphorus), TPP (Total Particulate Phosphorus) = POP (Particulate Organic Phosphorus) + PIP (Particulate Inorganic Phosphorus).

Microorganisms are a potential bioremediation tool not only for P recovery in wastewater treatment plants (WWTP) (Tarayre et al., 2016), but also for heavy metal sequestration such as uranium (Newsome et al., 2014), or even mineral phosphate mobilization in agriculture (Ramamoorthy et al., 2020). In particular, the ability of microorganisms to efficiently sequester P as intracellular PolyP, from around  $\text{nmol.L}^{-1}$  in open-oceanic waters to around  $\text{mmol.L}^{-1}$  intracellularly (Martin et al., 2014), has been shown to be highly promising for the sustainable management of P as demonstrated by WWTPs (Yuan et al., 2012; Tarayre et al., 2016; Stockholm-Bjerregaard et al., 2017). Moreover, in addition to the wide diversity of cellular functions PolyP can perform, PolyP can replace phosphate rocks as fertilizers due to its inexpensiveness, non-

toxicity, and biodegradability. The negatively charged polymers can also induce complexation of diverse metal cations from the environment, such as iron, which minimizes their toxic effects. For these reasons PolyP are extensively studied for agricultural, industrial, medicinal and bacterial ecological purposes (Kulakovskaya et al., 2012).

### 1.1.2.1 Biotic and abiotic reservoirs of P

P reservoirs are usually classified into particulate and dissolved groups, each of which contain organic and inorganic compounds. While the total particulate phosphorus (TPP) is composed of particulate inorganic phosphorus (PIP) and particulate organic phosphorus (POP) respectively, the total dissolved phosphorus (TDP) is composed of dissolved inorganic phosphorus (DIP), also described as soluble reactive phosphorus (SRP), and the dissolved organic phosphorus (DOP).

P is essential for organisms as cell components for intracellular energy, cell growth, and metabolic functions (Ruttenberg, 2003). Both organic and inorganic molecules compose the microbial cells. P reservoirs and their transformation induced by microbial activities are illustrated in Fig. 1.2. In cells, the POP is found in nucleic acids such as DNA or RNA; in nucleosides as reservoir of biochemical energy (e.g., adenosine triphosphate (ATP); creatine phosphate and phosphoenolpyruvate); in phospholipidic membranes; in intermediary metabolites involved in biochemical syntheses and degradation (Westheimer, 1987; Ruttenberg, 2003; Paytan and McLaughlin, 2007; Labry et al., 2013; Ehrlich et al., 2015); and in phosphonates, which are known to be produced by many primitive life forms (Quinn et al., 2007; Hilderbrand, 2018) such as cyanobacteria (Dyhrman et al., 2009). The PIP cellular fraction includes orthophosphates, pyrophosphates, and PolyP, the latter two being polymers of orthophosphates (Labry et al. (2013); see Fig. 1.3).

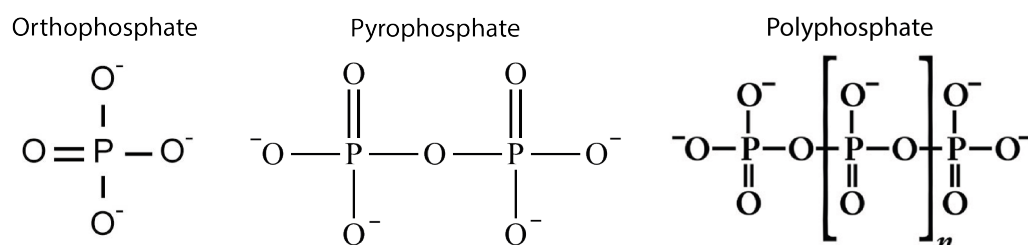


**Figure 1.3: Monomeric and polymeric forms of orthophosphate constitute the intracellular inorganic P molecules (PIP).** From left to right: molecule structure of an orthophosphate, a pyrophosphate and polyphosphate (with n central phosphate groups).

At the extracellular level, PIP includes P adsorbed to mineral phases or cells, and phosphate minerals such as phosphorites in upwelling continental margins environments (e.g. Namibia;



Goldhammer et al. (2010); Mänd et al. (2018)). In parallel, POP mainly represent detrital organic molecules (Labry et al., 2013; Yoshimura et al., 2007).

The TDP represents the main source of P for microorganisms. DIP (i.e.,  $P_i$ ) is the main form of P that microorganisms are able to uptake and directly incorporate into their biomass. The DOP is comprised of a complex mixture of organic constituents such as monophosphate esters, diesters, phosphonates, and PolyP. This P pool must be transformed into orthophosphate before it can be used by microorganisms (Yoshimura et al., 2007; Karl and Björkman, 2015; Diaz et al., 2016).

### **Polyphosphates are ubiquitous molecules with diverse functions**

PolyP are synthesized by all kingdoms of life (Kulaev et al., 2004). These polymers are composed of several hundreds of orthophosphates linked together by high energy phosphoanhydride bonds (see Fig. 1.3; Kornberg et al., 1999).

PolyP can be found in many different compartments of the cell. In prokaryotes, it can be found in the vicinity of nucleoids (Kulaev and Vagabov, 1983), in the periplasmic region (Rao and Torriani, 1988), in the flagellar pole and the cell membrane (Bode et al., 1993), and as part of the cell capsule (Tinsley et al., 1993; Tinsley and Gotschlich, 1995). For the eukaryotes, PolyP can be sequestered in different compartments constituting the cell (Kulaev and Kulakovskaya, 2000) and often in acidocalcisomes (i.e., organelles rich in P and metal ions such as calcium; Jendrossek (2020)). The PolyP, being negatively charged, usually interacts with counter-ions such as  $Mg^{2+}$ ,  $Ca^{2+}$  or  $K^+$ .

Hydrolysis of PolyP yields large amounts of energy that is used for a wide diversity of biological reactions (Kulaev, 1975). Microorganisms use PolyP in a variety of ways (Albi and Serrano, 2016), with the most common function being as a source of energy and phosphate storage, as it can be used as adenosine triphosphate (ATP) or a phosphorus substitute (Bonting et al., 1991; Kornberg, 1995). This energy can be used for the upkeep of motility to leave unsuitable growth conditions or move to a more preferable environment (Seufferheld et al., 2008; Varela et al., 2010; Möller et al., 2019); it also provides a cellular "safety system" in case no suitable electron acceptor is available (Brock and Schulz-Vogt, 2011), and is used by microorganisms in waste water treatment plants to sequester polyhydroxyalkanoate (PHA) (Bunce et al., 2018). PolyP can act against stresses by providing chaperone activity (i.e., prevent protein damage from stresses such as temperature, low pH, and oxidants; Kampinga (2014)), as a buffer system (Pick et al., 1990), as chelator for metal ions (as a detoxifying agent for e.g.  $Ca^{2+}$ ,  $Mg^{2+}$ ,  $Al^{2+}$ , ...; Kornberg (1995)) and as a regulator for gene activity (Blum et al., 1997). It is also linked to colonization, pathogenicity, virulence, and antibiotic resistance (Bowlin and Gray, 2021; Wang et al., 2018). Lechaire et al. (2002) propose that the PolyP might constitute a reservoir for oxygen in anoxic conditions.

Because of the many functions PolyP can perform, it is found in every type of cell and, in some

of them, in large quantities. Therefore, PolyP provides great potential for the possible bioremediation of polluted areas.

### 1.1.2.2 Transformation of P reservoirs induced by microbial activities

#### **Incorporation of P into the microbial biomass**

Microorganisms have developed strategies involving enzymes, acids, or other compounds to retrieve bioavailable orthophosphate from other less available pools of P (Ruttenberg, 2019). The enzymes, used for the recycling of the organic molecules, can be phosphatase (catalyse the hydrolysis of both esters and anhydrides of phosphoric acid), nucleases and nucleotidase (to retrieve a phosphate molecule from nucleic acid), or phosphomono- and phosphodiesterases (to release a  $P_i$  from phosphoproteins, phospholipids, glycerol phosphates,...) (Banik and Dey, 1983; Ruttenberg, 2019). Through microbial remineralization activities, the DOP supports division and growth of a large fraction of microorganisms and communities in zones depleted in DIP (Nausch et al., 2018).

Some microorganisms can solubilize phosphates adsorbed to mineral surfaces by releasing inorganic and organic acids or phosphatase into the medium (Tarafdar and Claassen, 1988; Rodríguez and Fraga, 1999), and also by releasing chelators and electron-shuttling compounds which can then complex onto the cations present on the mineral, forcing its dissolution (Lovley et al., 2004). Another process involves indirect solubilization and sulfate reducing bacteria (SRB): hydrogen sulfide ( $H_2S$ ) can be produced by these microorganisms and reduce iron from an iron-phosphate mineral, releasing  $P_i$  and reduced iron into the local medium (Roden and Edmonds, 1997).

The local release of phosphate in the medium provides bioavailable P that can be further incorporated in by the cells for the various P compounds of the cells including PolyP storage.

These processes participate in the recycling of P by the biomass and may also induce some active or passive immobilization.

#### **Immobilization of P in mineral phases induced by microbial activities**

Biom mineralization of metal-phosphates. Biom mineralization encompasses diverse processes in which cells trigger the precipitation of metal-phosphate phases, whether it be controlled by specific cellular activity or induced by the indirect modification of chemical conditions in the environment through biological activity (Benzerara et al., 2011).

Phosphate biom mineralization can occur upon microbial mobilization or solubilization of orthophosphates from mineral-adsorbed phosphate. Cell death can also lead to the release of orthophosphates, resulting in higher water saturation levels with respect to phosphate minerals and the induction of phosphatogenesis (Youssef, 1965; Piper and Codispoti, 1975).

In microorganisms accumulating intracellular PolyP, the PolyP can hydrolyze upon the death

of the cell or specific stresses can create a flux of  $\text{PO}_4^{3-}$  ions and thus trigger the precipitation of authigenic phosphorite (Gächter and Meyer, 1993; Sannigrahi and Ingall, 2005; Schulz and Schulz, 2005; Hupfer et al., 2007; Goldhammer et al., 2010).

Another, more indirect, case of P biomineralization may occur in a P-rich solution where the presence of Fe-reducing bacteria can increase the concentration of reactive Fe(II), thus creating conditions in which the solution is supersaturated with respect to different iron-phosphate phases or vivianite (Zachara et al., 1998; Glasauer et al., 2003; Peretyazhko et al., 2010). In a similar P-rich solution, and with low oxygen or anoxic conditions, Fe-oxidation can occur through both anoxygenic photosynthesis or nitrate reduction, increasing the concentration of Fe(III). This additional Fe(III) can then precipitate under the form of insoluble iron phases with phosphate (Widdel et al., 1993; Weber et al., 2006).

Cell competition with mineral phases. Microorganisms can also compete with mineral surfaces for phosphorus adsorption. This adsorption can occur in the presence of various extracellular polymeric substances such as negatively charged polysaccharides, surface proteins, or lipids. These compounds can promote the adsorption of different cations (e.g.,  $\text{Fe}^{2+}$ ) and the nucleation and biomineralization of Fe-phosphate crystals (Ferris and Beveridge, 1985; Konhauser et al., 1994; Konhauser, 1998; Peretyazhko et al., 2010).

### **PolyP metabolism and the current paradigm for P accumulation/hydrolyze**

Synthesis and hydrolysis of PolyP in microorganisms is being recognized for its impact within the different P reservoirs, and especially with respect to the formation of phosphorites in continental margins (Crosby and Bailey, 2012).

Because the sequestration or the hydrolysis of PolyP are potentially excellent processes for bioremediation strategies, it is important to understand how it is genetically controlled and in which conditions both occur. Prokaryotes and eukaryotes do not use PolyP for the same functions: prokaryotes use PolyP mainly as an energy source, whereas eukaryotes are using them more for regulatory functions (Kulaev and Kulakovskaya, 2000). Genes involved in the metabolism of PolyP (synthesis and hydrolysis) have been identified in different kingdoms. It was found that the enzyme responsible for the synthesis of PolyP and addition of further orthophosphate residues is the polyphosphate kinase (PPK) (Ahn and Kornberg, 1990; Zhang et al., 2002). This enzyme uses the gamma phosphate of the ATP, which is the primary phosphate group in the ATP molecules, that hydrolyzes to produce the energy needed to drive anabolic reactions, and to add P residue. On the contrary, the enzyme responsible for the hydrolysis of PolyP is either exopolyphosphatase (PPX) or endopolyphosphatase (PPN) (Ault-Riché et al. (1998); see Fig. 1.4).

The current paradigm suggests that few bacterial genera, e.g., marine sulfoxidizers *Thiomar-*

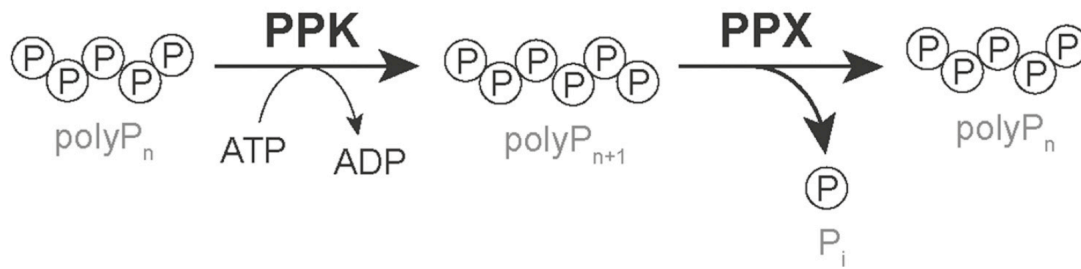


**Figure 1.4: Schematic representation of the PolyP PPK and PPX enzymes functions for the PolyP synthesis and hydrolysis.** Figure adapted from Bowlin and Gray (2021).

*garita* and *Beggiatoa* (Brock et al., 2012; Mußmann et al., 2007), are particularly efficient at sequestering large amounts of inorganic P from the water column as PolyP under oxic conditions. When shifting to anoxic/sulfide-rich conditions at the water-sediment interface, they release orthophosphates by actively hydrolyzing these PolyP (Brock and Schulz-Vogt, 2011; Jones et al., 2016).

In parallel, few genera of polyphosphates accumulating organisms (PAO) have been described in wastewater treatment systems, based on anaerobic/aerobic cycling at the interface between water and sewage sludge. Under carbon rich anaerobic conditions, polyhydroxyalkanoates (PHAs) are stored intracellularly thanks to the energy provided by either glycogen or PolyP stored aerobically. In the subsequent aerobic phase, the PHAs are used to regenerate the intracellular glycogen and store in excess the PolyP (Stokholm-Bjerregaard et al., 2017). As the uptake of P in each aerobic phase exceeds the amount of P released in each anaerobic phase, the PAO accumulate more and more PolyP through the each cycle. After several cycles, the wastewater is filtrated and the particulate fraction is then enriched in P enriched cells. Among these mixed communities, abundant bacteria were identified: *Accumulibacter* spp. (Martín et al., 2006; Oyserman et al., 2016), *Gemmatimonas aurentiaca* (Zhang et al., 2003), *Micrococcus phosphovorus* (Kawakoshi et al., 2012), *Tetrasphaera* isolates (Kristiansen et al., 2013), and *Candidatus Halomonas phosphatis* (Nguyen et al., 2012). The genome of most of these bacteria has been sequenced and functionally characterized, providing clues to the molecular processes possibly involved in the accumulation vs release of PolyP: e.g., polyphosphate kinases, exopolyphosphatases, transport of inorganic P, transport of counter cations used to balance the negative charge of PolyP. Comparison of gene expression profiles when *Accumulibacter* cells were alternatively switched between aerobic and anaerobic phases evidenced (i) a regulation at the transcriptional level and (ii) a coupling of metabolisms that cycle P and C storage polymers (He and McMahon, 2011). However, the specific metabolic traits of the P-hyperaccumulating phenotype remains to be determined. *Candidatus Accumulibacter phosphatis*, the dominant bacterium responsible for enhanced biological phosphorus removal in wastewater treatment plants, was also recently detected in a natural estuary water-sediment interface where large diel fluctuations of redox conditions and dissolved oxygen concentrations occur (Watson et al., 2019).

Overall, only a few models of microorganisms with high P sequestration capabilities are known, most of which have been identified at water-sediment interfaces, in marine environments, or both.

### 1.1.3 The *Magnetococcaceae* family as a new model for polyphosphate sequestration

Recent studies on new models of bacteria accumulating P challenge the prevailing environmental paradigm in which the combination of anoxia and sulfidic waters are responsible for the hydrolysis of PolyP and oxic conditions that trigger PolyP accumulation. These models were shown to keep their PolyP in anoxic conditions or even actively accumulate them in anoxic and rich-sulfur conditions proving that the oxygen does not represent a sufficient parameter to explain the PolyP accumulation and hydrolysis (Schulz-Vogt et al., 2019; Möller et al., 2019; see details later in this section).

Using a correlative  $\mu$ -X-ray fluorescence (XRF) and SEM microscopy to identify P carriers, P sequestering MTB were identified in the water column of Lake Pavin around the OATZ under the oxycline, where the maximum gradient of oxygen is detected (Rivas-Lamelo et al., 2017). These MTB have been shown to be affiliated with the *Magnetococcaceae* family in the *Candidatus* Etaproteobacteria class - also proposed as the phylum Magnetococcia in the GTDB taxonomy (Ji et al., 2017). These *Magnetococcaceae* are magnetotactic cocci and thus will be qualified as MTBc for the rest of this thesis. Similarly to the marine *Beggiatoa* and *Thiomargarita* that hyperaccumulate PolyP they can store PolyP up to 90% of their cell volume, or 10 to 30 times more than other microbes in the same environment (see Fig. 1.5; Rivas-Lamelo et al., 2017). Moreover, like the marine *Thiomargarita* and *Beggiatoa* P-hyperaccumulators, the MTBc from Lake Pavin are sulfoxidizers with intracellular S-granules. But in the contrary to these models, these MTBc store and likely accumulate their PolyP in anoxic conditions. Rivas-Lamelo et al. (2017) calculated the PolyP fraction of the MTB as a function of the total particulate P fraction. The PolyP of the MTB only accounted for ~ 1% of the total particulate P, but constituted a P-content of 6- to 23-fold higher than the other particles.

MTB biomineralize intracellular nano-sized crystals of a magnetic iron mineral called magnetosomes (see the electron dense chains of minerals in STEM-HAADF image and in green in the XEDS map Fig. 1.5). The magnetic properties of these magnetosomes allow MTB cells to passively align parallel to the geomagnetic field lines and swim actively along them (Lefevre and Bazylinski, 2013). Because of this capacity, MTB have been repeatedly suggested as interesting targets for bioremediation since they can be easily recovered via magnetic sorting (Bahaj

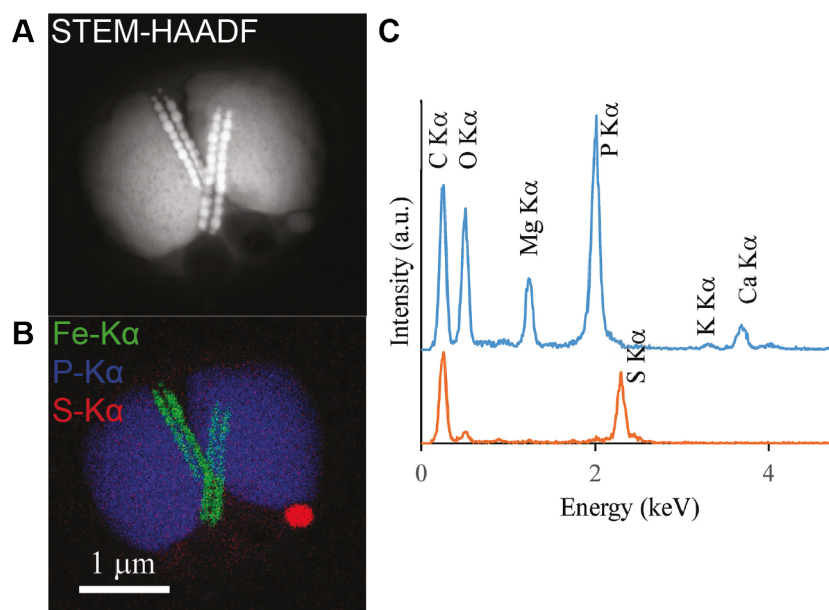


**Figure 1.5: STEM-HAADF and STEM-XEDS images of a MTBc accumulating P under the form of PolyP in Lake Pavin.** A/ STEM-HAADF image of a Lake Pavin MTBc with two double chains of magnetosomes, two large and one small electron dense inclusions, and two organic-deficient vacuoles. B/ The associated XEDS chemical map shows the cartography of the Fe, P and S elements within the MTBc cell. C/ Two spectra (blue and orange) respectively associated to the XEDS chemical map of P and S showing the presence of two PolyP granules (blue) and a sulfur granule (red). The green on the XEDS chemical map represents chains of magnetosomes characteristic of magnetotactic bacteria. Figure adapted from Rivas-Lamelo et al. (2017).

et al., 1993).

MTB from the *Magnetococcaceae* family showed an important accumulation capability for PolyP (Cox et al., 2002; Chen et al., 2015; Schulz-Vogt et al., 2019; Koziaeva et al., 2019). These data indicate a potentially more global impact of this MTB family on P cycle beyond Lake Pavin. This proposition was later reinforced by the discovery of MTB from the same family accumulating PolyP and impacting the environment in the Black Sea (Schulz-Vogt et al., 2019). One explanation could be that these MTBc accumulate PolyP to the same extent as bacteria known as P-hyperaccumulators, but with a higher efficiency compared to other known MTB models. Thus, the MTB from the *Magnetococcaceae* family represent a new and valuable model to the study of the cycling of P by microorganisms, including its molecular mechanisms and how it is impacted by environmental parameters.

Since the discovery of these MTBc, new models of bacteria have also been shown to challenge the current paradigm of PolyP accumulation. One of them is the marine magnetotactic bacteria also related to the *Magnetococcaceae* family which have been found to keep PolyP in

the suboxic, i.e., anoxic and sulfide-poor, zone of the Black Sea (Schulz-Vogt et al., 2019). In the water column of the Black Sea these bacteria have been shown to be responsible for the presence of a strong phosphate gradient. Similarly to the marine sulfoxidizers *Beggiatoa* and *Thiomargarita*, they appear to be uptaking P near the OATZ, where they create a minimum phosphate concentration, and to be hydrolyzing their PolyP to orthophosphate upon reaching the sulphidic zone of the water column. Another marine sulfoxidizing bacteria, the *Sulfurimonas*, have been reported to accumulate PolyP in the anoxic part of the Baltic Sea water column, this time not at the OATZ but in a zone of redox gradients with inverse gradients of nitrate and hydrogen sulfide (Möller et al., 2019). They have been studied *in situ* directly and also isolated in anoxic axenic cultures and studied in different conditions. In Möller et al. (2019), they show that the *Sulfurimonas* necessitate nitrate but also the access of sulfur (thiosulfate or sulfide) in order to accumulate PolyP.

These new data bring to light the necessity of indentifying new models of P-hyperaccumulators in new environmental areas, and especially in freshwater environments for which there is a paucity of data. Since all of these microorganisms are located in zones of redox or oxygen gradients, the exploration of the microbial diversity in these zones seems especially pertinent for the identification of new models of P sequestration.

### 1.1.4 Lake Pavin as a model site for the identification of geochemical drivers of polyphosphate sequestration by magnetotactic cocci

Lake Pavin represents a unique site for the study of these P-sequestering MTB. It is the first freshwater environment where MTB populations have been followed seasonally in the water column, over several meters in depth near the OATZ. In this section, the several chemical gradients present in Lake Pavin water column over several meters in depth where the MTB are observed are discussed. Lake Pavin thus allows for the study of the MTB physiology and their P-accumulation capabilities as a function of varying chemical conditions.

#### 1.1.4.1 General presentation

Lake Pavin is a ferruginous, i.e. sulfide-poor ( $< 20 \mu\text{M}$ , Bura-Nakić et al. (2009)) and iron-rich (up to  $1200 \mu\text{M}$ , Busigny et al. (2016)), freshwater lake. This lake is a ~7000 year old meromictic lake, i.e. permanently stratified, whose layers do not interact with each other all year round. The lake is a crater located in the Massif Central in France at 1300 m a.s.l (Michard et al. (1994), see Fig. 1.6), which originated from a large volcanic explosion. It appears today almost circular in shape and 400 m in diameter, with the deepest point at 92 m. The lake was for a long time the source of many local legends, which fostered fear among the local population (Meybeck, 2016). After a limnic explosion event in Nyos Lake (Cameroon) in 1986 (Cotel,

1999), provoking the death of many people, the lake became an even more studied place, this time not only historically but also scientifically.

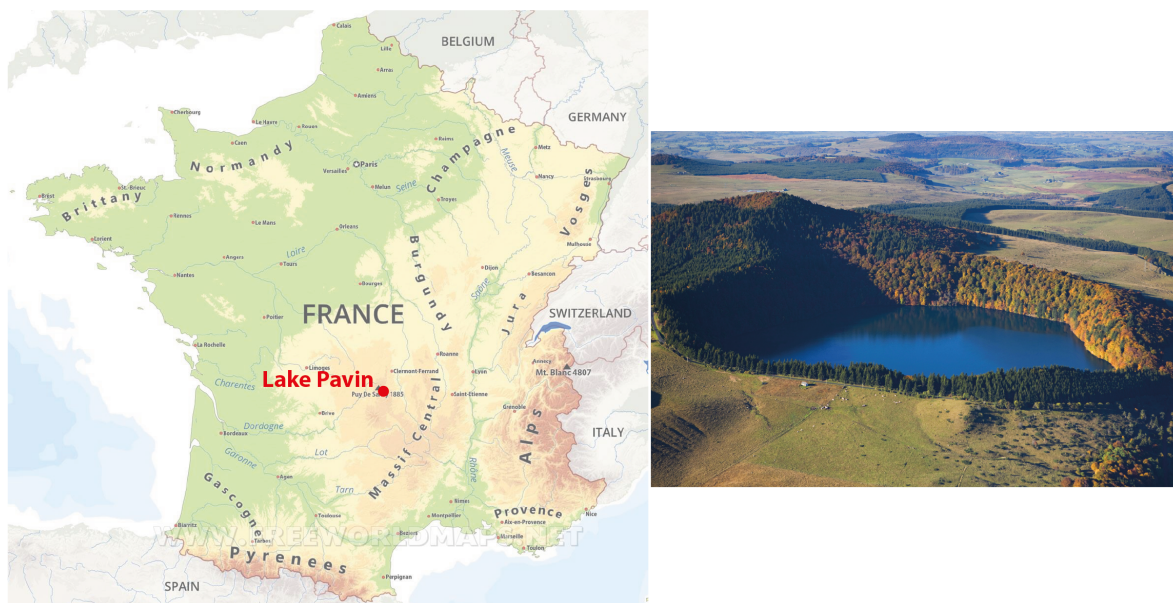


**Figure 1.6: Geographical map of France locating Lake Pavin (red dot), in addition to an aerial view of the lake (right) (photo credited to Pierre Soisson - ens.puy-de-dome.fr).**

The lake water balance is realized through rainfall, snowfall and groundwater springs, it also usually gets frozen during winter for approximately 3-4 months and is therefore hardly accessible for scientific exploration during that time (Sime-Ngando et al., 2016).

#### 1.1.4.2 Chemical gradients

Twice per year the lake undergoes mixing when the waters reaches 4°C in its top oxic layer, the mixolimnion (0- ~50-60 m). The freeze scale of the lake during winter can impact the mixing efficiency and duration of the top layer, and thus shift the depth at which the OATZ occurs (~50-65 m; Michard et al. (1994)). The lake's bottom part, the monimolimnion (~ 70 - 92 m), however, never sees any mixing throughout the year and remains anoxic.

In most aquatic habitats, the OATZ is located at the water-sediment interface, where most of the known MTB have so far been isolated and in which most of the P-sequestering MTB have been found. This interface usually consists of a thin, ~100  $\mu\text{m}$  in thick layer with overlapping reducing and oxidizing conditions that are difficult to study. The chemical gradients, being dispersed over several meters in the Lake Pavin water column, allow higher resolution analyses. Thus, facilitating the study bacteria physiology and potential P-accumulation capabilities as a function of varying chemical conditions and redox transitions.



Oxygen in the monimolimnion of Lake Pavin is completely consumed due to the presence of high organic matter fluxes coming from the surface of the lake. Dissolved substance concentrations and conductivity are markedly greater in the monimolimnion compared to the mixolimnion, which aids in maintaining the stratification. As a result, the mesolimnion, the intermediate layer between the mixolimnion and the monimolimnion, is characterized by steep chemical gradients (redox potential, conductivity, Fe, S, P,...etc.) (Michard et al., 1994; Bonhomme et al., 2016).

In this ferruginous lake, iron is the main dissolved element and its cycle is driven by redox processes. The low concentrations of sulfide permit dissolved iron to accumulate in the monimolimnion and its distribution in the water column is explained by the "iron wheel" system (Busigny et al., 2016). The "iron wheel" is a term illustrating the Fe dissolution and precipitation cycle between the redox boundary, called the redoxcline, and the anoxic part of the water column. Dissolved Fe, diffusing from the deeper anoxic part of the water column or from the sediments, gets oxidized upon reaching the redoxcline, either by oxygen or other oxidized components such as Mn(IV) and nitrate. The Fe(III) phase then precipitates into insoluble ferric-iron particles, which then sink back into the anoxic and more reduced monimolimnion. These particles get reduced along the water column into soluble iron again by either reductive dissolution or by organic matter upon reaching the sediments. This soluble fraction then diffuses again toward the redoxcline and gets re-oxidized. This perpetual cycle particularly involves not only the P cycle, but also the C, S and Mn cycles (Hongve (1997); Busigny et al. (2016); see Fig. 1.7 for these elements gradients along the water column).

Fe and P cycles are tightly linked, as shown by Cosmidis et al. (2014) and Busigny et al. (2016). Dissolved iron and orthophosphate concentrations in the anoxic bottom layer of the lake gradually decrease from high concentrations ( $Fe < 1,2\text{mM}$  and  $P < 300\ \mu\text{M}$ ) near the sediments to very low values at the OATZ (see Fig. 1.7). Moreover, P and Fe particulate concentrations at and below the redoxcline are linearly correlated suggesting direct interaction between the two element cycles at the redoxcline and in the monimolimnion (Busigny et al., 2016). Fe and P dissolved fraction gradients show their diffusion from the bottom of the lake toward the OATZ. At the redox boundary, phosphogenesis occurs, iron is oxidized and phosphorus is either adsorbed on Fe-oxyhydroxides, incorporated in P-rich hydrous ferric oxides (HFO), or forming Fe(II)-Fe(III)-phosphate or Fe(III)-phosphate minerals (Cosmidis et al., 2014). This dissolved P scavenging process thus limits the escape of  $PO_4^{3-}$  to the mixolimnion.

The turbidity profile, between the OATZ and the bottom part of the water column, is mainly explained by the iron precipitated particles and phosphogenesis (Cosmidis et al., 2014; Busigny et al., 2016). Turbidity shows a peak at the redox boundary, and then a gradual increase toward

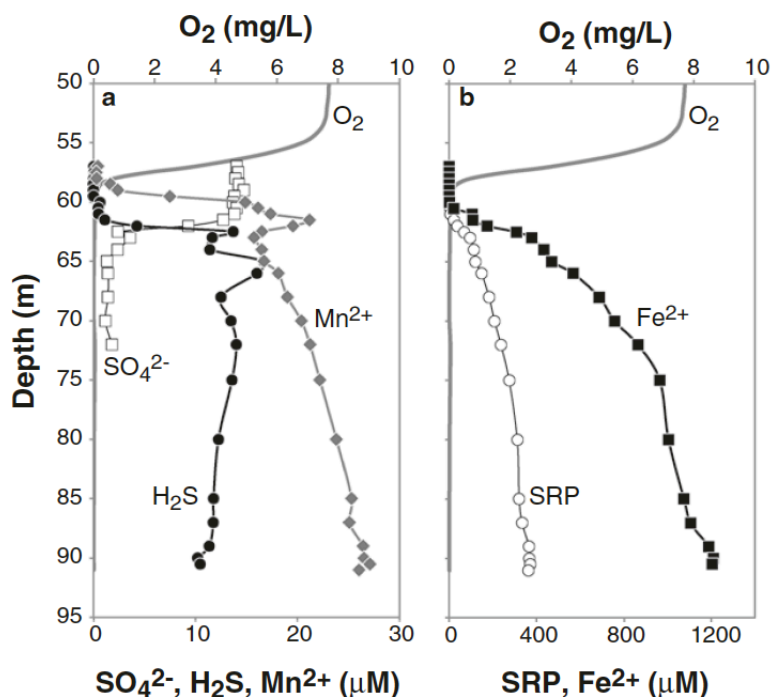


**Figure 1.7: Concentration profiles of dissolved  $O_2$ ,  $SO_4^{2-}$ ,  $Mn^{2+}$ ,  $H_2S$ ,  $Fe^{2+}$  and SRP chemical species (a and b) in Lake Pavin water samples and collected in July 2007.** At the exception of  $O_2$  and  $SO_4^{2-}$  the water column shows an increase of these dissolved species with depth in anoxic water. The redox transition zone occurs between 50 and 60 m and the water column is in fully anoxic conditions below 60 m. The bottom of the lake reaches 92 m depth. Figure from Busigny et al. (2016).

the bottom of the monimolimnion. This gradual increase is explained by the precipitation of further Fe-bearing phases (i.e. vivianite -  $Fe_3(PO_4)_2 \cdot 8H_2O_{(s)}$ ) when reductive dissolution of the insoluble iron minerals from the redox boundary provoke a local supersaturation of dissolved Fe and P. In the sediments the Fe-bearing minerals are mainly represented by vivianite, and in lesser amount by pyrite ( $FeS_2$ ) and siderite ( $FeCO_3$ ) (Cosmidis et al., 2014).

As a result of its chemical conditions and enduring stratification, Lake Pavin became a model site for the exploration of the OATZ (Bonhomme et al., 2016), the iron, phosphorus and sulfur cycles (Bura-Nakić et al., 2009; Cosmidis et al., 2014; Busigny et al., 2016), archaeobacteria communities (Lehours et al., 2005; Biderre-Petit et al., 2011; Miot et al., 2016; Berg et al., 2019), and as an ocean analogue during the Archean (i.e. anoxic, sulfate poor and ferruginous) (Busigny et al., 2014).

#### 1.1.4.3 Potential relationships between microbial activities and phosphogenesis

In the water column of Lake Pavin, a rich diversity of bacteria, archaea (Lehours et al., 2005; 2007) and even unicellular eukaryotes (Lepère et al., 2016) exist. In the anoxic zone of the lake, iron and sulfur reducing or oxidizing bacteria, as well as ammonium-oxidizing, nitrate reducing

and methane-oxidizing and reducing bacteria populations could be found along the water column and the sediments (Biderre-Petit et al., 2011; Berg et al., 2019; Biderre-Petit et al., 2019). They were shown to be stratified as a function of the depth with a bigger fraction of sulfur oxidizing bacteria (SOB), ammonium-oxidizing, iron- and nitrate-reducing bacteria, methanogens and methanotrophs congregating in suboxic conditions and a bigger fraction of SRB being found deeper in the water column in more sulfidic conditions (Biderre-Petit et al., 2019; Berg et al., 2019). The diffusion of large amounts of methane produced in the anoxic zone and the deposited sediments of the lake generally ceases in water column as it is instead consumed by methanogens. The sulfur-reducing and the iron-reducing bacteria show interaction with each other and strong influence on the iron mineralogy. For example, at the redox gradient, dissolved iron can interact with  $H_2S$  when  $SO_4^{2-}$  is reduced into sulfide by sulfate-reducing bacteria and form into  $FeS$  particles (Berg et al., 2019).

As mentioned in the previous section (see part 1.1.4.2), phosphogenesis is occurring around the redoxcline. Some studies propose that microbial biomineralization is involved in this process (Cosmidis et al., 2014; Miot et al., 2016). In these studies, several samples collected near the redoxcline observed under an electronic microscope are shown to contain iron-phosphate particles shaped with morphologies similar to bacteria, suggesting part of their formation onto the surfaces of microorganisms. Moreover, to support this hypothesis, in Cosmidis et al. (2014) STXM analyses at the C K- and Fe  $L_{2,3}$ -edges showed Fe distributed around potential bacterial cells suggesting Fe-bearing phases nucleation on the cell membranes. And finally, in Miot et al. (2016), they could not only found the same cell-shaped iron-phosphate particles but also the presence of nanoparticles of iron-phosphate scattered at the surface of numerous cells.

Several ways in which the cells interact with their local environment and lead to biomineralization have been described in this chapter (see part 1.1.2). Few of them being metabolic activities which can increase  $PO_4^{3-}$  concentrations to reach the critical saturation state for iron-phosphate minerals. In this case, the situation may arise when microorganisms release  $PO_4^{3-}$ , hydrolyzing intracellular storage of PolyP. Several cells in the water column of Lake Pavin have been identified accumulating PolyP (Cosmidis et al., 2014; Miot et al., 2016), but these bacteria were only seen in the mixolimnion and are only capable of accumulating P in small amounts of PolyP. The P-sequestering MTBc thus constitute good candidates as actors of phosphogenesis occurring in the water column. In terms of quantity, the MTB may not account for a lot of the total particulate P, but their potential capabilities to release or store it in short amount of time might favor the precipitation of the phosphate mineral phases. One hypothesis is that the MTBc are an important reservoir of P in Lake Pavin by size (compared to other microbes), turnover rate (i.e., the in-flux or out-flux from this microbial reservoir to the dissolved inorganic P reservoir), or both. The release of P by these MTB could take place in the water column or in the sediments following cell sedimentation. It is also possible that the chemical variations such as those

encountered in the water column of Lake Pavin could impact the storage/hydrolysis balance of PolyP by these MTBc.

In Lake Pavin, both the MTB and the chemical gradients, including the OATZ, span several meters, allowing us to study the MTB physiology and their P-accumulation capabilities as a function of varying chemical conditions and redox transitions at unprecedented resolution. The MTBc from the *Magnetococcaceae* family, and in particular in the context of Lake Pavin, provide an excellent model of study with which to improve our understanding of the metabolic processes associated with PolyP.

## 1.2 Thesis objectives and strategy

Phosphorus, which is ubiquitous in living organisms, is also a limiting and pollutant element in several environments due to the slow geochemical processes controlling its bioavailability and the extreme use of phosphate sedimentary rocks leading to the eutrophication of numerous aquatic systems. Microorganisms can have a predominant impact on their local environment by either actively or passively mobilizing phosphates into or out of their cells and immobilizing P into phosphate minerals. In this context, PolyP accumulators constitute major actors and their characterization represent a current challenge for the elaboration of bioremediation strategies. The recent discovery of new models P-sequestering and challenging the prevailing paradigm for PolyP accumulation and hydrolyze make the need to understand the biogeochemical and genetic determinants an even more important issue.

The goal of my thesis is to describe the biological and environmental parameters related to the P accumulation process for the newly observed model of P sequestration in the stratified freshwater Lake Pavin. A major challenge of this thesis is to quantify the relative proportions of the MTBc sequestering P among the other MTB, and thus to describe the MTB diversity throughout the water column. This challenge also includes identifying the MTBc distribution, their habitat, and the chemical gradients with depth in the water column, as well as isolating the bacteria in an appropriate growth media. Another issue is to determine the environmental conditions favoring or not the MTBc P accumulation and to isolate them with respect to their P accumulation capabilities thanks to flow cytometry.

In this thesis, I combined multiple *in situ* (physico-chemical measurements, bulk geochemistry, optical and electron microscopy), *in vitro* (MTB growth cultures) and *in silico* (multivariate statistics) methods. The source of our data mostly focused on *in situ* sampling and measures in Lake Pavin and the data were further processed and analyzed in the laboratory.

In the first part of my thesis, I present my contribution on the characterization of a new abundant **MTB** species from Lake Pavin forming  $\text{CaCO}_3$ , and similarly to the **MTBc** located in the zone of steep geochemical gradients right under the **OATZ**. A new technique of sampling for which I contributed as well was developed to increase the volume and the vertical sampling resolution in the water column. The improved sampling allowed us to precisely compare certain physicochemical parameters to the bulk **MTB** distribution and a thin profile of the **MTB** and its different morphotypes as a function of the magnetosomes organisation, shape and abundance was done. This profile was compared to a wide range of geochemical and physicochemical parameters, and correlation tests were performed using multivariate statistics to determine if any environmental drivers could be found for the distribution of the **MTB** and the P-sequestering **MTBc**. Then, preliminary tests were made to create a specific medium for the isolation of the **MTBc** using semi-solid media culture techniques with inverse gradients to mimic the environment in which **MTB** live.

In the second part of this thesis, I present a detailed characterisation of the **MTBc** with respect to their magnetosome organisation and P-accumulation capabilities. All of the **MTBc** morphotypes encountered along the water column were then compared to the different environmental parameters present along the water column. This work is followed by preliminary tests using flow cytometry, with the goal of analyzing and sorting the cocci **MTBc** based on their accumulation of **PolyP**.





---

# Chapter 2. Vertical structure of magnetotactic bacteria populations in the water column of Lake Pavin

---

*"Spilling coffee is the adult equivalent of loosing your balloon."*

Gemma Etc

## Contents

---

2.1	<b>Introduction</b> . . . . .	57
2.1.1	Known diversity and biogeography of magnetotactic bacteria . . . . .	57
2.1.2	Magnetosomes diversity can be a proxy of environments, taxonomy or metabolism . . . . .	58
2.1.3	Magnetotactic bacteria: a life at the interfaces . . . . .	59
2.1.4	Magnetotactic bacteria sorting, isolation and methods of study . . . . .	61
2.1.5	Objectives and strategy of the chapter . . . . .	63
2.2	<b>Discovery of a magnetotactic bacteria group capable of sequestering intracellularly amorphous calcium carbonate in the water column of Lake Pavin - Monteil et al. (2021)</b> . . . . .	65
2.3	<b>Improvement of the magnetotactic bacteria collection with a higher vertical resolution sampling and a proxy to detect their abundance - Busigny et al. (2021)</b> . . . . .	85
2.4	<b>Thin description of the magnetotactic bacteria profile as a function of the depth and varying chemical parameters in the water column of Lake Pavin</b>	103
2.4.1	Material and methods . . . . .	103



## Chapter 2. Vertical structure of magnetotactic bacteria populations in the water column of Lake Pavin

---

2.4.1.1	Site description and water sampling strategy . . . . .	103
2.4.1.2	<i>In situ</i> measurements of physicochemical parameters . . . . .	104
2.4.1.3	Chemical analyses of dissolved and particulate fractions in the water column . . . . .	104
2.4.1.4	Estimation of the magnetotactic bacteria population sizes and analysis of morphotypes diversity . . . . .	104
2.4.1.5	Statistical analyses . . . . .	105
2.4.2	Results . . . . .	107
2.4.2.1	Magnetotactic bacteria communities are localized just below the OATZ in a zone spatially structured in discrete geochemical niches . . . . .	107
2.4.2.2	Magnetotactic bacteria are diverse and predominantly composed of MTBc . . . . .	109
2.4.2.3	The abundance of MTBc is correlated to the concentration of dissolved sulfates, mass percentage of organic N and C, particulate magnesium and phosphorus . . . . .	111
2.4.3	Discussion . . . . .	112
2.5	<b>Design of culture media for the isolation of the Lake Pavin MTBc and preliminary results . . . . .</b>	<b>114</b>
2.5.1	Materials and methods . . . . .	114
2.5.1.1	Design of double gradient media . . . . .	114
2.5.1.2	Media oxygen profile - oxygen microsensor . . . . .	115
2.5.1.3	Magnetotactic bacteria sampling and isolation protocol . . . . .	116
2.5.2	Results . . . . .	118
2.5.2.1	Four double gradient media presenting different redox gradients	118
2.5.2.2	The resazurin is a redox indicator allowing the visualization of oxygen gradients . . . . .	119
2.5.2.3	Culture of magnetospirillum-like magnetotactic bacteria . . . . .	120
2.5.3	Discussion . . . . .	121
2.6	<b>Conclusions and perspectives . . . . .</b>	<b>125</b>

---

## 2.1 Introduction

### 2.1.1 Known diversity and biogeography of magnetotactic bacteria

MTB are highly diverse microorganisms which can be found in every types of aquatic environments (freshwater, marine,...). They favor gradients and thus present specific requirement in terms of oxygen levels. Moreover, their diversity can be impacted by environmental parameters.

MTB constitute a group of microorganisms showing a broad phylogenetic, physiologic, morphologic and metabolic diversity (Lefevre and Bazylinski, 2013).

Most of them have been described in various classes of the Proteobacteria and Nitrospirae phyla, but recent studies seem to indicate that bacteria from other phyla such as the *Nitrospinota*, *Bdellovibrionota*, *Fibrobacterota*, and *Riflebacteria* phyla could produce magnetosomes (Amann et al., 2007; Lin et al., 2020). They present a wide morphological and physiological diversity, they occur in the form of a spirilla, rod-shaped, vibrio, coccoid-to-ovoid cells, and they can even be multicellular bacteria (Keim et al., 2006; Lefevre and Bazylinski, 2013; Qian et al., 2020).

MTB are ubiquitous, they are found in a wide range of environments, from freshwater, brackish, marine, hypersaline habitats (Bazylinski and Frankel, 2004) to cold or high temperature (respectively Abreu et al., 2016, Lefevre et al., 2010) and strongly alkaline conditions (Lefèvre et al., 2011a).

MTB are generally considered to be gradient-seekers as they are found in the vicinity of the oxic-anoxic interface or in anoxic conditions in a context of redox gradients. They can be microaerophiles (Spring et al., 1993), anoerobes or both (Petermann and Bleil, 1993) and therefore require specific and strict conditions to grow (Bazylinski et al., 2013a). For example, most cultured species from the *Alpha*- and *Gammaproteobacteria* classes are microaerophiles using reduced sulfur compounds for autotrophic growth and organic acids for heterotrophic growth (Bazylinski and Williams, 2007).

A wide diversity of MTB can be found in most environmental samples (Kolinko et al., 2013; Chen et al., 2015; Lin et al., 2017; Koziyeva et al., 2020; Liu et al., 2020), but this diversity and global distribution can be impacted by environmental parameters (chemical or physical) but also spatial differences (i.e. geographic distance between two sampling site) as reported by Lin et al. (2013). It was shown that salinity is one of the strongest driver of global distribution for the MTB by influencing their phylogenetic distribution across the world, and a separation in the phylogenetic tree between MTB from freshwater and saline water was evidenced (Spring et al., 1998; Zhang et al., 2010). MTB communities can change as a function of total iron concentra-

tion (Lin et al., 2013) and MTB phylogenetic lineages are suggested to be influenced by nitrate concentrations (Lin and Pan, 2010). South-seeking MTB have also been shown to be positively correlated with redox potential, being even more concentrated when redox potential increases (Simmons et al., 2006). Postec et al. (2012) have shown that sulfate concentrations was positively correlated to the concentration of MTB and suggested a link with the presence of SRB. Another parameter that have been shown to impact MTB diversity is the strength of the Earth's magnetic field. It was shown by Wang et al. (2008); Pan et al. (2009); Lin et al. (2012a) that the magnetic field's variation could change the velocity or the cell metabolism of some MTB. MTB communities can also change with high temperature as shown by Lin et al. (2012b; 2013). Overall, several parameters can impact the MTB diversity and distribution in the environment, but until now no correlation between a MTB taxon and a biotope has been found.

One of the most common MTB morphotype to be observed in the environment, sediments and stratified water columns, is the MTBc (Lefevre and Bazylinski, 2013; Liu et al., 2020), with a coccoid to ovoid-shaped cell and two flagellar bundles on one side of its cell (Frankel et al., 1997). Based on 16S rRNA phylogenetic analyses it was first thought that these MTBc were affiliated to the Alphaproteobacteria class. But recent studies proposed a novel class, the *Candidatus Etaproteobacteria*, to classify the MTBc (Ji et al., 2017). A lot of the uncultured MTBc accumulate sulfur granules suggesting an autotrophic or mixotrophic metabolism involved in the oxidation of reduced sulfur compounds (Lefevre and Bazylinski, 2013).

### 2.1.2 Magnetosomes diversity can be a proxy of environments, taxonomy or metabolism

The biomineralization of magnetosomes by MTB is unique and genetically controlled. Magnetosomes can show different compositions, shape, numbers, organization or axis ratio and some of these characteristics can constitute proxies for bacteria class, phylum or species and even for metabolism.

Magnetosomes formation is an emblematic biomineralization as it represents the only evidenced case of controlled intracellular biomineralization of crystalline phases in prokaryotic cells (Lefevre and Bazylinski, 2013). Magnetosome formation is a genetically controlled process by a gene cluster encoding for proteins involved in magnetosome formation and arrangement (Schüler, 2008; Murat et al., 2010; Komeili, 2012). Many magnetosome genes could be found in all characterized MTB (Nakazawa et al., 2009; Lefèvre et al., 2013b) but the content and organization of the magnetosome genes is distinct from one group of MTB to another. These differences might then explain the differences in magnetosome compositions, number, shapes,

and organizations found in the different MTB species.

Magnetosomes can contain magnetite ( $\text{Fe}_3\text{O}_4$ ) or greigite ( $\text{Fe}_3\text{S}_4$ ) crystals enveloped by a bilayer membrane (Blakemore, 1975; Bazylinski and Frankel, 2004; Jogler et al., 2011). MTB producing magnetite are found in all known taxa of MTB, whereas MTB producing greigite are affiliated to the *Deltaproteobacteria* (Wenter et al., 2009; Abreu et al., 2011; Lefevre et al., 2011). Some MTB from the *Deltaproteobacteria* class have also been detected to form simultaneously magnetite and greigite (Lefevre et al., 2011; Wang et al., 2013). Magnetite forming MTB have been described to usually have either a heterotrophic but facultatively chemolithoautotrophic metabolism (Bazylinski et al., 2004; Williams et al., 2006; Geelhoed et al., 2010) or obligatory chemolithoautotrophic metabolism (Lefèvre et al., 2012).

Most of the magnetosomes belong to three main morphological groups: cuboctahedral, elongated prismatic or bullet-shaped (Bazylinski and Frankel, 2004; Isambert et al., 2007; Lefèvre et al., 2011b) with the hypothesis that bullet-shaped magnetite magnetosomes constitute the most primitive type (Lefèvre et al., 2013a). Cuboctahedral and elongated prismatic magnetosomes only occur in MTB phylogenetically affiliated to the *Alpha*- and *Gammaproteobacteria*, whereas the bullet-shaped magnetosomes were only found in MTB affiliated to the *Nitrospirae* and the *Deltaproteobacteria* (Lefèvre et al., 2011b).

Magnetosomes can also present diverse organization: one chain, two chains, two double chains and even multiple chains of magnetosomes, or disorganized magnetosomes (Jogler et al., 2011; Li et al., 2015; Lefevre and Bazylinski, 2013; Liu et al., 2020). For example, the multiple chains occur in the *Candidatus Magnetobacterium bavaricum* within the *Nitrospirae* phylum. These diverse organizations have been observed in MTBc as well, and their different magnetosome morphologies were shown to be species-specific (Liu et al., 2020).

### 2.1.3 Magnetotactic bacteria: a life at the interfaces

MTB are organisms with the aptitude to use magnetoreception. Magnetoreception define the capacity of organisms to detect and navigate along the Earth's geomagnetic field lines (Monteil and Lefevre, 2020). Magnetoreception has been for a long time thought to be only characteristic of MTB. Some recent studies have brought into light that this is not the case and that magnetoreception not only is present in prokaryotes but also in eukaryotes. The current knowledge shows that eukaryotes can acquire magnetoreception by either: (i) preying on MTB, (ii) forming an holobiont by being in mutual symbiosis with ectosymbiotic MTB, or (iii) forming their own magnetosomes (Monteil et al., 2019; Monteil and Lefevre, 2020; Leão et al., 2020).

It has been found that the majority of MTB, located either on the southern or northern hemisphere, do not seek the same geomagnetic pole, respectively seeking the South and the North

## Chapter 2. Vertical structure of magnetotactic bacteria populations in the water column of Lake Pavin

---

pole (Blakemore et al., 1980). Doing so, given the direction of the geomagnetic field lines, MTB of each hemisphere can then swim downward toward microaerobic/anaerobic zones and potentially away from toxic conditions such as high oxygen concentrations. Even if this MTB distribution of north and south-seeking is in majority true, it is also possible to find significant amount of south-seeking MTB in the Northern hemisphere (Simmons et al., 2006; Shapiro et al., 2011). For this reason, it has been suggested that MTB might have other mechanisms to overcome vertical variations of the geochemical conditions and high oxygen concentrations. These other mechanisms can be chemotaxis or redox taxis working in coordination with magnetotaxis that MTB use. Chemotaxis or redox taxis are respectively mechanisms biasing the organism's movements toward preferred chemical or less toxic zones, or favoured redox potential. The involvement of chemotaxis or redox taxis is supported by the studies of the MTB isolate *Magnetococcus marinus* and *Magnetospirillum magnetotacticum* for which it has been shown that an aerotaxis behaviour is used in addition to magnetotaxis (Frankel et al., 1997). Both MTB strains prefer to be located near the oxic-anoxic interface (OAI) rather than to swim downward and grow in the bottom of the culture tubes as they would have done if they were only influenced by their magnetotaxis behaviour. Moreover, Mao et al. (2014) showed for a *Candidatus Magnetobacterium bavaricum* (MBV) and an unspecified MTBc that they relied both on magnetotaxis for their survival but using it for different mobility requirements. MBV was shown to migrate over macroscopic distances relying only on chemotaxis, thus using magnetotaxis only as a mean to efficiently shuttle between different chemical layers of the sediments. In the contrary, MTBc were shown to only use chemotaxis as a mean to detect the specific chemical properties in which they thrive and use magnetotaxis to overcome sediment perturbations. In zero field with sediment perturbations, MBV can thus survive at the expense of a population decrease but not MTBc.

Phototaxis is also another mechanism that can supplant magnetotaxis and help MTB to move toward a zone with a lower exposition to light. For example, some multicellular magnetotactic prokaryotes (MMPs) use phototaxis to move away from white light and wavelength ranging below 480 nm (Shapiro et al., 2011; Almeida et al., 2013). Another example is *Magnetococcus marinus* which is also sensitive to light and swim toward zones where light below 500 nm do not reach. This process thus makes them swim downward similarly to aerotaxis upon oxygen diffusion (Frankel et al., 1997).

All these mechanisms can act similarly to magnetotaxis by making the MTB swim in a vertical search for optimal conditions in chemical, redox or even light gradients rather than at a three-dimensional search.

### 2.1.4 Magnetotactic bacteria sorting, isolation and methods of study

The study of most microorganisms is tributary to how easy they can be isolated and identified in their natural habitat. Thanks to their magnetosomes **MTB** can be quickly enriched from environmental samples and thus can be more easily studied than other microorganisms in the same environment. However, **MTB** common magnetic enrichment is not always enough for some specific analyses. As a consequence, other methods have been developed for bulk observations of high **MTB** biomass or more specifically for single-cell observations. The success at isolating a **MTB** in an axenic culture can help study them specifically without the complexity inherent to an environmental sample.

The presence of magnetosomes is what makes the **MTB** so easy to enrich from a natural sample by using different magnetic sorting techniques such as the hanging drop technique (Bazylin-ski et al., 2013a), the orientation magnetic separation or the channel separator (Bahaj et al., 2002; Wang et al., 2020). Their repulsion to complete oxic conditions and their swimming abilities can also help concentrating them, for example by aerotactic concentration and the diffusion of oxygen in a recipient from which the surface water is retrieved regularly while the **MTB** move downward and concentrate at the bottom (Busigny et al., 2021).

An axenic culture enables the study of the **MTB** in a controlled environment without the interference of any other microorganism, therefore simplifying the interpretations of experimental results. A controlled environment means being able to control the medium and the conditions in which the microorganisms evolve, allowing the description of the organism metabolism, or of the genes expressed at a given time or for specific conditions. The processes observed in the culture medium are either abiotic processes or processes linked to the bacteria of interest. The ambiguity of the source of a certain phenomenon or compound, inherent from the presence of multiple microorganisms in the same sample in the environment, is thus avoided. Overall, increasing the number of axenic cultures contribute to a better understanding of the biomineralization, biochemistry and physiology of **MTB**.

**MTB** isolation in a culture media is difficult and not a lot of them have been isolated in an axenic culture so far (Lefevre and Bazylin-ski, 2013), with only a tenth of successes of isolation in the last decade (Lefèvre et al., 2009; 2011a; Morillo et al., 2014; Shimoshige et al., 2021). The difficulties come from the need of a specific oxygen gradient medium, necessity due to their unique life in gradient-conditions. Moreover, they possess long cell-dividing times and they are therefore prone to be outcompeted by other fast growing microorganisms (Bazylin-ski et al., 2013a).

Isolating **MTBc** from Lake Pavin would greatly help better understand their physiology and their taxonomy, but despite the ubiquity of the **MTBc** in the environment, only three **MTBc**

## Chapter 2. Vertical structure of magnetotactic bacteria populations in the water column of Lake Pavin

---

have been isolated in a growth medium so far and only from marine environments. Two are coming from the northern hemisphere, the first isolated is the *Magnetococcus marinus* strain MC-1 [Meldrum et al. \(1993\)](#), and the other one is the magneto-ovoid MO-1 both from the Pettaquamscutt Estuary in Rhode Island, USA [Lefèvre et al. \(2009\)](#). The third cultivated MTBc is *Magnetofaba australis* strain IT-1 from the southern hemisphere in the Itaipu Lagoon in Rio de Janeiro in Brazil ([Morillo et al., 2014](#)). They are obligately microaerophilic and can grow autotrophically on sulfide or thiosulfate and also heterotrophically for MC-1 and IT-1 while using acetate or succinate. These isolated MTBc all show only one magnetosome chain of magnetite, but it is known that the MTBc can be very diverse in terms of magnetosome organisation, size, number and axial axis ([Liu et al., 2020](#)). In parallel, none freshwater MTBc have been isolated, even with the already important amount of phylogenetic and genomic information gathered on them and their phylogenetic relatedness with their marine counterparts ([Lefevre and Bazylinski, 2013](#)).

Since MTB are not easily cultivable, sampling methods need to be efficient in terms of volume and/or enrichment. Usually MTB present in a water column are collected using a Geopump™ peristaltic pump ([Simmons et al., 2004](#); [Moskowitz et al., 2008](#)), a Niskin bottle ([Rivas-Lamelo et al., 2017](#)), or a free-flow bottle or automatic flow injection sampler ([Schulz-Vogt et al., 2019](#)). These sampling methods are followed by a magnetic sorting to enrich the MTB, but it usually does not yield the high MTB density necessary for certain approaches. A recent study presented different approaches in order to alleviate this problem and help gather a large number of MTB (see part 2.3 of this chapter for details; [Busigny et al. \(2021\)](#)).

In general, numerous different cell morphotypes can be present in relatively large number in a single environmental sample ([Lefevre and Bazylinski, 2013](#); [Lin et al., 2017](#)), thus the analyze of a specific morphotype of MTB taxon can be difficult. Along the years, different approaches have been set up to be able to characterize the MTB at the single cell level. If a specific MTB is distinguishable from the other by its morphology, a micromanipulator associated with an optical microscope can be used for a single-cell sorting and further genomic analyses ([Jogler et al., 2011](#); [Kolinko et al., 2012](#); [Monteil et al., 2021](#)). A taxonomic identification of MTB cells, confirmed by fluorescence *in situ* hybridization (FISH) with rRNA-targeted oligonucleotide probes, can also be used in association with an electron microscope (SEM or TEM) to characterize the MTB specific structural features and to reveal the MTB affiliations ([Li et al., 2017](#); [Zhang et al., 2017](#); [Liu et al., 2020](#)). Moreover, the association of synchrotron based synchrotron-based scanning transmission X-ray microscopy (STXM) and electron microscopy can also helps the joint analyses of the MTB chemistry and structural features (e.g. magnetosomes, intracellular inclusions; [Leão et al. \(2020\)](#); [Li et al. \(2020a\)](#)).

### 2.1.5 Objectives and strategy of the chapter

The majority of **MTB** and **MTBc** have been studied at water-sediment interfaces, where their distribution spreads on a few hundred micrometers, limiting our understanding of the precise ecological niche in which they live and which potentially impact their metabolism. In this chapter, I present the first study of the **MTB** diversity along varying chemical conditions on several meters in the water column of a freshwater and ferruginous environment. This study aims to describe the different **MTB** populations (i.e. the morphotypic **MTB** diversity), their relative abundance as a function of their habitats, and at characterizing the specific environmental conditions in which the **MTBc** are found by using microscopic, chemical and statistical analyses. Comparing the different **MTB** in the water column of Lake Pavin will help determine if the **MTBc** harbor a specific ecological niche, or if their ecological niche is common to all **MTB** in the water column of Lake Pavin.

The first part of this chapter introduces my contribution to the recent discovery of an abundant population of rod-shaped **MTB** with intracellular inclusions of amorphous calcium carbonates (hereafter described as **iACC**-forming rods) in the sediment and the water column of Lake Pavin. I co-authored this study which was published in *The ISME Journal* (Monteil et al. (2021)). This study extends the known biomineralization capabilities of **MTB** but also the known diversity of **MTB** present in the water column of Lake Pavin.

The second part of this chapter is the object of a published article I also coauthored (Busigny et al., 2021) and in which the development of a technique for the mass collection of **MTB** populations in Lake Pavin is the main focus. During the optimization of the mass collection techniques a new sampling method was elaborated for a better vertical resolution, and some physicochemical parameters were associated with the **MTB** peak of abundance.

The results presented in these articles later allowed in the third part of this chapter a precise characterization of the **MTB** profile and that of their diversity as a function of the environmental parameters with multivariate statistics. In the fourth and final part, I present preliminary tests carried out during this thesis to elaborate a growth medium for the Lake Pavin **MTBc**.





## **2.2 Discovery of a magnetotactic bacteria group capable of sequestering intracellularly amorphous calcium carbonate in the water column of Lake Pavin - [Monteil et al. \(2021\)](#)**

In the context of PolyP sequestration by microorganisms, the OATZ is of great interest. While studying the bacterial populations present in the vicinity of the oxycline of Lake Pavin water column, [Rivas-Lamelo et al. \(2017\)](#) discovered the MTBc hyperaccumulating PolyP. Later on, the study of the water column MTB where the MTBc are located lead to the discovery of a unique new morphotype of rod-shaped MTB accumulating large amounts of iACC, further on called iACC-forming rods. This discovery lead to the publication of an article that I co-authored and for which an overview is following:

In parallel to their unique capability to biomineralize magnetosomes, MTB may also show the capacity to sequester diverse intracellular elements such as sulfur, phosphorus, magnesium, calcium and potassium under the form of sulfur granules ([Liu et al., 2020](#)) or PolyP ([Bazylinski et al., 2004](#); [Cox et al., 2002](#); [Rivas-Lamelo et al., 2017](#)). In ([Monteil et al., 2021](#)) the MTB capabilities were extended to the formation of iACC granules in both the sediments and the water column of Lake Pavin. The number of microbial groups capable of sequestering calcium carbonate were increased from two to three, with formerly the *Achromatium* species in the Gammaproteobacteria class ([Schewiakoff, 1893](#); [Head et al., 1996](#)) and several species of the Cyanobacteria phylum ([Couradeau et al., 2012](#)). Such intracellular biomineralization being found in only few microorganisms, these inclusions occurrences, functions, ultrastructures and genetic determinants remain poorly constrained.

In [Monteil et al. \(2021\)](#), the iACC-forming rods were shown to be affiliated to the Alphaproteobacteria class using single-cell, molecular typing and FISH/SEM correlative approaches. The ultrastructure and composition of these inclusions was described as well thanks to TEM, cryo-electron microscopy of vitreous sections (CEMOVIS) and synchrotron-based STXM. It showed that the inclusions are amorphous and form in a membrane-enclosed compartment in which calcium is probably greatly concentrated compared to the extracellular under-saturated medium with respect to calcium carbonate precipitation. This indicates an active process of sequestration which costs energy to the cell. A possible function of these inclusion is their use as ballasts to adjust their vertical position in chemical vertical gradients.

For this study, my contribution consisted in participating in the field trips for the recovery of the sediments and water column samples, in the preparation of the MTB samples for CEMOVIS

## Chapter 2. Vertical structure of magnetotactic bacteria populations in the water column of Lake Pavin

---


analyses, and in providing a large amount of [TEM](#) images of the [iACC](#)-forming rods for the elaboration of different hypotheses for cellular division mechanisms.

This work allowed me to learn how to observe and sort the [MTB](#) in both the sediments and the water column and use [TEM](#) and [XEDS](#).

See next the [Monteil et al. \(2021\)](#) article and in appendices the [supplementary information](#).



# Intracellular amorphous Ca-carbonate and magnetite biomineralization by a magnetotactic bacterium affiliated to the Alphaproteobacteria

Caroline L. Monteil <sup>1,2</sup> · Karim Benzerara<sup>2</sup> · Nicolas Menguy<sup>2</sup> · Cécile C. Bidaud<sup>1,2</sup> · Emmanuel Michot-Achdjian<sup>1</sup> · Romain Bolzoni<sup>1,2</sup> · François P. Mathon<sup>1,3</sup> · Margot Coutaud<sup>2</sup> · Béatrice Alonso<sup>1</sup> · Camille Garau<sup>1</sup> · Didier Jézéquel<sup>3</sup> · Eric Viollier<sup>3</sup> · Nicolas Ginet<sup>4</sup> · Magali Floriani <sup>5</sup> · Sufal Swaraj<sup>6</sup> · Martin Sachse<sup>7</sup> · Vincent Busigny<sup>3,8</sup> · Elodie Duprat <sup>2</sup> · François Guyot<sup>2,8</sup> · Christopher T. Lefevre <sup>1</sup>

Received: 1 May 2020 / Revised: 30 July 2020 / Accepted: 10 August 2020  
© The Author(s), under exclusive licence to International Society for Microbial Ecology 2020

## Abstract

Bacteria synthesize a wide range of intracellular submicrometer-sized inorganic precipitates of diverse chemical compositions and structures, called biominerals. Their occurrences, functions and ultrastructures are not yet fully described despite great advances in our knowledge of microbial diversity. Here, we report bacteria inhabiting the sediments and water column of the permanently stratified ferruginous Lake Pavin, that have the peculiarity to biomineralize both intracellular magnetic particles and calcium carbonate granules. Based on an ultrastructural characterization using transmission electron microscopy (TEM) and synchrotron-based scanning transmission X-ray microscopy (STXM), we showed that the calcium carbonate granules are amorphous and contained within membrane-delimited vesicles. Single-cell sorting, correlative fluorescent in situ hybridization (FISH), scanning electron microscopy (SEM) and molecular typing of populations inhabiting sediments affiliated these bacteria to a new genus of the Alphaproteobacteria. The partially assembled genome sequence of a representative isolate revealed an atypical structure of the magnetosome gene cluster while geochemical analyses indicate that calcium carbonate production is an active process that costs energy to the cell to maintain an environment suitable for their formation. This discovery further expands the diversity of organisms capable of intracellular Ca-carbonate biomineralization. If the role of such biomineralization is still unclear, cell behaviour suggests that it may participate to cell motility in aquatic habitats as magnetite biomineralization does.

---

These authors contributed equally: Caroline L. Monteil, Karim Benzerara, Nicolas Menguy

---

**Supplementary information** The online version of this article (<https://doi.org/10.1038/s41396-020-00747-3>) contains supplementary material, which is available to authorized users.

---

✉ Christopher T. Lefevre  
christopher.lefevre@cea.fr

<sup>1</sup> Aix-Marseille University, CNRS, CEA, UMR7265 Institute of Biosciences and Biotechnologies of Aix-Marseille (BIAM), CEA Cadarache, F-13108 Saint-Paul-lez-Durance, France

<sup>2</sup> Sorbonne Université, Muséum National d'Histoire Naturelle, UMR CNRS 7590, IRD. Institut de Minéralogie, de Physique des Matériaux et de Cosmochimie (IMPMC), 4 Place Jussieu, 75005 Paris, France

<sup>3</sup> Université de Paris, Institut de Physique du Globe de Paris, CNRS, F-75005 Paris, France

## Introduction

Biomineralization is a process whereby organisms trigger the formation of minerals by sequestering diverse chemical elements such as Fe, Mn, Ca, As, O, S or P into relatively stable solid phases [1, 2]. Produced minerals are chemically diverse

<sup>4</sup> Laboratoire de Chimie Bactérienne, UMR 7283 CNRS, Aix-Marseille Université, Institut de Microbiologie de la Méditerranée, 13402 Marseille, France

<sup>5</sup> Institut de Radioprotection et de Sécurité Nucléaire (IRSN), PRP-ENV/SERIS/LECO, Cadarache, Saint-Paul-lez-Durance 13115, France

<sup>6</sup> Synchrotron SOLEIL, L'Orme des Merisiers, Saint-Aubin-BP 48, 91192 Gif-sur-YVETTE cedex, France

<sup>7</sup> Ultrastructural Bioimaging unit, Institut Pasteur, 24-28 rue du Docteur-Roux, 75015 Paris, France

<sup>8</sup> Institut Universitaire de France, 75005 Paris, France

including oxides, oxy-hydroxides, carbonates, phosphates, sulphates and sulphides, some of which involve metals and metalloids [2]. This process can have a significant impact on the geochemical cycles of these diverse chemical species. Two types of biomineralization pathways are distinguished: (i) biologically-induced mineralization, which refers to all cases where mineral precipitation results from chemical shifts in the environment of the organisms induced by their metabolic activity, and (ii) biologically controlled mineralization, for which specific genes and cell structures are involved [3].

Biomineralization is not restricted to eukaryotes; many prokaryotes developed mechanisms to nucleate and grow diverse minerals as well. However, only few cases of controlled biomineralization are reported in prokaryotes. The most emblematic case of prokaryotic controlled biomineralization is that of magnetotactic bacteria (MTB), which produce intracellular magnetic crystals enclosed within compartments delimited by a lipid bilayer and called magnetosomes [4]. The underlying genetic determinism, molecular machinery, ecologic role and evolution of this biomineralization pathway have been the focus of interdisciplinary investigations and represent the most documented case of biomineralization in prokaryotes [5, 6].

A much less documented case is provided by bacteria biomineralizing intracellular calcium carbonate inclusions. Two phylogenetically distinct groups have been shown to be capable of this biomineralization: (i) several species of the Cyanobacteria phylum, and (ii) some *Achromatium* species in the Gammaproteobacteria class. The large sulphur bacterium *Achromatium oxaliferum* was first described by Schewiakoff in 1893 [7]. It accumulates numerous calcium carbonate inclusions filling most of the cell volume [8–11]. This group of Proteobacteria was observed worldwide in the microoxic-anoxic zone of the sediment-water interface of both freshwater and marine environments. Population densities can be as high as  $10^5$  cells/mL and account for over 90% of the total local bacterial volume [9, 10, 12]. Despite the large biomass represented by *Achromatium* populations, their impact on biogeochemical cycles is not well understood. However, it has been shown that calcium carbonates accumulating within *Achromatium* cells can represent most of the solid calcium in some sediments, especially when (extracellular) pore waters are undersaturated with calcium carbonate phases [12–14]. No cultured representative strain is available, which limits the physiological characterization of cells to culture-independent field and microcosm analyses. Only some *Achromatium* populations have been shown to be able to fix inorganic carbon, while others are not able to do so. Since all *Achromatium* populations can form intracellular Ca-carbonates, this suggests that inorganic C fixation is not key to intracellular Ca-carbonate biomineralization. Moreover,

they gain energy from sulphur oxidation and may use oxygen or nitrate as potential electron acceptors [15–19]. Transmission electron microscopy (TEM) analyses suggested the presence of membranes surrounding the calcium carbonate inclusions of *Achromatium* [12, 13].

The biomineralization of intracellular amorphous calcium carbonate (ACC) by phylogenetically and geographically widespread cyanobacteria species, has been discovered more recently [19]. They include deep-branching species, suggesting the possibility that intracellularly calcifying cyanobacteria may have thrived on the early Earth. Similarly to *Achromatium*, it was shown that they can form intracellular ACC even in extracellular solutions undersaturated with respect to ACC, again demonstrating some energy cost which has been attributed to active uptake of Ca [20]. Also similar with *Achromatium*, ACC biomineralization in cyanobacteria occurs within a microcompartment but in this case, it is delimited by an envelope that is not composed of a lipid bilayer but of a yet-to-be-determined nature [21]. Two distinct patterns of ACC distribution were described within the cyanobacterial cells: one with ACC inclusions scattered throughout the cell cytoplasm and another one in which inclusions start forming at the septum and lie at the cell poles after cell division [22, 23]. In contrast to *Achromatium*, ACC-producing cyanobacteria were shown to live in oxic environments where they perform oxygenic photosynthesis [23]. These cyanobacteria can be abundant in some habitats. For example, they reach up to 10% of all the operational taxonomic units (OTUs) identified in a geothermal pool at Little Hot Creek in California [24]. Due to its ability to sequester abundant alkaline earth elements within ACC, the cyanobacterium *Gloeomargarita lithophora* [19, 25], was shown to be particularly interesting for the remediation of radionuclides such as  $^{90}\text{Sr}$  and Ra [20, 26]. Moreover, this cyanobacterium is the closest modern relative of plastids, questioning the possibility that this capability to sequester Ca was transferred to the first photosynthetic eukaryotes [27].

The biological role of intracellular calcium carbonate biomineralization is still unclear, but some functions have been hypothesized: intracellular carbonates may be involved in (i) the buffering of intracellular pH [10, 28], (ii) a buoyancy-regulating mechanism [13, 17, 19, 29] or (iii) the storage of inorganic carbon that may serve in some cases as an electron acceptor in carbonate respiration [13, 17]. However, in both Cyanobacteria and *Achromatium*, the biochemical pathways and the genetic determinants involved in calcium carbonate formation remain unknown. Moreover, the evolutionary history of this process has yet to be determined to test whether it appeared independently in distinct phyla by convergent evolution, or derived from a common ancestor, and/or spread by transfer.

For this purpose, a better assessment of the biology and ecology of intracellular calcium carbonate biomineralizing bacteria as well as the phylogenetic distribution of this capability is crucial. Considering that this process was detected only very recently in cyanobacteria, it is likely that we do not have an exhaustive view of the phylogenetic distribution of intracellular calcium carbonate biomineralization, and much less of the ecological niches where such a biomineralization is performed.

Recent observations in the ferruginous and permanently stratified (meromictic) Lake Pavin, Massif Central, France [30], support this assumption by revealing intracellular calcium carbonates biomineralizing microorganisms within a broad uncharacterized diversity of biomineralizing microorganisms. Here, we report a magnetotactic bacterium in the water column and sediments of Lake Pavin that biomineralizes both intracellular magnetite and calcium carbonate. Molecular typing of single cells sorted from sediments revealed that the double biomineralization is performed by members of an undescribed genus within Alphaproteobacteria with no close MTB relatives. Hereafter, we characterize the ultrastructure and intracellular mineral phases biomineralized by these bacteria to finally give some insight into magnetite biomineralization using a partial genome sequence.

## Materials and methods

### Site description and sample collection

Sediment samples were collected from the shore of Lake Pavin. This was done by fully filling 1 L glass bottles with 300–400 mL of sediments and 600–700 mL of water overlaid on the sediments. Air bubbles were excluded. Once in the laboratory, bottles were stored with their cap closed, under dim light and at room temperature (ca. 25 °C). Two locations were sampled at Lake Pavin during the different sampling campaigns that took place between May 2015 and October 2019: (i) 45.499107°N, 2.886273°E and (ii) 45.499101°N, 2.889239°E.

Water column samples were collected in October 2018 at depths ranging between 45 and 65 m from a platform located near the centre of Lake Pavin (45.495792°N, 2.888117°E). Water was collected using a Niskin bottle at the targeted depths and was then transferred in 1 L glass bottles filled to their capacity and tightly closed. Bacteria of interest collected from the water column could be conserved for a few days only when stored at 4 °C, whereas those from sediments could be observed and magnetically sorted up to 5 years after their sampling and storage in the laboratory, at room temperature. This is the

reason why the majority of our study focused on bacteria from sediments.

### Solution chemistry analyses

Solutions in the sampling bottles were filtered at 0.22 µm before analyses. The pH was measured with a CyberScan pH 5500 pH-metre (Eutech instruments) using a combined pH microelectrode (Fisherbrand) calibrated with Hanna pH standard buffer solutions (4.010, 7.010, 10.010) and an uncertainty of 0.01 pH unit. Elemental analyses of  $[Ca^{2+}]$  were performed on samples acidified with HNO<sub>3</sub> (2%) by ICP-AES (iCAP6200 Thermofisher) with an uncertainty of 0.7%. All measurements were far above the quantification limit (ca. 0.1 ppb).

### Dissolved orthophosphate concentration and alkalinity of sediment pore water

Alkalinity measurements were carried out according to the protocol previously described [31, 32]. The standard range was tested with Evian® water before sample alkalinity measurements. Here, alkalinity was approximately equivalent to the concentration of HCO<sub>3</sub><sup>-</sup> under the present conditions [33].

The saturation index was defined as:  $SI = \log(IAP/K_{sp})$ , where IAP corresponds to the ion activity product and  $K_{sp}$  to the thermodynamic solubility product for a mineral phase. A solution was supersaturated with respect to a mineral phase when  $SI > 0$ . Here  $Ca^{2+}$  and HCO<sub>3</sub><sup>-</sup> activities were approximated to the measured concentrations. The solubility constant ( $pK_{sp}$ ) at 25 °C of amorphous Ca carbonate (ACC) used in the present study was 6.278, as determined by Purgstaller et al. [34].

### Magnetic enrichment and light microscope observation

North-seeking magnetic cells were concentrated by placing the south pole of a neodymium-iron-boron magnet (disc magnet with a diameter of 5 mm and a height of 5 mm) for 3 h next to the bottles, above the sediment-water interface (for the sediment samples) or at mid-height against the bottle (for water column samples). Examination of magnetically concentrated cells was carried out using the hanging drop technique [35] under a Zeiss Primo Star light microscope equipped with phase-contrast and differential interference contrast optics. Magnetotaxis was evidenced by rotating a stirring bar magnet at 180° on the microscope stage to reverse the local magnetic field. Motility and the magnetotactic behaviour were also observed and recorded under a Leica LMD6000 light microscope equipped with a Leica DMC 4500 camera.

## In situ and in microcosms measurements of chemical and cell count profiles

Dissolved oxygen profiles were measured in the sediments, using a fibre-optic oxygen sensor (50- $\mu\text{m}$  tip diameter, REF OXR50) and a FireStingO<sub>2</sub> metre, both from Pyroscience. High-resolution profiles (100  $\mu\text{m}$  steps, from 10 mm above the sediment to -25 mm below the sediment) were achieved with a Pyroscience MU1 motorized micro-manipulator. Sensor calibration was made against saturated humid air (O<sub>2</sub> sat.=100%) and a water solution flushed with N<sub>2</sub>. Magnetotactic cells were highly concentrated and diverse in sediment samples, those with large refractive granules could be easily distinguishable from other bacteria and sediment particles; they were counted using a Malassez counting chamber. Measurements were systematically carried out on three replicates of three different samples. For each replicate, the number of cells was counted at three different locations in the sediment sample. Cell counts were reported as the means of triplicate counts for each sample.

In the water column, dissolved oxygen and redox potential were measured in situ using a CTD O<sub>2</sub>-pH-redox probe (YSI 6600). Three 1 L bottles of water were collected every metre above and below the oxycline in order to determine the depth distribution of magnetotactic bacteria. For each depth, three drops of 40  $\mu\text{L}$  were observed using the hanging drop technique [35]. Magnetotactic cells accumulating at the edge of the drops when a magnetic field was applied from one side of the drop were counted under a ZEISS Primo Star light microscope. The number of cells counted in each drop was multiplied by a factor of 25 to obtain the concentration of cells per millilitre. Cell counts were reported as the means of triplicate counts for each depth.

## Cell sorting and whole-genome amplification (WGA)

Cell sorting was carried out on sediment samples collected in Lake Pavin with an InjectMan<sup>®</sup> NI2 micromanipulator and a CellTram<sup>®</sup> vario, hydraulic, manual microinjector from Eppendorf mounted on a Leica DM IL LED microscope equipped with a 63 $\times$ /0.70 PH objective. The microscope and micromanipulator were placed inside a clean chamber, sterilized beforehand by 1 h germicidal irradiation with ultraviolet (wavelength of the lamp: 254 nm). A 10- $\mu\text{L}$  drop containing magnetically concentrated cells was gently added to a 30- $\mu\text{L}$  drop of filtered Lake Pavin water on a hydrophobic coverslip in order to magnetically transfer magnetotactic cells toward the filtered water. One to ten cells with bright granules were transferred with a sterile microcapillary (TransferTip<sup>®</sup> (ES), 4  $\mu\text{m}$  inner diameter, Fig. S1) into a 4  $\mu\text{L}$  drop of phosphate buffer saline (PBS). This drop was stored at -20 °C before WGA. To obtain

sufficient gDNA for 16S rRNA gene and shotgun metagenomic sequencing, WGA was carried out using the multiple displacement amplification (MDA) technique with the REPLI-g Single Cell Kit (QIAGEN) following the manufacturer's instructions. The concentration of double strand gDNA was measured using a QuBit<sup>™</sup> 4 fluorimeter (ThermoFisher Scientific).

## Cloning and sequencing of the 16S rRNA gene of magnetically concentrated and sorted cells

The 16S rRNA gene of all processed DNA samples was amplified using the Phusion<sup>®</sup> Hot Start Flex DNA Polymerase following the manufacturer's recommendations, a DNA template of 50–70 ng/ $\mu\text{L}$  and the 27 F 5'-AGAGT TTGATCMTGGCTCAG-3' and 1492 R 5'-TACGGHTA CCTTGTTACGACTT-3' primers [36]. Blunt-end fragments of 16S rRNA gene sequences were cloned using a Zero Blunt<sup>®</sup> TOPO<sup>®</sup> PCR Cloning Kit with One Shot<sup>®</sup> TOP10 chemically competent *E. coli* cells. The inserts of the resulting clones were digested using the restriction enzyme EcoRI to select five operational taxonomic units (OTUs) representative of the sediment-sorted-cell populations and were sent for sequencing (Eurofins Genomics Germany GmbH). Sequences were compared to data from the NCBI nucleotide database with Basic Local Alignment Search Tool [37]. The 16S rRNA gene sequences of the sorted MTB OTUs were checked using the UCHIME2 chimera detection algorithm [38] and deposited in GenBank under accession numbers MT021453 to MT021457.

## Phylogenetic analyses

All the 16S rRNA gene sequences of Rhodospirillaceae and Acetobacteraceae type strains (NCBI taxonomy) available in the public databases NCBI in January 2020 were downloaded and completed with the five OTUs obtained in this study. This database was reduced to one species per genus keeping the highest quality sequences to draw a first tree with the BioNJ software [39] after sequences were aligned using MAFFT 7 [40] and trimmed with the relaxed parameters of Gblocks (Fig. S2) [41]. This tree was used to remove genetic redundancy by randomly selecting few representative species only per cluster to get a final database of 45 sequences including 7 Acetobacteraceae type strains as an external group. All sequences were aligned and trimmed following the same method to get a final alignment of 1381 bp. A maximum-likelihood tree was built using IQ-TREE [42] and a TIM3 + F + R4 model for describing nucleotide evolution selected by Modelfinder [43] using the Bayesian Information Criterion (BIC). Robustness of tree topology was tested using a non-parametric bootstrap approach and 500 replicates.

### Correlative fluorescent in situ hybridization (FISH) and scanning electron microscopy (SEM)

FISH was performed according to the procedure described by Pernthaler et al. [44]. First, an ATTO488-labelled probe was designed, specific to the bacteria producing refractive inclusions that were sorted from sediment samples (CCPp, 5'- GTCATTATCGTCGCGTGCGAAAGAGCTTTACAA CCGG -3', complementary to nucleotides 383 to 419 of the 16S rRNA molecule of OTU1, one mismatch with OTU5 at position 414). This was based on the alignment of the most similar 16S rRNA gene sequences of the Rhodospirillaceae family found in GenBank in August 2018. Probe specificity was evaluated by using the PROBE\_MATCH programme in the RDP-II [45]. The nearest non-target hits contain at least one mismatch with the specific probe CCPp. Oligonucleotide probes used in this study were purchased from Eurofins Genomics (Ebersberg, Germany).

Then, a 20  $\mu$ L drop of magnetically concentrated cells was deposited on an 18 mm  $\times$  18 mm coverslip covered with poly-L-lysine. After 10 min, the drop was removed and the cells adsorbed on the coverslip were fixed overnight with 30  $\mu$ L of a 4% paraformaldehyde solution. Fixed cells were dehydrated by serial incubations in 50%, 80% and 100% ethanol during 5 min each. The hybridization solution contained 10 ng/mL of the probe, 0.9 M NaCl, 20 mM Tris-HCl (pH 7.4), 1 mM Na<sub>2</sub>EDTA, and 0.01% sodium dodecyl sulphate (SDS), using the hybridization and washing stringencies recommended for each probe (30% for CCPp). Hybridization was performed at 46 °C for 2 h. For some samples, 10  $\mu$ L of a solution of 1  $\mu$ g/mL of 4,6-diamidino-2-phenylindole (DAPI) was added to the coverslip, incubated 10 min at 4 °C and rinsed with water. Coverslips were stored at 4 °C in a humidity chamber before observation.

Finally, hybridization assays were analysed using a Zeiss LSM780 confocal microscope available on the Zoom platform at the Institute of Biosciences and Biotechnologies of Aix-Marseille. Correlative fluorescence light and electron microscopy, combining the specificity of fluorescence labelling with the high spatial resolution of scanning electron microscopy (SEM), was carried out with a Zeiss LSM710 confocal laser scanning microscopy at the Institut de Minéralogie, de Physique des Matériaux et de Cosmochimie in Paris. Correlation with SEM was performed using the KorrMik Life Sciences sample holder and the correlative Shuttle and Find software implemented in ZEN as previously described [46]. Images were collected in the backscattered and secondary electron modes using a Zeiss Ultra 55 FEG-SEM operating at 10 kV, a working distance of 5 mm and an aperture of 30  $\mu$ m.

### Transmission electron microscopy (TEM)

The ultrastructure of CaCO<sub>3</sub>-producing MTB was observed by developing an alternative protocol to fix cells on a TEM carbon-coated grid. Indeed, only few or no cell at all of CaCO<sub>3</sub>-producing MTB were fixed on TEM grids when using the standard protocol consisting simply in drying a droplet containing the bacteria. Here, we pipetted 2  $\mu$ L of liquid from the edge of the northern side of a hanging drop, at the bottom of the drop, where magnetic cells aggregated and settled down due to their magnetotactic behaviour and their density. Then, we slowly deposited these cells at the centre of the TEM grid. The grid and the drop were kept in place during the fixation of the cells. Indeed, if the grid was moved upside down as it is usually done for other MTB, cells with CaCO<sub>3</sub> granules did not adsorb onto the carbon film of the TEM grid and instead settled down at the bottom of the drop likely because of their high density. Once the drop started to dry, the grid was washed with filtered deionized water. Although most of the CaCO<sub>3</sub>-producing bacteria formed large aggregates of cells, this technique facilitated their observation and enabled optimal adsorption of the MTB onto the carbon film.

Electron micrographs were recorded with a Tecnai G<sup>2</sup> BioTWIN (FEI Company) equipped with a CCD camera (Megaview III, Olympus Soft imaging Solutions GmbH) using an accelerating voltage of 100 kV. High-resolution transmission microscopy (HRTEM), z-contrast imaging in the high-angle annular dark field (STEM-HAADF) mode, and elemental mapping by X-ray energy-dispersive spectrometry (XEDS) were carried out using a JEOL 2100 F microscope. This machine, operating at 200 kV, was equipped with a Schottky emission gun, an ultrahigh resolution pole piece, and an ultrathin window JEOL XEDS detector. HRTEM images were obtained with a Gatan US4000 charge-coupled-device (CCD) camera.

The sizes of magnetosomes and other mineral inclusions as well as the estimation of the area occupied by these inclusions were measured from TEM images using the ImageJ software (1.48 v).

### Cryo-electron microscopy of vitreous sections (CEMOVIS)

For CEMOVIS, a pellet of cells magnetically enriched from a Lake Pavin sediment sample was harvested. The pellet was carefully mixed with an equal volume of 40% PBS. The suspension was transferred in a gold coated copper sample holder type A with a 200- $\mu$ m diameter cavity and closed with a flat sample holder type B (Wohlwend GmbH, Sennwald, Switzerland) before vitrification with a HPM 100 (Leica microsystems, Vienna, Austria). Vitrified samples



were placed in the cryo-chamber of a Leica cryo-ultramicrotome at  $-150\text{ }^{\circ}\text{C}$ . Ultrathin cryo-sections with a nominal feed of 40 nm were obtained using a  $35^{\circ}$  cryo-diamond knife and were collected on quantifoil grids covered with a carbon film. Grids were stored in liquid nitrogen before observations by cryo-TEM in the low dose mode with a Tecnai G2 microscope equipped with a Gatan US 4000 CCD camera.

### Shotgun genomic sequencing, assembly and functional annotation

One single-cell of  $\text{CaCO}_3$ -producing MTB, named CCP1 (Calcium Carbonate Producing bacterium #1), was sorted using a micromanipulator (as described above) from a sample collected on the shore of Lake Pavin in May 2015. After WGA of this cell, gDNA was quantified using a QuBit Fluorimeter (ThermoFisher Scientific) and quality was evaluated on a 1% TAE agarose gel.

The genome of CCP1 was sequenced on an Illumina MiSeq platform with a MiSeq<sup>®</sup> Reagent Kit v2 (300 cycles, Illumina Inc.) using a Nextera<sup>®</sup> XT kit for the library preparation. A total of  $1.9 \times 10^6$  paired-end reads was obtained, trimmed and filtered using Trimmomatic [47] and the default settings. A draft assembly of 2.5 Mbp was assembled using SPAdes v.3.12.0 (with -k 21,33,55,77,99,127 —only-assembler —sc options) into 3365 contigs longer than 250 bp and annotated using the fast method implemented in Prokka 1.14.0 [48]. The genome completeness was assessed using CheckM v1.1.2 [49].

### Scanning transmission X-ray microscopy (STXM)

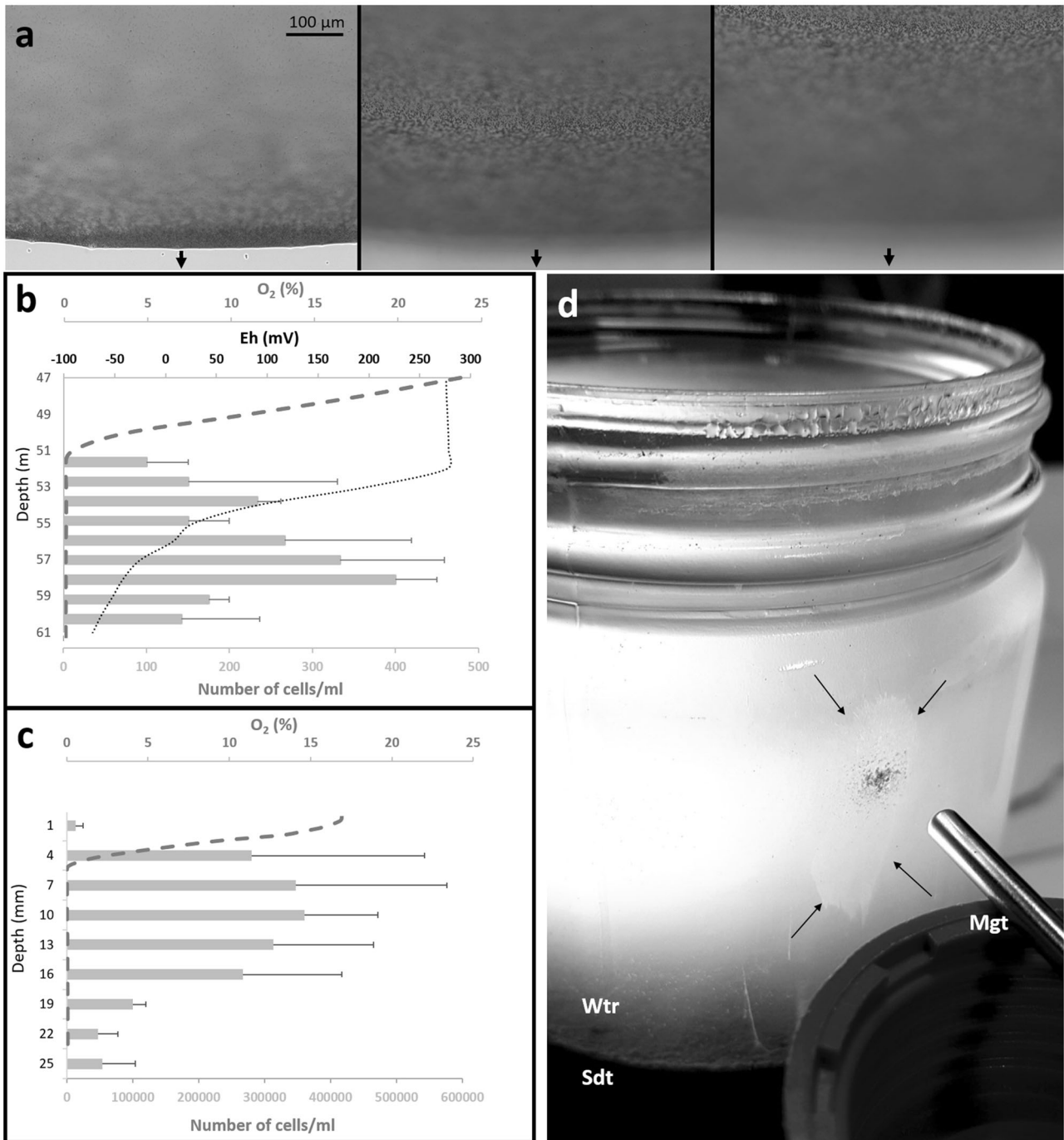
STXM analyses were performed on the HERMES beamline at the SOLEIL synchrotron (St. Aubin, France) [50, 51]. Details on the STXM technique and its application to biomineralization can be found in e.g., [52, 53]. This microscopy uses X-rays in the soft X-ray energy domain to provide images with a  $\sim 25$  nm spatial resolution and spatially-resolved speciation information of light elements such as C based on X-ray absorption near edge structure (XANES) spectroscopy. For this purpose, monochromated X-rays are focused to a  $\sim 25$  nm spot by a Fresnel zone plate. An image is obtained by positioning the sample at the focal point of the lens and raster scanning it in  $x$  and  $y$ , while recording the intensity of the transmitted X-rays. After localizing cells of interest by optical microscopy beforehand, we could easily localize them by STXM. A stack of STXM images of the cells at a sequence of photon energies was acquired at the C K-edge. The step size was 75 nm and images were obtained at 140 energy steps varying between 270 and 345 eV with an increment of 0.12 eV in the 282–291.5 eV energy range, where most of the

narrowest XANES peaks were present. The imaged area also contained a sub-area free of cells to measure the incident flux (I<sub>0</sub>). This allowed to convert images from transmitted intensity units to optical density units (OD). The XANES spectra at the C K-edge of the  $\text{CaCO}_3$  inclusions and the cells were extracted and mapped using the aXis 2000 software (McMaster University, <http://unicorn.mcmaster.ca/axis/aXis2000-IDLVM.html>).

## Results

### Observation of bacteria with electron dense granules and an unusual magnetotactic behaviour

Over the different sampling campaigns performed since 2015 at Lake Pavin, a large diversity of MTB morphotypes, mostly represented by cocci, was observed close to the oxic-anoxic boundary of the water column (45–60 m depth) [46]. MTB were also very diverse in the sediments collected from the shore down to a water depth of 40 m [54]. In most collected samples, one MTB morphotype escaped our first light and electron microscopy observations because of its atypical magnetotactic behaviour. Indeed, some slightly-curved rod-shaped MTB with large inclusions were only weakly magnetic, i.e., their rotation was slow compared to other MTB when the applied magnetic field was switched  $180^{\circ}$  to the initial direction. They did not, for the majority, accumulate at the edge of the hanging drop. Instead, they aligned along the magnetic field and slowly swam back and forth at the bottom of the drop without reaching the edge of the drop where light microscopy observations of MTB usually focus (Fig. 1a). Overall, these particular MTB cells were more efficiently concentrated by increasing the duration of the magnetic enrichment from 30 min to 3 h and applying a stronger magnetic field (neodymium, iron and boron magnet of 400 mT). As most of the other members of the MTB community, these bacteria were located in oxygen-depleted areas, i.e. below the oxycline [46]. The cell density of this new MTB morphotype in the water column was generally higher in autumn and its maximum was observed during the October 2018 campaign at a depth of 58 m, reaching  $4.0 \times 10^2$  cells/mL (Fig. 1b). However, this cell density was probably underestimated since the used hanging drop technique likely biased the counting of such MTB downward. This new MTB morphotype was always observed in the hanging drop assay without previous magnetic enrichment in autumn. During the other seasons (spring and summer), they were observed after magnetic enrichment only (i.e., abundance  $<25$  cells/mL). In sediment samples, these bacteria generally represented the dominant magnetotactic population and reached up to



$5.8 \times 10^5$  cells/mL of porewater. In the sediments, the majority of the cells were detected below the oxic-anoxic interface as in the water column (Fig. 1c). After magnetic enrichment of sediment samples, aggregated cells formed a thin irregular whitish pellet measuring up to 4 cm in diameter and located against the magnet. The pellet was wider below the magnet, suggesting that the population was sensitive to gravity (Fig. 1d). In most samples collected on the shore, MTB pellets aggregated after 3 h

against magnets were of similar size whenever the north or the south poles of the magnets were directed toward the sampling bottle. This suggests that there was an equal proportion of north- and south-seeking cells.

Bacteria with this atypical magnetotactic behaviour contained 2 to 4 characteristic large refractive inclusions measuring  $856 \pm 95$  nm in width ( $n = 147$ , Fig. 2). They also showed poor adsorption onto the carbon film covering TEM grids and a specific protocol had to be developed for

**◀ Fig. 1 Observation of the refractive magnetotactic bacterium from Lake Pavin.** **a** Light microscope images of north-seeking magnetotactic bacteria (MTB) sampled in the sediment of Lake Pavin. The microscope was focused at the edge of the water drop closest to the south pole of the bar magnet, producing a local field direction indicated by the black arrow (left panel). The microscope was focused at 200  $\mu\text{m}$  (middle panel) and 400  $\mu\text{m}$  (right panel) from the edge of the water drop showing the presence of MTB cells (seen as grey dots in the images) aligned with the magnetic field but not aggregated at the edge of the hanging drop. **b** Vertical concentration profiles of oxygen (grey dashed line), redox potential (black dotted line) and rods with large refractive inclusions (histogram) through the water column of samples collected in Lake Pavin in October 17th, 2018. Note that the measurements extend through the oxic-anoxic interface and the deeper regions of the anaerobic zone of the water column. Cell counts are reported as the mean of triplicate measurements and line extensions represent the positive standard deviation of the total number of MTB. Rods with refractive inclusions were also observed above 52 m and below 60 m but at densities < 25 cells/mL and thus escaped our counting assay. **c** Vertical concentration profiles of  $\text{O}_2$  (grey dashed line) and cell density of rods with large refractive inclusions (histogram) in a sediment sample collected from the shore of Lake Pavin. Cell counts are reported as the mean of triplicate measurements and line extensions represent the positive standard deviation. **d** Image of a one-litre sample collected from the shore of Lake Pavin. The bottle was filled to about 1/3 of its volume with sediment (Sdt) and the remainder of the bottle is filled to its capacity with water (Wtr) that overlaid the sediment. A large whitish pellet (black arrows) of magnetotactic cells clustered against the magnet (Mgt) 2 h after magnetic enrichment. Note the presence of black particles, in the centre of the pellet, composed of magnetic sediments.

their fixation on the grids (see Materials and Methods). Most of the cells formed large aggregates on the TEM grids. Analysis of the cells ultrastructure revealed the presence of a single polar flagellum (Fig. 2a). Inclusions were very dense to the electron beam and occupied the majority of the cytoplasm, which significantly complicated the observation of the magnetosomes using conventional TEM bright field mode (Fig. 2b, c). Magnetosomes overlapping with the inclusions were only observed when using the HAADF mode in STEM (Fig. 2d, e). Some inclusions were observed to form at the septum of dividing cells (Figs. 2f and S3). Shortly after cell division, each daughter cell contained two inclusions of different sizes: a large one located at the flagellum pole and a small one at the other pole (Figs. 2a, d, e and S3). When observed under the light microscope with an applied magnetic field, recently divided cells always showed their smallest inclusion in the front and their largest one in the back, at the flagellum pole (Fig. 2g). Based on the observation of 186 STEM-HAADF images of cells from a water column sample, two scenarios linking cell division and the formation of the inclusions could be proposed (Supplementary Information on cell division). However, we cannot exclude the possibility that different species or sub-species of calcium carbonate-producing MTB have different number and/or organization of inclusions.

## Chemical analyses indicate the presence of both calcium carbonate and magnetite inclusions forming in environmental conditions undersaturated with Ca-carbonate phases

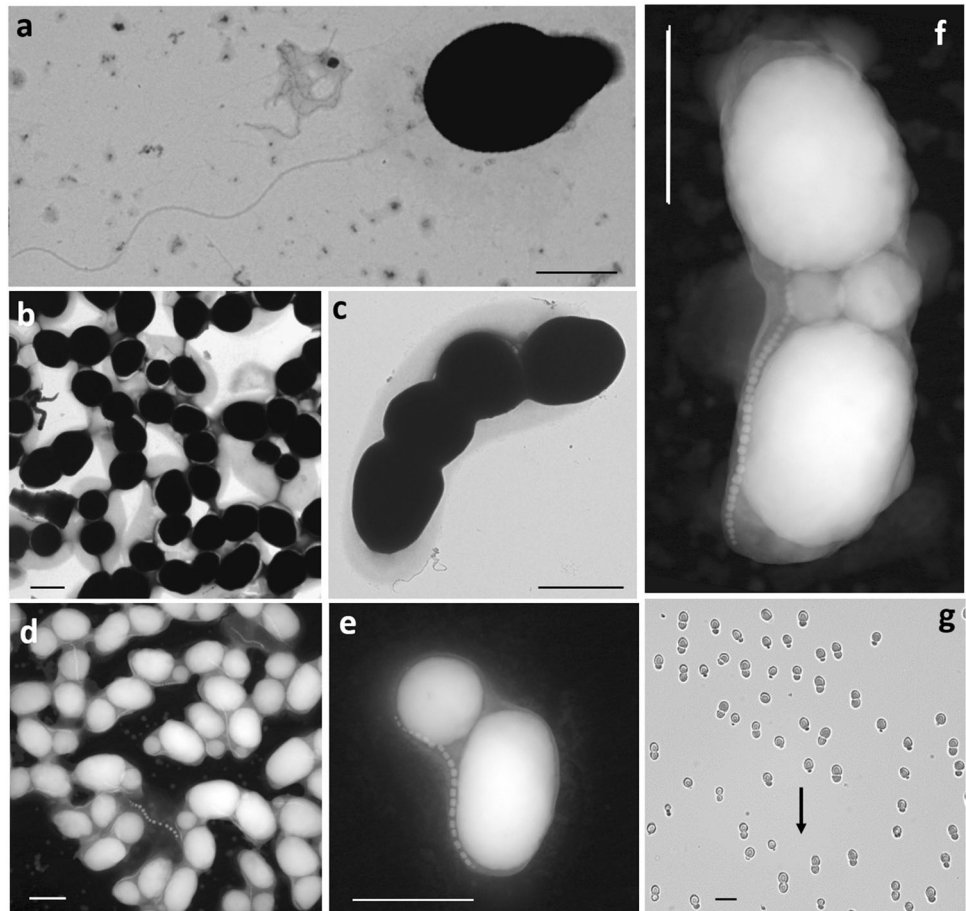
The majority of cells, from sediment samples, producing the large electron-dense inclusions contained a single chain of  $14 \pm 4$  ( $n = 35$ ) prismatic magnetite particles measuring  $58 \pm 4$  nm in length and  $40 \pm 3$  nm in width ( $n = 223$ ) (Fig. 3a, c). Similar cells were also observed with cuboctahedral magnetite particles in the sediments (Fig. 3d, f). Moreover, cells producing such large inclusions in the water column were always observed with cuboctahedral particles. TEM image analysis revealed that these large electron-dense inclusions represent  $73 \pm 9\%$  ( $n = 134$ ) of the cell area. Usually, extrapolation from 2D TEM images to 3D volumes is not straightforward. Here, we assumed that both cell and electron-dense inclusions exhibited an ellipsoidal morphology, which is fairly supported by the numerous images of randomly oriented cells. Based on this assumption, the volume of the large electron-dense inclusions could be roughly estimated to 65% of the total cell volume. X-ray energy-dispersive spectrometry (XEDS) and elemental mapping in the STEM-XEDS mode indicated that the large inclusions contained mostly calcium, carbon and oxygen (Fig. 3b, e, Fig. S3 and Supplementary Information), with weak peaks assigned to strontium and barium (Fig. 4). Phosphorus-rich granules were also observed in some cells (Figs. 3b and 4b). Selected-area electron diffraction patterns obtained on these inclusions showed that they were amorphous (Fig. S4).

STXM analyses were carried out on MTB cells collected in the water column and the sediments to further characterize these amorphous Ca-, O- and C-containing inclusions. XANES spectra at the C K-edge extracted from the cells showed peaks at 285.2, 286.6, 288.2 and 290.3 eV which were interpreted as carbon  $1s \rightarrow \pi^*$  electron transitions in aromatic, ketonic/phenolic, amide carbonyl and carbonate functional groups, respectively [55]. Spectra measured on large inclusions were very similar to those of reference amorphous calcium carbonate (ACC) particles and showed a pronounced  $1s \rightarrow \pi^*$  carbonate-C peak at 290.3 eV together with broader peaks at 296.2 and 301.6 eV that were attributed to a  $1s \rightarrow \sigma^*$  electron transitions in carbonate C. Overall, this allowed to unambiguously determine that inclusions in the MTB were composed of ACC [55] (Fig. 5).

In parallel, we measured the alkalinity (approximated to  $[\text{HCO}_3^-]$ ), pH, and  $[\text{Ca}^{2+}]$  in 10 sampling bottles of onshore sediments to better understand the environmental conditions that led to the formation of such inclusions. The pH of the pore water was between 6.88 and  $7.64 \pm 0.01$ , the  $[\text{Ca}^{2+}]$  between  $83.9 \pm 0.7$  and  $634 \pm 3.7$   $\mu\text{M}$  and the alkalinity

**Fig. 2 Microscopy images of magnetotactic bacteria with electron-dense inclusions isolated from Lake Pavin sediment samples.**

**a** Transmission electron microscopy (TEM) image of a cell stained with 1% uranyl acetate, showing the presence of one single polar flagellum. **b, c** Bright-field TEM images of cells showing the electron-dense granules that make the observation of the magnetosomes difficult. **d–f** Scanning TEM-high-angle annular dark field (HAADF) images showing the magnetosome chain partially overlapping the electron-dense inclusions in the cytoplasm of the cells. **f** The formation of small inclusions at the septum of a dividing cell. **g** Light microscopy image of cells magnetically orientated in the same direction (north direction pointed by the black arrow) showing that the smaller inclusions are always at the front of the cells. Scale bars represent 1  $\mu\text{m}$  (a–f) and 2  $\mu\text{m}$  (g).



between 725 and 3824  $\mu\text{M}$ . Overall, the ion activity product (IAP),  $(\text{Ca}^{2+}) \times (\text{CO}_3^{2-})$ , varied between  $3.32 \times 10^{-11}$  and  $1.23 \times 10^{-9}$  and was therefore systematically lower than the solubility products at 25°C of ACC ( $5.27 \times 10^{-7}$ , [34]) and calcite ( $3.31 \times 10^{-9}$ ). As a result, we could conclude that all solutions in contact with the sediments and MTB were undersaturated with ACC, at least at the bulk scale. Available water chemistry data indicate that ACC produced by MTB present in the water column also form in a solution undersaturated with ACC [56].

### ACC-producing MTB represent a new genus within the Alphaproteobacteria and harbour an atypical magnetosome gene cluster

The identity of ACC-producing MTB isolated from the Lake Pavin sediments was investigated by sequencing the 16S rRNA genes amplified from magnetically purified populations and sorted single-cells (Fig. S1). We obtained 18 sequences (between 1450 and 1492 bp) composed of 5 operational taxonomic units (OTUs) defined at a 99% identity level. These 5 OTUs shared 92.8–98.3% identity indicating that this morphotype of ACC-producing MTB

was composed of several species, likely belonging to at least two genera based on a 95% sequence identity threshold [57]. Based on BLASTN hits, the closest cultured species belonged to the *Azospirillum* and *Skermanella* genera of the Rhodospirillaceae family of the Alphaproteobacteria class (following the current NCBI taxonomy). However, sequence identities with these genera were low (between 91.7 and 93.8%) suggesting that ACC-producing MTB belonged to at least two genomic undescribed genera. As a result, based on the phylogeny inferred from the 16S rRNA gene sequences, these biomineralizing MTB formed a distinct new monophyletic clade within Rhodospirillaceae, related to a group composed of the *Niveispirillum*, *Rhodocista*, *Nitrospirillum*, *Azospirillum*, *Desertibacter* and *Skermanella* genera (Fig. 6a). However, the tree topology was not well statistically supported and could not entirely resolve the evolutionary relationships between Lake Pavin MTB and the closest Rhodospirillaceae genera. Indeed, the 16S rRNA sequences harboured too much interspecific polymorphism with important genetic saturation effects suggesting that the current Rhodospirillaceae family (NCBI taxonomy) may actually gather very divergent organisms.

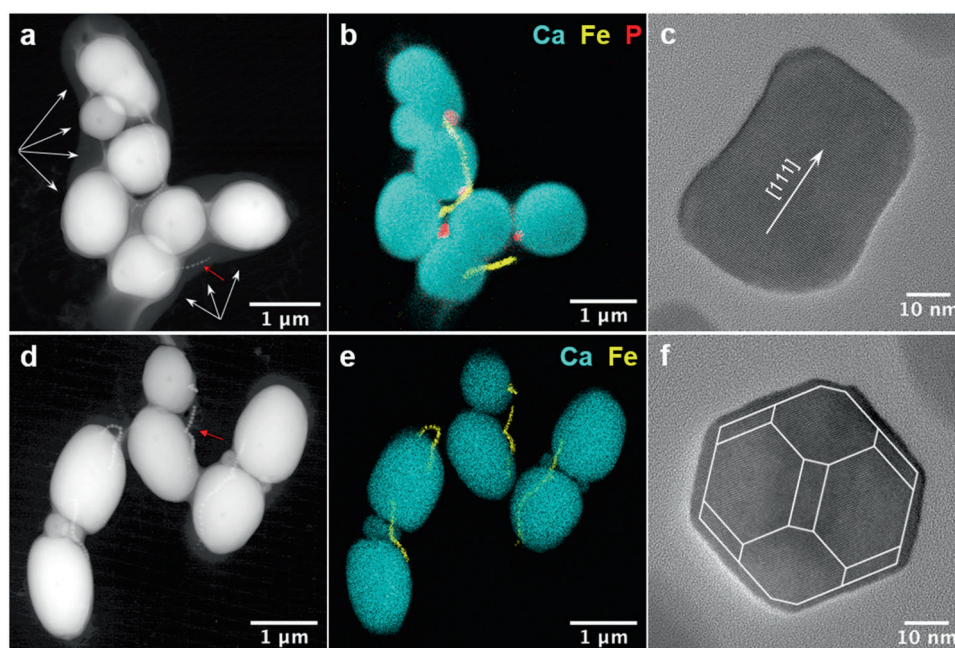


**Fig. 3** Chemical identification of the mineral phase in the magnetosomes and the large inclusions of bacteria isolated from sediment samples. **a** STEM-HAADF image of two cells producing four (left cell) and three (right cell) large inclusions (indicated by white arrows). **b** Composite XEDS elemental mapping of calcium, iron and phosphorus. **c** High-resolution TEM image of a prismatic magnetosome (shown by a red arrow in panel a) elongated along the [111] axis.

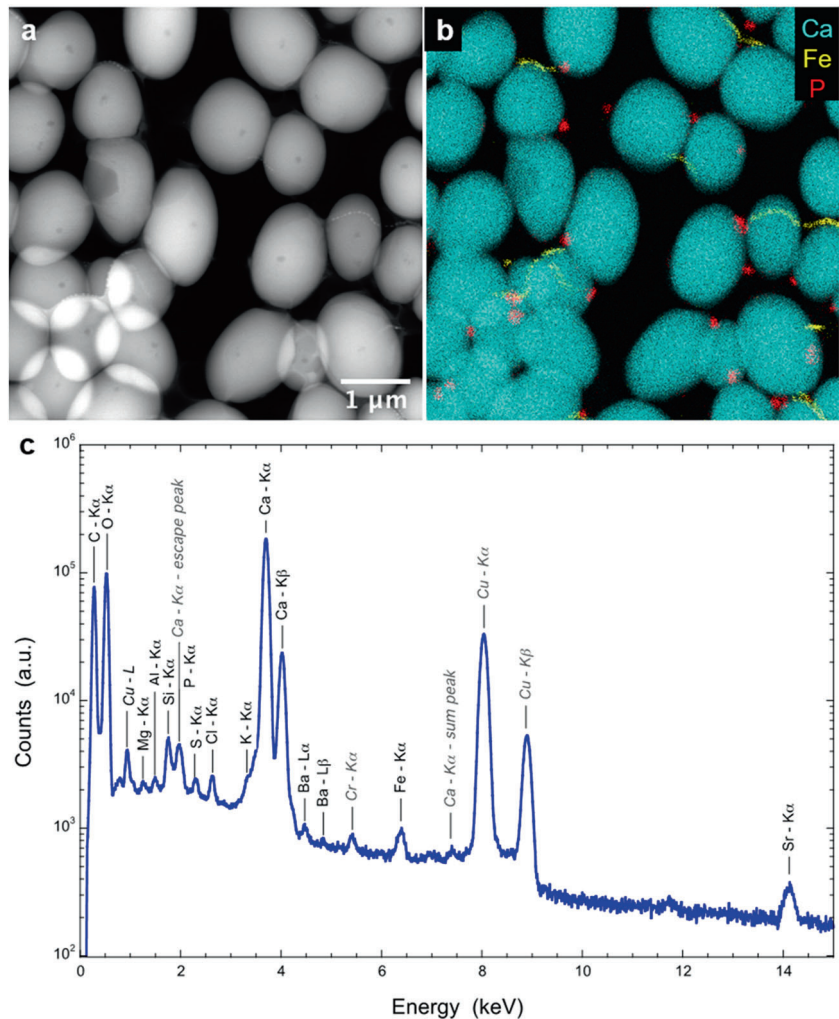
**d** STEM-HAADF image of three cells producing large and small inclusions). **e** composite XEDS elemental mapping of calcium and iron. **f** HR-TEM image of a cuboctahedral magnetosome (shown by a red arrow in panel d), an ideal model of a cuboctahedron with small {110} faces is superimposed. Detailed information on the chemical and shape identification of the mineral phases present in these bacteria is given in Supplementary Information.

Fluorescent in situ hybridization (FISH) using specific fluorescently-labelled oligonucleotide probes and combining confocal microscopy with scanning electron microscopy observations further validated the ACC-producing MTB identity (Fig. 7). As expected from similar observations on ACC in cyanobacteria [22], the MTB ACC inclusions dissolved during the preparation of the FISH samples because of the detrimental impact of fixation followed by incubation in buffers undersaturated with ACC (Fig. 7e). A similar loss of ACC inclusions was observed in these bacteria when preparing ultrathin TEM sections following conventional ultramicrotomy protocols (Fig. S5a-c). In contrast, ACC inclusions were preserved by cryo-electron microscopy of vitreous sections (CEMOVIS) and showed the existence of a lipid bilayer-delimited intracellular compartment enclosing ACC (Fig. S5d-f).

The genome of the representative ACC-producing MTB clone CCP-1 was tentatively assembled. Single-cell sorting coupled with whole-genome amplification and sequencing allowed to assemble a partial genome sequence of 2.5 Mb, in which a single 16S rRNA gene copy identical to the OTU1 sequence was detected. Completeness was estimated to be lower than 22%, which was not satisfactory enough to get a reliable phylogeny reconstruction based on ribosomal proteins or to reconstruct full metabolic pathways. This

result indicates that ACC-producing MTB may have an atypical large genome over 10 Mbp, compared to its closest relatives whose genomes size range between approximately 3 and 8 Mb in average. Despite this low genome coverage, a full magnetosome gene cluster was retrieved from the longest contig of 72.5 kbp using the BLASTP algorithm and the bank of *mam* sequences publicly available for all Alphaproteobacteria (RefSeq non-redundant proteins database). Its sequence was deposited in Genbank under the accession number MT411893. Indeed, up to 30 genes were unambiguously identified with a high sequence similarity with known magnetosome genes (See Table S1 and Fig. 6b). Comparative analysis of the magnetosome gene cluster (MGC) from representative magnetotactic Rhodospirillaceae showed the presence of the main operons described in *Magnetospirillum* species but with an atypical organization compared to both marine and freshwater strains (Fig. 6c). For example, the *mamAB* operon was complete with the exception of *mamJ*, which is a gene involved in ultrastructural organisation of the magnetosome chain specific to the *Magnetospirillum* genus. However, gene synteny was not conserved in the *mamAB* operon, just as for the *mamXZ* operon in which no *mamY* was detected. Finally, the canonical form of the *mamGFDC* operon was not present.

**Fig. 4 Evidence of strontium and barium in the calcium-rich inclusions.** **a** STEM-HAADF image of cells with calcium-rich inclusions, isolated from the sediment of Lake Pavin. **b** Composite XEDS elemental mapping of calcium, iron and phosphorus. **c** XEDS elemental spectrum of an inclusion showing the presence of calcium as well as traces of strontium and barium. Note that the coordinate axis is in logarithmic scale.



## Discussion

The ability to mineralize calcium carbonates has been described in very few prokaryotic taxa so far and despite the tremendous importance that such a function may have had in the Earth's history, very little is known about its distribution in the tree of Bacteria, its genetic basis and its ecological role. This gap may be partially reduced by describing new organisms producing calcium carbonates in very divergent phyla with different ecological niches. Here, we not only described a bacterium able to perform two different types of biomineralization, but we also extended the record of microorganisms able to perform intracellular Ca-carbonate biomineralization from two to three far-related groups of Bacteria: Gammaproteobacteria, Cyanobacteria and Alphaproteobacteria. The MTB performing both magnetic iron oxide and calcium carbonate biomineralization in the ferruginous Lake Pavin undoubtedly form a monophyletic group composed at least of one or two genera that are distinct from those currently described within the

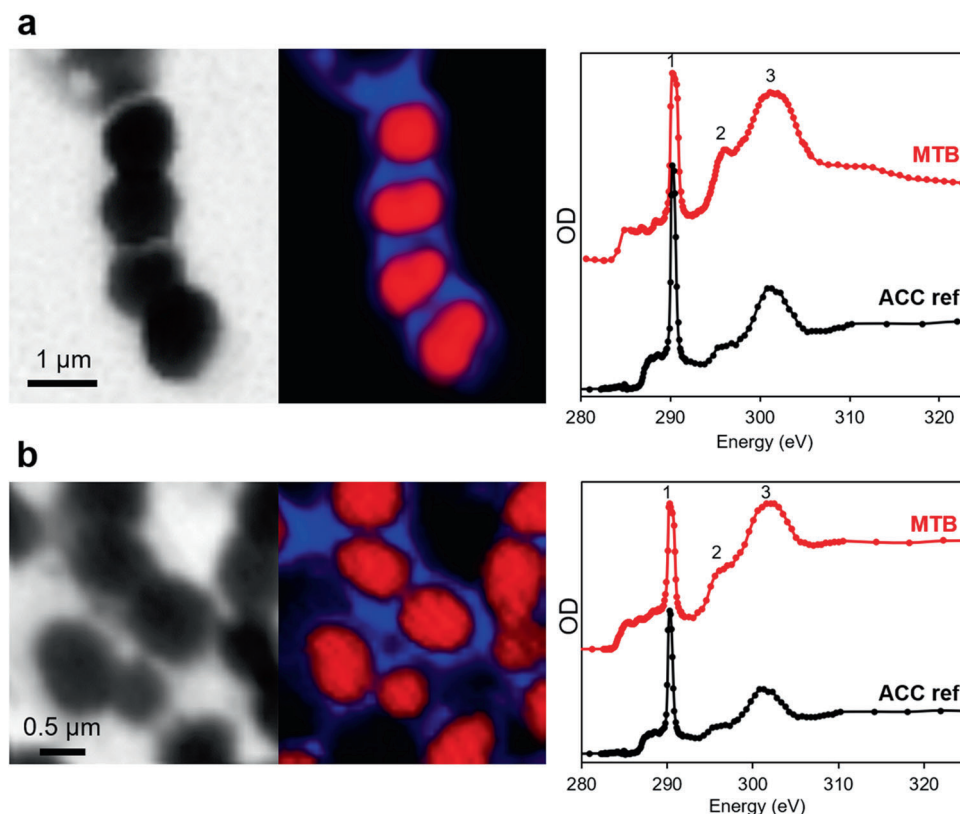
Alphaproteobacteria. The majority of the phylogenetically closest genera, *i.e.* *Niveispirillum*, *Rhodocista*, *Nitrospirillum*, *Azospirillum* and *Skermanella*, includes species isolated from the rhizosphere or freshwater environments. None of the species from these genera has been reported to biomineralize ACC [58–62]. Most of these species are chemoorganoheterotrophic and aerobic, but some can also be anaerobically phototrophic. Future culture assays and genome sequencing will determine if ACC-accumulating MTB have similar metabolisms and will help resolving the ancestry of both biomineralization processes in Alphaproteobacteria.

MTB have often been used to illustrate how the cell functioning and compartmentalization can be complex in prokaryotes through the description of numerous morphotypes with diverse cell ultrastructures and physiologies in very chemically contrasted environments [63, 64]. Besides magnetosomes, other large inclusion bodies storing elemental sulphur, polyphosphates, or polyhydroxybutyrates (PHB) have been regularly observed in MTB [46, 65–73].

**Fig. 5 STXM analyses measured at the C K-edge on intracellular inclusions of magnetotactic bacteria isolated from Lake Pavin.**

**a** Bacterial cell isolated from the water column. From left to right: STXM image at 320 eV; Map of two spectroscopically different compounds derived from the analysis of a hyperspectral image: an ACC-like compound (red) and an organic, cell-like compound (blue); XANES spectrum at the C K-edge of the ACC-like compound and of a reference synthetic ACC sample. Y-axis shows optical density (OD) values. Peaks 1, 2 and 3 seen in both reference and MTB inclusions are located at 290.3, 296.2 and 301.6 eV.

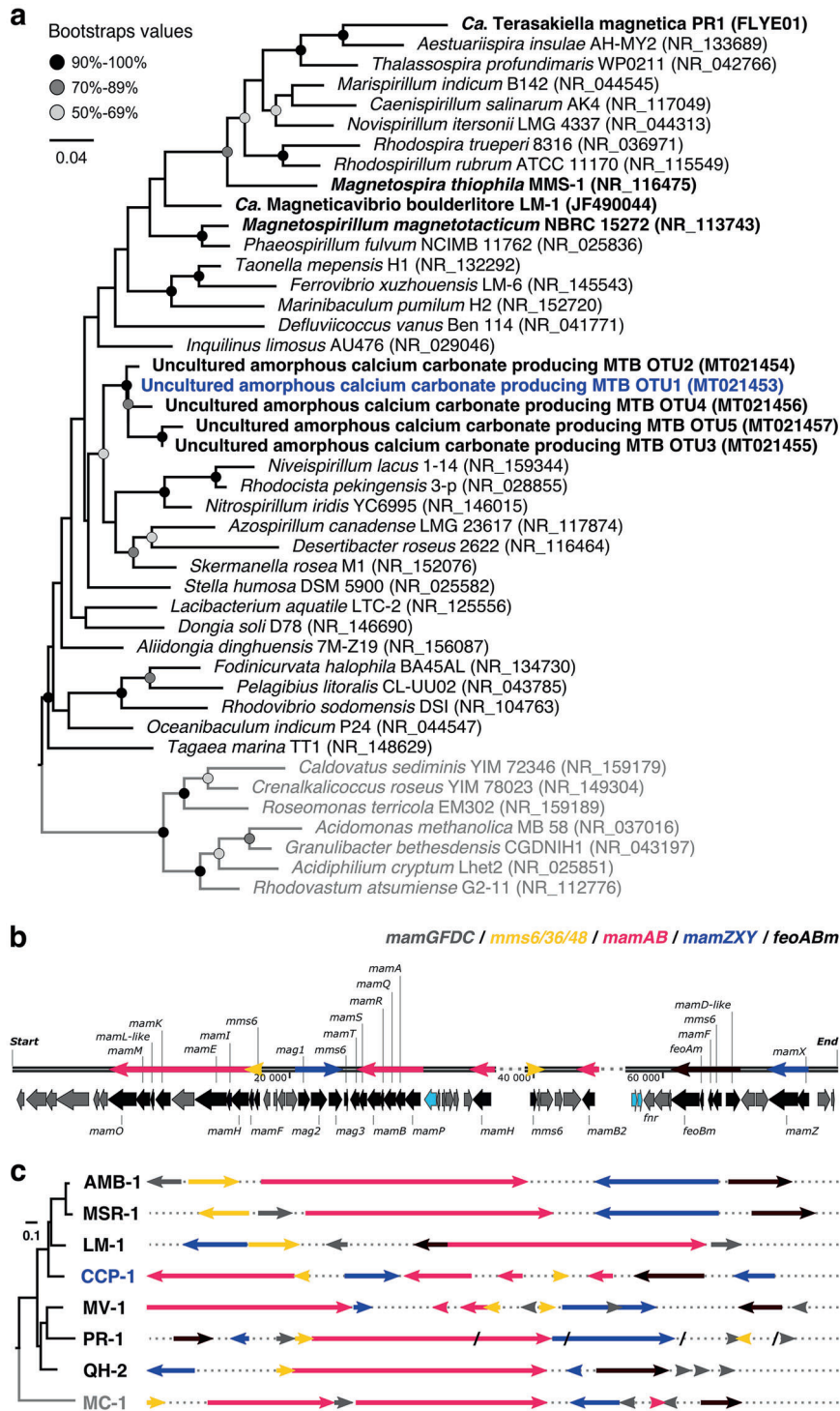
**b** Bacterial cell isolated from the sediment. From left to right: same as in panel a.



Here, we extend the range of inclusions that MTB may form and give insights into the ultrastructure, chemistry and formation of ACC inclusions during the cell cycle. TEM analyses showed that the inclusions were amorphous and CEMOVIS confirmed the presence of a surrounding membrane. Interestingly, XEDS analyses showed the presence of Sr and Ba in the ACC granules. The accumulation of the alkaline earth elements such as Ca, Sr and Ba at a high level has been demonstrated for the ACC-biomineralizing cyanobacterium *Gloeomargarita lithophora* [74]. For this reason, it has been suggested that these prokaryotes could be used to remediate pollutions by alkaline earth elements [26]. If such high accumulation abilities were proven for these ACC-producing MTB, they may similarly be suitable for designing new remediation strategies or other applications under physicochemical conditions different from those allowing the use of cyanobacteria [75]. In the light of our data, it is still unclear how ACC-containing vesicles form and how cytosolic conditions initiate the formation of ACC. However, similarly to what has been shown for three strains of cyanobacteria [76] and for *Achromatium* [12], we showed that Alphaproteobacteria MTB also form Ca-carbonates intracellularly in solutions undersaturated with respect to ACC phases. In other words, these extracellular conditions are thermodynamically unfavourable to mineral precipitation, which indicates that ACC formation in MTB

is an active process and costs energy to the cell to maintain an intracellular environment supersaturated with ACC, most likely within the membrane-enclosed compartment observed by CEMOVIS.

TEM observations provided additional information on the biogenesis of these inclusions. During cell division, each daughter cell systematically harboured one significantly smaller ACC inclusion in the vicinity of the septum, that remained at one cell pole once cells detached. Interestingly, a similar connection between ACC biomineralization and cell division was observed in cyanobacteria species belonging to the *Thermosynechococcus elongatus* BP-1 clade [23]. These observations raise questions about the formation, inheritance and maintenance of the polarity of the cells, that of the magnetosome chain and ACC inclusions over generations. Indeed, it is known that magnetosomes formation is a complex process where chains of magnetosome particles are concatenated, positioned and segregated by a multi-partite cytoskeletal network, called the magnetoskeleton [77, 78]. The atypical MGC found in the genome of ACC-producing MTB could be an indication of a specific adaptation of these bacteria to produce straight magnetosome chains in such a crowded cytoplasm. Monotrichously flagellated MTB developed specific dividing strategies or sensory apparatus to keep a sustainable magnetotaxis and produce two daughter cells with a similar



magnetic polarity, *i.e.* swimming in the same direction along magnetic field lines [79]. Here, in ACC-producing Alphaproteobacteria, the flagellum was always observed at the oldest pole where the largest and likely oldest ACC inclusion stands. This suggests that similarly to *Magnetovibrio blakemorei* strain MV-1, they divide according to a

scheme whereby the newly synthesized flagellum emerges from the mother pole initially devoid of a flagellum [79]. This represents a most common dividing scheme similar to that observed in *Caulobacter crescentus* [80]. In strain MV-1, all daughter cells swim in the same direction (north-seeking), so it was suggested that the flagellum pushes the



◀ **Fig. 6 Phylogenetic and magnetosome gene cluster (MGC) analyses of ACC-producing MTB isolated from sediment samples of Lake Pavin.** **a** Maximum-likelihood tree of the Rhodospirillaceae family (NCBI taxonomy) based on the 16S rRNA gene and rooted with representative members of the Acetobacteraceae (grey group). Branch length represents the number of substitutions per site. Bootstrap values were estimated with a non-parametric bootstrap approach and 500 replicates. Representative MTB species and ACC producing MTB are in bold. The OTU to which the clone CCP-1 was affiliated is in dark blue. **b** MGC organization of the ACC-producing MTB clone CCP-1 representing OTU1. All genes homologous to any known magnetosome gene are coloured in black. Any gene with unknown function conserved in the vicinity of other MGCs is highlighted in light blue. The map of the contig was drawn to scale and its sequences can be retrieved under the Genbank accession number MT411893. Main operons organisation described in *Magnetospirillum* species [5] are symbolized with arrows above the map. **c** Comparative analysis of the MGCs from the ACC producing clone CCP-1 and different representative magnetotactic Rhodospirillaceae strains previously reviewed in detail in Monteil et al. [90]. (AMB-1: *Magnetospirillum magneticum*, MSR-1: *Magnetospirillum gryphiswaldense*, LM-1: *Ca. Magneticavibrio boulderlitore*, MV-1: *Magnetovibrio blakemorei*, PR-1: *Ca. Terasakiella magnetica*, QH-2: *Ca. Magnetospira* sp.). MGCs were organized according to the phylogeny based on MTB 16S rRNA gene sequences, rooted with the sequence of *Magnetococcus marinus* strain MC-1 (NR\_074371.1). The arrows symbolize operons described by Uebe and Schüler [5]; they were drawn to scale and the direction symbolizes the relative position of genes within the operons in respect to that described in species of the *Magnetospirillum* genus. Dotted lines symbolize continuous genomic regions and were not drawn to scale, while slashes represent contigs edges.

cell body for one half of the population while pulling it for the other half of the population. In contrast, magnetic enrichments of ACC-producing MTB populations collected from the shore of Lake Pavin revealed a similar fraction of south-seeking and north-seeking cells. This observation suggests that for these MTB, two daughter cells swim in opposite direction along magnetic field lines: the cell inheriting the ancient flagellum will keep swimming in the same direction than the mother cell, while the cell inheriting the newly synthesized flagellum will swim toward the opposite direction. This observation is of ecological significance since it means that these population of MTB use the magnetic field only as an axis of motility. Their chemotactic machinery is then responsible for their stabilization in their optimal habitat [81].

Magnetotaxis is not the only strategy developed by microorganisms to facilitate their vertical motility in the water column. For instance, some microorganisms living in anoxic environments developed a negative phototactic response to the shorter wavelengths of visible light that penetrate the deepest in the water column [82]. This behaviour, allowed by specific photoreceptors, drives these microorganisms toward and into the anaerobic zone of aquatic habitats where they are found at their highest abundance. Similarly, gas vesicles formed by some organisms are used as positive or negative buoyant to perform

vertical migrations in the water column [83]. For some cyanobacteria, gas vesicles increase their residence time in the euphotic zone and are responsible for surface water-blooms [84]. May ACC inclusions contribute to the vertical motility of these MTB in the water column? The role of Ca-carbonate inclusions in the vertical motility of bacteria has been postulated for *Achromatium* as well as cyanobacteria [13, 17, 19, 29]. Interestingly, the ACC-producing MTB described here had a magnetotactic behaviour different from that usually observed for environmental magnetically-responsive microorganisms. Indeed, they did not aggregate at the edge of hanging drops after their magnetic enrichment from aquatic samples. Instead, cells settled down at the bottom of the drops, swimming along the magnetic field lines applied and displaying a back and reverse motility. Similarly, when deposited between a microscope slide and a coverslip, cells were systematically observed swimming in the deepest part of the preparation. We showed that ACC inclusions could occupy up to two-thirds of the cytoplasm, representing a considerable increase of cell negative buoyancy. This indicates the potential of ACC to serve as ballasts and could represent an adaptation to a benthic lifestyle, cells adjusting their vertical positioning using their flagellum. It is possible that this process functions in coordination with magnetotaxis where the axis of motility and orientation of the cell would be directed by the magnetosomes chain while the direction of motility would be given by gravitaxis associated with ACC inclusions.

This unique behaviour, the potential ACC loss upon standard TEM sample preparation and the difficulty to observe their magnetosomes due to the electron dense ACC inclusions filling the cytoplasm, could explain why these microorganisms have been overlooked so far. In some samples, these bacteria could reach a cell density above  $10^5$  cells/mL but yet remained invisible when standard protocols were used to quantify MTB [63]. Recently, it was shown that the adaptation of new protocols for the sampling, magnetic enrichment and observation allowed the discovery of new magnetically-responsive microorganisms [85–87]. It is thus important to permanently reassess how to observe magnetotactic organisms to unravel their whole diversity. Here, the new ACC-accumulating microorganisms were discovered owing to the observation of an unusual magnetotactic behaviour that gives the opportunity to concentrate rare organisms from complex communities. This double biomineralization may be more widespread than we currently think. Indeed, some Ba- and Ca-rich inclusions were observed in environmental MTB collected in the Seine River (France) [88] and another study reported the presence of Ca-rich granules occupying most of the intracellular volume of the giant freshwater magnetotactic rod-shaped strain GRS-1, affiliated with the Gammaproteobacteria [89],

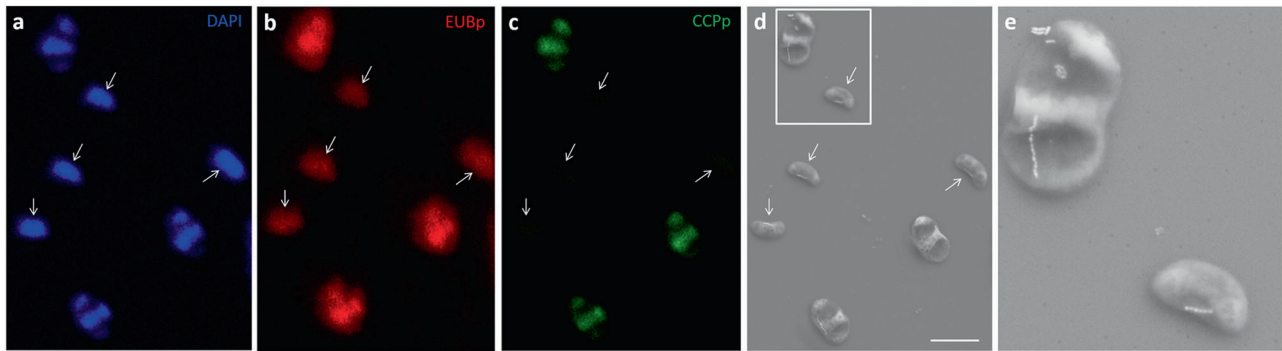


**Fig. 7** Fluorescence in situ hybridization (FISH) of magnetically concentrated MTB from the sediments of Lake Pavin. The specific oligonucleotide rRNA probe (CCPp) was used to authenticate the 16S rRNA gene sequence of MTB with CaCO<sub>3</sub> inclusions. **a** Fluorescence microscope image of three rods with large inclusions and four smaller vibrio (shown by white arrows) stained with 4',6-diamidino-2-phenylindole (DAPI). **b** Fluorescence microscope image of the same cells

hybridized with the Bacteria specific probe Eubp. Note that both cell morphotypes fluoresce with this probe. **c** Fluorescence microscope image of the same cells hybridized with the CCP-specific probe. Only cells with large inclusions fluoresce with this probe. **d** Scanning electron microscope (SEM) image of the same cells showing their ultrastructure and magnetosomes. White frame indicates the position of the SEM image in panel **e**. Scale bar represents 2 μm.

although none of these studies confirmed or infirmed that these inclusions are made of amorphous or crystalline carbonates. Presuming that the above-mentioned inclusions were amorphous carbonate phases, all these observations suggest the phylogenetic diversity of ACC-producing MTB may be even higher than what is reported here. Indeed, although strain GRS-1 and *Achromatium* belong to the same order, *i.e.* Thiotrichales, both strains remain phylogenetically distant [89]. Besides finding the origin of such processes, future comparative genomics and molecular phylogenies will infer the ancestry and evolutionary forces associated to their diversification.

**Acknowledgements** This work was supported by the CNRS: “Programme national Ecosphère Continentale et Côtière (EC2CO)” (BACCARAT2 – N°13068) and the French National Research Agency (SIGMAG: ANR-18-CE31-0003 and PHOSTORE: ANR-19-CE01-0005-02). CCB was supported by the Frontières de l’Innovation en Recherche et Éducation (FIRE) Ph.D. programme from the Centre de Recherches Interdisciplinaires (CRI). Support for the confocal microscope was provided by the Région Provence Alpes Côte d’Azur, Conseil Général des Bouches du Rhône, French Ministry of Research, CNRS and Commissariat à l’Energie Atomique et aux Energies Alternatives. We acknowledge the Institut de Radioprotection et de Sûreté Nucléaire (IRSN) at CEA Cadarache for the access of the transmission electron microscope Tecnai G<sup>2</sup> BioTWIN. We are grateful to the INRA MIGALE bioinformatics platform (<http://migale.jouy.inra.fr>) for providing computational resources. We thank Stefan Stanescu and Rachid Belkhou for user support on the HERMES STXM beamline at Synchrotron SOLEIL, Fériel Skouri-Panet and Cynthia Travert for user support on the IMPMC Biology facility, Jean-Michel Guigner for user support on the IMPMC TEM facility and Imène Esteve, Béatrice Doisneau and Stéphanie Delbrel for user support on the IMPMC SEM facility. We are grateful to the genomic platform at the Institut de Microbiologie de la Méditerranée (IMM) and to Yann Denis for helpful advices. We thank Alexis Canette from the Service de Microscopie Electronique at the IBPS for his help in CEMOVIS sample preparation. We thank Maria Pilar Asta and

Alejandro Fernandez-Martinez from ISTERre, University Grenoble Alpes, for providing a reference ACC sample.

### Compliance with ethical standards

**Conflict of interest** The authors declare that they have no conflict of interest.

**Publisher’s note** Springer Nature remains neutral with regard to jurisdictional claims in published maps and institutional affiliations.

### References

- Weiner S, Dove PM. An overview of biomineralization processes and the problem of the vital effect. *Rev Miner Geochem.* 2003;54:1–29.
- Benzerara K, Miot J, Morin G, Ona-Nguema G, Skouri-Panet F, Féraud C. Significance, mechanisms and environmental implications of microbial biomineralization. *Comptes Rendus Geosci.* 2011;343:160–7.
- Lowenstam HA. Minerals formed by organisms. *Science.* 1981;211:1126–31.
- Blakemore R. Magnetotactic bacteria. *Science.* 1975;190:377–9.
- Uebe R, Schüler D. Magnetosome biogenesis in magnetotactic bacteria. *Nat Rev Microbiol.* 2016;14:621–37.
- Grant CR, Wan J, Komeili A. Organelle formation in bacteria and archaea. *Annu Rev Cell Dev Biol.* 2018;34:217–38.
- Schewiakoff W. Über einen neuen bacterienähnlichen organismus des Süßwassers. *Heidelb Habilit.* 1893;1–38.
- West GS, Griffiths BM. The lime-sulphur bacteria of the genus *hillhousia*. *Ann Bot.* 1913;os-27:83–91.
- Head IM, Gray ND, Clarke KJ, Pickup RW, Jones JG. The phylogenetic position and ultrastructure of the uncultured bacterium *Achromatium oxaliferum*. *Microbiol Read Engl.* 1996;142(Pt 9):2341–54.
- Salman V, Yang T, Berben T, Klein F, Angert E, Teske A. Calcite-accumulating large sulfur bacteria of the genus *Achromatium* in Sippewissett Salt Marsh. *ISME J.* 2015;9:2503–14.
- Mansor M, Hamilton TL, Fantle MS, Macalady J. Metabolic diversity and ecological niches of *Achromatium* populations

- revealed with single-cell genomic sequencing. *Front Microbiol.* 2015;6:822.
12. Gray N, Head I. The family achromatiaceae. In: Rosenberg E, DeLong EF, Lory S, Stackebrandt E, Thompson F, editors. *The Prokaryotes: Gammaproteobacteria*. Berlin, Heidelberg: Springer; 2014. p. 1–14.
  13. Head IM, Gray ND, Howarth R, Pickup RW, Clarke KJ, Jones JG. *Achromatium oxaliferum* Understanding the Unmistakable. In: Schink B, editor. *Advances in microbial ecology*. Boston, MA: Springer US; 2000. p. 1–40.
  14. Babenzien H-D, Sass H. The sediment-water interface—habitat of the unusual bacterium *Achromatium oxaliferum*. *Adv Limnol.* 1996;48:247–51.
  15. Gray ND, Pickup RW, Jones JG, Head IM. Ecophysiological evidence that achromatium oxaliferum is responsible for the oxidation of reduced sulfur species to sulfate in a freshwater sediment. *Appl Environ Microbiol.* 1997;63:1905–10.
  16. Gray ND, Howarth R, Pickup RW, Jones JG, Head IM. Substrate uptake by uncultured bacteria from the genus *Achromatium* determined by microautoradiography. *Appl Environ Microbiol.* 1999;65:5100–6.
  17. Babenzien H-D. *Achromatium oxaliferum* and its ecological niche. *Zentralblatt Für Mikrobiol.* 1991;146:41–49.
  18. Gray ND, Comaskey D, Miskin IP, Pickup RW, Suzuki K, Head IM. Adaptation of sympatric *Achromatium* spp. to different redox conditions as a mechanism for coexistence of functionally similar sulphur bacteria. *Environ Microbiol.* 2004;6:669–77.
  19. Couradeau E, Benzerara K, Gérard E, Moreira D, Bernard S, Brown GE, et al. An early-branching microbialite cyanobacterium forms intracellular carbonates. *Science.* 2012;336:459–62.
  20. Cam N, Benzerara K, Georgelin T, Jaber M, Lambert J-F, Poinot M, et al. Selective Uptake of Alkaline Earth Metals by Cyanobacteria Forming Intracellular Carbonates. *Environ Sci Technol.* 2016;50:11654–62.
  21. Blondeau M, Sachse M, Boulogne C, Gillet C, Guigner J-M, Skouri-Panet F, et al. Amorphous calcium carbonate granules form within an intracellular compartment in calcifying cyanobacteria. *Front Microbiol.* 2018;9:1768.
  22. Li J, Margaret Oliver I, Cam N, Boudier T, Blondeau M, Leroy E, et al. Biom mineralization patterns of intracellular carbonatogenesis in cyanobacteria: molecular hypotheses. *Minerals.* 2016;6:10.
  23. Benzerara K, Skouri-Panet F, Li J, Féraud C, Gugger M, Laurent T, et al. Intracellular Ca-carbonate biomineralization is widespread in cyanobacteria. *Proc Natl Acad Sci USA.* 2014;111:10933–8.
  24. Bradley JA, Daille LK, Trivedi CB, Bojanowski CL, Stamps BW, Stevenson BS, et al. Carbonate-rich dendrolitic cones: insights into a modern analog for incipient microbialite formation, Little Hot Creek, Long Valley Caldera, California. *NPJ Biofilms Microbiomes.* 2017;3:32.
  25. Moreira D, Tavera R, Benzerara K, Skouri-Panet F, Couradeau E, Gérard E, et al. Description of *Gloeomargarita lithophora* gen. nov., sp. nov., a thylakoid-bearing, basal-branching cyanobacterium with intracellular carbonates, and proposal for *Gloeomargaritales* ord. nov. *Int J Syst Evol Microbiol.* 2017;67:653–8.
  26. Mehta N, Benzerara K, Kocar BD, Chapon V. Sequestration of radionuclides radium-226 and strontium-90 by cyanobacteria forming intracellular calcium carbonates. *Environ Sci Technol.* 2019;53:12639–47.
  27. Ponce-Toledo RI, Deschamps P, López-García P, Zivanovic Y, Benzerara K, Moreira D. An early-branching freshwater cyanobacterium at the origin of plastids. *Curr Biol CB.* 2017;27:386–91.
  28. la Rivière JWM, Schmidt K. Morphologically Conspicuous Sulfur-Oxidizing Eubacteria. In: Starr MP, Stolp H, Trüper HG, Balows A, Schlegel HG, editors. *The prokaryotes: a handbook on habitats, isolation, and identification of bacteria*. Berlin Heidelberg: Springer; 1981. p. 1037–48.
  29. Gray ND. The unique role of intracellular calcification in the genus *achromatium*. In: Shively JM, editor. *Inclusions in prokaryotes*. Berlin, Heidelberg: Springer; 2006. p. 299–309.
  30. Miot J, Jezequel D, Benzerara K, Cordier L, Rivas-Lamelo S, Skouri-Panet F, et al. Mineralogical diversity in lake pavin: connections with water column chemistry and biomineralization processes. *Minerals.* 2016;6:UNSP 24.
  31. Podda F, Michard G. Mesure colorimétrique de l'alcalinité. *Comptes Rendus Acad Sci - Sér II.* 1994;319:651–7.
  32. Sarazin G, Michard G, Prevot F. A rapid and accurate spectroscopic method for alkalinity measurements in sea water samples. *Water Res.* 1999;33:290–4.
  33. Zeyen N, Daval D, Lopez-Garcia P, Moreira D, Gaillardet J, Benzerara K. Geochemical conditions allowing the formation of modern lacustrine microbialites. *Procedia Earth Planet Sci.* 2017;17:380–3.
  34. Purgstaller B, Goetschl KE, Mavromatis V, Dietzel M. Solubility investigations in the amorphous calcium magnesium carbonate system. *CrystEngComm.* 2018;21:155–64.
  35. Schüler D. The biomineralization of magnetosomes in *Magnetospirillum gryphiswaldense*. *Int Microbiol J Span Soc Microbiol.* 2002;5:209–14.
  36. Lane DJ. 16S/23S sequencing. In: Stackebrandt E, Goodfellow M, editor. *Nucleic acid techniques in bacterial systematics*. New York: John Wiley & Sons; 1991. p. 115–75.
  37. Altschul SF, Madden TL, Schaffer AA, Zhang JH, Zhang Z, Miller W, et al. Gapped BLAST and PSI-BLAST: a new generation of protein database search programs. *Nucleic Acids Res.* 1997;25:3389–402.
  38. Edgar RC. UCHIME2: improved chimera prediction for amplicon sequencing. *bioRxiv* 2016. <https://www.biorxiv.org/content/10.1101/074252v1>.
  39. Gascuel O. BIONJ: an improved version of the NJ algorithm based on a simple model of sequence data. *Mol Biol Evol.* 1997;14:685–95.
  40. Katoh K, Standley DM. MAFFT multiple sequence alignment software version 7: improvements in performance and usability. *Mol Biol Evol.* 2013;30:772–80.
  41. Talavera G, Castresana J. Improvement of phylogenies after removing divergent and ambiguously aligned blocks from protein sequence alignments. *Syst Biol.* 2007;56:564–77.
  42. Nguyen L-T, Schmidt HA, von Haeseler A, Minh BQ. IQ-TREE: a fast and effective stochastic algorithm for estimating maximum-likelihood phylogenies. *Mol Biol Evol.* 2015;32:268–74.
  43. Kalyaanamoorthy S, Minh BQ, Wong TKF, von Haeseler A, Jermini LS. ModelFinder: fast model selection for accurate phylogenetic estimates. *Nat Methods.* 2017;14:587–9.
  44. Pernthaler J, Glockner FO, Schonhuber W, Amann R. Fluorescence in situ hybridization (FISH) with rRNA-targeted oligonucleotide probes. *Methods Microbiol Vol 30.* 2001; 30:207–26.
  45. Cole JR, Chai B, Marsh TL, Farris RJ, Wang Q, Kulam SA, et al. The Ribosomal Database Project (RDP-II): previewing a new autoaligner that allows regular updates and the new prokaryotic taxonomy. *Nucleic Acids Res.* 2003;31:442–3.
  46. Rivas-Lamelo S, Benzerara K, Lefèvre CT, Jézéquel D, Menguy N, Viollier E, et al. Magnetotactic bacteria as a new model for P sequestration in the ferruginous Lake Pavin. *Geochem Perspect Lett.* 2017;5:35–41.
  47. Bolger AM, Lohse M, Usadel B. Trimmomatic: a flexible trimmer for Illumina sequence data. *Bioinforma Oxf Engl.* 2014;30:2114–20.
  48. Seemann T. Prokka: rapid prokaryotic genome annotation. *Bioinformatics.* 2014;30:2068–9.
  49. Parks DH, Imelfort M, Skennerton CT, Hugenholtz P, Tyson GW. CheckM: assessing the quality of microbial genomes recovered

- from isolates, single cells, and metagenomes. *Genome Res.* 2015;25:1043–55.
50. Belkhou R, Stanescu S, Swaraj S, Besson A, Ledoux M, Hajlaoui M, et al. HERMES: a soft X-ray beamline dedicated to X-ray microscopy. *J Synchrotron Radiat.* 2015;22:968–79.
  51. Swaraj S, Belkhou R, Stanescu S, Rioult M, Besson A, Hitchcock AP. Performance of the HERMES beamline at the carbon K-edge. *J Phys Conf Ser.* 2017;849:012046.
  52. Le Nagard L, Zhu X, Yuan H, Benzerara K, Bazylinski DA, Fradin C, et al. Magnetite magnetosome biomineralization in *Magnetospirillum magneticum* strain AMB-1: A time course study. *Chem Geol.* 2019;530:119348.
  53. Cosmidis J, Benzerara K. Soft x-ray scanning transmission spectro-microscopy. In: Elaine DiMasi, Laurie B. Gower, editors. *Biomineralization sourcebook: characterization of biominerals and biomimetic materials.* CRC Press; 2014.
  54. Lefèvre CT. Genomic insights into the early-diverging magnetotactic bacteria. *Environ Microbiol.* 2016;18:1–3.
  55. Benzerara K, Yoon TH, Tyliczszak T, Constantz B, Spormann AM, Brown GE. Scanning transmission X-ray microscopy study of microbial calcification. *Geobiology.* 2004;2:249–59.
  56. Michard G, Viollier E, Jézéquel D, Sarazin G. Geochemical study of a crater lake: Pavin Lake, France — Identification, location and quantification of the chemical reactions in the lake. *Chem Geol.* 1994;115:103–15.
  57. Konstantinidis KT, Rosselló-Móra R, Amann R. Uncultivated microbes in need of their own taxonomy. *ISME J.* 2017;11:2399–406.
  58. Cai H, Wang Y, Xu H, Yan Z, Jia B, Majid Maszenan A, et al. *Niveispirillum cyanobacteriorum* sp. nov., a nitrogen-fixing bacterium isolated from cyanobacterial aggregates in a eutrophic lake. *Int J Syst Evol Microbiol.* 2015;65:2537–41.
  59. Zhang D, Yang H, Zhang W, Huang Z, Liu S-J. *Rhodocista pekingensis* sp. nov., a cyst-forming phototrophic bacterium from a municipal wastewater treatment plant. *Int J Syst Evol Microbiol.* 2003;53:1111–4.
  60. Chung EJ, Park TS, Kim KH, Jeon CO, Lee H-I, Chang W-S, et al. *Nitrospirillum irinus* sp. nov., a diazotrophic bacterium isolated from the rhizosphere soil of Iris and emended description of the genus *Nitrospirillum*. *Antonie Van Leeuwenhoek.* 2015;108:721–9.
  61. Bashan Y, Holguin G, de-Bashan LE. *Azospirillum*-plant relationships: physiological, molecular, agricultural, and environmental advances (1997-2003). *Can J Microbiol.* 2004;50:521–77.
  62. Guo Q, Zhou Z, Zhang L, Zhang C, Chen M, Wang B, et al. *Skermanella pratensis* sp. nov., isolated from meadow soil, and emended description of the genus *Skermanella*. *Int J Syst Evol Microbiol.* 2020;70:1605–9.
  63. Lefèvre CT, Bazylinski DA. Ecology, diversity, and evolution of magnetotactic bacteria. *Microbiol Mol Biol Rev.* 2013;77:497–526.
  64. Lin W, Bazylinski DA, Xiao T, Wu L-F, Pan Y. Life with compass: diversity and biogeography of magnetotactic bacteria. *Environ Microbiol.* 2014;16:2646–58.
  65. Bazylinski DA, Dean AJ, Williams TJ, Long LK, Middleton SL, Dubbels BL. Chemolithoautotrophy in the marine, magnetotactic bacterial strains MV-1 and MV-2. *Arch Microbiol.* 2004;182:373–87.
  66. Schultheiss D, Handrick R, Jendrossek D, Hanzlik M, Schüler D. The presumptive magnetosome protein Mms16 is a poly(3-hydroxybutyrate) granule-bound protein (phasin) in *Magnetospirillum gryphiswaldense*. *J Bacteriol.* 2005;187:2416–25.
  67. Lefèvre CT, Bernadac A, Yu-Zhang K, Pradel N, Wu L-F. Isolation and characterization of a magnetotactic bacterial culture from the Mediterranean Sea. *Environ Microbiol.* 2009;11:1646–57.
  68. Qian X-X, Liu J, Menguy N, Li J, Alberto F, Teng Z, et al. Identification of novel species of marine magnetotactic bacteria affiliated with Nitrospirae phylum. *Environ Microbiol Rep.* 2019;11:330–7.
  69. Lefèvre CT, Frankel RB, Abreu F, Lins U, Bazylinski DA. Culture-independent characterization of a novel, uncultivated magnetotactic member of the Nitrospirae phylum. *Environ Microbiol.* 2011;13:538–49.
  70. Cox BL, Popa R, Bazylinski DA, Lanoil B, Douglas S, Belz A, et al. Organization and elemental analysis of P-, S-, and Fe-rich inclusions in a population of freshwater magnetococci. *Geomicrobiol J.* 2002;19:387–406.
  71. Byrne ME, Ball DA, Guerquin-Kern J-L, Rouiller I, Wu T-D, Downing KH, et al. *Desulfovibrio magneticus* RS-1 contains an iron- and phosphorus-rich organelle distinct from its bullet-shaped magnetosomes. *Proc Natl Acad Sci USA.* 2010;107:12263–8.
  72. Keim CN, Solórzano G, Farina M, Lins U. Intracellular inclusions of uncultured magnetotactic bacteria. *Int Microbiol J Span Soc Microbiol.* 2005;8:111–7.
  73. Schulz-Vogt HN, Pollehne F, Jürgens K, Arz HW, Beier S, Bahlo R, et al. Effect of large magnetotactic bacteria with polyphosphate inclusions on the phosphate profile of the suboxic zone in the Black Sea. *ISME J.* 2019;13:1198–208.
  74. Blondeau M, Benzerara K, Ferard C, Guigner J-M, Poinot M, Coutaud M, et al. Impact of the cyanobacterium *Gloeomargarita lithophora* on the geochemical cycles of Sr and Ba. *Chem Geol.* 2018;483:88–97.
  75. Anbu P, Kang C-H, Shin Y-J, So J-S. Formations of calcium carbonate minerals by bacteria and its multiple applications. *Springerplus.* 2016;5:250.
  76. Cam N, Benzerara K, Georgelin T, Jaber M, Lambert J-F, Poinot M, et al. Cyanobacterial formation of intracellular Ca-carbonates in undersaturated solutions. *Geobiology.* 2018;16:49–61.
  77. Toro-Nahuelpan M, Müller FD, Klumpp S, Plietzko JM, Bramkamp M, Schüler D. Segregation of prokaryotic magnetosomes organelles is driven by treadmilling of a dynamic actin-like MamK filament. *BMC Biol.* 2016;14:88.
  78. Toro-Nahuelpan M, Giacomelli G, Raschdorf O, Borg S, Plietzko JM, Bramkamp M, et al. MamY is a membrane-bound protein that aligns magnetosomes and the motility axis of helical magnetotactic bacteria. *Nat Microbiol.* 2019;4:1978–89.
  79. Lefèvre CT, Bennet M, Klumpp S, Faivre D. Positioning the flagellum at the center of a dividing cell to combine bacterial division with magnetic polarity. *mBio.* 2015;6:e02286.
  80. Judd EM, Ryan KR, Moerner WE, Shapiro L, McAdams HH. Fluorescence bleaching reveals asymmetric compartment formation prior to cell division in *Caulobacter*. *Proc Natl Acad Sci USA.* 2003;100:8235–40.
  81. Klumpp S, Lefèvre CT, Bennet M, Faivre D. Swimming with magnets: From biological organisms to synthetic devices. *Phys Rep.* 2019;789:1–54.
  82. Lefèvre CT, Abreu F, Lins U, Bazylinski DA. Nonmagnetotactic multicellular prokaryotes from low-saline, nonmarine aquatic environments and their unusual negative phototactic behavior. *Appl Environ Microbiol.* 2010;76:3220–7.
  83. Walsby AE. Gas vesicles. *Microbiol Rev.* 1994;58:94–144.
  84. Walsby A. The properties and buoyancy-providing role of gas vacuoles in *trichodesmium ehrenbergi*. *Br Phycol J.* 1978;13:103–16.
  85. Monteil CL, Menguy N, Prévéral S, Warren A, Pignol D, Lefèvre CT. Accumulation and dissolution of magnetite crystals in a magnetically responsive ciliate. *Appl Environ Microbiol.* 2018;84:e02865-17.
  86. Monteil CL, Vallenet D, Menguy N, Benzerara K, Barbe V, Fouteau S, et al. Ectosymbiotic bacteria at the origin of magnetoreception in a marine protist. *Nat Microbiol.* 2019;4:1088–95.

- 
87. Leão P, Nagard LL, Yuan H, Cypriano J, Silva-Neto ID, Bazylinski DA, et al. Magnetosome magnetite biomineralization in a flagellated protist: evidence for an early evolutionary origin for magnetoreception in eukaryotes. *Environ Microbiol.* 2020;22:1495–506.
  88. Isambert A, Menguy N, Larquet E, Guyot F, Valet J-P. Transmission electron microscopy study of magnetites in a freshwater population of magnetotactic bacteria. *Am Miner.* 2007;92:621–30.
  89. Taoka A, Kondo J, Oestreicher Z, Fukumori Y. Characterization of uncultured giant rod-shaped magnetotactic Gammaproteobacteria from a freshwater pond in Kanazawa, Japan. *Microbiol Read Engl.* 2014;160:2226–34.
  90. Monteil CL, Perrière G, Menguy N, Ginet N, Alonso B, Waisbord N, et al. Genomic study of a novel magnetotactic Alphaproteobacteria uncovers the multiple ancestry of magnetotaxis. *Environ Microbiol.* 2018;20:4415–30.

## 2.3 Improvement of the magnetotactic bacteria collection with a higher vertical resolution sampling and a proxy to detect their abundance - [Busigny et al. \(2021\)](#)

In the water column, [MTB](#) are localized in the vicinity of sharp chemical gradients. In order to describe the precise [MTB](#) distribution as a function of different chemical conditions in these gradients, a high resolution sampling method has to be used. In [Busigny et al. \(2021\)](#), a study mainly focused on the development of sampling methods for the recovery of high amount of [MTB](#), such a method was developed and consisted of an online pumping system with a high spatial resolution along the water column. This study also lead to the development of a technique allowing *in situ* physico-chemical measurements and the highlight of the conductivity as proxy for the detection of the [MTB](#) maximum abundance in the water column.

Following is an overview of the article problematic and different methods for an efficient recovery of the [MTB](#) in Lake Pavin:

In the frame of the ANR project SIGMAG (Signature of magnetite produced by magnetotactic bacteria: chemical and isotopic perspectives), a high amount of [MTB](#) was required to investigate the magnetic, chemical and isotopic features of environmental magnetosomes. Therefore, efforts were made to gather and compare different methods to accumulate high amounts of [MTB](#), either in the water column or sediments of Lake Pavin.

Several methods were elaborated by using the magnetotactic and aerotactic behaviors of the [MTB](#). The sediments harbor a really diverse and concentrated pool of [MTB](#) but a great amount of magnetic particles is present and can be magnetically concentrated alongside the [MTB](#). A migration track device was elaborated allowing the separation of the magnetic particles from the north-seeking [MTB](#) with an average efficiency of 72 %.

In the water column, one of the issues involve the commonly used sampling technique (i.e. Niskin bottle) which take a long time to gather large volume of water and which possesses a low sampling resolution. In addition, vertical perturbations of the chemical gradients with time can shift the [MTB](#) peak of abundance, and thus represents another problematic encountered in the water column. An online pumping system helped increase both the water collection speed rate (x12) and the vertical resolution sampling (up to x10). The water recovered from the water column was contained in 20 L Nalgene, and thanks to the aerotactic behavior of the [MTB](#), a concentration method was developed with an average [MTB](#) recovery efficiency of 80 %. In order to deal with the problem of vertical perturbations, some tests were made to find physicochemical parameters, directly measurable *in situ*, correlated with the [MTB](#) peak of abundance. The [MTB](#) peak of abundance was found to not occur at oxygen concentrations superior than 2  $\mu\text{mol.L}^{-1}$ ,

## Chapter 2. Vertical structure of magnetotactic bacteria populations in the water column of Lake Pavin

---

and in addition the conductivity was found to be a good proxy to track this peak with average values of  $65.8 \mu\text{S}\cdot\text{cm}^{-1}$ .

Using several vertical **MTB** profiles over different seasons, the study also highlighted the systematic observation of the **MTB** under the oxygen detection limit but also their abundance peak near the maximum decrease of the redox potential and the peak of turbidity (mainly iron phosphate precipitates).

My contribution in this study mainly consisted in my participation to the field trips and in measurements of chemical vertical profiles in the water column.

The development in the water column of this improved sampling technique is of great importance for the detection and the precise analysis of the **MTB** population distribution in the water column as a function of the different environmental parameters. This **MTB** population analysis is at the base of the main work of my thesis presented below.

See next the [Busigny et al. \(2021\)](#) article and in appendices the [supplementary information](#).

# Mass collection of magnetotactic bacteria from the permanently stratified ferruginous Lake Pavin, France

Vincent Busigny<sup>1,2\*</sup>, François P. Mathon,<sup>1,3</sup>  
Didier Jézéquel,<sup>1,4</sup> Cécile C. Bidaud,<sup>5</sup> Eric Viollier,<sup>1</sup>  
Gérard Bardoux,<sup>1</sup> Jean-Jacques Bourrand,<sup>1</sup>  
Karim Benzerara,<sup>5</sup> Elodie Duprat<sup>1,5</sup>, Nicolas Menguy,<sup>5</sup>  
Caroline L. Monteil<sup>3</sup> and Christopher T. Lefevre<sup>1,3\*</sup>

<sup>1</sup>Université de Paris, Institut de Physique du Globe de Paris, CNRS, Paris, F-75005, France.

<sup>2</sup>Institut Universitaire de France, Paris, 75005, France.

<sup>3</sup>Aix-Marseille University, CNRS, CEA, UMR7265 Institute of Biosciences and Biotechnologies of Aix-Marseille, CEA Cadarache, Saint-Paul-lez-Durance, F-13108, France.

<sup>4</sup>INRAE & Université Savoie Mont Blanc, UMR CARTELE, Thonon-les-Bains, 74200, France.

<sup>5</sup>Sorbonne Université, Muséum National d'Histoire Naturelle, UMR CNRS 7590, IRD. Institut de Minéralogie, de Physique des Matériaux et de Cosmochimie (IMPMC), Paris, France.

## Summary

**Obtaining high biomass yields of specific microorganisms for culture-independent approaches is a challenge faced by scientists studying organism's recalcitrant to laboratory conditions and culture. This difficulty is highly decreased when studying magnetotactic bacteria (MTB) since their unique behaviour allows their enrichment and purification from other microorganisms present in aquatic environments. Here, we use Lake Pavin, a permanently stratified lake in the French Massif Central, as a natural laboratory to optimize collection and concentration of MTB that thrive in the water column and sediments. A method is presented to separate MTB from highly abundant abiotic magnetic particles in the sediment of this crater lake. For the water column, different sampling approaches are compared such as *in situ* collection using a Niskin bottle and online pumping. By monitoring several physicochemical parameters of the water column, we identify the**

**ecological niche where MTB live. Then, by focusing our sampling at the peak of MTB abundance, we show that the online pumping system is the most efficient for fast recovering of large volumes of water at a high spatial resolution, which is necessary considering the sharp physicochemical gradients observed in the water column. Taking advantage of aerotactic and magnetic MTB properties, we present an efficient method for MTB concentration from large volumes of water. Our methodology represents a first step for further multidisciplinary investigations of the diversity, metagenomic and ecology of MTB populations in Lake Pavin and elsewhere, as well as chemical and isotopic analyses of their magnetosomes.**

## Introduction

The recent technological advances are increasingly allowing the study of microorganisms using culture-independent approaches in many fields of research. These advances include the development of tools to analyse genomes at the single cell scale, as well as the ultrastructure and/or chemistry of microorganisms (Blainey, 2013). However, some analytical approaches still require high biomass and thus often rely on cultured microorganisms or natural enrichment (e.g. bloom). Magnetotactic bacteria (MTB) represent one example of microorganisms at the origin of numerous interdisciplinary studies using culture-independent approaches over the last decades mainly because most strains are recalcitrant to growth (Abreu *et al.*, 2007; Lefèvre and Bazylinski, 2013; Lin *et al.*, 2017). For instance, significant progress has been achieved on MTB diversity, chemistry and magnetosome biomineralization based on culture-independent approaches such as single-cell analysis (Jogler *et al.*, 2010; Kolinko *et al.*, 2016), coupled FISH-SEM/TEM (Li *et al.*, 2017, 2019; Kozaieva *et al.*, 2020; Liu *et al.*, 2020; Qian *et al.*, 2020), comprehensive TEM (Li *et al.*, 2015; Zhang *et al.*, 2017; Li *et al.*, 2020a; Li *et al.*, 2020b) and the combination of TEM and synchrotron-based STXM (Li *et al.*, 2020c). MTB can be concentrated and purified magnetically from natural aquatic environments thanks to their magnetosome chain at the origin of their magnetotactic

Received 11 December, 2020; revised 4 March, 2021; accepted 7 March, 2021. \*For correspondence. E-mail busigny@ipgp.fr; christopher.lefevre@cea.fr



behaviour (Bazylnski and Frankel, 2004). Magnetosomes are membrane-enveloped ferrimagnetic nanocrystals, which serve as magnetic field sensors (Blakemore, 1975). Their alignment in linear chains imposes a magnetic moment to the bacteria, which ensures navigation in the weak geomagnetic field along vertical redox gradients (Bazylnski and Frankel, 2004). This behaviour, named magnetotaxis, is based on MTB chemo-aerotactic capability and active swimming motility. It likely represents a selective fitness advantage in their natural habitat, which is the oxic–anoxic transition zone (OATZ) of aquatic ecosystems. Most cultured MTB are micro-aerophilic (Lefèvre *et al.*, 2014). Consequently, sampling for MTB is generally based on the collection of sediment or water samples that comprise the OATZ. MTB present in sediments can be sampled from the shore (Liu *et al.*, 2018), by free diving (Lefèvre *et al.*, 2009), or using a bottom sampler (Kolinko *et al.*, 2013). In contrast, MTB present in the water column of stratified ecosystems have previously been collected using Geopump peristaltic pump (Simmons *et al.*, 2004; Moskowitz *et al.*, 2008), Niskin bottle (Rivas-Lamelo *et al.*, 2017), free-flow bottle or automatic flow injection sampler (Schulz-Vogt *et al.*, 2019).

Their detection in environmental water and sediment samples is relatively easy due to their magnetotactic behaviour. Indeed, MTB can be enriched magnetically by placing a bar magnet adjacent to the outer wall of a bottle filled with environmental sample. If MTB are abundant in the sample, a brownish or greyish-to-white spot containing mainly MTB will form next to the inside of the glass wall closest to the bar magnet. Cells can be easily harvested from the bottle and examined using light microscopy. Few improvements of the magnetic concentration of MTB have been proposed such as (i) a glass apparatus containing a capillary end allowing the concentration of MTB from a large volume of sediment when the apparatus is introduced in a coiled tube that generates a homogenous magnetic field (Lins *et al.*, 2003), (ii) an apparatus containing a separating chamber for an initial enrichment of MTB and a sampling chamber where MTB are further concentrated and harvested (Xiao *et al.*, 2007), (iii) a ‘MTB trap’ where south- and north-seeking MTB are magnetically directed towards the tips of collection tubes, from which they can be conveniently collected for further analyses (Jogler *et al.*, 2009b) and (iv) a MTB column separation, the MTB-CoSe method, that allows collection of magnetotactic cells directly from sediment samples (Koziaeva *et al.*, 2020). The modification of the techniques commonly used for sampling and observation of environmental magnetotactic microorganisms recently allowed to extend our knowledge of the diversity and ecology of magnetotaxis in bacteria (Lin *et al.*, 2018; Monteil *et al.*, 2019, 2021; Monteil and

Lefevre, 2019; Koziaeva *et al.*, 2020). Even if all these techniques allow to get biological material in sufficient concentrations for biodiversity studies, the abundance of bacterial populations recovered is not high enough to properly investigate some important magnetic, chemical and isotopic features of the magnetic minerals they form. These aspects are yet essential to understand the molecular and geochemical biomineralization processes. Indeed, the separation of magnetite from MTB in the laboratory for subsequent Fe isotope analyses requires a minimum of 0.1 mg of magnetite (Amor *et al.*, 2016, 2018). This represents a total amount of MTB of  $\sim 10^{10}$  cells, assuming typically 30 magnetosomes per cell and a magnetosome length of 50 nm. To improve our ability to harvest large amount of MTB from natural environment for multidisciplinary studies, including biological, mineralogical and geochemical analyses, we tested and optimized several approaches to collect and concentrate MTB.

Lake Pavin (Massif Central, France) was selected as a natural laboratory for the following reasons: (i) it is a ferruginous meromictic lake, i.e. permanently stratified with an OATZ located in the water column instead of the sediment (Michard *et al.*, 1994; Aeschbach-Hertig *et al.*, 1999, 2002); (ii) the physicochemical conditions of the lake and associated sediments have been studied extensively, and geochemical cycles are well constrained (Michard *et al.*, 1994; Viollier *et al.*, 1995; Albéric *et al.*, 2000; Schettler *et al.*, 2007; Assayag *et al.*, 2008; Busigny *et al.*, 2014; Cosmidis *et al.*, 2014) and (iii) recent exploratory field trips at Lake Pavin demonstrated that MTB are exceptionally abundant in concentration and biodiversity in the water column and sediments and may contribute to the geochemical cycles of P, Ca and C (Miot *et al.*, 2016; Rivas-Lamelo *et al.*, 2017; Monteil *et al.*, 2021).

Lake Pavin is the youngest crater lake of the Massif Central volcanic area (about 7000 years cal BP; Chapron *et al.*, 2010). It is redox-stratified, with anoxic and ferruginous deep waters extending between 50–55 and 92 m in depth (monimolimnion), and topped by oxic waters (mixolimnion; Cosmidis *et al.*, 2014; Rivas-Lamelo *et al.*, 2017; Berg *et al.*, 2019). The position of the OATZ varies slightly with time in a depth range comprised between 50 and 60 m (Michard *et al.*, 1994; Cosmidis *et al.*, 2014; Rivas-Lamelo *et al.*, 2017; Berg *et al.*, 2019). In the deep waters, ferrous iron ( $\text{Fe(II)}_{\text{aq}}$ ) along with  $\text{NH}_4^+$ , are the main dissolved cations, with concentrations up to 1 mM (Michard *et al.*, 1994; Viollier *et al.*, 1995; Busigny *et al.*, 2014, 2016). Iron is efficiently confined below the oxic-anoxic boundary due to the formation of insoluble ferric iron species,  $\text{Fe(III)}_{\text{s}}$ , by oxidation with  $\text{O}_2$  and other oxidants in the mixolimnion (e.g.,  $\text{NO}_3^-$ ,  $\text{Mn}^{4+}$ ; Lopes *et al.*, 2011). The  $\text{Fe(III)}_{\text{s}}$  particles settle down and

are reduced to soluble Fe(II)<sub>aq</sub> in the anoxic waters and at the lake bottom by reaction with organic matter. Dissolved Fe(II)<sub>aq</sub> then diffuses upward in the water column and is finally re-oxidized to Fe(III) at the redox boundary. This process, known as the 'iron wheel' has been described in details from available data for dissolved and particulate matter in the water column, settling particles collected by sediment traps and sediment cores (Cosmidis *et al.*, 2014; Busigny *et al.*, 2016). Additionally, the lake's water column has remarkably low sulfate concentrations (< 20 µM), which also keep low level of sulfides (Bura-Nakic *et al.*, 2009). The redox boundary fed by a downward flux of dissolved O<sub>2</sub> and other oxidants, and an upward flux of dissolved Fe(II) represents ideal conditions for magnetosome formation by MTB, as observed in similar stratified aquatic environments (Simmons *et al.*, 2004; Schulz-Vogt *et al.*, 2019).

This contribution first presents a method for sampling MTB from the sediments, with particular emphasis on the separation between MTB and abiotic (volcanic) magnetic particles. Then, the global distribution of MTB in the water column of Lake Pavin is presented. The results of several tests for harvesting MTB from the water column are described and compared, including water sampling using Niskin bottles and online pumping system. Finally, a technique for the concentration and isolation of MTB from a large environmental water volume based on magnetotaxis and chemotaxis is presented. Our results allow the identification of optimal physicochemical parameters for the presence of MTB in the water column. This work is paving the way for future multidisciplinary studies of MTB in Lake Pavin and others natural sites.

## Results and discussion

### *Magnetotactic bacteria are abundant and diverse in the sediments of Lake Pavin*

Over the different sampling campaigns performed since 2016 on Lake Pavin, a large abundance (up to  $5.8 \times 10^5$  cells ml<sup>-1</sup> of porewater; Monteil *et al.*, 2021) and diversity of MTB morphotypes has been observed in the sediments collected from the shore (Fig. 1). MTB abundance determined in sediments of other aquatic systems generally falls in a range from 10<sup>5</sup> to 10<sup>6</sup> cells ml<sup>-1</sup> (Spring *et al.*, 1993; Jogler *et al.*, 2009a) with some studies reporting up to 10<sup>7</sup> cells ml<sup>-1</sup> (Flies *et al.*, 2005), magnetotactic cocci being in most aquatic habitats the dominant population of MTB. Although only future studies using molecular typing methods will be able to specify the phylogenetic affiliation of these MTB morphotypes, the unique ultrastructure of some of these MTB allows speculations on their taxonomy. First, the recently published calcium-carbonate producing MTB were easy to

distinguish thanks to their refractive inclusions, their slow motility and their unique magnetotactic behaviour when observed under the light microscope (Figs. 1A and S1A; Monteil *et al.*, 2021). This MTB morphotype was among the most abundant in sediment samples along with MTB with an ultrastructure typical of the Magnetococcaceae family (e.g. coccoid cells, helical motion, two flagella bundles; Fig. 1B–E; Bazylinski *et al.*, 2013). Cell's shapes similar to that of *Magnetospirillum* bacteria (e.g. thin, i.e. < 500 nm, and long, i.e. > 5 µm, helical-shaped with one chain of cuboctahedral magnetosomes; Fig. 1F) could also be recognized based on TEM observations (Lefèvre *et al.*, 2012). Rod-shaped MTB producing polyphosphate inclusions very similar to previously described MTB affiliated to the Magnetococcaceae family were also observed (Figs 1G and H and S1B; Spring *et al.*, 1994; Oestreicher *et al.*, 2011; Kolinko *et al.*, 2013). Magnetotactic spirilla very similar (e.g. large, i.e. between 0.5 and 1 µm, and short, i.e. < 3 µm, helical-shaped cells with one chain of prismatic magnetosomes) to described species of the *Magnetospira* genus were also present in sediments of Lake Pavin (Fig. 1I). Then, cells resembling previously described MTB of the Nitrospirae phylum (e.g. large rod or ovoid cells with electron dense inclusions and several chain bundles of bullet-shaped magnetosomes) such as *Candidatus* Magnetoovum sp. (Fig. 1J; Lefèvre *et al.*, 2011; Lin *et al.*, 2012) and *Ca.* Magnetobacterium bavaricum (Fig. 1K; Spring *et al.*, 1993; Jogler *et al.*, 2010; Li *et al.*, 2020b) could also be observed (Lefèvre, 2016). Finally, various rods to curved rods producing bullet-shaped magnetosomes were observed and could be tentatively affiliated to the Deltaproteobacteria since their ultrastructure was similar to described magnetotactic species of the *Desulfovibrio* and *Desulfamplus* genera (Fig. 1L–O; Lefèvre *et al.*, 2016; Descamps *et al.*, 2017; Pan *et al.*, 2019).

Lake Pavin sediments appeared as a natural environment particularly suitable to obtain high MTB biomass. Indeed, after magnetic enrichment of sediment samples using neodymium–iron–boron magnets for 2–3 h, aggregated cells formed a thin irregular whitish pellet measuring up to 5 cm in diameter, containing an estimated number of up to 10<sup>8</sup> magnetotactic cells located against the magnet. However, abiotic magnetic particles were also very abundant in the sediments of this lake and were generally trapped in the pellets during MTB concentration. These abiotic particles were predominantly identified as ilmenite (i.e. titanium–iron oxide, FeTiO<sub>3</sub>) by scanning electron microscopy (SEM) analyses (Fig. S2). Ilmenite is a slightly magnetic, black and steel-grey mineral. It is a paramagnetic mineral, explaining its attraction during magnetic concentration of Lake Pavin sediments. At the macroscopic scale, it can easily be mistaken with magnetite.

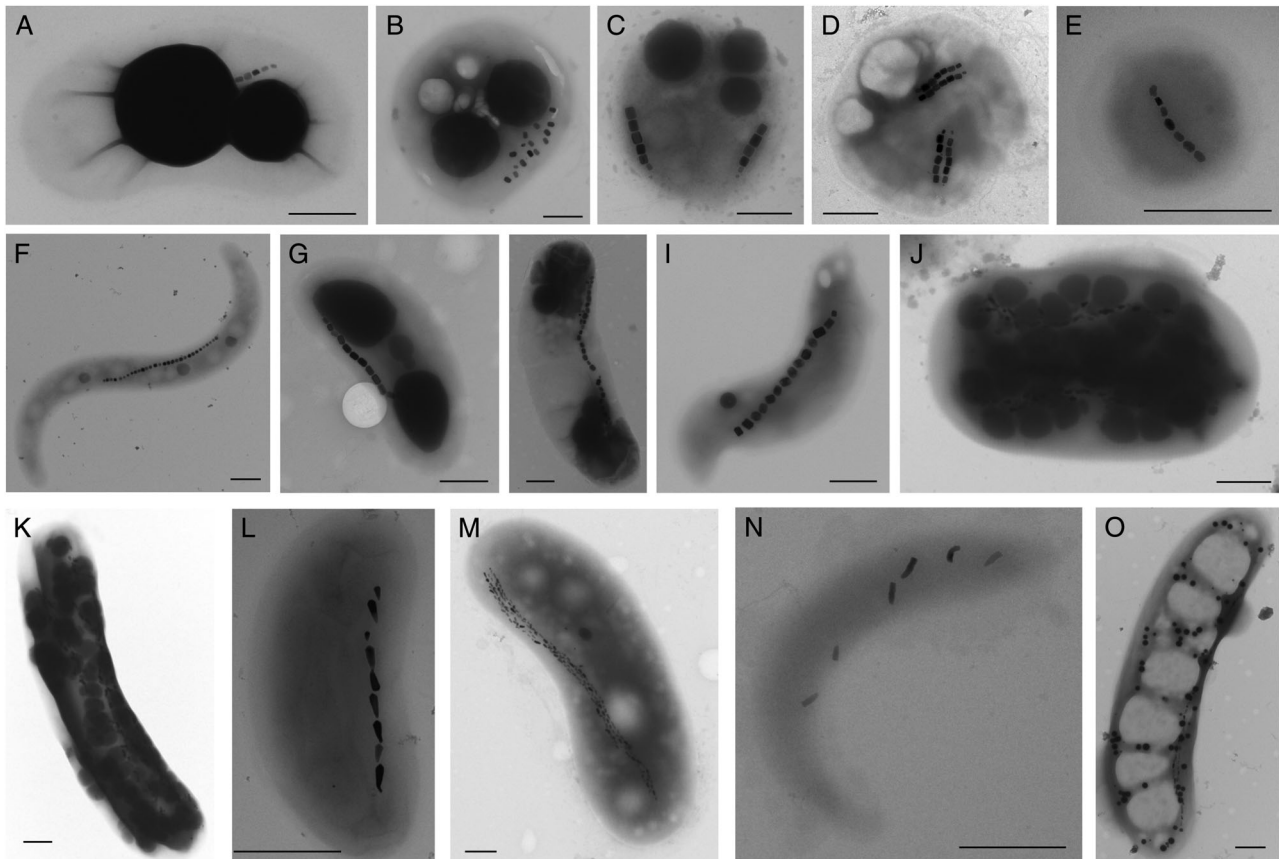


**Fig. 1.** Transmission electron microscope images of different magnetotactic bacteria morphotypes observed in Lake Pavin sediments. See main text for morphotypes description. Scale bars represent 0.5  $\mu\text{m}$ .

We attempted at purifying a maximum proportion of MTB after their magnetic concentration. Our system, named 'migration track', is similar to the racetrack method developed in previous studies (Wolfe *et al.*, 1987; Li *et al.*, 2010). It improved the purification of north seeking MTB and was used directly on the field (Figs 2 and S3). The pellets containing abiotic particles, MTB and other microorganisms, were collected with a 1 ml micropipette on the inner wall of the bottles and placed next to the north pole of a strong bar magnet (15 mT at the edge of the drop). Magnetic particles were retained at this extremity while most north-seeking MTB were repulsed and swam in the opposite direction where the south pole of another magnet was placed (3 mT at the edge of the drop). A folded parafilm sheet was used to create a channel filled with a 0.22- $\mu\text{m}$ -filtered drop of Lake Pavin water overlying the sediments in the sample. Such a protocol avoids the formation of chemical gradients and thus facilitates the northern migration of MTB. The migration time was adjusted in order to obtain a maximum proportion of MTB purified at the extremity of the device. As the majority of MTB were fast swimming bacteria such as magnetotactic

cocci with a motility above  $200 \mu\text{m s}^{-1}$ , the drop was spread (i.e. 4–4.5 cm length) in order to optimize the transfer of magnetotactic cells in the filtered water. Up to 88.0% (71.9% in average) of MTB were efficiently purified and concentrated after 60 min of migration in the channel (Fig. 2). A whitish/greyish spot appeared close to the south pole of the magnet where MTB were harvested. A majority of magnetotactic cocci along with other rod-shaped magnetotactic cells composed this pellet containing more than  $10^7$  cells. This approach combining the standard method for magnetic concentration of sediment samples and our migration track technique allowed us harvesting an important quantity of MTB free of abiotic magnetic particles. These MTB were composed by different populations with proportions likely not representative of their proportions in the environment, as the protocols used for magnetic enrichment and purification do not have the same efficiency for all MTB (e.g. Lin *et al.*, 2008). Purified MTB from dozens of migration track devices were pulled together and concentrated by centrifugation, thus representing a large pellet of purified MTB available for further analyses.

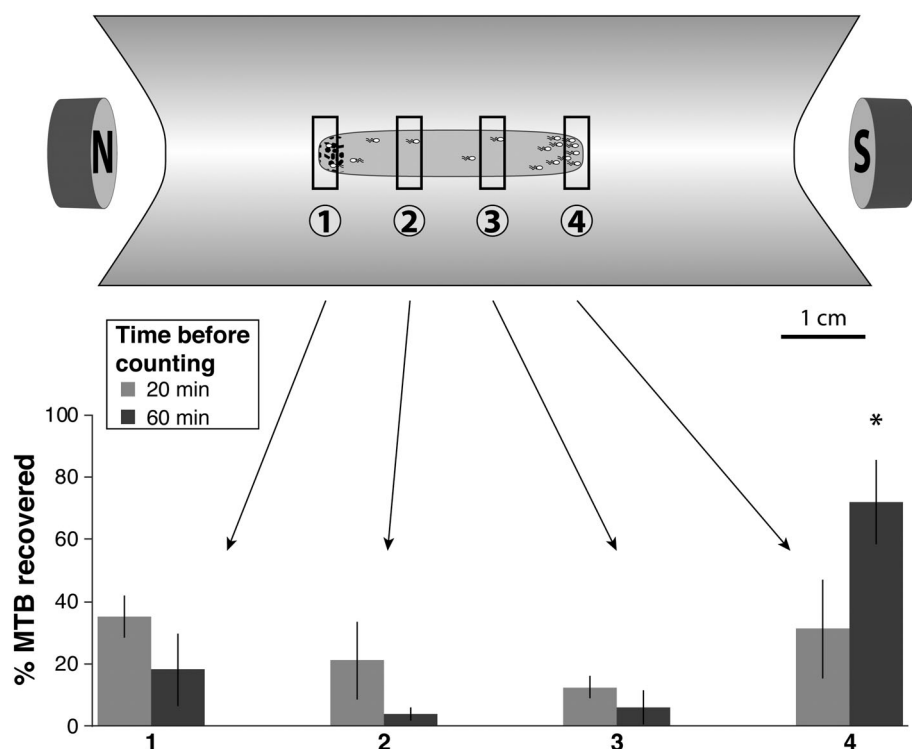


**Fig. 2.** Magnetic purification of MTB from Lake Pavin sediments using the migration track device, developed in the present work. The pellet of magnetically enriched cells is deposited on the left side of the system (i.e., position 1) and magnetic particles (represented by the black dots) and south seeking MTB are trapped by the left magnetic bar. North seeking MTB swim towards the right magnetic bar with the majority accumulating at position 4. Histograms on the lower part of the figure represent the proportion of cells counted at each position (1, 2, 3 and 4) after 20 or 60 min of magnetic purification, illustrating the efficiency of our migration track device. Cell counts are reported as the mean of triplicate measurements, with vertical lines indicating  $2\sigma$  uncertainties. The zone 4 after 60 min of magnetic purification is the only condition that concentrates significantly MTB relative to others. This is supported by a pairwise student t-test ( $P < 0.034$ ).

#### *Magnetotactic bacteria are distributed below the oxygen detection limit in the water column of Lake Pavin*

Over the different field works in Lake Pavin, the abundance and proportion of the different MTB morphotypes observed in the water column greatly varied depending on the season. Eight MTB morphotypes could be distinguished based on microscopy observations. Among these morphotypes, the most abundant (up to  $5.0 \times 10^3$  cells  $\text{ml}^{-1}$ ) were cells affiliated to the Magnetococcaceae family that produced polyphosphate inclusions of various sizes along with various organizations of magnetosomes (Figs 3A–C and S1C; Rivas-Lamelo *et al.*, 2017; Liu *et al.*, 2020). MTB producing calcium carbonate inclusions were observed at a lower abundance but could reach a cell density of  $4.0 \times 10^2$  cells  $\text{ml}^{-1}$  (Fig. 3D; Monteil *et al.*, 2021). Two rod-shaped MTB, one producing a single chain of octahedral magnetosomes along with polyphosphate (Figs 3E and S1C) and the other one producing a single chain of bullet-shaped magnetosomes (Fig. 3F) were also always present in our samples but at a low cell density ( $< 8$  cells  $\text{ml}^{-1}$ , the lower limit of the technique used to count MTB density using the hanging drop assay). A small vibrio producing one chain of bullet-shaped magnetosomes (Fig. 3G) and some helical MTB resembling cells of the *Magnetospirillum* genus (Fig. 3H) were occasionally observed in samples collected in the water column of Lake Pavin. Other studies on MTB populations living in the water column of stratified aquatic

environments also revealed the presence of a majority of magnetotactic cocci affiliated to the Magnetococcaceae family (Simmons *et al.*, 2007; Schulz-Vogt *et al.*, 2019) with abundance up to  $3.5 \times 10^6$  cells  $\text{ml}^{-1}$  at the top of the oxycline in Salt Pond, Massachusetts (Simmons *et al.*, 2004, 2007).

From April 2016 to October 2019, 10 vertical profiles of MTB distribution along with several physicochemical parameters were obtained across the OATZ of the water column using a Niskin bottle for water collection (Figs 4 and S4). These profiles could bring important information concerning the MTB distribution in the water column of Lake Pavin. For instance, although there are important variations of the oxygen and redox gradients over the seasons and years, MTB were always distributed below the oxygen detection limit (Figs 4 and S4). The maximum abundance of MTB in the water column was systematically detected near the maximum decrease of the redox potential, i.e. between 51.0 and 57.2 m depth depending on seasons/years (Fig. 4). The peak of turbidity, corresponding mainly to the precipitation of iron phosphate and (oxy)hydroxide (Cosmidis *et al.*, 2014; Busigny *et al.*, 2016), was either at the same depth level as the peak of MTB abundance or just below. In most cases, their depths evolved similarly depending on the season (Figs 4 and S4). However, it should be noted that the intensities of the turbidity and MTB peaks did not correlate with each other. For instance, in October 2017, a

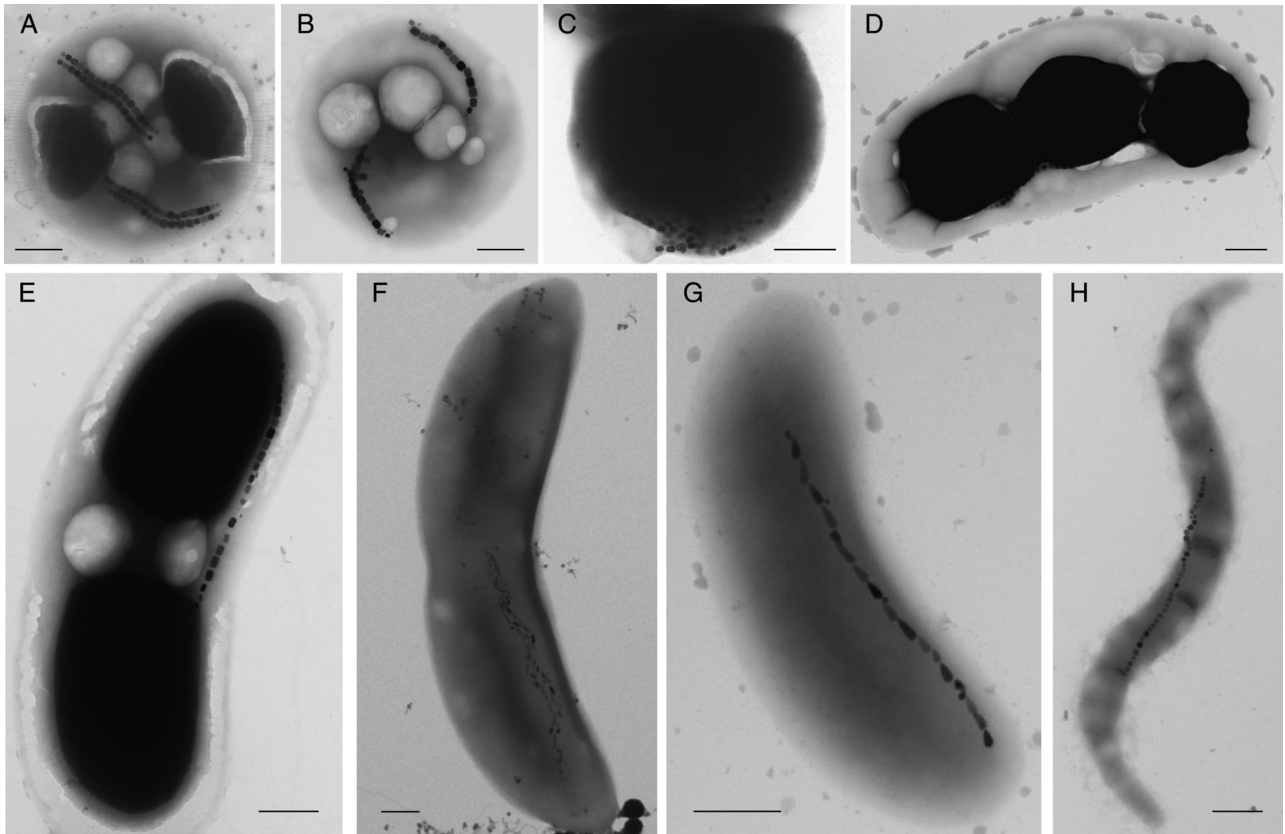


**Fig. 3.** Transmission electron microscope images of different magnetotactic bacteria morphotypes from Lake Pavin water column. See main text for morphotypes description. Scale bars represent 0.5  $\mu\text{m}$ .

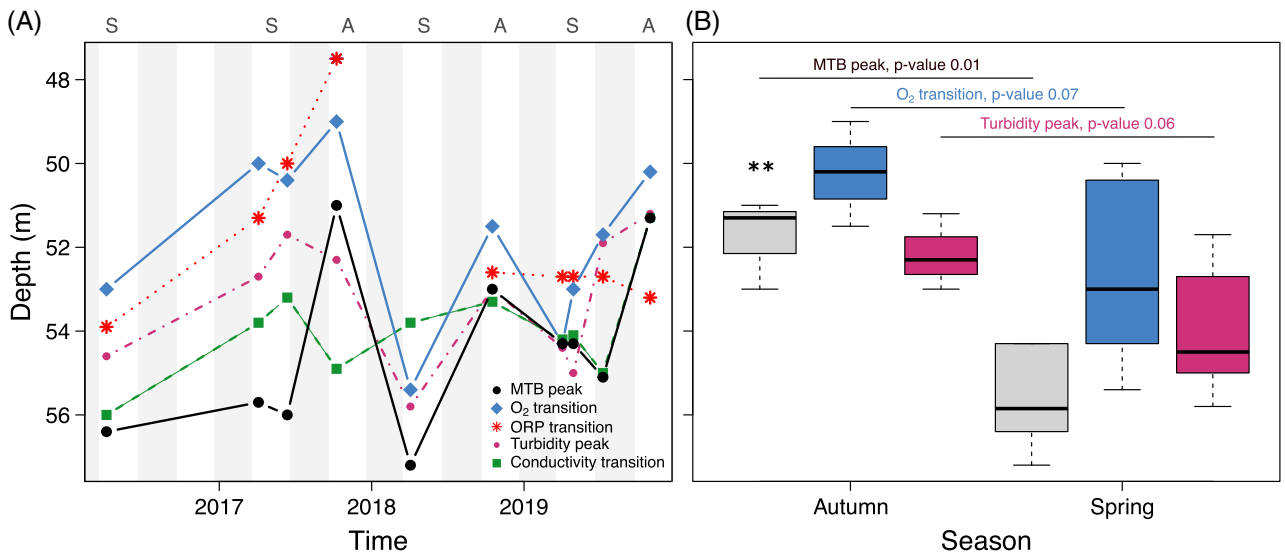


**Fig. 4.** A. Depth variations of the MTB and turbidity peaks, as well as conductivity, oxygen and redox potential transitions upper boundary (i.e. depth where the maximum gradient starts) over time.

B. Box plots showing the distribution of these depths as a function of the sampling season for the variables with the most significant mean differences according to a pairwise Student's *t*-test ( $P < 0.1$ ). [Color figure can be viewed at [wileyonlinelibrary.com](http://wileyonlinelibrary.com)]

high MTB concentration of  $7.4 \times 10^3$  cells  $\text{ml}^{-1}$  was observed at 51.0 m depth while the peak of turbidity was very weak. Reciprocally, in April 2016, a strong peak of

turbidity was observed at 54.6 m depth while the number of MTB reached only  $1.4 \times 10^3$  cells  $\text{ml}^{-1}$ . Accordingly, the contribution of MTB populations to the turbidity of the

water column is insignificant and the turbidity value cannot be used unequivocally as a proxy for MTB. The peak of MTB was always observed at the level of or below the break of conductivity at value of  $78.9 \pm 13.0 \mu\text{S cm}^{-1}$  ( $n = 10$  sampling campaigns using Niskin bottles) which corresponds to the region where iron concentration starts to increase (Cosmidis *et al.*, 2014; Busigny *et al.*, 2016).

In spring and summer, the maximum number of MTB counted in the water column was located between 54.3 and 57.2 m depth, while in autumn, the maximum number of MTB was generally located at a lower depth in the water column, between 51.0 and 53.0 m (Figs 4B and S5). This zonation can be explained by the dynamics of the upper water column. In winter, shallow waters (0–10 m) cool down and eventually become denser than deeper waters (10 to c. 50–55 m) thus creating an instability and a mixing of the upper water column (i.e. mixolimnion). This brings dissolved  $\text{O}_2$  to the deep part and slightly deepens the OATZ, turbidity peak and the maximum MTB abundance zone. In contrast, during summer and autumn, shallow waters are warmer and the water column is strongly stratified by the thermocline (c. 8–12 m depth) that limits  $\text{O}_2$  renewal in the hypolimnion, inducing an upward shift of chemocline, turbidity

and MTB peaks to shallower depth (due to upward  $\text{Fe(II)}$  diffusion from deep anoxic waters).

Sampling with a Niskin bottle is thus an efficient method to decipher the global distribution of MTB in the water column. Nevertheless, the use of Niskin bottles is associated with several drawbacks. First, the bottles are, in general, vertical and, in our case, with a height of  $\sim 50$  cm for the 5.7-L bottle and  $\sim 100$  cm for the 20-L bottle (Fig. 5). As a result, this method provides a limited depth resolution for the assessment of MTB distribution in the water column, not better than 50–100 cm. However, near the OATZ of Lake Pavin, the strong stratification at relatively small scale, as measured by *in situ* probes, requires a better depth resolution for water collection. Moreover, water collection takes a long time, especially at a 60 m depth: about 30 min in total are required for bottle opening, descent, closing, ascent, and emptying on the platform. Then, when a water sample is collected, the only direct control over the depth is a meter counter connected to the pulley of the winch, which provides a poor precision. The depth is precisely known thanks to a depth gauge fixed to the Niskin bottle only when the bottle is pulled out from the water. Thus, there is no direct indication that the bottle is located at the peak

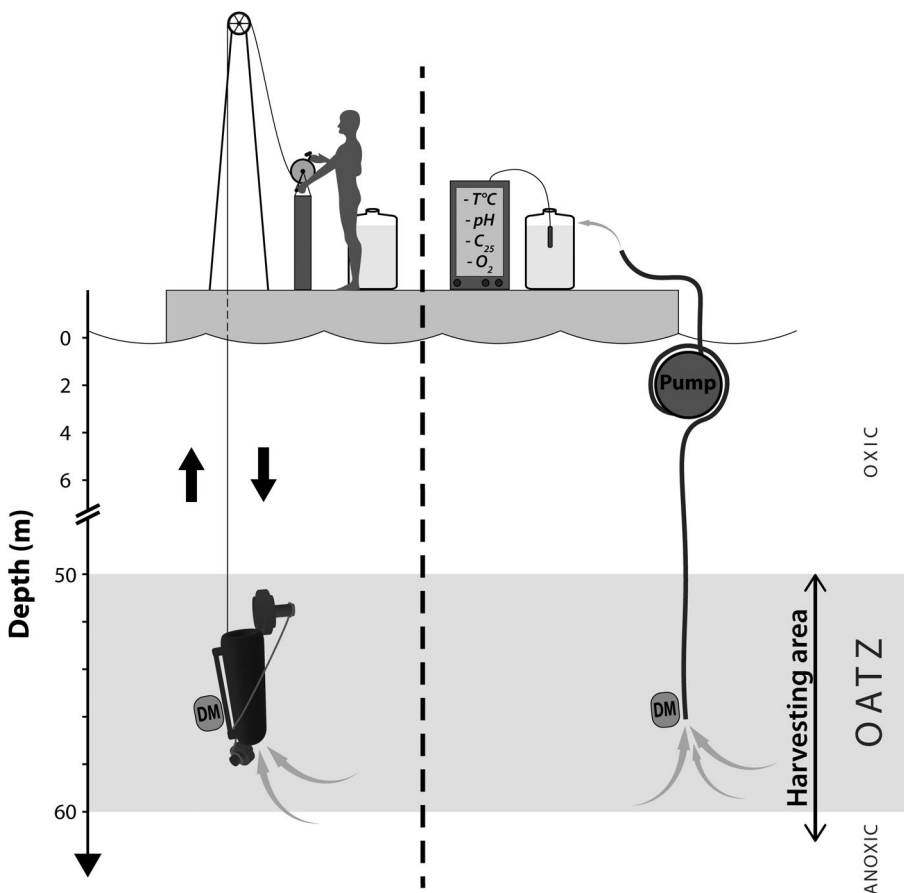


**Fig. 5.** Schematic representation of the methods used to sample the water column of Lake Pavin using a Niskin bottle (left side) and online pumping (right side). DM refers to the depthmeter used to control the pipe depth. The oxic-anoxic transition zone (OATZ) represents the region where oxygen concentrations are at the micromolar to sub-micromolar levels and where populations of magnetotactic cells are present.

of MTB abundance. Therefore, the method of water collection using Niskin bottle is adapted for a study of global MTB distribution in the water column but (i) can hardly target the peak of MTB abundance reproducibly and (ii) cannot be used to establish a precise distribution profile of MTB at high depth resolution.

*Online pumping allows a sampling at high depth resolution, showing that MTB distribution is correlated with conductivity and oxygen*

We developed an alternative method for water sampling using a vertical graduated pipe settled at depth and connected at the other side of the pipe to a submersible pump (Fig. 5). The water transfer from depth to surface can be rapid and efficient but depends on the pump flow capacity. In the present work, the maximum pump flow reached  $8 \text{ L min}^{-1}$  (BLDC Pump, model DC50E-1250), filling a 20-L Nalgene bottle in c. 150 s. This is much faster compared to the 30 min required to collect 20 l with a Niskin bottle. A clear advantage of our online sampling system is that several Nalgene bottles could be filled from the same depth on a time scale where evolution of the water physico-chemistry and MTB abundance are insignificant. We compared MTB abundances in several Nalgene bottles successively filled and found them statistically identical (data not shown). Moreover, the abundance of cells collected at the same depth using a Niskin bottle was similar or lower compared to our pipe system showing that the flow generated by the pump has no impact on MTB motility and integrity. Indeed, electron microscopy analyses of cells sampled with the two approaches show similar MTB morphology and magnetosomes organization. For sampling another depth in the water column, the graduated pipe can simply be shifted to a shallower or deeper position. A waiting time is required to flush the water contained in the 60-m-long pipe, corresponding roughly to 150 s. Another benefit of our online sampling system is that it allows the collection of water at relatively high depth resolution of approximately 10–20 cm.

In Lake Pavin, although MTB-rich waters can be efficiently collected at a specific depth using our online sampling system, imprecisions persist because the depth of the MTB abundance peak can change over days, and even hours, due to slight variation of the redox boundary and internal waves of the lake (Bonhomme, 2008; Bonhomme *et al.*, 2011). In order to overcome this problem, we evaluated whether physicochemical parameters of the water could be used as a proxy for MTB abundance in the water column. Over several days in July 2019, we monitored MTB cell density around the peak of MTB abundance identified beforehand, as well as temperature, conductivity at  $25^\circ\text{C}$  (i.e.  $C_{25}$ ), dissolved oxygen concentration

and pH of the water samples (measured *in situ* directly at the extremity of the pipe). The results indicate that MTB cell density ranged from 13 to  $1.18 \times 10^4 \text{ cells ml}^{-1}$ , temperature from  $6.3$  to  $7.0^\circ\text{C}$ ,  $C_{25}$  from  $63.3$  to  $78 \mu\text{S cm}^{-1}$  and pH from 6.1 to 6.3. Figure 6 illustrates that MTB cell density is not correlated with pH and temperature, but displays specific distribution with  $C_{25}$  and dissolved  $\text{O}_2$  concentration. MTB cell density tends to increase with decreasing  $\text{O}_2$  level, and  $\text{MTB} > 4.0 \times 10^3 \text{ cells ml}^{-1}$  are only found when dissolved  $\text{O}_2$  is lower than  $2 \mu\text{mol L}^{-1}$ . However, low MTB cell densities are also observed in some water samples with low  $\text{O}_2$  (i.e. around  $2 \mu\text{mol L}^{-1}$ ; Fig. 6A) showing that  $\text{O}_2$  concentration is an important parameter controlling MTB distribution but is not sufficient to monitor online MTB abundance. The conductivity is also a relevant parameter since the peak of MTB abundance was systematically found in a restrictive range of  $C_{25}$  values, between  $64.7$  and  $67.1 \mu\text{S cm}^{-1}$  (Fig. 6B). Considering the 12 richest samples with  $\text{MTB} > 4.0 \times 10^3 \text{ cells ml}^{-1}$ , the average  $C_{25}$  value is  $65.8 \pm 1.4 \mu\text{S cm}^{-1}$  ( $2\sigma$ ). The conductivity represents the concentration of dissolved ionic species, including iron. Thus, the peak of MTB abundance in the water column of Lake Pavin occurs at an ideal set of conditions including an oxygen concentration below  $2 \mu\text{mol L}^{-1}$  and a conductivity around  $65.8 \mu\text{S cm}^{-1}$ . The conductivity can be instantaneously measured in the water collected by our online system and was further used as a proxy for MTB abundance.

The MTB abundance,  $\text{O}_2$  concentrations and specific conductivity measured along three depth profiles in Lake Pavin water column are reported in Fig. 7. While  $C_{25}$  showed a progressive increase with depth for the different sampling days, MTB cell density and  $\text{O}_2$  concentration showed stronger variabilities and scattering. Oxygen concentration typically decreased with depth but displayed unexpected bursts at depths of 51.5 m (14 July 2019) and 52.0 m (15 July 2019). This  $\text{O}_2$  increase was not observed in 17 July 2019 although there might be subtle variations at low level. The presence of  $\text{O}_2$  anomalies (i.e. concentration burst in anoxic waters) may reflect an inflow of a sub-lacustrine intermittent spring, as described previously in Lake Pavin at a depth ranging between 50 and 55 m (Bonhomme *et al.*, 2011). Interestingly, the MTB concentration is anticorrelated with these  $\text{O}_2$  burst, with no MTB in elevated  $\text{O}_2$  regions (Fig. 7).

Using the online pumping system, we noticed that the MTB abundance exhibited several peaks at different depths in the water column. Two peaks were observed on July 14<sup>th</sup> and 15<sup>th</sup>, and three peaks on July 17<sup>th</sup> (Fig. 7). This was not the case on July 9<sup>th</sup> and during the other sampling campaigns while performing the MTB abundance profiles with the Niskin bottle. Although MTB are distributed along several meters in the water column, a high depth resolution is thus required to study precisely

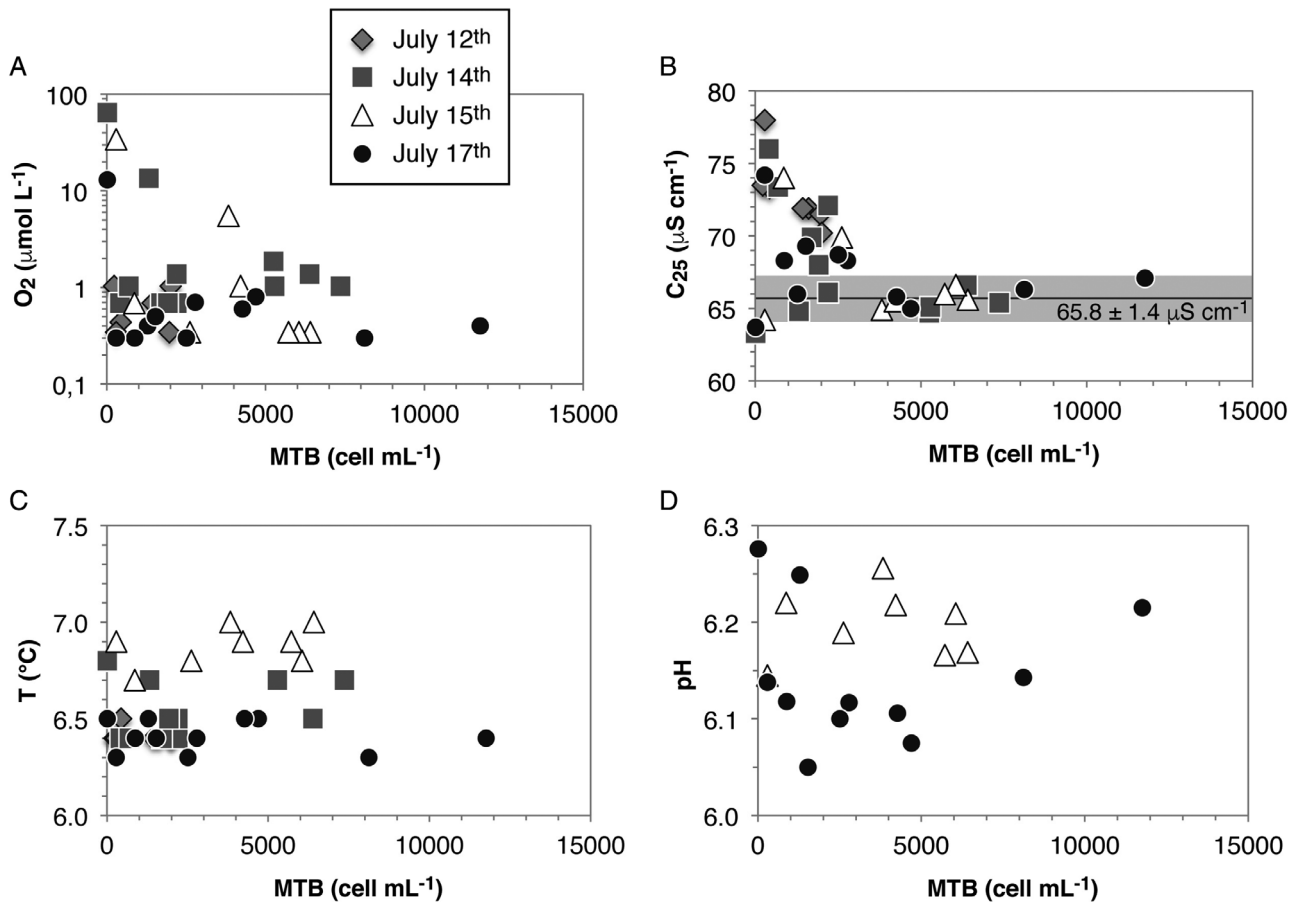


**Fig. 6.** Relations between MTB cell abundance and various physicochemical parameters from Lake Pavin water column in the vicinity of the redox boundary, during the July 2019 sampling campaign.

A, Dissolved oxygen concentration ( $\mu\text{mol L}^{-1}$ ); B, specific conductivity at  $25^\circ\text{C}$  ( $\mu\text{S cm}^{-1}$ ); C, temperature ( $^\circ\text{C}$ ); and D, pH. All samples were collected with our online pumping system (Fig. 5 left panel). Note that the temperature measured on the platform could slightly differ from the temperature at depth (i.e. approximately  $4^\circ\text{C}$  (Michard *et al.*, 1994; Bonhomme *et al.*, 2011)) due to thermal exchange in the 60-m long pipe.

MTB distribution in the water column of Lake Pavin. The origin of multiple MTB peaks is still poorly constrained. Future studies will have to examine the potential link between physico-chemical conditions and associated MTB populations by monitoring in detail physico-chemical properties of the water, MTB morphotypes and molecular typing methods.

Finally, two important questions must be discussed concerning our online pumping system. First, when the pipe is left at depth for relatively long time (e.g. several minutes or more), where is the water collected at the pipe mouth coming from? It is unknown if the water collected for a long time is derived from a roughly constant depth level, all around, below or above the pipe mouth. Because of strong vertical density gradient in the vicinity of the OATZ in Lake Pavin, we can reasonably assume that the zone of water collection around the pipe mouth is similar at each sampling depth (regardless of the water flow direction). This is supported for instance by the progressive increase in

conductivity with depth on the different profiles of July 2019 (Fig. 7, in particular the smooth shape of the profiles in July 14th and 15th). The second important question to address is whether the physico-chemical conditions of water are preserved or not during transfer through the pipe from depth to surface. Again, the smooth shape of the conductivity profile suggests that the water was well preserved during ascension. In addition, we noted a clear oxo-anoxic transition of the water samples (even though the oxoic zone was not monitored and reported here due to the absence of MTB). The anoxic conditions (i.e. below probe detection limit) measured at depth  $> 52.5$  m (Fig. 7) indicate that  $\text{O}_2$  diffusion through the pipe did not occur or was negligible during water ascension. The only parameter significantly modified was temperature due to high exchange surface with ambient water around the pipe. The water temperature measured on the platform was between  $6.3$  and  $7^\circ\text{C}$  (Fig. 6), while *in situ* measurement provided values near  $4^\circ\text{C}$ . Overall our online pumping



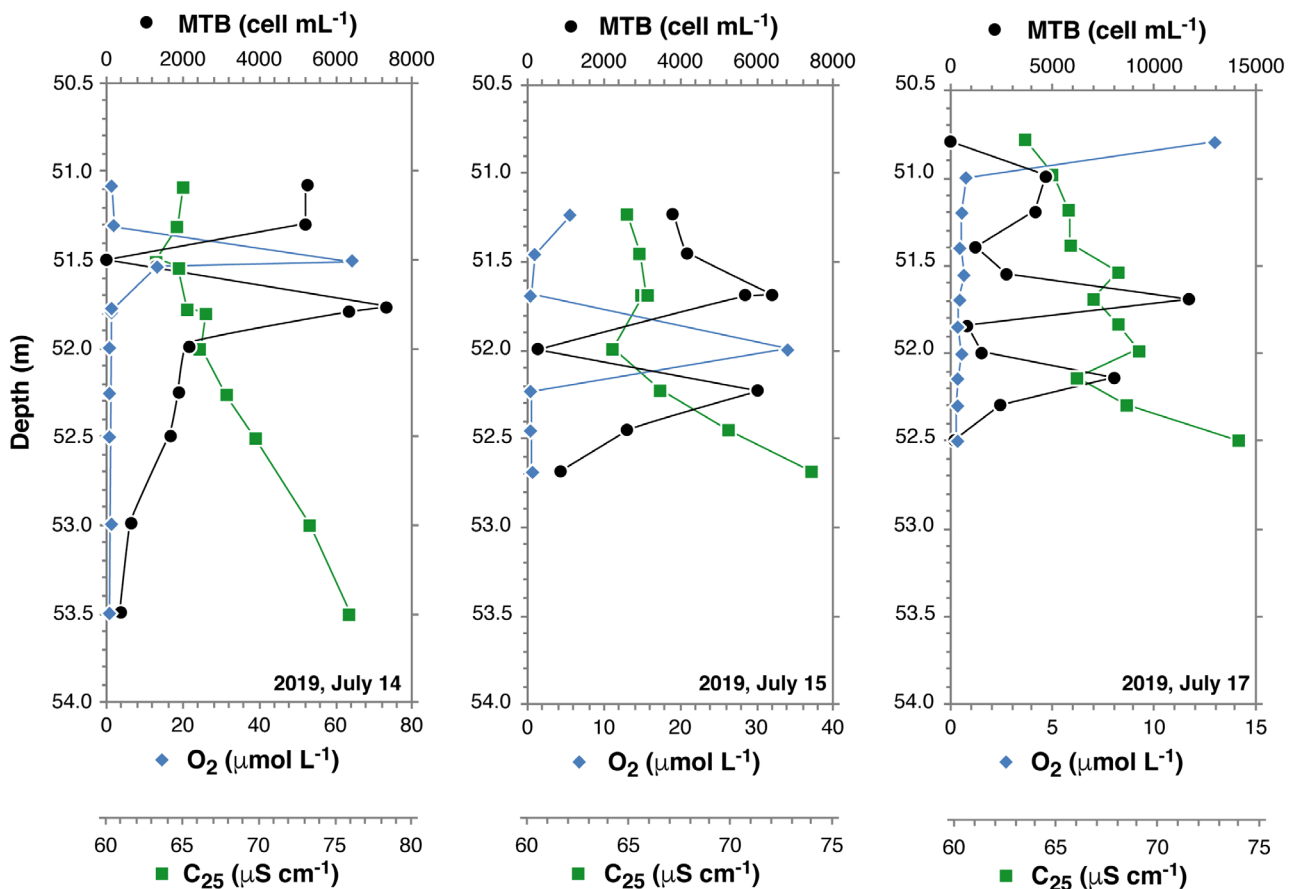


**Fig. 7.** Magnetotactic cell abundance ( $\text{cell mL}^{-1}$ ), dissolved oxygen concentration ( $\mu\text{mol L}^{-1}$ ) and specific conductivity ( $\mu\text{S cm}^{-1}$ ) profiles from Lake Pavin water column, on 14<sup>th</sup>, 15<sup>th</sup> and 17<sup>th</sup> July 2019. The high-spatial resolution of water collection was reached using online collecting system. [Color figure can be viewed at [wileyonlinelibrary.com](http://wileyonlinelibrary.com)]

system allows to achieve a high spatial resolution together with consistent water conditions and associated MTB abundance.

#### *Chemotaxis and magnetotaxis allow an efficient MTB concentration from large water samples*

Most previous studies of environmental MTB focused on water-saturated sediment samples (Jogler *et al.*, 2010; Lefèvre *et al.*, 2011; Lin *et al.*, 2013, 2018) and a few explored the stratified water column of freshwater or saline lakes (Simmons *et al.*, 2004; Rivas-Lamelo *et al.*, 2017; Schulz-Vogt *et al.*, 2019). In all of these studies, MTB were isolated using magnetic enrichment (Jogler and Schüller, 2009; Lefèvre and Bazylinski, 2013; Lin *et al.*, 2017). This magnetotaxis-based procedure is well adapted for samples of small volume (i.e. below 1 L) but is not efficient for large volumes such as 10 or 20 L, which are needed for studies that require high MTB biomass, for instance, to combine mineralogical, biological and geochemical analyses of magnetosomes.

In order to concentrate MTB cells from a 20-L volume to 1 L and subsequently perform magnetic enrichment, we explored the possibility to concentrate them using their aerotaxis. Indeed, MTB are known to display strong microaerophilic, aerophilic or -phobic response (Frankel *et al.*, 1997; Lefèvre *et al.*, 2014; Popp *et al.*, 2014). Using our online pumping system, we collected water samples from Lake Pavin (near the peak of MTB abundance) and filled six Nalgene bottles of 20 L each. After sampling, the bottles were left open to air so that  $\text{O}_2$  could diffuse into the water (Fig. 8). MTB were expected to swim downwards to the bottom of the bottle. Because  $\text{O}_2$  diffusion in water was extremely slow, the experiment was speeded up by gently removing water from the upper part of the bottle by pumping 4 L every 30 or 60 min, so that  $\text{O}_2$  could diffuse deeper in the bottle while aerotactic cells were swimming downward. Among the six bottles, three of them were pumped every 30 min and the three others every 60 min. This provided a triplicate of each condition (30 or 60 min idle time between pumping). For every volume interval, water was collected and MTB

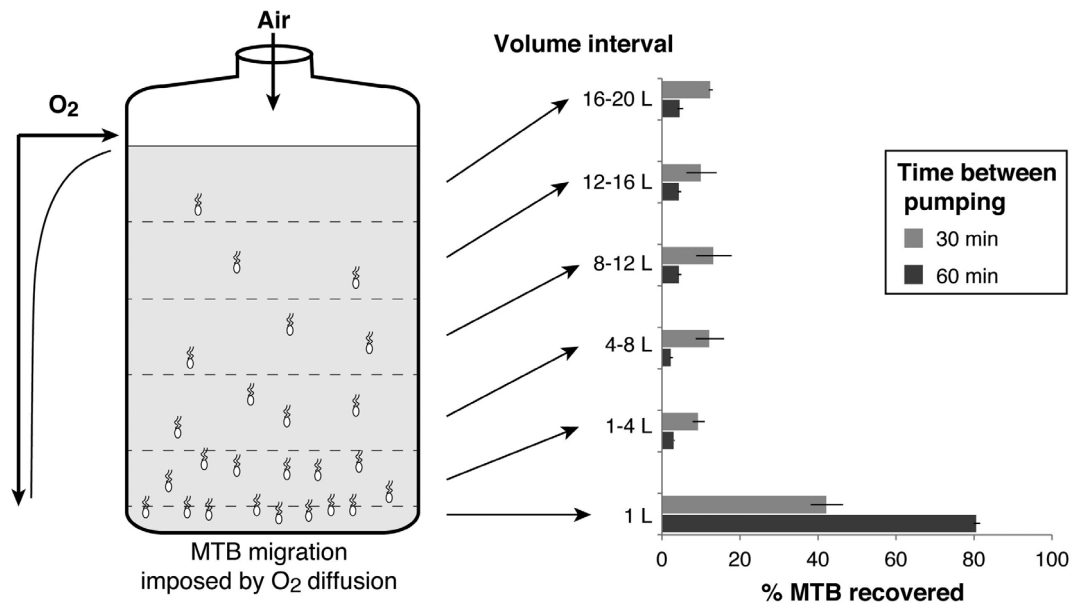


**Fig. 8.** Schematic representation (left panel) of the aerotactic concentration of magnetotactic bacteria after collection from the water column with the online pumping system and transferred in a 20-L Nalgene bottle. Histograms (right panel) represent the percentage of MTB cells recovered in each water layer after 30 or 60 min of idle time between pumping, showing the efficiency of our device. The percentage of MTB recovered is reported as the mean of triplicate counts and line extensions represent the positive and negative standard deviations. The thickness of each water layer in the Nalgene bottle was about 10 cm.

concentration was quantified in triplicate under a light microscope. The distribution of MTB concentration was very consistent and reproducible between triplicates (see error bars on Fig. 8). The results of the experiment with 30 min idle time between pumping showed that MTB swam and concentrated in the bottom water. However, only  $42.3 \pm 4.1\%$  of the total MTB cells were found in the bottom water (1 L), while  $\sim 60\%$  were lost in the upper oxygenated waters. In contrast, the experiment with 60 min idle time gave a higher concentration yield with  $80.7 (\pm 0.8)\%$  of the total MTB cells present in the bottom water. Overall, this shows that downwards MTB migration imposed by  $O_2$  diffusion in the bottle is an efficient pre-concentration procedure. These data allowed to estimate the motion speed of the slowest MTB from Lake Pavin water column. The vertically travelled distance in the 20 L Nalgene bottle was 10 cm in 60 min. This corresponds to MTB motion speed  $c. 28 \mu\text{m s}^{-1}$ , which is in the speed range to that previously described for MTB (Lefèvre *et al.*, 2014) and in agreement with light microscope observation where we could distinguish highly motile magnetotactic cocci and some slow motile magnetotactic large rods. A further magnetic enrichment of the chemotactically enriched samples allowed the formation of a large pellet against the magnet that could be easily harvested and used for further analyses of magnetotactic cells or their magnetosomes. For a 20 L bottle sampled at the peak of MTB abundance in Lake Pavin water column, more than  $10^8$  cells could be collected. Similarly to

the magnetic concentration carried out in the sediments, coupling aerotactic and magnetic concentration allows to obtain large pellets of cells composed by several populations of MTB in proportions likely different from the natural ones as the sensitivity to oxygen probably differs between the different MTB present in our samples.

## Conclusion

The present work on Lake Pavin provides several analytical methods for optimizing MTB collection in sediments and the water column. In sediments, MTB were efficiently separated from magnetic abiotic particles (i.e. volcanic ilmenite) using a 'migration track' system, where MTB are left swimming towards a magnet. In the water column, a comparison of sampling protocols based on Niskin bottle and online pumping system demonstrates a stronger potential of online technique, with fast collection of large volumes (20 L in 150 s) and at high depth resolution (about 10–20 cm). Another strong advantage of the online pumping technique is the capacity to evaluate the zone of maximum MTB abundance using empirical calibration coupling dissolved oxygen and conductivity measurements. While only one peak of MTB was identified on depth profile performed using Niskin bottles, high resolution profile using online pumping system indicates that two to three peaks of MTB are present. Likewise, we anticipate a stratification of MTB morphotypes and a

potential link to geochemical parameters in the water column. This aspect will need to be explored in future studies and may help to decipher the ecological niche specific of the different MTB populations present in the water column.

After collection of large volumes of water at depth, MTB can now be efficiently recovered by coupling their aerotactic and magnetic behaviours. This opens a new avenue for chemical and isotopic studies that require large amount of MTB and are usually limited to laboratory cultures. In the case of Lake Pavin, MTB present at the OATZ of the water column show a maximum concentration slightly higher than  $10^4$  cells  $\text{ml}^{-1}$ . Therefore, the mass requirement for Fe isotope analysis ( $\sim 0.1$  mg of magnetite, i.e.  $10^{10}$  cells) implies that about 1000 L of water will have to be collected and treated. Although this represents a large volume of water, this can reasonably be achieved by the present protocols. The application of these methods to others chemically stratified aquatic environments such as Salt Pond, Massachusetts (Simmons *et al.*, 2004) or the Black Sea (Schulz-Vogt *et al.*, 2019) could be of high interest to carry out a comparative study of MTB ecology, diversity and isotope characteristics from different ecosystems.

## Experimental procedures

### *Sample collection and in situ physicochemical measurements*

Sampling in the water column was carried out at 10 different dates between April 2016 and October 2019. Samples were collected from a platform located near the centre of Lake Pavin (45.495792°N, 2.888117°E) using a 5.7 L or 20 L Niskin bottle (General Oceanics, USA) connected to a winch or by pumping directly the water using a speed-adjustable 12 V brushless pump (see details in the Results section). For initial MTB counting, water collected at the targeted depths was transferred in one-litre glass bottles filled to their capacity and tightly closed. *In situ* environmental parameters of the water column were acquired with different profiler probes: YSI 6600 (CTD-O<sub>2</sub>-pH-ORP), EXO2 (CTD-O<sub>2</sub>-pH-ORP-turbidity-chlorophyll-phycoyanine-fDOM), SDOT 300 nke (O<sub>2</sub>-T), AQUAlogger 210TYPT Aquatec (turbidity-T-depth), STBD 300 nke (turbidity-T-depth), where CTD stands for conductivity-temperature-depth, ORP for oxidation reduction potential and fDOM for fluorescent dissolved organic matter. Detection limit for dissolved O<sub>2</sub> is c. 0.1% or about  $0.3 \pm 0.2$   $\mu\text{M}$ .

Sediments were sampled along the edge of the dock, near the main access road to Lake Pavin (45.499162°N, 2.886399°E). They were recovered onshore with a scooper by fully filling one-litre glass bottles with

300–400 mL of sediments and overlying 600–700 mL water. During sampling, air bubbles were avoided. Once in the laboratory, bottles were stored with their cap closed, under dim light and at room temperature ( $\sim 25^\circ\text{C}$ ).

### *Magnetic enrichment and light microscope observation*

North-seeking magnetic cells were concentrated by placing the south pole of a magnetic stirring bar or neodymium-iron-boron magnet (disc magnet with a diameter of 5 mm and a height of 5 mm) for 1–3 h next to the bottle wall, above the sediment–water interface or at mid-height of the water bottle. Examination of magnetically concentrated cells was carried out using the hanging drop technique (Schüler, 2002) under a Zeiss Primo Star light microscope equipped with phase-contrast, differential interference contrast optics and a camera Axiocam 105. Magnetotaxis was evidenced by rotating a stirring bar magnet at  $180^\circ$  on the microscope stage to reverse the local magnetic field.

### *Cell count profiles*

For counting MTB cells in the water column, two 1-L bottles of water were collected at the different investigated depths. For each bottle, three 40- $\mu\text{l}$  drops were immediately observed using the hanging drop technique. Magnetotactic cells accumulated at the edge of the drops when a magnetic field was applied at one side of the drop and were subsequently counted under the light microscope. The counting occurred 2 min after the cells in the hanging drop were exposed to the magnetic field. The number of cells counted in each drop was multiplied by a factor of 25 to obtain the abundance of cells per millilitre. Cell counts were reported as the means of two triplicates counts for each depth. Using this counting method, the lower limit of MTB abundance is 8 cells  $\text{ml}^{-1}$  (i.e. minimum of 1 cell/3 replicates  $\times$  25).

Magnetotactic cells in sediment samples were counted using a Malassez counting chamber. Measurements were systematically carried out on three replicates. Cells were not immobilized during counting. Although some MTB are fast swimmers, we were able to count the number of cells in the chamber reproducibly. Counts were performed as fast as possible, a task facilitated by the fact that most MTB cells contain refractile inclusions (e.g. sulphur or calcium carbonate) which makes their identification under the microscope easy.

### *Transmission and scanning electron microscopy (TEM and SEM)*

The morphology of MTB as well as the shape and arrangement of magnetosomes were observed after

fixation of the cells on a TEM carbon-coated grid. Electron micrographs were recorded with a Tecnai G<sup>2</sup> BioTWIN (FEI Company) equipped with a CCD camera (Megaview III, Olympus Soft imaging Solutions GmbH) using an accelerating voltage of 100 kV. Z-contrast imaging in the high-angle annular dark field (STEM-HAADF) mode, and elemental mapping by X-ray energy-dispersive spectrometry (XEDS) were carried out using a JEOL 2100F microscope. This machine, operating at 200 kV, was equipped with a Schottky emission gun, an ultrahigh resolution pole piece, and an ultrathin window JEOL XEDS detector.

Bulk magnetic particles extracted from the sediments were observed by SEM in back-scattered electron and secondary electron imaging modes to characterize both the shape and chemical composition of particles in the samples. Analyses were carried out at Institut de Physique du Globe de Paris (IPGP) using a Carl Zeiss EVO MA10 SEM. Standard operating conditions for SEM imaging and EDS (energy dispersive spectroscopy) analyses were 15 kV accelerating voltage, working distance of 12 mm, and electron beam current of 2–3 nA. Samples were coated with a few nanometres of Au prior to analysis.

#### Statistical analyses

Statistical analyses were performed in R, version 4.0.0 (R Core Team, 2018). For each variable, groups' averages were compared either by a paired Student's *t*-test or by a paired non-parametric Mann–Whitney *U* test if variables were not normally distributed. Differences were considered as significant when *P*-values were below 0.05.

#### Acknowledgements

This work was supported by the French National Research Agency (SIGMAG: ANR-18-CE31-0003 and PHOSTORE: ANR-19-CE01-0005), the CNRS: 'DEFI Instrumentation aux limites' (MAGNETOTRAP project) and 'Programme National Ecosphère Continentale et Côtière (EC2CO)' (BACCARAT2 project – N°13068). C.C. Bidaud was supported by the Frontières de l'Innovation en Recherche et Éducation (FIRE) PhD program from the Centre de Recherches Interdisciplinaires (CRI). Part of this work was supported by IPGP multidisciplinary program PARI and by Region Île-de-France SESAME Grant no. 12015908. We acknowledge the Institut de Radioprotection et de Sécurité Nucléaire (IRSN) at CEA Cadarache for the access of the transmission electron microscope Tecnai G<sup>2</sup> BioTWIN. We would like to thank the town of Besse for the work facilities in the field, and particularly Marie Léger from the heritage service as well as the technical staff.

#### References

Abreu, F., Martins, J.L., Silveira, T.S., Keim, C.N., de Barros, H.G.P.L., Filho, F.J.G., and Lins, U. (2007)

- “Candidatus Magnetoglobus multicellularis”, a multicellular, magnetotactic prokaryote from a hypersaline environment. *Int J Syst Evol Microbiol* **57**: 1318–1322.
- Aeschbach-Hertig, W., Hofer, M., Kipfer, R., Imboden, D.M., and Wieler, R. (1999) Accumulation of mantle gases in a permanently stratified volcanic lake (Lac Pavin, France). *Geochim Cosmochim Acta* **63**: 3357–3372.
- Aeschbach-Hertig, W., Hofer, M., Schmid, M., Kipfer, R., and Imboden, D.M. (2002) The physical structure and dynamics of a deep, meromictic crater lake (Lac Pavin, France). *Hydrobiologia* **487**: 111–136.
- Albéric, P., Voillier, E., Jézéquel, D., Grosbois, C., and Michard, G. (2000) Interactions between trace elements and dissolved organic matter in the stagnant anoxic deep layer of a meromictic lake. *Limnol Oceanogr* **45**: 1088–1096.
- Amor, M., Busigny, V., Louvat, P., Gélabert, A., Cartigny, P., Durand-Dubief, M., et al. (2016) Mass-dependent and -independent signature of Fe isotopes in magnetotactic bacteria. *Science* **352**: 705–708.
- Amor, M., Busigny, V., Louvat, P., Tharaud, M., Gélabert, A., Cartigny, P., et al. (2018) Iron uptake and magnetite biomineralization in the magnetotactic bacterium *Magnetospirillum magneticum* strain AMB-1: an iron isotope study. *Geochim Cosmochim Acta* **232**: 225–243.
- Assayag, N., Jézéquel, D., Ader, M., Viollier, E., Michard, G., Prévot, F., and Agrinier, P. (2008) Hydrological budget, carbon sources and biogeochemical processes in Lac Pavin (France): constraints from  $\delta^{18}\text{O}$  of water and  $\delta^{13}\text{C}$  of dissolved inorganic carbon. *Appl Geochem* **23**: 2800–2816.
- Bazyliński, D.A., and Frankel, R.B. (2004) Magnetosome formation in prokaryotes. *Nat Rev Microbiol* **2**: 217–230.
- Bazyliński, D.A., Williams, T.J., Lefèvre, C.T., Berg, R.J., Zhang, C.L., Bowser, S.S., et al. (2013) *Magnetococcus marinus* gen. nov., sp. nov., a marine, magnetotactic bacterium that represents a novel lineage (Magnetococcaceae fam. nov.; Magnetococcales ord. nov.) at the base of the Alphaproteobacteria. *Int J Syst Evol Microbiol* **63**: 801–808.
- Berg, J.S., Jezequel, D., Duverger, A., Lamy, D., Laberty-Robert, C., and Miot, J. (2019) Microbial diversity involved in iron and cryptic sulfur cycling in the ferruginous, low-sulfate waters of Lake Pavin. *PLoS One* **14**: e0212787.
- Blainey, P.C. (2013) The future is now: single-cell genomics of bacteria and archaea. *FEMS Microbiol Rev* **37**: 407–427.
- Blakemore, R. (1975) Magnetotactic bacteria. *Science* **190**: 377–379.
- Bonhomme, C. (2008) Turbulences et ondes en milieu naturel stratifié: deux études de cas: étude du mélange turbulent et des ondes internes du lac Pavin (Auvergne, France); influence des ondes de Rossby sur la concentration en chlorophylle de surface dans l'upwelling du Pérou.
- Bonhomme, C., Poulin, M., Vincon-Leite, B., Saad, M., Groleau, A., Jezequel, D., and Tassin, B. (2011) Maintaining meromixis in Lake Pavin (Auvergne, France): the key role of a sublacustrine spring. *C R Geosci* **343**: 749–759.
- Bura-Nakic, E., Viollier, E., Jezequel, D., Thiam, A., and Ciglenecki, I. (2009) Reduced sulfur and iron species in

- anoxic water column of meromictic crater Lake Pavin (Massif Central, France). *Chem Geol* **266**: 311–317.
- Busigny, V., Jézéquel, D., Cosmidis, J., Viollier, E., Benzerara, K., Planavsky, N.J., et al. (2016) The iron wheel in Lac Pavin: interaction with phosphorus cycle. In *Lake Pavin: History, Geology, Biogeochemistry, and Sedimentology of a Deep Meromictic Maar Lake*, Sime- Ngando, T., Boivin, P., Chapron, E., Jezequel, D., and Meybeck, M. (eds). Cham: Springer International Publishing, pp. 205–220.
- Busigny, V., Planavsky, N.J., Jézéquel, D., Crowe, S., Louvat, P., Moureau, J., et al. (2014) Iron isotopes in an Archean Ocean analogue. *Geochim Cosmochim Acta* **133**: 443–462.
- Chapron, E., Alberic, P., Jezequel, D., Versteeg, W., Bourdier, J.-L., and Sitbon, J. (2010) Multidisciplinary characterisation of sedimentary processes in a recent maar Lake (Lake Pavin, French Massif Central) and implication for natural hazards. *Nat Hazards Earth Syst Sci* **10**: 1815–1827.
- Cosmidis, J., Benzerara, K., Morin, G., Busigny, V., Lebeau, O., Jezequel, D., et al. (2014) Biomineralization of iron-phosphates in the water column of Lake Pavin (Massif Central, France). *Geochim Cosmochim Acta* **126**: 78–96.
- Descamps, E.C.T., Monteil, C.L., Menguy, N., Ginet, N., Pignol, D., Bazylinski, D.A., and Lefèvre, C.T. (2017) *Desulfamplus magnetovallimortis* gen. nov., sp. nov., a magnetotactic bacterium from a brackish desert spring able to biomineralize greigite and magnetite, that represents a novel lineage in the Desulfobacteraceae. *Syst Appl Microbiol* **40**: 280–289.
- Flies, C.B., Jonkers, H.M., de Beer, D., Bosselmann, K., Bottcher, M.E., and Schüler, D. (2005) Diversity and vertical distribution of magnetotactic bacteria along chemical gradients in freshwater microcosms. *FEMS Microbiol Ecol* **52**: 185–195.
- Frankel, R.B., Bazylinski, D.A., Johnson, M.S., and Taylor, B.L. (1997) Magneto-aerotaxis in marine coccoid bacteria. *Biophys J* **73**: 994–1000.
- Jogler, C., Kube, M., Schübbe, S., Ullrich, S., Teeling, H., Bazylinski, D.A., et al. (2009a) Comparative analysis of magnetosome gene clusters in magnetotactic bacteria provides further evidence for horizontal gene transfer. *Environ Microbiol* **11**: 1267–1277.
- Jogler, C., Lin, W., Meyerdieks, A., Kube, M., Katzmann, E., Flies, C., et al. (2009b) Toward cloning of the magnetotactic metagenome: identification of magnetosome Island gene clusters in uncultivated magnetotactic bacteria from different aquatic sediments. *Appl Environ Microbiol* **75**: 3972–3979.
- Jogler, C., Niebler, M., Lin, W., Kube, M., Wanner, G., Kolinko, S., et al. (2010) Cultivation-independent characterization of “*Candidatus Magnetobacterium bavaricum*” via ultrastructural, geochemical, ecological and meta-genomic methods. *Environ Microbiol* **12**: 2466–2478.
- Jogler, C., and Schüler, D. (2009) Genomics, genetics, and cell biology of magnetosome formation. *Annu Rev Microbiol* **63**: 501–521.
- Kolinko, S., Richter, M., Glöckner, F.-O., Brachmann, A., and Schüler, D. (2016) Single-cell genomics of uncultivated deep-branching magnetotactic bacteria reveals a conserved set of magnetosome genes. *Environ Microbiol* **18**: 21–37.
- Kolinko, S., Wanner, G., Katzmann, E., Kiemer, F., Fuchs, B.M., and Schüler, D. (2013) Clone libraries and single cell genome amplification reveal extended diversity of uncultivated magnetotactic bacteria from marine and freshwater environments. *Environ Microbiol* **15**: 1290–1301.
- Koziaeva, V.V., Alekseeva, L.M., Uzun, M.M., Leão, P., Sukhacheva, M.V., Patutina, E.O., et al. (2020) Biodiversity of magnetotactic bacteria in the freshwater Lake Beloe Bordukovskoe, Russia. *Microbiology* **89**: 348–358.
- Lefèvre, C.T. (2016) Genomic insights into the early-diverging magnetotactic bacteria. *Environ Microbiol* **18**: 1–3.
- Lefèvre, C.T., and Bazylinski, D.A. (2013) Ecology, diversity, and evolution of magnetotactic bacteria. *Microbiol Mol Biol Rev* **77**: 497–526.
- Lefèvre, C.T., Bennet, M., Landau, L., Vach, P., Pignol, D., Bazylinski, D.A., et al. (2014) Diversity of magneto-aerotactic behaviors and oxygen sensing mechanisms in cultured magnetotactic bacteria. *Biophys J* **107**: 527–538.
- Lefèvre, C.T., Bernadac, A., Yu-Zhang, K., Pradel, N., and Wu, L.-F. (2009) Isolation and characterization of a magnetotactic bacterial culture from the Mediterranean Sea. *Environ Microbiol* **11**: 1646–1657.
- Lefèvre, C.T., Frankel, R.B., Abreu, F., Lins, U., and Bazylinski, D.A. (2011) Culture-independent characterization of a novel, uncultivated magnetotactic member of the Nitrospirae phylum. *Environ Microbiol* **13**: 538–549.
- Lefèvre, C.T., Howse, P.A., Schmidt, M.L., Sabaty, M., Menguy, N., Luther, G.W., and Bazylinski, D.A. (2016) Growth of magnetotactic sulfate-reducing bacteria in oxygen concentration gradient medium. *Environ Microbiol Rep* **8**: 1003–1015.
- Lefèvre, C.T., Schmidt, M.L., Vilorio, N., Trubitsyn, D., Schüler, D., and Bazylinski, D.A. (2012) Insight into the evolution of magnetotaxis in *Magnetospirillum* spp., based on mam gene phylogeny. *Appl Environ Microbiol* **78**: 7238–7248.
- Li, J., Ge, X., Zhang, X., Chen, G., and Pan, Y. (2010) Recover vigorous cells of *Magnetospirillum magneticum* AMB-1 by capillary magnetic separation. *Chin J Ocean Limnol* **28**: 826–831.
- Li, J., Liu, P., Wang, J., Roberts, A.P., and Pan, Y. (2020c) Magnetotaxis as an adaptation to enable bacterial shuttling of microbial sulfur and sulfur cycling across aquatic oxic-anoxic interfaces. *J Geophys Res-Biogeosci* **125**: e2020JG006012.
- Li, J., Menguy, N., Gatel, C., Boureau, V., Snoeck, E., Patriarche, G., et al. (2015) Crystal growth of bullet-shaped magnetite in magnetotactic bacteria of the Nitrospirae phylum. *J R Soc Interface* **12**: 20141288.
- Li, J., Menguy, N., Leroy, E., Roberts, A.P., Liu, P., and Pan, Y. (2020a) Biomineralization and magnetism of uncultured *Magnetotactic coccus* strain THC-1 with non-chained magnetosomal magnetite nanoparticles. *J Geophys Res Solid Earth* **125**: e2020JB020853.
- Li, J., Menguy, N., Roberts, A.P., Gu, L., Leroy, E., Bourgon, J., et al. (2020b) Bullet-shaped magnetite

- biomineralization within a magnetotactic delta-proteobacterium: implications for magnetofossil identification. *J Geophys Res Biogeosci* **125**: e2020JG005680.
- Li, J., Zhang, H., Liu, P., Menguy, N., Roberts, A.P., Chen, H., *et al.* (2019) Phylogenetic and structural identification of a novel magnetotactic delta-proteobacteria strain, WYHR-1, from a freshwater lake. *Appl Environ Microbiol* **85**: e00731–19.
- Li, J., Zhang, H., Menguy, N., Benzerara, K., Wang, F., Lin, X., *et al.* (2017) Single-cell resolution of uncultured magnetotactic bacteria via fluorescence-coupled electron microscopy. *Appl Environ Microbiol* **83**: pii: e00409-17.
- Lin, W., Li, J., and Pan, Y. (2012) Newly isolated but uncultivated magnetotactic bacterium of the phylum Nitrospirae from Beijing, China. *Appl Environ Microbiol* **78**: 668–675.
- Lin, W., Pan, Y., and Bazylinski, D.A. (2017) Diversity and ecology of and biomineralization by magnetotactic bacteria. *Environ Microbiol Rep* **9**: 345–356.
- Lin, W., Tian, L., Li, J., and Pan, Y. (2008) Does capillary racetrack-based enrichment reflect the diversity of uncultivated magnetotactic cocci in environmental samples? *FEMS Microbiol Lett* **279**: 202–206.
- Lin, W., Wang, Y., Gorby, Y., Nealson, K., and Pan, Y. (2013) Integrating niche-based process and spatial process in biogeography of magnetotactic bacteria. *Sci Rep* **3**: 1643.
- Lin, W., Zhang, W., Zhao, X., Roberts, A.P., Paterson, G.A., Bazylinski, D.A., and Pan, Y. (2018) Genomic expansion of magnetotactic bacteria reveals an early common origin of magnetotaxis with lineage-specific evolution. *ISME J* **12**: 1508–1519.
- Lins, U., Freitas, F., Keim, C.N., de Barros, H.L., Esquivel, D.M.S., and Farina, M. (2003) Simple home-made apparatus for harvesting uncultured magnetotactic microorganisms. *Braz J Microbiol* **34**: 111–116.
- Liu, J., Zhang, W., Du, H., Leng, X., Li, J.-H., Pan, H., *et al.* (2018) Seasonal changes in the vertical distribution of two types of multicellular magnetotactic prokaryotes in the sediment of Lake Yuehu, China. *Environ Microbiol Rep* **10**: 475–484.
- Liu, P., Liu, Y., Zhao, X., Roberts, A.P., Zhang, H., Zheng, Y., *et al.* (2020) Diverse phylogeny and morphology of magnetite biomineralized by magnetotactic cocci. *Environ Microbiol* **23**, 1115–1129.
- Lopes, F., Viollier, E., Thiam, A., Michard, G., Abril, G., Groleau, A., *et al.* (2011) Biogeochemical modelling of anaerobic vs. aerobic methane oxidation in a meromictic crater lake (Lake Pavin, France). *Appl Geochem* **26**: 1919–1932.
- Michard, G., Viollier, E., Jézéquel, D., and Sarazin, G. (1994) Geochemical study of a crater lake: Pavin Lake, France—identification, location and quantification of the chemical reactions in the lake. *Chem Geol* **115**: 103–115.
- Miot, J., Jezequel, D., Benzerara, K., Cordier, L., Rivas-Lamelo, S., Skouri-Panet, F., *et al.* (2016) Mineralogical diversity in Lake Pavin: connections with water column chemistry and biomineralization processes. *Minerals* **6**: 24.
- Monteil, C.L., Benzerara, K., Menguy, N., Bidaud, C.C., Michot-Achdjian, E., Bolzoni, R., *et al.* (2021) Intracellular amorphous Ca-carbonate and magnetite biomineralization by a magnetotactic bacterium affiliated to the Alphaproteobacteria. *ISME J* **15**: 1–18.
- Monteil, C.L. and Lefevre, C.T. (2019) Magnetoreception in microorganisms. *Trends Microbiol* **28**: 266–275.
- Monteil, C.L., Vallenet, D., Menguy, N., Benzerara, K., Barbe, V., Fouteau, S., *et al.* (2019) Ectosymbiotic bacteria at the origin of magnetoreception in a marine protist. *Nat Microbiol* **4**: 1088–1095.
- Moskowitz, B.M., Bazylinski, D.A., Egli, R., Frankel, R.B., and Edwards, K.J. (2008) Magnetic properties of marine magnetotactic bacteria in a seasonally stratified coastal pond (Salt Pond, MA, USA). *Geophys J Int* **174**: 75–92.
- Oestreicher, Z., Lower, S., and Lower, B. (2011) Magnetotactic bacteria containing phosphorus-rich inclusion bodies. *Microsc Microanal* **17**: 140–141.
- Pan, H., Dong, Y., Teng, Z., Li, J., Zhang, W., Xiao, T., and Wu, L.-F. (2019) A species of magnetotactic delta-proteobacterium was detected at the highest abundance during an algal bloom. *FEMS Microbiol Lett*: 366:fnz253.
- Popp, F., Armitage, J.P., and Schüller, D. (2014) Polarity of bacterial magnetotaxis is controlled by aerotaxis through a common sensory pathway. *Nat Commun* **5**: 5398.
- Qian, X.-X., Santini, C.-L., Kosta, A., Menguy, N., Le Guenno, H., Zhang, W., *et al.* (2020) Juxtaposed membranes underpin cellular adhesion and display unilateral cell division of multicellular magnetotactic prokaryotes. *Environ Microbiol* **22**: 1481–1494.
- R Core Team. (2018) *R: A Language and Environment for Statistical Computing*. Vienna, Austria: R Foundation for Statistical Computing. <https://www.R-project.org/>.
- Rivas-Lamelo, S., Benzerara, K., Lefèvre, C.T., Jézéquel, D., Menguy, N., Viollier, E., *et al.* (2017) Magnetotactic bacteria as a new model for P sequestration in the ferruginous Lake Pavin. *Geochem Perspect Lett* **5**: 35–41.
- Schettler, G., Schwab, M.J., and Stebich, M. (2007) A 700-year record of climate change based on geochemical and palynological data from varved sediments (Lac Pavin, France). *Chem Geol* **240**: 11–35.
- Schüler, D. (2002) The biomineralization of magnetosomes in *Magnetospirillum gryphiswaldense*. *Int Microbiol* **5**: 209–214.
- Schulz-Vogt, H.N., Pollehne, F., Jürgens, K., Arz, H.W., Beier, S., Bahlo, R., *et al.* (2019) Effect of large magnetotactic bacteria with polyphosphate inclusions on the phosphate profile of the suboxic zone in the Black Sea. *ISME J* **13**: 1198–1208.
- Simmons, S.L., Bazylinski, D.A., and Edwards, K.J. (2007) Population dynamics of marine magnetotactic bacteria in a meromictic salt pond described with qPCR. *Environ Microbiol* **9**: 2162–2174.
- Simmons, S.L., Sievert, S.M., Frankel, R.B., Bazylinski, D. A., and Edwards, K.J. (2004) Spatiotemporal distribution of marine magnetotactic bacteria in a seasonally stratified coastal salt pond. *Appl Environ Microbiol* **70**: 6230–6239.
- Spring, S., Amann, R., Ludwig, W., Schleifer, K.H., Schuler, D., Poralla, K., and Petersen, N. (1994) Phylogenetic analysis of uncultured magnetotactic bacteria from the alpha-subclass of Proteobacteria. *Syst Appl Microbiol* **17**: 501–508.
- Spring, S., Amann, R., Ludwig, W., Schleifer, K.H., Vangemerden, H., and Petersen, N. (1993) Dominating

- role of an unusual magnetotactic bacterium in the micro-aerobic zone of a fresh-water sediment. *Appl Environ Microbiol* **59**: 2397–2403.
- Viollier, E., Jezequel, D., Michard, G., Pepe, M., Sarazin, G., and Alberic, P. (1995) Geochemical study of a Crater Lake (Pavin Lake, France)—trace-element behavior in the monimolimnion. *Chem Geol* **125**: 61–72.
- Wolfe, R.S., Thauer, R.K., and Pfennig, N. (1987) A ‘capillary racetrack’ method for isolation of magnetotactic bacteria. *FEMS Microbiol Lett* **45**: 31–35.
- Xiao, Z., Lian, B., Chen, J., and Teng, H.H. (2007) Design and application of the method for isolating magnetotactic bacteria. *Chin J Geochem* **26**: 252–258.
- Zhang, H., Menguy, N., Wang, F., Benzerara, K., Leroy, E., Liu, P., et al. (2017) Magnetotactic coccus strain SHHC-1 affiliated to Alphaproteobacteria forms octahedral magnetite magnetosomes. *Front Microbiol* **8**: 969.

### Supporting Information

Additional Supporting Information may be found in the online version of this article at the publisher’s web-site:

**Appendix S1:** Supporting information

## **2.4 Thin description of the magnetotactic bacteria profile as a function of the depth and varying chemical parameters in the water column of Lake Pavin**

### **2.4.1 Material and methods**

#### **2.4.1.1 Site description and water sampling strategy**

The water column of the ferruginous meromictic Lake Pavin, France (45.495792°N, 2.88-8117°E) was sampled in October 2019 from a platform anchored at its center where the lake is the deepest (~90 m). Previous campaigns showed that **MTB** have been systematically found right under the oxycline at depths where dioxygen becomes undetectable in a specific range of conductivity (Busigny et al., 2021). The localization of this zone varies over the seasons which influences the depth where **MTB** are found (Busigny et al., 2021). Therefore, a first geochemical profiling (notably, O<sub>2</sub> and redox potential) of the water column was done in October 29<sup>th</sup> 2019 (1<sup>st</sup> day) to localize the **OATZ** and the **MTB** communities with a 50 cm resolution and was checked again the 30<sup>th</sup> in the morning (2<sup>nd</sup> day). These profiles did not significantly change overnight and were then used to establish a fine sampling strategy along the few meters from above to below the **OATZ** the 2<sup>nd</sup> day afternoon. When reaching 50.7 m, a depth close to the one of first **MTB** appearance on the 1st day, a total of 9 samples spaced of ~20 cm in average were collected and further used to determine the **MTB** concentration, diversity and physicochemical features. Samples were collected using a metered flexible hose attached in parallel with a metered cable with the approach described in Busigny et al. (2021). The hose of ~65 m long, was connected to a speed-adjustable 12 V brushless pump (DC50E-1250A). When reaching the depth to sample, a ~5 min break was respected to ensure the hose purge and the collection of the water at the corresponding depth. At each depth, several samples were collected either for chemical or biological analyses. For **MTB** populations analyses, samples were collected in several 1 L glass bottles filled to their capacity and tightly closed for optical and electron microscopy preparation. For chemical analyses at each sampled depth of the water column, 3 L of sample were in-line filtrated under anoxia (N<sub>2</sub> influx and control of oxygen with a multi-parameter portable meter) through 45 mm quartz filters with a 0.7 μm nominal threshold. A triplicate of 10 mL soluble fraction was recovered and then acidified with 3 to 4 drops of 65% HNO<sub>3</sub>—suprapur to prevent any precipitation. In parallel, the particulate fraction was dried by the continuous N<sub>2</sub> influx in the filtration system after the water entry stopped. The filters were then stored in Petri dishes until further treatments.



## Chapter 2. Vertical structure of magnetotactic bacteria populations in the water column of Lake Pavin

---

### 2.4.1.2 *In situ* measurements of physicochemical parameters

Some physicochemical features were measured *in situ* using an YSI EXO2 Multiparameter probe, such as the conductivity (CTD), pH, redox potential, oxygen concentration, turbidity, fluorescent dissolved organic matter (fDOM) concentration and temperature. Detection limit for dissolved O<sub>2</sub> is ca 0.1% or about  $0.3 \pm 0.2 \mu\text{M}$ . Turbidity was also measured simultaneously *in situ* with an Aquatec AQUAlogger 210TYPT (Seapoint turbidity sensor, 880 nm) probe to get a higher sensitivity threshold. Oxygen sensor calibration was made against ambient air (pO<sub>2</sub> = 100%), and conductivity against two buffers standard solutions at 25°C. The different *in situ* probes were fixed at the extremity of the sampling hose.

### 2.4.1.3 Chemical analyses of dissolved and particulate fractions in the water column

For the measurement of the particulate fraction using Inductively Coupled Plasma-Optical Emission Spectroscopy (ICP-OES), a triplicate of 17 mm disks was sliced from each filter and submitted to an acidified solution of 1 M HNO<sub>3</sub>-suprapur for a period of at least a day. The subsequent solution was then recovered and diluted in order to stay in the measurement accuracy range of the spectrometer (ICP-OES iCAP6200 ThermoScientific). The ICP-OES was also used to measure the dissolved fraction retrieved and acidified directly on the field. The reduced forms such as H<sub>2</sub>S and Fe<sup>2+</sup> were not measured due to (i) an unavoidable too large delay between the sampling and the analyses and (ii) the presence of oxygen in our samples. Duplicates of 9 mm sliced disks from the same filters as for the ICP-OES were recovered for the quantification of carbon and nitrogen elements. These quantification were done using an Organic Elemental Analyzer CHNS Flash 2000 ThermoScientific. For each water sample, filtrated solution with an addition of zinc acetate were used for the measurement of anions (fluoride, chloride, bromide, nitrate, sulfate) using ion chromatography with a Dionex Chromatograph.

### 2.4.1.4 Estimation of the magnetotactic bacteria population sizes and analysis of morphotypes diversity

Populations of north-seeking MTB were quantified by retrieving 40  $\mu\text{L}$  of water sample and cells were counted using the hanging drop technique (Schüler, 2002) with a Zeiss Primo Star light microscope equipped with contrast and differential interference contrast optics. South-seeking MTB were also counted but corresponded to either really small amount or none. The final concentration of MTB per litre at each depth of the water column was estimated with two biological replicates. For each of the 9 samples collected at or around the OATZ, the diversity of MTB morphotypes was also estimated. As previously done (Rivas-Lamelo et al., 2017; Monteil et al., 2021), each cell counted (~5 to 130 cells per sample) was classified according to their shape (e.g. spirillum, coccoid, rod shape), their size and the presence/absence of bright

## 2.4. Thin description of the magnetotactic bacteria profile as a function of the depth and varying chemical parameters in the water column of Lake Pavin

---

intracellular granules.

MTB can also be differentiated by their magnetosomes shape, composition, numbers and organization. These characteristics are not observable in optical microscopy, thus the morphotype heterogeneity of the MTB was further analyzed using STEM and XEDS approaches. MTB were concentrated using a magnetic enrichment protocol. The magnetic enrichment, for each depth, consisted in placing the south pole of a stirring-magnet against the side of a 1 L bottle at its center for 1 h. These bottles correspond to a duplicate of the ones used for optical microscopy. 15  $\mu$ L of MTB pellet was deposited, onto TEM grids coated with poly-L-lysine, for 20 min with a stirring magnet below with the south pole facing up (i.e. to attract north-seeking MTB). The grids were then washed twice with filtered sterilized water and the excess each time absorbed after 5 min with a Whatman paper until complete dry. STEM observations were performed in the HAADF mode using a JEOL 2100F, operating at 200 kV, and equipped with a JEOL XEDS detector. The number of cells observed and counted on the TEM grid averaged a few hundred to several hundreds of cells. However, when the number of cells was low we counted all the cells present on the grid.

### 2.4.1.5 Statistical analyses

Statistical analyses of the environmental and biological datasets were performed using the R software, version 4.0.0 (R Core Team, 2020). Our dataset describing the environmental context where MTB have been detected in October 2019 consisted in 8 physicochemical variables (*in situ* measurements) and 38 geochemical variables, with observations corresponding to 9 water column depths. Geochemical variables with values under the detection limits for all the 9 depths were excluded (i.e. the concentrations of particulate fractions for Lithium, Boron and Silicon; concentrations of dissolved fractions for Aluminum and Lithium; concentrations of Bromide in the dissolved fraction). Our final geochemical dataset consisted in a total of 32 variables. We faced some missing value issues for the physicochemical dataset, which we addressed by using modeling strategies. Because of a sudden failure of the real-time recording device 1 to 3 out of 9 values could not be recorded for the following *in situ* measurements: conductivity, temperature, pH, redox potential (ORP), turbidity, chlorophyll concentration and fDOM. For each of these variables, we built linear regression models using the 6 to 8 values recorded on the 2<sup>nd</sup> day afternoon and those corresponding to the same depths in the complete profile realized in the 2<sup>nd</sup> day morning. Missing values were replaced with values predicted by the model if the linearity was significant (Pearson test P-value < 0.05) when all test assumptions were satisfied (i.e. independency of residuals, normal distribution of residuals, homogeneous distribution). If not, the variable was excluded from the whole analysis. This approach was successful for the following variables only: conductivity, temperature, pH, and fDOM concentrations. The other

## Chapter 2. Vertical structure of magnetotactic bacteria populations in the water column of Lake Pavin

---

variables: redox potential (ORP), turbidity, chlorophyll concentration, were excluded from the final environmental dataset which consisted in a total of 36 variables.

First, strength and direction of the pairwise linear or monotonous relationships between the 36 environmental variables on 9 water column depth samples were evaluated by the Pearson's (when bivariate normality assumptions were satisfied) or Spearman's correlation coefficient, respectively (values ranging from  $-1$  to  $+1$ ). The statistical significance of each correlation was assessed and indicated by a P-value: correlations were considered as significant when the P-value was lower than 0.0014 (Bonferroni correction corresponding to a false positive error rate lower than 5% per test). Pairwise relationships of the variables were drawn.

In order to define environmental niches in the water column depth zone where **MTB** populations were observed, an additional clustering of the environmental variables into directional groups associated with a Latent Variable (LV) was performed. Based on the variation of the clustering criterion after consolidation of the partitions by means of the partitioning algorithm, an important loss in homogeneity of the clusters with 9 clusters was observed which means that a partition into 10 clusters of variables should be retained (appendices Fig. S1). We performed a standardized principal component analyses (PCA) on the 9 water column depths described by these latent variables (potentially indicative of niche structuring).

Our dataset describing the **MTB** populations thriving at 9 depths in the water column (Table S1) consisted in the abundance of **MTB** cells and of the two main **MTB** populations (**MTBc** and **iACC**-forming rods, as counted by optical microscope with triplicates).

## 2.4. Thin description of the magnetotactic bacteria profile as a function of the depth and varying chemical parameters in the water column of Lake Pavin

### 2.4.2 Results

#### 2.4.2.1 Magnetotactic bacteria communities are localized just below the OATZ in a zone spatially structured in discrete geochemical niches

The first geochemical profiling of the Lake Pavin water column performed on the first day localized the OATZ and the MTB communities in the water column (Fig. 2.1).

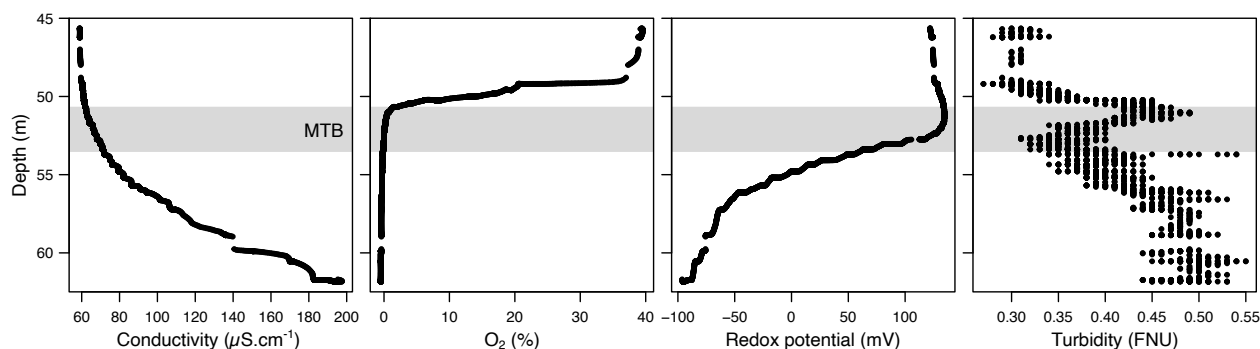


**Figure 2.1:** Physicochemical depth profiles in the water column of Lake Pavin measured *in situ* in October 30<sup>th</sup>. The light gray zone corresponds to the localization of the MTB peak.

In details, the oxygen concentration of the water column underwent a steep diminution around 49.7 m in depth where it decreased from ~40 % to the probe detection limit and complete anoxia around 50.3 m. In line with previous observations (Busigny et al., 2021), conductivity, dissolved organic matter concentration and temperature gradually increased with depth from ~ 60 to > 200  $\mu\text{S}\cdot\text{cm}^{-1}$ , from 1 to 5 RFU and from 4°C to > 4.5°C, respectively. Moreover, a typical slight peak of turbidity was observed at the depth just after the oxygen disappeared. A rough estimation of MTB population sizes confirmed their localization in the anoxic part of the water column between 51.3 and 53.5 m.

Based on these data, a second fine sampling strategy was defined for the transect of a few meters where MTB were observed specifically and slightly upper. When reaching 50.7 m, a total of 9 additional samples spaced of ~20 cm in average were collected the afternoon and further used to identify geochemical niches in relation to MTB concentration and diversity. By analysing a total of 36 geochemical variables at each depth, we identified groups of variables fluctuating similarly (Fig. 2.2A).

Two big clusters of positively correlated variables can be seen that are negatively correlated to each other. This is mainly the dissolved element fractions negatively correlated to the particulate fraction, with the exception of dissolved sulfate negatively correlated to the other dissolved elements and strongly correlated to particulate Ca, Fe, P and the mass percentage of C and N. The two first axes of a principal component analysis built from this matrix explained 73.6 % of the total variance and showed that depths could be distinguished in three global niches; one at 50.7 m (1 sample), a second from 51 m to 52 m (5 samples), and a third one from 52,5 and

## Chapter 2. Vertical structure of magnetotactic bacteria populations in the water column of Lake Pavin

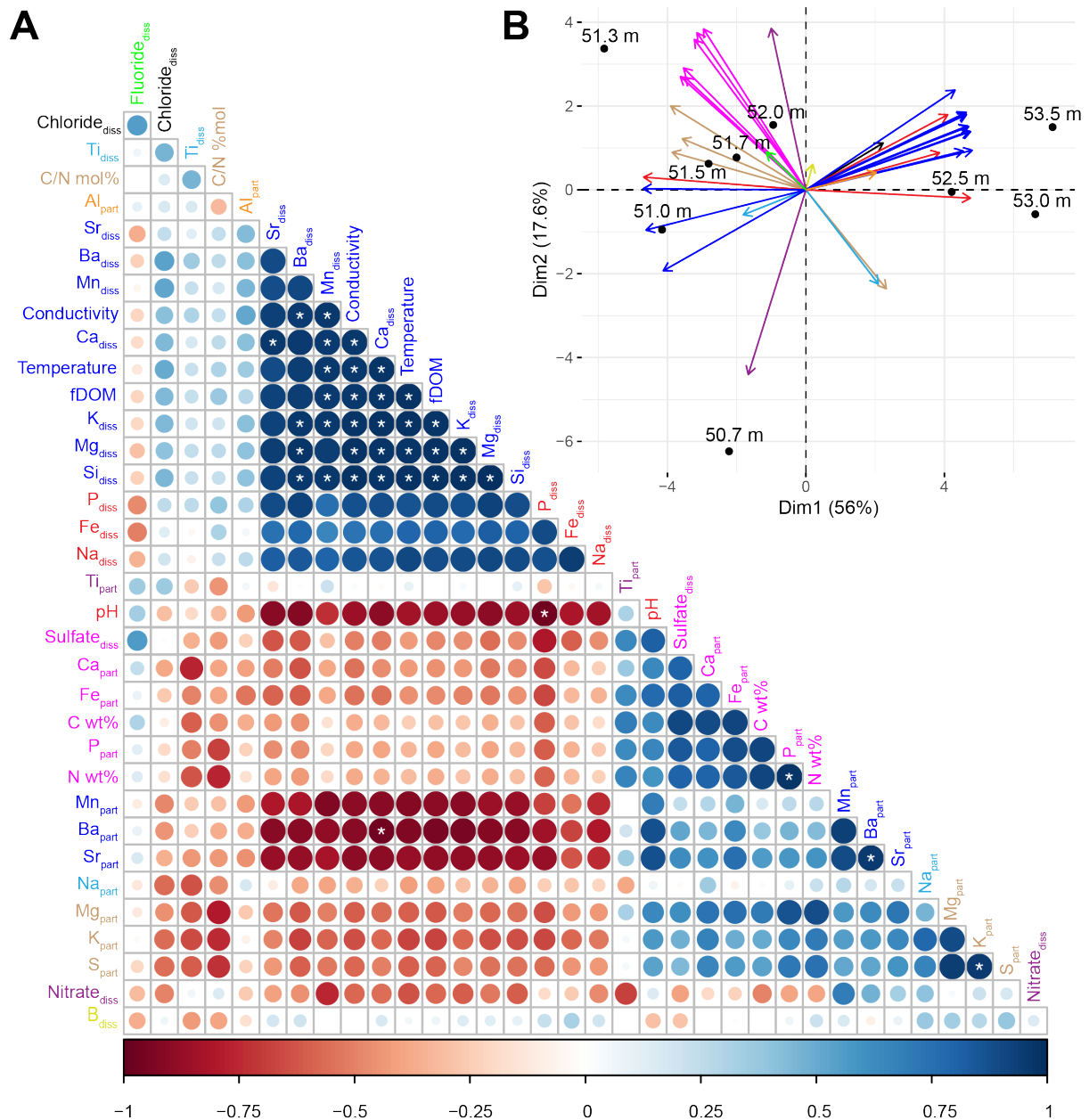


**Figure 2.2: Environmental structuring of depths according to their geochemical features.** (A) Correlation matrix built from 36 geochemical variables reordered according to the correlation coefficient and (B) associated principal component analysis showing covariance of these variables according to the sampling depth. Depths 1 to 9 refer to depths 50.7 m to 53.5 m. Variables and vectors in both panels with the same colour belong to the same cluster defined by the Clustering of Variables around Variables (CLV) approach. Ten directional groups (i.e. clusters of positively and negatively highly correlated variables) were identified and are represented in a dendrogram and in separated PCA in the appendices Fig. S1.

53.5 m (3 samples) (Fig. 2.2B). While the first niche is mainly structured by a higher nitrate concentration, niche 2 differs from niche 3 mainly by (i) the concentration of particulate iron, phosphorus, magnesium, calcium, sulfur and potassium, (ii) the concentration of dissolved sul-

## 2.4. Thin description of the magnetotactic bacteria profile as a function of the depth and varying chemical parameters in the water column of Lake Pavin

---

fate and (iii), the mass percentage of N and C.

### 2.4.2.2 Magnetotactic bacteria are diverse and predominantly composed of MTBc

In parallel of the geochemistry, each sample was analysed regarding MTB diversity and concentration using magnetic sorting and optical microscopy approaches. The morphotypic diversity was estimated by classifying cells according to their shape (e.g. spirillum, coccoid, rod shape), their size and the presence/absence of bright intracellular granules, as previously done in [Monteil et al. \(2021\)](#) under the light microscope. The total concentration of MTB and of the two main morphotypes were then represented in Fig. 2.3A.

Seven different morphotypes were then observed by electron microscopy across the nine depths (Fig. 2.4), among which MTBc able to hyperaccumulate P under the form of PolyP represented the most abundant morphotype (Fig. 2.4A, XEDS supplied in the appendices Fig. S2A), reaching between 52 and 94% of the total MTB population (Table S1).

Rod shaped bacteria forming granules of amorphous calcium carbonate and prismatic magnetosomes represent the second more abundant MTB morphotype (Fig. 2.4B, XEDS measurements supplied in the appendices Fig. S2B). This morphotype represents between 2% and 47% of the total MTB population (Table S1). Together with the MTBc, they account for between 88.5 and 98.8% of the MTB cells observed at each depth (Figure 2.3A).

In a minor extent, few other morphotypes could be observed in the lower zone where the populations of MTBc and iACC-forming rods are decreasing. One also accumulating P as PolyP (Fig. 2.4C, XEDS supplied in the appendices Fig. S2C), is a rod with a chain of prismatic magnetosomes and has been previously affiliated to the *Magnetococcaceae* family ([Monteil et al., 2021](#)). This morphotype of MTB seemed to have been encountered as well in other marine and freshwater environments ([Spring et al., 1995](#); [Oestreicher et al., 2011](#); [Kolinko et al., 2013](#)). Although this MTB morphotype is not abundant, we could find a peak of abundance at 52.5 m in depth corresponding to a slight drop of MTBc and iACC-forming rods percentage (Fig. 2.3A). A small type of vibrio with similar ultrastructural features of *Desulfovibrio magneticus* RS-1 ([Pósfai et al. \(2006\)](#); [Chariaou et al. \(2015\)](#); Fig. 2.4D) was also found along with another magnetotactic sulfate-reducing Deltaproteobacteria-like ([Descamps et al., 2017](#)) below 52.5 m (Fig. 2.4E). Another small vibrio forming one chain of prismatic magnetosomes was observed in few amounts as well (Fig. 2.4F). The last morphotype of MTB is a large curved rod mineralizing a chain of prismatic magnetosomes and observed only once (Fig. 2.4G).

## Chapter 2. Vertical structure of magnetotactic bacteria populations in the water column of Lake Pavin

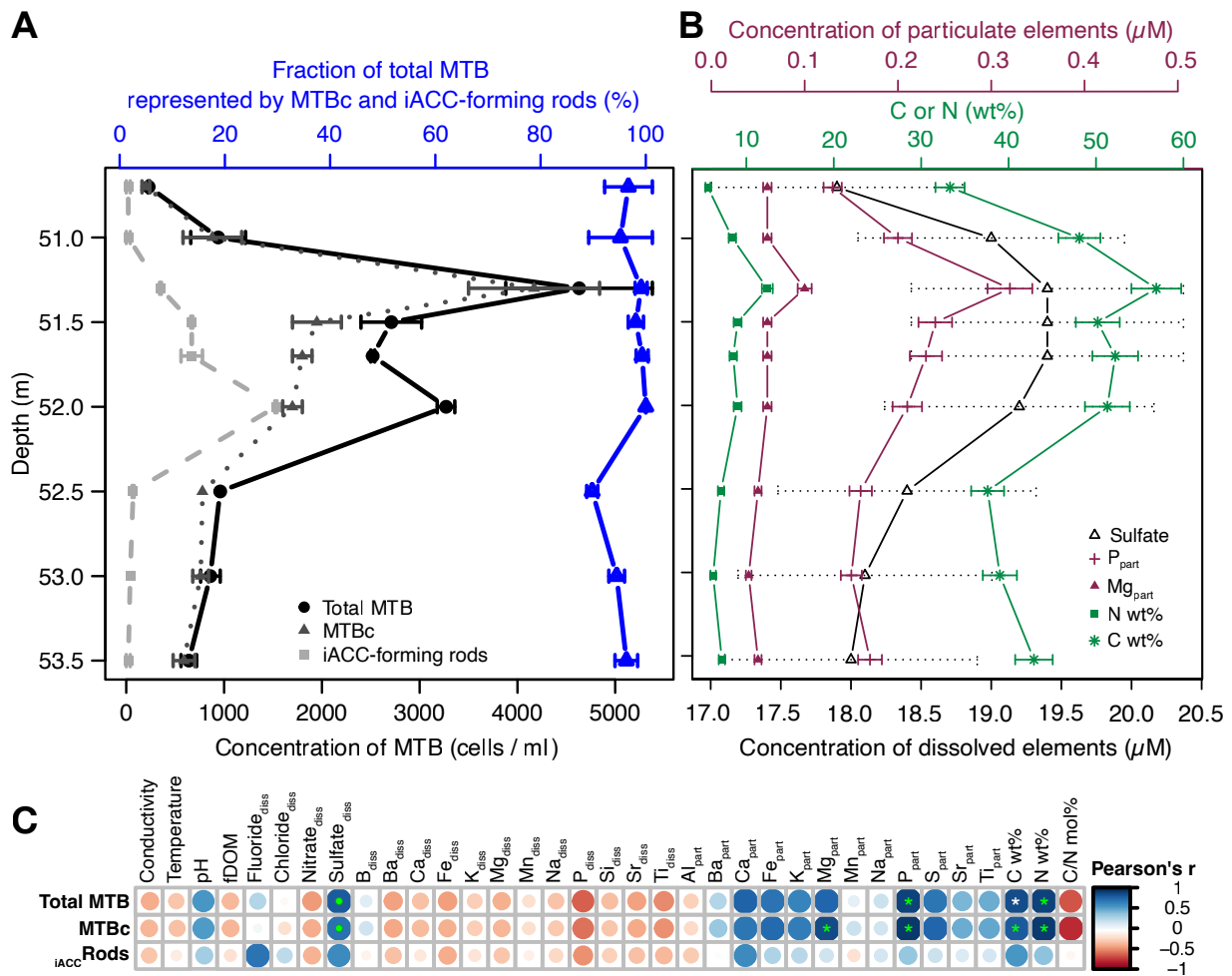


**Figure 2.3: Relationships between the MTB population structure and abundance and the environmental features in the water column.** (A) Cell concentration of the total MTB and those of the two main morphotypes, i.e. the iACC-forming rods and the MTBc for the nine sampled depths. The fraction of total MTB represented by these two morphotypes are given for each depth. Error bars represent the standard deviation on biological duplicates (see wTable S1 for details) (B) Concentration profiles of the different geochemical variables significantly and positively correlated to either the total MTB or/and MTBc using Pearson's and Spearman's correlations tests. Particulate organic N and C are expressed in weight percent (wt%) of the total particulate organic matter. Error bars represent the maximal absolute error on measurement ( $\pm 5\%$  for dissolved sulfate and particulate organic N and C,  $\pm 7.5\%$  for particulate P and Mg, respectively). (C) Statistical analysis of the correlation between the environmental variables and the cell concentrations of total MTB, MTBc and iACC-forming rods. The plot shows the Pearson's correlation matrix. The size and the color of the circles are related to the correlation coefficient value, meaning that: the bigger and the darker the circle, the better the correlation. Blue and red circles refer positive and negative correlations respectively. The white and the green stars indicate significant linear correlations (Pearson's test) or monotonic correlations (Spearman's test), respectively. A green dot indicates that both tests were statistically significant. All statistics are given in the appendices in Table S2.

## 2.4. Thin description of the magnetotactic bacteria profile as a function of the depth and varying chemical parameters in the water column of Lake Pavin

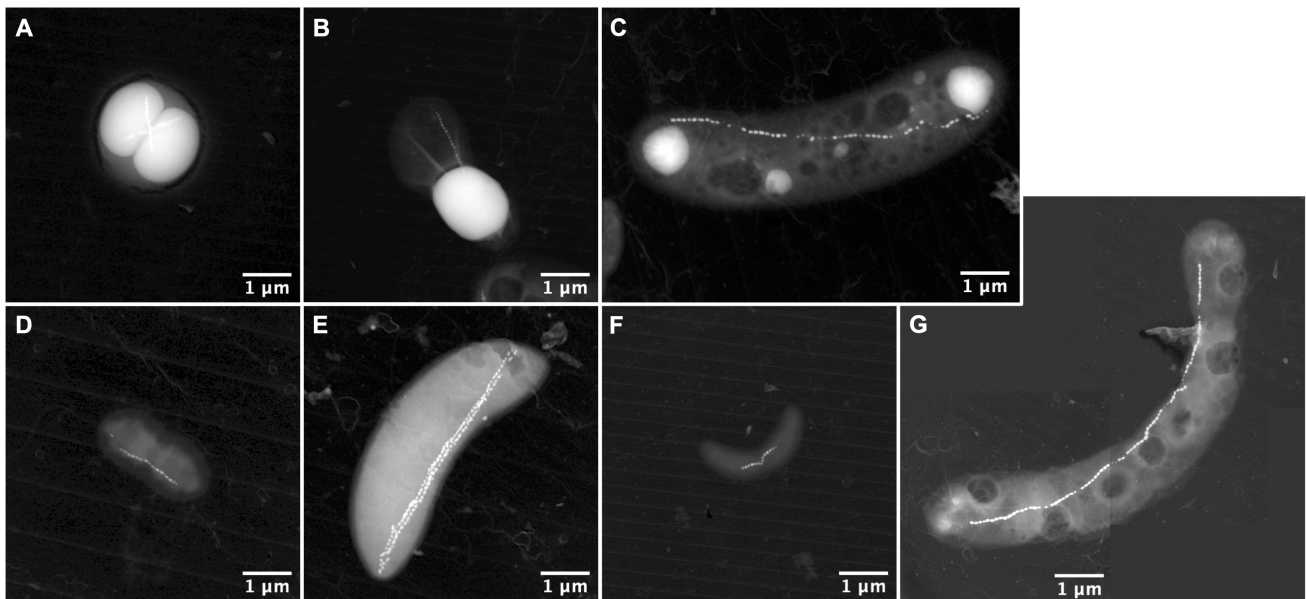


**Figure 2.4: Scanning transmission electron microscopy images of magnetotactic bacteria with different morphology found in Lake Pavin water column.** It includes **MTBc** cells of the *Magnetococcaceae* family producing polyphosphate inclusions (A); calcium-carbonate producing **MTB** (B); Rod-shaped **MTB** producing polyphosphate inclusions and affiliated to the *Magnetococcaceae* family (C); small vibrio resembling the *Desulfovibrio magneticus* RS-1 bacteria with bullet-shaped magnetosomes (D); rods resembling sulfate-reducing **MTB** producing bullet-shaped magnetosomes affiliated to the Deltaproteobacteria (E); small vibrio resembling some species of the *Magnetospirillum* genus (F); and long curved rod forming hexagonal magnetic crystal (G).

### 2.4.2.3 The abundance of **MTBc** is correlated to the concentration of dissolved sulfates, mass percentage of organic N and C, particulate magnesium and phosphorus

The structure of the total **MTB** population and that of the main morphotypes along the water column transect, in connection to geochemical niches was investigated, to get insight into **MTB** biology and ecology. In agreement with previous observations during a recent campaign (Busigny et al., 2021), the **MTB** distribution was structured in two distinct peaks over the water column at 51.3 m and 52 m (Fig. 2.3A) where the population could reach up to  $4.6 \cdot 10^3$  and  $3.2 \cdot 10^3$  cells per mL of water respectively. While the concentration of **MTBc** was the highest at 51.3 m, that of **iACC**-forming rods was the highest at 52 m.

Pairwise correlation analyses identified several geochemical variables linked to the abundance of **MTB** populations (Fig. 2.3B and C, data in appendices Table S2). The most striking results were obtained for the concentration of **MTBc** that was significantly correlated to the concentration of particulate phosphorus and magnesium (Pearson's  $r$  of 0.94 and 0.8 respectively,  $P < 0.0014$ ) and mass percentage of nitrogen (0.91,  $P < 10^{-5}$ ). When looking at non-linear but monotonous relationships, we could observe an additional correlation between the concentration of dissolved sulfates and the concentration of both **MTBc** and total **MTB** populations (Spearman's rho of



0.90,  $P < 10^{-5}$ ). Lowering the stringency on the P-value threshold, mass percentage of carbon appeared as positively correlated both to the concentration of both total **MTB** and **MTBc** (Spearman's rho of 0.78 and 0.78 respectively,  $P < 0.003$ ). **MTBc** being the major **MTB** in the water column, the profile of **MTBc** concentration follows that of total **MTB** (Pearson's  $r$  of 0.90,  $P = 0$ ) and therefore similar relationships were obtained for total **MTB** and **MTBc** concentrations (Fig. 2.3C). No variable measured in this study was significantly associated to the concentration of rods forming intracellular amorphous calcium carbonate.

### 2.4.3 Discussion

As **MTBc** dominate the **MTB** profile, i.e. representing a minimum of 52% and up to 94% of all **MTB** at any depth, a similar pattern of correlations with different geochemical parameters was observed for the total abundance of **MTB** and the abundance of **MTBc**. In particular, both abundances were correlated to the wt% of N and C. The C/N mol% ratio average value calculated in our samples is 6.63, which correspond to the Redfield ratio of C/N in aquatic biomass (6.625) (Tyrrell, 2001). The ratio of **MTB** versus other microorganisms in the water column of Lake Pavin only accounts to ~1:1000 (Lehours et al., 2005). It is thus likely that wt% N and C correspond to a proxy for the presence of the biomass represented at these depths by eubacteria and archaea, and that the optimal conditions for prokaryotic biomass development in this anoxic layer also favours **MTBc** growth.

Significant correlations were found between the concentration of dissolved sulfate and **MTBc**-related quantitative variables (optical counting), providing clues to metabolic features of these bacteria (Fig. 2.3C). The **MTB** zone most likely correspond to the maximum concentration of dissolved sulfate encountered in the water column of Lake Pavin as compared with the different chemical profiles obtained in Miot et al. (2016); Busigny et al. (2016); Rivas-Lamelo et al. (2017). A positive linear correlation between the concentration of this sulfur compound and the bulk abundance of **MTBc** could suggest either a metabolic dependency or a release related to **MTBc** growth, corresponding respectively to sulfate-reduction or sulfur-oxidation, respectively.

The sulfur oxidizing bacteria (**SOB**) and the sulfate reducing bacteria (**SRB**) are usually found around the redoxcline, in suboxic or euxinic waters (Vliet et al., 2020). In a recent study using 16S rRNA analyses, it has been shown that **MTBc** were at their highest abundance at the same depth where the **SOB** and **SRB** are present (Berg et al., 2019). In addition, Berg et al. have shown that at the **MTBc** maximum abundance depth, in suboxic conditions, the **SOB** were dominant compared to the **SRB** (Berg et al., 2019), the **SRB** becoming dominant deeper in the water column. Berg et al. also found that **MTBc** corresponded to 8% of the **SOB** sequences, which supports our hypothesis that they are sulfur-oxidisers as they sequester intracellular sul-

#### 2.4. Thin description of the magnetotactic bacteria profile as a function of the depth and varying chemical parameters in the water column of Lake Pavin

---

fur granules. Our present observations evidenced in TEM the succession as a function of depth of the MTBc, then deeper the *Magnetococcaceae* rods accumulating PolyP and sulfur granules and finally, based on their ultrastructure, potential sulfate-reducing Deltaproteobacteria. These observations confirm the vertical succession of SOB and SRB in the water column. Dissolved sulfate increases slightly around the MTBc abundance peak (figure 2.3B), this increase could be due to MTBc oxidizing their sulfur storage as well as species of the *Sulfuritalea* genus that represent the most abundant SOB in the water column (Berg et al., 2019). The *Sulfuritalea* are known to oxidize thiosulfate, S<sup>0</sup> and hydrogen but not sulfide, with sulfate as an end product. They can also use nitrate as an electron acceptor. With the hypothesis that MTBc use sulfide when the *Sulfuritalea* do not, it might explain their coexistence at the same depths and they might not compete between each other for their electron donor but only for the electron acceptor. Intracellularly accumulated nitrate could then be a good survival process for the MTBc to thrive at these depths.

This study did not find a specific biogeochemical niche for the iACC-forming rods or the other minor morphotypes of MTB. The reasons may be that (i) a high biomass concentration is necessary for efficient statistical analyses along the entire MTB profile and (ii) parameters which structure their vertical distribution were not measured (e.g. pCO<sub>2</sub>, methane...).

## 2.5 Design of culture media for the isolation of the Lake Pavin MTBc and preliminary results

### 2.5.1 Materials and methods

#### 2.5.1.1 Design of double gradient media

Cells for Lake Pavin MTBc growth media were inoculated during the field trip of October 2019. The media tested were elaborated based on media commonly used for MTBc and magnetite forming MTB, but also based on the potential physiology of MTBc and the chemical conditions met in the water column.

In Lake Pavin, the MTBc are found right under the oxic-anoxic interface in anoxia, where a lot of different chemical gradients are co-located (see Chapter 1 part 1.1.4 for more details), moreover, the MTBc in Lake Pavin have been shown to accumulate elemental sulfur granules, indicating a metabolism of sulfur-oxidation and thus the use of sulfur compounds. For these reasons, the first culture media tested for their isolation were inspired from the marine *Beggiatoa* strain medium where oxygen and sulfide gradients are opposed (Nelson and Jannasch, 1983; Brock and Schulz-Vogt, 2011). This strain, similarly to our MTBc in Lake Pavin, is accumulating P in high amount and sulfur granules as well. This type of inverse gradient culture medium has also been previously used with successful results for the enrichment of freshwater and marine MTB located in similar inverse gradients of oxygen and sulfide (Schüler et al., 1999; Bazylnski and Williams, 2007). Finally, the components of the Lake Pavin MTBc growth media were inspired and modified from the culture of the phylogenetically close cultivated marine MTBc MC-1 (Bazylnski et al., 2013b).

The media consisted of 12 mL of semi-solid medium (0.2% agar) overlying 6 mL of solid plug of agar (2%) in a anoxic cap clipped glass tube of ~25 mL. The agar was previously washed three times to remove impurities. The semi-solid agar composed the part where the MTB were inoculated thus the growth medium, whereas the solid plug of agar only served to create an overlying gradient of sulfide or thiosulfate. The semi-solid medium was amended with ammonium chloride (5.6 mM), magnesium sulfate (162  $\mu$ M), potassium nitrate (5 mM), iron chloride (30  $\mu$ M), sodium carbonate (15 mM), dipotassium phosphate (100  $\mu$ M), a filter sterilized solution of vitamins (Vitamines, see appendices 4.2 for composition), and a solution of trace metals (Wolf mineral solution, see appendices for composition). 20 mM of PIPES was also added to the medium to buffer the system at pH 6.2 (pH close to the one observed in the MTB zone in Lake Pavin), especially because the bottom plug of sulfide can acidify the medium with time. Resazurin was implemented in the medium to follow the formation of the redox and oxygen gradient in the semi-solid medium. See the details in the schematic figure 2.5.

## 2.5. Design of culture media for the isolation of the Lake Pavin **MTBc** and preliminary results

Four different media were tested, two had a bottom agar plug containing  $\text{Na}_2\text{S}$  and two other thiosulfate. One of each plug was also implemented with 0.04% neutralized and fresh filtered cystein to help counter the oxygen diffusion and create a different gradient with respect to oxygen versus sulfide or thiosulfate.

The media were prepared before the field trip and kept at  $4^\circ\text{C}$  until a few hours before the inoculation, approximately five days later. Five tubes of each media were prepared. Once inoculated, the culture media were placed at  $18^\circ\text{C}$  in the dark.

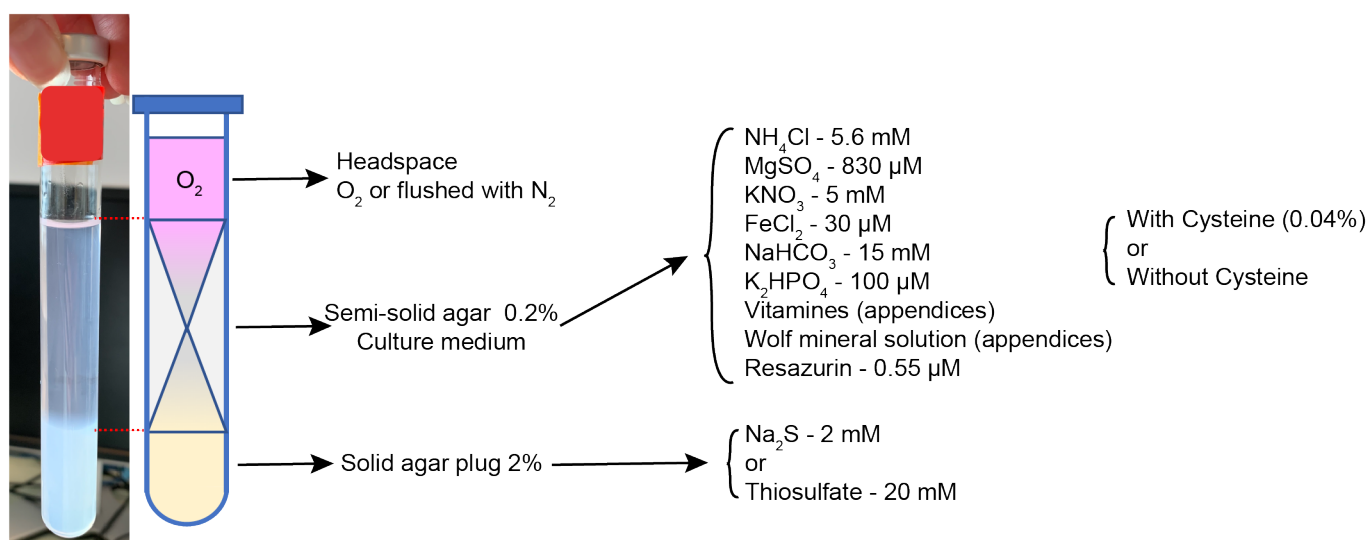


**Figure 2.5: Schematic of the different inverse gradient media (oxygen versus a sulfur compound) tested for the **MTBc** growth.** The four different media possess a common central growth medium and an upper oxygen gradient. Two of the media are supplemented with a  $\text{Na}_2\text{S}$  bottom plug of agar whereas the other other two with  $\text{S}_2\text{O}_3^{2-}$ .

### 2.5.1.2 Media oxygen profile - oxygen microsensor

Vertical oxygen microprofiles were acquired in order to measure the oxygen gradient in our media, using an OXR50-UHS optical microsensor (Pyroscience GmbH) with a 50  $\mu\text{m}$  sharp tip, connected to a FirestingPro oxygen meter (Pyroscience GmbH). Microprofiling was done using a M33 micromanipulator (UNISENSE A/S). The zero point-calibration of the oxygen-sensor was made against a freshly-made solution of saturated sodium sulfide while the 100% point-calibration was made with the ambient atmosphere.

Oxygen gradients were measured only for the media with the plug of  $\text{Na}_2\text{S}$ , with or without cystein. The *in situ*  $\text{O}_2$  measurements were done two days after making the media to allow sulfide and oxygen gradients to stabilize.

The micromanipulator attached with the micro-electrode was fixed above the culture medium glass tubes (see Fig. 2.6) and the extremity of the electrode positioned at the exact beginning of the semi-solid medium. While measuring, the electrode was then vertically moved by the

## Chapter 2. Vertical structure of magnetotactic bacteria populations in the water column of Lake Pavin

micromanipulator with a 100 to 500  $\mu\text{m}$  step downward until anoxia was reached.

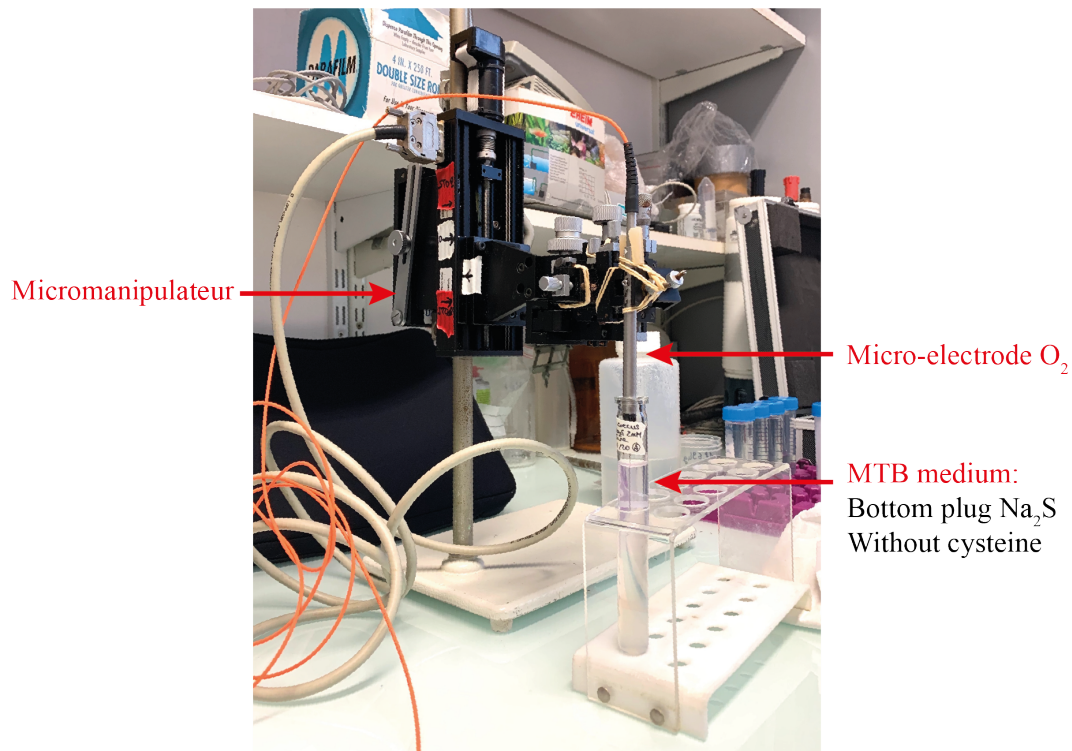


**Figure 2.6:** Photo of the microelectrode-micromanipulator setup for O<sub>2</sub> measurement in Lake Pavin growth media.

### 2.5.1.3 Magnetotactic bacteria sampling and isolation protocol

MTB samples were retrieved during the October 2019 mission using the online pumping system described in (Busigny et al., 2021). Upon reaching the zone of MTB maximum abundance, water samples were retrieved and kept either in 1-L bottles or 20-L Nalgene bottles. The water in the Nalgene bottles was quickly transferred in several aquariums of 30 L. Then, whether it was on a bottle or an aquarium, a magnetic sorting of 1-5h was done thanks to neodymium magnetic disks. Only the bigger MTB pellets obtained were used and a further magnetic purification was made. The enriched sample of MTB obtained after the magnetic sorting can contain other microorganisms present in the vicinity of the pellet. An additional purification step is thus highly recommended before the inoculation into the growth medium. The 'capillary racetrack' is a purification process (Wolfe et al., 1987) carried out in sterile conditions to further purify MTB from other microorganisms (see Fig. 2.7). A Pasteur pipette and a small piece of hydrophilic cotton are necessary to make this device. The pipette tip is melted closed thanks to a flame, and the cotton is inserted and loosely packed into the narrow neck of the large part of the pipette. Filtered water from Lake Pavin is inserted in the capillary until the piece of cotton is totally soaked. The dispositive is fixed on the table and a magnet is placed south-side next to the

## 2.5. Design of culture media for the isolation of the Lake Pavin MTBc and preliminary results

closed tip to attract the MTB from the larger part of the pipette through the cotton filter. Once everything is set, the pellet of MTB magnetically sorted is added in the large part of the pipette and the MTB are then attracted through the cotton toward the closed tip leaving the non magnetotactic microorganisms behind. After ~20 min, fast motile MTB such as MTBc accumulated at the tip of the pipette, the pipette tip was then carefully broken and the MTB retrieved thanks to a thin needle. The pellet was then directly inoculated in the middle of the semi solid part of one of the media.

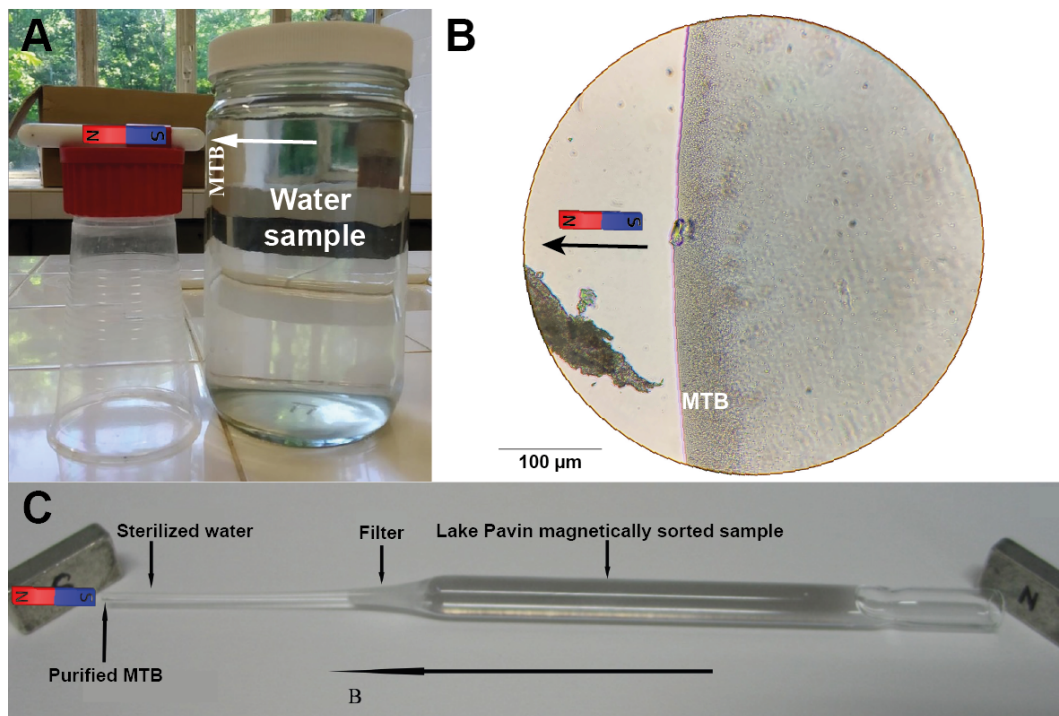


**Figure 2.7: MTB sampling and purification setup for inoculation in the MTBc growth media.** This setup consists in 3 successive steps. (A) A magnetic sorting of the MTB sampled from the water of Lake Pavin by using a magnet south-pole against the side of the bottle. (B) Observation and verification of their presence under the light microscope using the hanging drop technique. (C) 'Capillary racetrack' purification technique by using a Pasteur pipette, a hydrophilic cotton as filter and a magnet.

MTB growing in a gradient medium are usually visually observable as a white-grayish band at the oxic-anoxic interface, i.e. the pink-transparent transition when resazurin is used (see Fig. 2.8). From time to time, the tubes were checked visually to see if any characteristic band appeared in the culture media. After three weeks, the growth media were checked for any viable MTB cells or growth. The semi-solid medium was split in slices of 1 mL and after mixing, a drop of 10 µL was observed using the hanging drop technique (Schüler, 2002) and a Zeiss Primo Star light microscope equipped with a phase contrast.



**Figure 2.8: MTB culture medium showing a band of MTB growing at the oxic-anoxic interface (pink-transparent transition).**

## **2.5.2 Results**

### **2.5.2.1 Four double gradient media presenting different redox gradients**

In the media supplemented with cystein the resazurin became blue, in contrast to the color pink observed in the media without addition of cysteine. As expected, the different media with or without cystein showed a different redox gradient as it can be seen from the color of the resazurin, whether it was blue or pink (see Fig. 2.9). The media harboring the solid bottom plug of thiosulfate showed a lower redox gradient in the semi-solid medium than those with a Na<sub>2</sub>S solid bottom plug (A and B1 versus C and D). In the medium with a thiosulfate plug and without cystein (D), there was almost no redox gradient as the color of the resazurin diffused almost until the bottom of the semi-solid part.

In our media with inverse gradient of Na<sub>2</sub>S and oxygen, without cystein, Na<sub>2</sub>S and oxygen interaction created elemental sulfur precipitation in the semi-solid medium after several days (reaction is as follow:  $\text{H}_2\text{S} + \text{O}_2 \longrightarrow 2\text{S} + 2\text{H}_2\text{O}$ ). As elemental sulfur is not soluble, it was possible to observe this interaction in the medium as a large white band in the middle of the semi-solid medium (see Fig. 2.9B2). This reaction was not yet observable in the B1 tube as it was only one day old.

## 2.5. Design of culture media for the isolation of the Lake Pavin **MTBc** and preliminary results

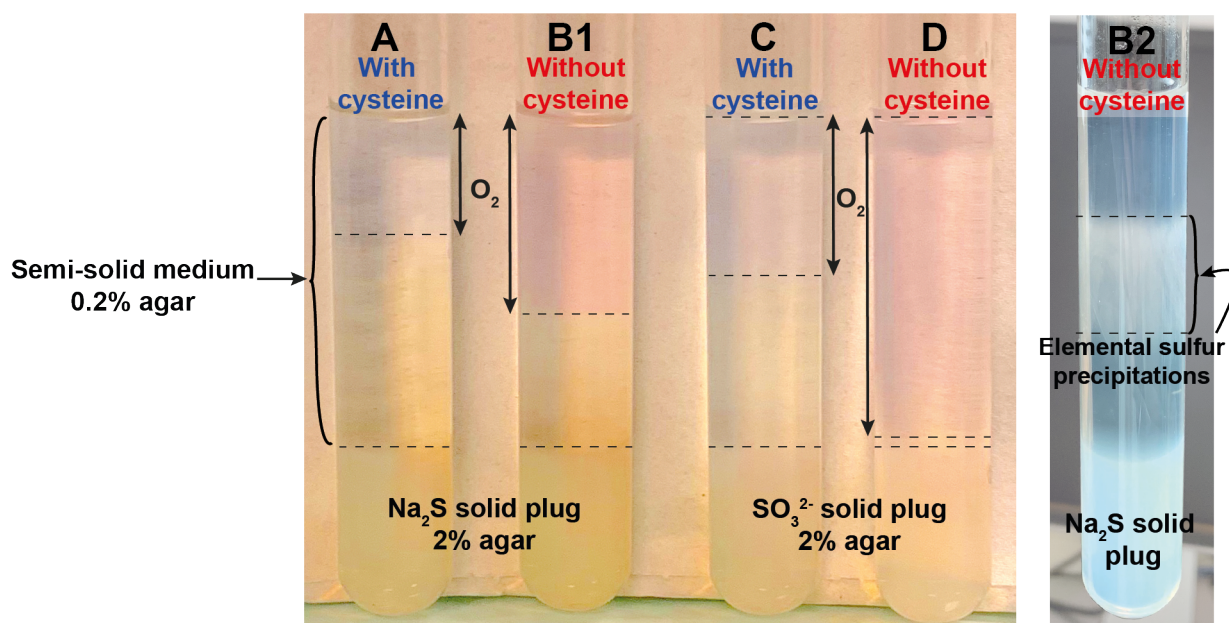


**Figure 2.9: Different inverse gradient media tested for the Lake Pavin **MTBc**.** The tubes A, B1, C and D correspond to one day old media, whereas B2 correspond to a 3 weeks old B1 medium. (A,B1) Media with a solid bottom plug of sodium sulfide and supplemented, or not, with cystein in the semi-solid medium respectively, (C,D) Same media with a solid bottom plug of thiosulfate. The color blue or pink passing to translucent with depth represents the redox gradient visualized thanks to the resazurin color indicator. (B2) Medium with an inverse gradient of oxygen and sulfide, without cystein, showing a large white band representing the precipitation of elemental sulfur.

### 2.5.2.2 The resazurin is a redox indicator allowing the visualization of oxygen gradients

The oxygen gradient of the two media, with a  $\text{Na}_2\text{S}$  bottom plug, were measured. This was done to check if both redox gradients, seen in blue and pink with the resazurin, were representative of the oxygen gradient. The oxygen was measured thanks to a microelectrode and a micromanipulator, the variation of oxygen concentration could therefore be checked with precision.

The medium with cystein and a blue gradient showed a steeper slope of the oxygen as a function of the depth ( $a=-160.85$ ) than the medium without cystein ( $a=-251.49$ ; see Fig. 2.10). In addition, the oxygen reached zero approximately where the passage from blue/pink to transparent could be detected (marked with the gold star on the figure 2.10). From our observation, we can thus conclude that in the media prepared for the culture of **MTBc**, cystein is a precise redox and oxygen indicator to visualize the oxic-anoxic boundary.



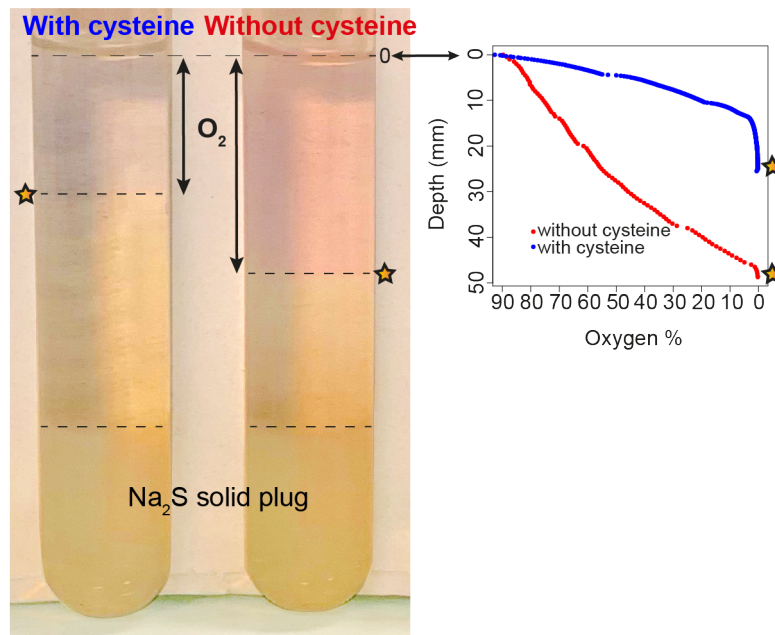


**Figure 2.10: Oxygen micro profiles comparison of the media with a  $\text{Na}_2\text{S}$  solid bottom plug with or without cysteine.** The oxygen reached 0% where the golden star is placed and corresponded to the transition of the color blue or pink to translucent.

### 2.5.2.3 Culture of magnetospirillum-like magnetotactic bacteria

After the Lake Pavin mission of October 2019 and the inoculation of the 4 different media with magnetically enriched and purified MTB, the media were incubated at 18°C for 3 weeks while looking for any characteristic MTB band in the tubes.

In three different tubes, of either a medium with a bottom plug of  $\text{Na}_2\text{S}$  without cysteine and a medium with a bottom plug of thiosulfate with cysteine, some moving cells could be observed but they did not present a magnetotactic behavior under the microscope. A TEM observation of these cells helped us identify some rods-like bacteria, resembling *Pseudomonas* cells, without any intracellular magnetosomes.

In one culture medium with a  $\text{Na}_2\text{S}$  bottom plug, non-motile and non-magnetotactic round-shaped cells resembling the MTBc were observed. In the other media with a thiosulfate bottom plug none moving cells or cells shape resembling the MTBc were spotted.

In one tube of the medium with a bottom plug of  $\text{Na}_2\text{S}$ , without cysteine, a white band could be observed in the half top part of the semi-solid medium (see Fig. 2.11). After light microscope observation, the slice of 1 mL including the band, contained magnetotactic cells resembling under the optical microscope (e.g. size and motility) magnetospirillum-like cells. Although I was able to isolate a magnetotactic bacterium, this culture was not further investigated as it was not a MTBc.

## 2.5. Design of culture media for the isolation of the Lake Pavin **MTBc** and preliminary results

---

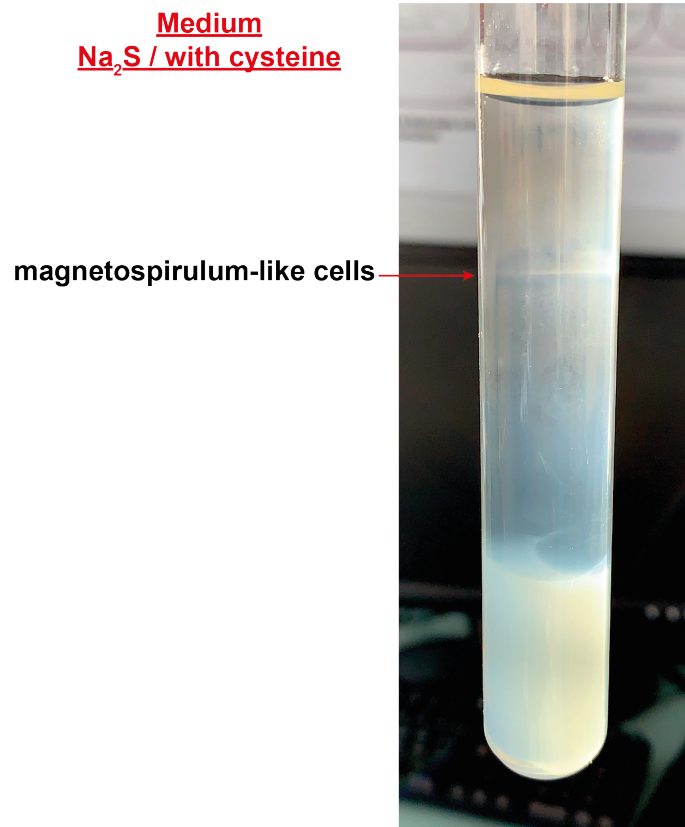


**Figure 2.11: Image of the tube which isolated the magnetospirillum-like cells.** Tube of medium, inoculated during the October 2019 mission, with a bottom plug of Na<sub>2</sub>S and its the semi-solid medium supplemented with cysteine. The thin white band located in the top part of the semi-solid medium represent the magnetospirillum-like cells observed after 3 weeks of incubation at 18°C in the dark.

### 2.5.3 Discussion

This first test of growth media showed that more or less steep oxygen gradients could be created. Cysteine is commonly used in the semi-solid media elaborated for the **MTB** as a reducing agent to limit the oxygen diffusion and form an oxygen gradient. In these media, not only did the cystein act as a reducing agent, but also the H<sub>2</sub>S produced by the bottom plug of Na<sub>2</sub>S. It is therefore not surprising that the oxygen gradient, for the medium having cystein in addition of H<sub>2</sub>S, was steeper and shorter than the one with only H<sub>2</sub>S to counteract O<sub>2</sub> diffusion. In parallel, the non existence of an oxygen gradient in the medium supplemented with a bottom agar plug of thiosulfate without cystein suggests that the thiosulfate does not have the capacity to reduce oxygen as H<sub>2</sub>S does. In the same medium with cystein, an oxygen gradient established in the overlaying semi-solid medium.

The day of the inoculation of magnetically sorted and purified **MTB**, the tubes were already 5 days old. The media were made on the Friday preceding the field mission which began on

## Chapter 2. Vertical structure of magnetotactic bacteria populations in the water column of Lake Pavin

---

the next Monday. As the inoculation occurred a few days after the beginning of the mission, it is possible that the diffusion of both the oxygen and the H<sub>2</sub>S in the growth medium was too advanced and that these gradients were overlapping or too diffused compare to the optimum conditions for the *MTBc*. In addition, the overlapping of these gradients may be less representative of the conditions in which the *MTBc* are found in Lake Pavin where both gradients are clearly distinct from each other with the *MTBc* in between (as seen in [Rivas-Lamelo et al. \(2017\)](#)).

The observation of some non-moving *MTBc-like* cells suggests that the *MTBc* might have survived longer in the media supplemented with Na<sub>2</sub>S than in the others, and that these conditions are more optimum for the *MTBc* than the ones with a thiosulfate bottom plug.

The success in isolating a magnetospirillum-like *MTB* in only one tube out of the five of the same medium may result from the two steps sorting technique (magnetic sorting and racetrack). In these two steps, it is possible that a lot of *MTB* have been lost and that the inocula were not equivalent between the different tubes.

Some components and concentrations of the MC-1 *MTB* growth medium were used for the semi-solid growth medium as their phylogenetic relatedness suggest that they might share common metabolism pathways ([Bazylnski et al., 2013b](#)). It is possible that even if they share phylogenetic information they do not share the same metabolic pathways. Usually the nutrient concentrations in the *MTB* isolation media have to be kept low to let the *MTB* take the advantage and compete against fast growing bacteria ([Bazylnski et al., 2013a](#)). For example, the carbon and nitrogen source should be kept low, with a concentration lower than 2 mM for the carbon source ([Schüler et al., 1999](#); [Bazylnski et al., 2013a](#)). In our media, the carbon source concentration was much higher than that, with a concentration of sodium carbonate of 15 mM, as it is used in the growth medium of the *MTBc* MC-1 ([Bazylnski et al., 2013b](#)). It would therefore be a good idea to reduce that concentration but also try some components used for known P-hyperaccumulators which might share similar metabolism with the *MTBc* of Lake Pavin, such as the *Beggiatoa* genus ([Brock and Schulz-Vogt, 2011](#)) which are accumulating S and P granules intracellularly or the *Sulfurimonas* ([Möller et al., 2019](#)) which are only present in anoxia and accumulate PolyP.

In the media supplemented with sulfide, the available iron initially present may be partly scavenged by sulfide and it may interfere with magnetosome biomineralization ([Lefèvre et al., 2011a](#)). If not enough iron is supplemented in the growth medium and as it is essential for magnetosomes formation ([Schüler and Müller, 2020](#)) *MTB* may not present magnetic responses.

Finally, after 3 weeks of incubation, it is possible that no more distinct oxygen and redox gradient were present in the tubes. The tubes being closed by anoxic clipped caps, no oxygen was able to enter after inoculation, and the gradient detected with resazurin was no more visible after 3 weeks of incubation. It therefore suggests that the oxygen was no more present in the tubes and that the tubes became anoxic. This oxygen/redox gradient might be essential for the *MTBc*, it may therefore be why the media did not show any growth.

## 2.5. Design of culture media for the isolation of the Lake Pavin **MTBc** and preliminary results

---

Overall, even if only one test could be made during this thesis, the isolation of a **MTB** in one of the medium already constitute a promising result. My results are thus paving the way for future attempts at isolating **MTBc** and other **MTB** from Lake Pavin.



## 2.6 Conclusions and perspectives

In this chapter, a new unique and abundant **MTB** sequestering calcium carbonates, the **iACC**-forming rods, was characterized in the water column of Lake Pavin (Monteil et al., 2021). This new **MTB** was found in a similar zone than **MTBc** hyperaccumulating **PolyP** under the oxycline. This characterization was followed by the development of a new high resolution sampling technique and the discovery of a proxy (conductivity) to track the **MTB** maximum abundance in the water column. The precise distribution and diversity of the **MTB** populations as a function of the different environmental parameters along the water column of Lake Pavin could then be assessed. Seven morphotypes were observed, they were characterized with respect to their cell shape and size and their magnetosomes organisation, shape and numbers. Optical microscopy evidenced the stratification of the two main populations of **MTB**, the **MTBc** accumulating **PolyP** and the **iACC**-forming rods, suggesting that these two abundant morphotypes inhabit two different biogeochemical niches. Only the corresponding geochemical parameters for the **MTBc** could be identified using multivariate statistics. Different environmental conditions, such as the wt% of C and N, the concentration of particulate P and Mg, and dissolved sulfate were positively and significantly correlated to the **MTBc** abundance. These results suggest that the **MTBc** are correlated to the local biomass and reinforce the hypothesis that they possess a metabolism linked to the sulfur cycle. These results have recently been submitted for publication in which I am the first author.

A preliminary test was made in an attempt to isolate the **MTBc**. The first media conditions, consisting of double and inverse gradients of oxygen and sulfur compounds, prepared for the isolation of the **MTBc** did not succeed but gave promising results. The media with a  $\text{Na}_2\text{S}$  bottom plug showed the presence of non-moving **MTBc**-shaped cells after three weeks. Moreover, a medium with an inverse gradient of oxygen and  $\text{Na}_2\text{S}$ , without cystein, succeeded at isolating magnetospirillum-like cells.

This chapter results are paving the way for future studies on other magnetotactic microorganisms that have this unique advantage to be magnetically concentrated and present a metabolic, taxonomic and ultrastructural diversity of interest for a large community of scientists.

### Perspectives:

In this study we characterized the morphotype diversity of the **MTB** in Lake Pavin water column and their relative abundances as a function of their habitat, we then identified a specific niche for the **MTBc** hyperaccumulating **PolyP**. However, we still miss the information of their metabolic and taxonomic diversity as a function of the same habitats. Apprehending these information would help constrain whether or not their magnetosomes morphologies or their different metabolism are dependent from their phylogeny or habitats. Their taxonomy and the number of species can be evaluated by using 16S rRNA gene sequencing. Thanks to the 16S rRNA

## Chapter 2. Vertical structure of magnetotactic bacteria populations in the water column of Lake Pavin

---

information, FISH probes can be created to serve as fluorescent markers of specific species of MTB. For samples collected in specific environmental conditions, FISH probes observation in fluorescence microscopy can allow the calculation of the species relative proportions as a function of the environmental conditions. In combination with electron microscopy, the species and their relative abundances can be linked to their magnetosome morphologies at the single-cell and correlated to a specific habitat (Li et al., 2017; Zhang et al., 2017; Liu et al., 2020). It would be interesting to determine if our MTBc with different magnetosome organizations are affiliated to different species or if the organization differences are due to different environmental conditions within the Lake Pavin water column. Li et al. (2017); Liu et al. (2020) could show for MTBc, thanks to this technique, a dependency of the magnetosomes morphologies, numbers, size and organization with the species, whereas Zhang et al. (2017) showed for other MTBc that their magnetosomes morphologies may be less biologically controlled and more impacted by unfavorable environmental conditions.

It is possible that different close related strains of bacteria possess the same 16S rRNA gene and that different MTB morphologies can not be separated as a function of their 16S rRNA gene. In that case, metagenomic analyses, and then the reconstitution of the different genomes present in the sample, can be done to gain access to the functional repertoire of the MTB and to gain insights on the number of MTB strains. The reconstitution can also help gain insight into the metabolic diversity of the MTB by modeling the different metabolic pathways. Such study could thus help to know if MTBc have the potential to use nitrate as electron acceptor in anoxic water instead of oxygen, and if their link to the sulfur cycle correspond to sulfur-oxidation or sulfate-reduction. Metagenomic analyses, allowing a better understanding of the MTBc and their metabolism, could also help to elaborate more appropriate growth media.

The MTBc isolation test was the only one made during this thesis due to COVID-19 events. One solution in the future could be to use sediments of Lake Pavin known to harbour the MTBc, similar to the ones met in the water column. These sediment MTBc belong to the *Magnetococcaceae* family as well, although it is still not known if they belong to the same species. Their large number in the sediments would facilitate the possibility to test further growth medium without having direct access to Lake Pavin, as these MTBc populations conserve well in microcosms stored in a lab for years.

A lot of different conditions of growth with different components concentrations could be further tested for the MTBc of Lake Pavin. Carbon and nitrogen concentrations can be diminished in order to help the MTB out-compete other potential contaminant organisms capable of outgrowing them, especially the carbon source. The media tested during this thesis should be retried but this time with screw caps to enable the oxygen to diffuse continuously in the semi-solid growth medium and compete with the H<sub>2</sub>S gradient and/or cystein (see Fig.2.12A). Because it is possible that the MTBc of Lake Pavin link sulfur-oxidation with denitrification, it would be

interesting to try a medium with an inverse gradient of sulfide and nitrate in anoxic conditions as it was done for the P accumulating *Sulfurimonas* in Möller et al. (2019) (see Fig.2.12B1). To prevent potential shortage, iron can be added in higher concentration in the semi-solid growth media, or a  $\text{Fe}^{2+}$  gradient could be added in addition to the sulfide one at the place of oxygen or nitrate (see Fig.2.12B2) thus helping to create a redox gradient favorable for the MTB.

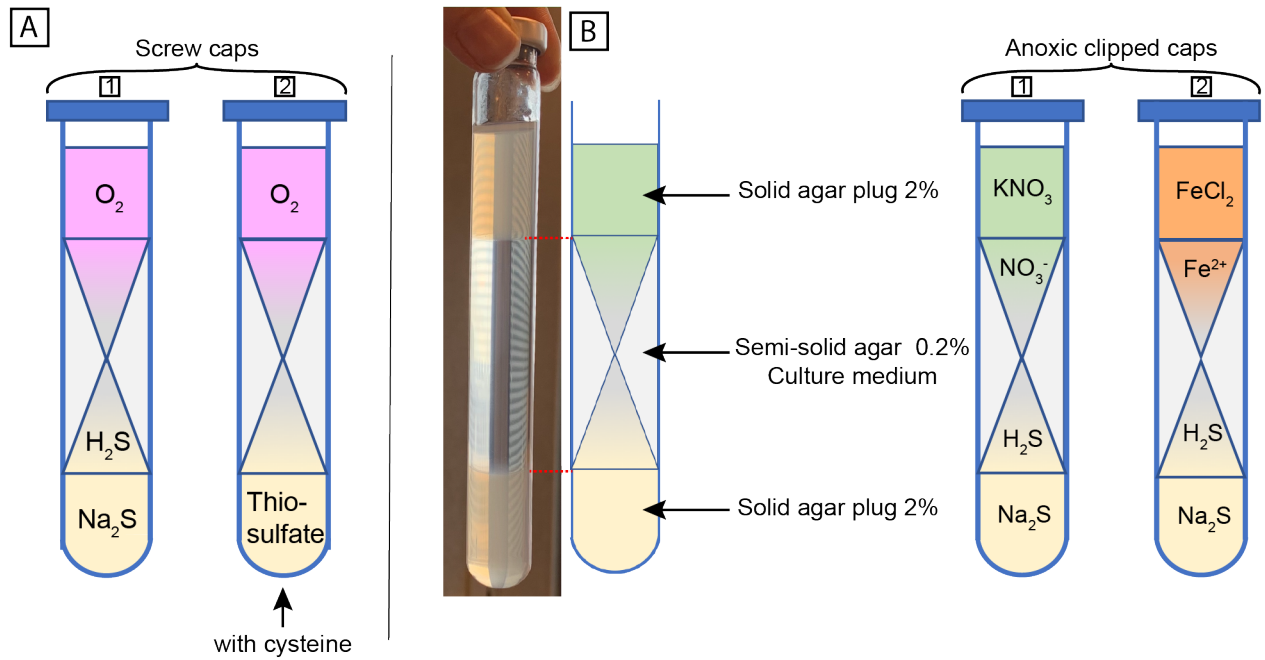


**Figure 2.12: Different ideas of media to test in the future for the isolation of the MTBc of Lake Pavin.** Panel A corresponds to inverse gradient media with presence of oxygen as electron acceptor whereas panel B corresponds to inverse gradient media as well but with an addition of a solid plug of agar on top of the tubes in anoxia with nitrate or iron as top gradient and nitrate as electron acceptor.





---

# Chapter 3. Magnetotactic cocci in the water column of Lake Pavin: morphotype classification and sorting of P-sequestering cells

---

*"You're never fully dressed without a smile."*

Annie (1982)

## Contents

---

<b>3.1</b>	<b>Introduction</b> . . . . .	<b>131</b>
3.1.1	Detection, quantification and characterization of PolyP in the cell fraction: state of the art . . . . .	133
3.1.1.1	Bulk analyses . . . . .	134
3.1.1.2	Localization of PolyP at cell scale . . . . .	135
3.1.1.3	Combination of techniques . . . . .	139
3.1.2	Questions and strategy of the chapter . . . . .	140
<b>3.2</b>	<b>Diversity and distribution of P-sequestering MTBc along the chemical gradients in the water column of Lake Pavin</b> . . . . .	<b>141</b>
3.2.1	Material and methods . . . . .	141
3.2.1.1	Water sampling strategy . . . . .	141
3.2.1.2	TEM grid deposition (optimization) . . . . .	141

## Chapter 3. Magnetotactic cocci in the water column of Lake Pavin: morphotype classification and sorting of P-sequestering cells

---

3.2.1.3	Classification of the magnetotactic cocci according to the magnetosome organization and the relative size of PolyP granules	143
3.2.1.4	Statistical analyses	146
3.2.2	Results	146
3.2.2.1	The proportion of MTBc sequestering PolyP differs with depth in the water column	146
3.2.3	Discussion	150
3.3	<b>Cell sorting of MTBc with large PolyP inclusions using flow cytometry: methodological developments and preliminary results</b>	<b>155</b>
3.3.1	Methodological strategy: samples and parameters	155
3.3.2	Material and methods	156
3.3.2.1	Staining protocols	156
3.3.2.2	Flow Cytometry set up	157
3.3.3	Bacterial models: choice and conditions to obtain negative and positive controls	159
3.3.4	Dual staining on the positive control	160
3.3.5	Cell sorting on the bacterial models	161
3.3.6	Sample preparation optimization for flow cytometry analyses - M2 Internship - Clémentin Bouquet	165
3.3.6.1	Optimization of the dual staining protocol	165
3.3.6.2	Cell sorting as a function of polyphosphate detection for a mix of both control cultures and for an environmental sample	166
3.4	<b>Conclusions and Perspectives</b>	<b>169</b>

---

### 3.1 Introduction

The magnetotactic cocci inhabiting a specific niche in the anoxic layer of the water column of Lake Pavin (see Chapter 2 part 2.4 for details) were previously proposed as a new model for P sequestration as intracellular PolyP (Rivas-Lamelo et al., 2017). However, Rivas-Lamelo et al., 2017 also show various MTBc cells with or without PolyP and with different organizations of their magnetosomes, in a given water sample collected with a low vertical resolution (Niskin sampling). In order to identify biological or environmental factors governing this phenotypical heterogeneity, the following questions remain to be addressed. Do these morphotypes colocalize in the water column within the MTBc niche? If so, what is their relative abundance? What is the range of PolyP sequestration capability at the cell scale and does this capability vary with depth along the geochemical gradients? Are the PolyP sequestration capability and magnetosome organization independent traits? Does this phenotypical diversity rely on a taxonomic diversity? As described in the previous chapter (Chapter 2 part 2.3) we now have at our disposal a high vertical resolution sampling technique that also measures physico-chemical parameters; however, it is not possible to specifically sort the MTBc nor cultivate them yet. Therefore, their PolyP accumulation capabilities have to be studied in complex environmental samples. A wide diversity of methods exist to analyze and monitor PolyP and the PolyP accumulating microorganisms (see Fig. 3.1). The following section will present these different methods to find the appropriate techniques necessary for the evaluation of the MTBc PolyP heterogeneity and their efficient sorting from the other MTB.

## Chapter 3. Magnetotactic cocci in the water column of Lake Pavin: morphotype classification and sorting of P-sequestering cells

Technique	Advantages	Disadvantages
Extraction/Digestion	<ul style="list-style-type: none"> <li>. Quantitative technique</li> <li>. Possibility to characterize different PolyP fractions</li> </ul>	<ul style="list-style-type: none"> <li>. Efficiency depending on the association of PolyP with other molecules</li> <li>. Effect of cations and chain length</li> <li>. Extraction can lead to the undesired modification of the PolyP</li> <li>. Destructive</li> </ul>
OMICS	<ul style="list-style-type: none"> <li>. Global overview of microbial consortia</li> <li>. Combination with FISH</li> </ul>	<ul style="list-style-type: none"> <li>. Do not measure PolyP content</li> <li>. Require up-to-date databases</li> <li>. Require living cells</li> </ul>
Enzymatic assay	<ul style="list-style-type: none"> <li>. Quantitative technique</li> <li>. Possibility to access the metabolism of PolyP extracts</li> </ul>	<ul style="list-style-type: none"> <li>. Sample preparation complexity</li> <li>. Enzymatic reaction complexity</li> <li>. Destructive</li> <li>. Chain length dependency</li> </ul>
<sup>31</sup> P- NMR	<ul style="list-style-type: none"> <li>. Non destructive</li> <li>. Differentiate the different P reservoirs</li> <li>. Relative quantification of PolyP</li> <li>. Determine PolyP size</li> <li>. Applicability to liquid and solid samples/ in vivo analyses</li> </ul>	<ul style="list-style-type: none"> <li>. Tagged substrates required</li> <li>. Unspecificity on nucleotides</li> <li>. High detection limit</li> <li>. Can not measure immobilized form of PolyP</li> <li>. Paramagnetic ions interferences</li> </ul>
Gel electrophoresis/ Chromatography	<ul style="list-style-type: none"> <li>. PolyP chain length and degree of polymerization measurements</li> <li>. Semi-quantitative</li> <li>. Combination with DAPI</li> </ul>	<ul style="list-style-type: none"> <li>. Pre-treatment step (PolyP extraction/ digestion)</li> <li>. Destructive</li> </ul>
EI-MS	<ul style="list-style-type: none"> <li>. Characterization of different PolyP fractions</li> <li>. High selectivity and sensitivity</li> <li>. Simple sample preparation protocol / No extraction/digestion step</li> </ul>	<ul style="list-style-type: none"> <li>. Destructive</li> <li>. Requires standard samples</li> </ul>
EM	<ul style="list-style-type: none"> <li>. Localization of the PolyP in cells</li> <li>. Resolution: &lt; 100 nm</li> <li>. Combination with staining and X-ray techniques</li> </ul>	<ul style="list-style-type: none"> <li>. Localization of the PolyP in cells</li> <li>. Resolution: &lt; 100 nm</li> </ul>
RAMAN	<ul style="list-style-type: none"> <li>. Simultaneous detection and quantification of different storage polymers</li> <li>. Label-free</li> <li>. Indicate mean concentration of PolyP and locate PolyP inside cells at a sub-cellular resolution</li> </ul>	<ul style="list-style-type: none"> <li>. Interferences due to impurities and fluorescence</li> </ul>
X-ray	<ul style="list-style-type: none"> <li>. Quantitative analysis</li> <li>. Spatial distribution of P compounds and their association to other chemical elements</li> </ul>	<ul style="list-style-type: none"> <li>. Destructive</li> <li>. Possible loss of PolyP during preparation protocol</li> </ul>
Colorimetry staining	<ul style="list-style-type: none"> <li>. Simplicity, rapidity</li> <li>. Direct visualization of PolyP inside the cells</li> </ul>	<ul style="list-style-type: none"> <li>. Not adapted to visualize small PolyP chains</li> <li>. Unspecificity toward nucleic acids</li> <li>. Non-quantitative/Low-resolution</li> <li>. Preparation protocol and acidic pH required</li> <li>. Destructive</li> </ul>
DAPI staining	<ul style="list-style-type: none"> <li>. Direct visualization of PolyP inside the cells</li> <li>. High sensitivity</li> </ul>	<ul style="list-style-type: none"> <li>. Expensive staining reagent</li> <li>. Unspecificity toward lipids, humic acids, RNA...</li> <li>. High background fluorescence at high concentrations</li> <li>. Destructive</li> </ul>
Tetracycline staining	<ul style="list-style-type: none"> <li>. Direct visualization of PolyP inside the cells</li> </ul>	<ul style="list-style-type: none"> <li>. Excitation and emission spectra depend on the manufacturer and solvent</li> </ul>
JC-D7/JC-D8 staining	<ul style="list-style-type: none"> <li>. Direct visualization of PolyP inside the cells</li> <li>. High specificity for PolyP</li> <li>. High sensitivity</li> </ul>	<ul style="list-style-type: none"> <li>. Highly expensive, production at the demand</li> <li>. Until now only used on mamalian, astrocytes and plants</li> </ul>

**Figure 3.1: Table of the techniques specificities for the detection and quantification of PolyP.** Adapted from Serafim et al. (2002); Majed et al. (2012); Tarayre et al. (2016).

### 3.1.1 Detection, quantification and characterization of PolyP in the cell fraction: state of the art

Most studied accumulators of PolyP are PAO from wastewater treatment plants WWTP. Because of the low amount of microorganisms isolated in the WWTP, approximately 1 to 10% of the overall microbial community (Ritz, 2007; Günther, 2011), a lot of culture-independent techniques have been developed to quantify and detect PolyP but also to detect and identify the P accumulators (reviewed in Serafim et al., 2002; Majed et al., 2012; Tarayre et al., 2016; Terashima et al., 2016). A classification of these methods is proposed in Fig. 3.2.

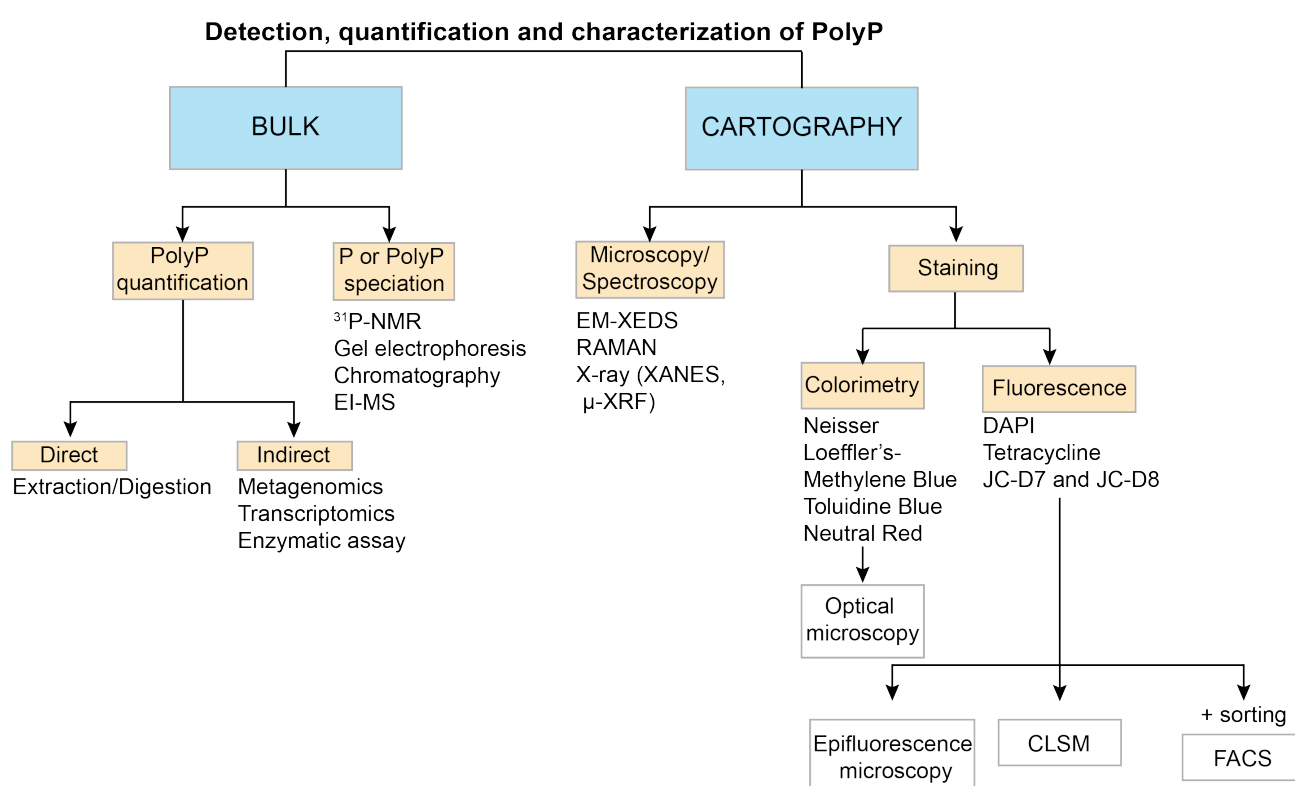


**Figure 3.2: Schematic view of the different methods for the detection of PolyP and PolyP accumulators** The techniques are separated as a function of the information obtained. The techniques can either focus on the bulk sample and give information on the bulk P or the entire microbial community, or can help to cartography the P inside the sample and at the single cell level. NMR: nuclear magnetic resonance; EI-MS: electron ionization mass spectrometry; EM-XEDS : electron microscopy - X-ray energy-dispersive spectrometry; XANES: X-ray absorption near-edge spectroscopy; XRF: X-ray fluorescence; DAPI: 4',6-diamidino-2-phenylindole; CLSM: confocal laser scanning microscopy; FACS: fluorescence-activated cell sorting. Adapted from (Majed et al., 2012; Günther et al., 2009; Angelova et al., 2014)

## Chapter 3. Magnetotactic cocci in the water column of Lake Pavin: morphotype classification and sorting of P-sequestering cells

---

### 3.1.1.1 Bulk analyses

Bulk methods quantify or determine the speciation of PolyP, the later allowing the relative quantification of the PolyP as a function of the other P forms or other types of PolyP, using diverse chemical or biological analyses.

#### Polyphosphate quantification

Several techniques exist to quantify particulate PolyP. They can be direct via PolyP extraction/digestion into orthophosphate, or indirect through the measurement of the microorganisms metabolic activities.

PolyP extraction and digestion methods usually use strong acids or alkali treatments (Hupfer et al., 2008; Tarayre et al., 2016). The effectiveness can be variable, often under or overestimating the PolyP, depending on the technique used, the different P fractions present in the sample, the PolyP associated components, and the PolyP solubility (Clark et al., 1986; Bonting et al., 1991; Ahlgren et al., 2007; Hupfer et al., 2008).

Indirect methods are based on the quantification of the genes, transcripts, and proteins linked with the PolyP metabolism to give insights on the functional potential of the sample or on the expression of the 16S rRNA or proteins.

Another indirect method is the enzymatic assay which is based on the use of the PPK and the PPX enzymes. The PPK enzymes synthesize ATP by adding a phosphate group, taken from the PolyP, to ADP, whereas PPX enzymes hydrolyzes PolyP into orthophosphates. The enzymes action is then followed by the respective quantification of the ATP with the luciferase system and the orthophosphate (Majed et al., 2012). These two methods are chain length dependent and can respectively be used on long and small chains of PolyP (Ault-Riché et al., 1998; Rao et al., 1998).

Because these techniques can be dependent on the PolyP chain length, different methods have been developed in order to determine the chain length. These techniques includes chromatography and filtration methods (Baba et al., 1984; Lorenz and Schröder, 1999; Hupfer et al., 2008) and electrophoresis (Clark and Wood, 1987) which separate the PolyP as a function of their chain length. Electron ionization mass spectrometry (EI-MS) is another technique that differentiates the PolyP species without pre-separation through chromatography or electrophoresis (Choi et al., 2000; Gross, 2017).

In Li and Dittrich (2019), extraction and measurements of the PolyP and total P particulate fractions in addition to enzymatic assays were used to evaluate the PolyP accumulation dynamics along the growth stages of cyanobacteria cultures. They could evidence a strong variability of PolyP levels depending on the cyanobacteria strain and different accumulation capabilities as a function of P availability and growth stage. Rapid accumulation of PolyP is witnessed during

the lag phase, whereas a smaller amount of PolyP is observed during the exponential phase due to the competition of P uptake and PolyP utilization for cell growth.

#### P speciation with $^{31}\text{P}$ NMR

$^{31}\text{P}$  nuclear magnetic resonance ( $^{31}\text{P}$  NMR) constitutes another method to look at the bulk P.  $^{31}\text{P}$  NMR can differentiate the different P species (PolyP, orthophosphate, phosphoesters, phosphonates) with respect to their characteristic P-bond. The method quantifies PolyP relative abundance over the other forms of P (Serafim et al., 2002; Diaz and Ingall, 2010). In addition, it can determine the size of the PolyP based on the ratio intensity of the main resonances characterizing the PolyP.

In contrast to the other bulk techniques, this method has the advantage of being non-invasive and non-destructive and thus was used in many *in vivo* analyses (Roberts and Jardetzky, 1981; Balaban, 1984; Fernandez and Clark, 1987; Lundberg et al., 1990; Santos et al., 1999; Boswell et al., 1999). However, some bias can exist between the detection of PolyP and the nucleotides which both hold a phosphoanhydride bond (Serafim et al., 2002). Moreover, this technique can not measure immobilized form of PolyP (Serafim et al., 2002) and paramagnetic ions such as iron or manganese can interfere with the signal (Cade-Menun and Preston, 1996; Turner, 2008) making it less interesting for the study of MTB.

This technique helped determine the type of PolyP accumulated in cells and revealed the presence of cyclic PolyP in *X. autotrophicus* cells (Mandala et al., 2020).

#### **3.1.1.2 Localization of PolyP at cell scale**

These techniques allow for the localization of PolyP at the cell scale, using specific dyes or taking advantage of the properties of P when involved with PolyP molecules (such as chemical bonds). These techniques are thus useful to characterize heterogeneous samples composed by cells with and without PolyP and to identify (and even sort) cells sequestering PolyP.

#### Colorimetric staining

Several dyes exist for the colorimetric visualization of PolyP and all depend on the metachromatic properties of a cationic dye which possess high affinity toward anionic compounds such as PolyP (Serafim et al., 2002). When bound to PolyP, the dye light absorption changes and the color perceived become dark-purple for the Neisser dye, pink-purple for the Loeffler's Methylene Blue and dark-red for Toluidine Blue. Another dye is Neutral Red which is sensitive to pH and is used as a probe for acidic cellular components such as the compartments containing PolyP (Tatsuhiko et al., 2001). Colorimetric visualization of PolyP is a relatively easy and fast method to carry out. These dyes can be used to quantify how much cells can accumulate PolyP among the other microorganisms, but they fail to detect small chain PolyP (Hupfer et al., 2008)



### Chapter 3. Magnetotactic cocci in the water column of Lake Pavin: morphotype classification and sorting of P-sequestering cells

---

and can be compatible with polyanions such as nucleic acids (Ohtomo et al., 2008). Moreover, with large accumulation of PolyP the technique fails to distinguish individual granules and thus can only indicate if the accumulation is null, small or large.

In Chaudhry and Nautiyal (2011) Toluidine Blue was used in the elaboration of an efficient technique for PAO screening and in the qualitative analysis of PolyP between different groups of organisms.

#### Fluorescent staining

Fluorescent dyes are commonly used with epifluorescence and confocal microscopy. The most common fluorescent dye used to observe PolyP is 4',6-Diamidino-2-phenylindole dihydrochloride (DAPI), which is usually used for DNA staining, but is also able to dye PolyP and lipids when used at high concentrations (i.e. 5-50  $\mu\text{g}\cdot\text{mL}^{-1}$ ; Tarayre et al. (2016)). When bound to DNA, the fluorescent dye emits a blue fluorescence ( $\sim 465$  nm), whereas it emits a yellow-green fluorescence ( $\sim 525$ - $550$  nm) when bound to PolyP (see Fig. 3.3; Hupfer et al. (2008)). In addition to high concentration of DAPI, the use of an excitation wavelength at about 415 nm allows a high sensitivity of detection (down to 25 ng  $\text{mL}^{-1}$ ) and the best specificity possible with a minimum DAPI-DNA signal (Aschar-Sobbi et al., 2008).

DAPI was shown to be unspecific toward several compounds such as lipids, humic acids and RNA. The fluorescence linked to the lipid only last few seconds (Streichan et al., 1990) but to help with that unspecific staining some studies combined polyhydroxyalkanoates (PHA) staining with Nile Blue to monitor PHA presence.

In Rugnini et al. (2017), DAPI staining seen in *Desmodesmus* sp. microalgae showed the impact of PolyP in detoxification and removal of copper and nickel from the local environment. In (Rivas-Lamelo et al., 2017), MTBc PolyP accumulation heterogeneity could be evidenced by using DAPI staining with confocal microscopy (see Fig. 3.3).

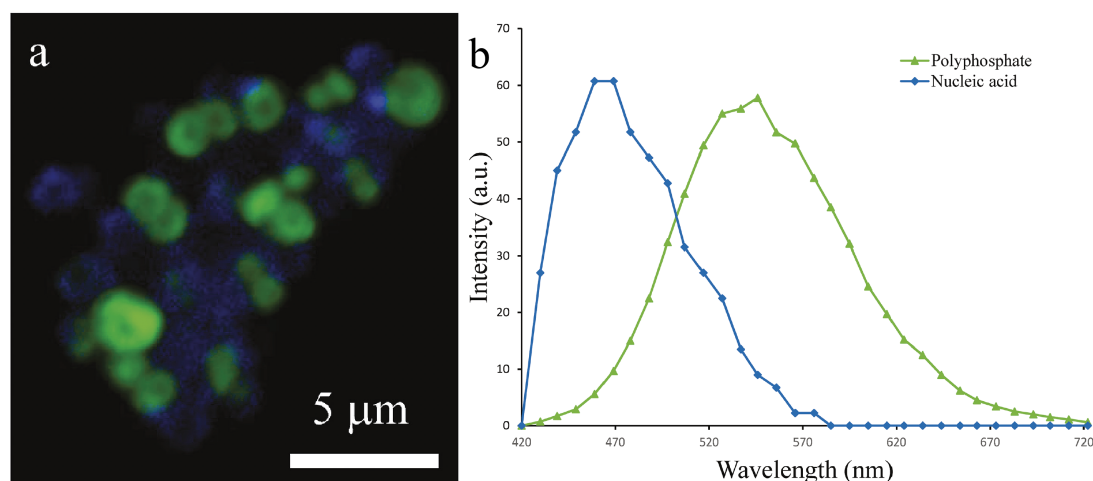


**Figure 3.3: Confocal analysis of cells stained with DAPI whose emission spectra are associated with DNA (blue) or PolyP (green).** (a) Confocal microscopy with an overlay of fluorescence maps of DAPI-stained nucleic acid (blue) and PolyP (green), (b) DAPI emission spectra obtained from a confocal analysis of DNA (blue) and PolyP (green). Figure adapted from Rivas-Lamelo et al. (2017).

Another fluorescent dye is Tetracycline (Tc). This dye is commonly used in medicine to identify calcium deposition on bones or teeth (Hallett et al., 1972). This dye has the ability to bind to the divalent cations associated with PolyP such as  $\text{Ca}^{2+}$  and  $\text{Mg}^{2+}$  and emits a green fluorescence with a maximum emission wavelength at 515 nm and a maximum excitation wavelength at 390 nm at pH 7.5 (Lee et al., 2003; Günther et al., 2009).

Günther (2011) showed that Tc possesses different excitation and emission spectra and varying fluorescent intensities depending on the manufacturer and the solvent used for the staining. It is then useful to perform protocol optimizations beforehand to guarantee an optimum detection of the PolyP.

Because of its binding to the divalent cations associated with PolyP, this dye was used as a quantitative fluorescent dye in single cell studies and aided in the identification and monitoring of bacteria proficient at PolyP sequestration within a highly diverse community in WWTP (Günther et al., 2009; Koch et al., 2013; Günther, 2011).

Based on the benzimidazolium dye library, JC dyes constitute other options for PolyP fluorescent staining. These dyes have only been used in eukaryotic, mammalian cells (Angelova et al., 2014), astrocytes (Angelova et al., 2018) and plants (Zhu et al., 2020). This may be due to its long synthesis process and its price. Two JC dyes have been shown to specifically bind PolyP in living cells and to have a high permeability: JC-D7 and JC-D8 (Angelova et al., 2014). The excitation wavelength and emission spectra are similar to DAPI at respectively 405 nm and 505-590 nm. Both dyes show an increase of fluorescence intensity with increasing concentration of PolyP and both have a low detection affinity (down to  $0.2 \mu\text{g mL}^{-1}$ ). Moreover unlike DAPI,

### Chapter 3. Magnetotactic cocci in the water column of Lake Pavin: morphotype classification and sorting of P-sequestering cells

---

JC dyes do not yield significant fluorescence when subject to diverse biological phosphates such as sodium orthophosphate, nucleotides, DNA and RNA (Angelova et al., 2014). JC dyes show an increase of fluorescence with Heparin but this compound is generally not found in cells.

JC dyes were used to visualize the PolyP granules in specific compartments of the astrocytes and to determine their PolyP release mechanism (Angelova et al., 2018).

#### Microscopies and spectroscopies

Electron microscopy (EM) combined with XEDS can help pinpoint, at the single-cell/submicron scale, the PolyP inclusions, and determine the chemistry of the intracellular compounds and associated elements attached to the PolyP (Serafim et al., 2002; Hupfer et al., 2008).

In Lake Pavin, STEM-XEDS analyses allowed the detection of several types of bacteria with intracellular PolyP granules at different depths along the water column (Cosmidis et al., 2014; Miot et al., 2016). This technique also helped demonstrate a heterogeneity of PolyP accumulation in MTBc (Rivas-Lamelo et al., 2017). In the Black Sea, TEM-XEDS analyses have revealed the presence of intracellular PolyP in MTBc. The method helped estimate an average volume ratio between the PolyP and the cell which contributed to explain the strong dissolved P gradient occurring in the water column (Schulz-Vogt et al., 2019).

Raman spectroscopy is a label-free technique coupled with a light microscope. The method requires minimal sample preparation and provides information about chemical composition and structure (Schuster et al., 2000). It indicates mean concentrations of PolyP (Moudříková et al., 2017), detecting simultaneously different chemical compounds and specific locations of PolyP within cells at a sub-cellular resolution (Dieing et al., 2010). This technique also enables the observation of interactions between PolyP and different cations such as Na<sup>+</sup>, Cs<sup>+</sup>, Ca<sup>2+</sup> and Ba<sup>2+</sup> for which a frequency shift and an intensity variation are observed (Koda et al., 1994). However, Raman analyses may show some photobleaching of fluorescence in chemically fixed or frozen cells (Moudříková et al., 2021).

The technical capability to concurrently detect PolyP and other intracellular inclusions makes it a very powerful method. In Majed and Gu (2010), Raman spectroscopy allowed for the separation of the PAO and the glycogen accumulating organisms (GAO) as a function of their respective inclusions. In addition, MTB and their magnetosomes were observed in Eder et al. (2014) by adapting this technique to overcome the size and chemical limitations of the magnetite magnetosomes. In this study, Raman allowed the simultaneous observation of the MTBc magnetite and the intracellular PolyP and sulfur granules.

Synchrotron analyses, such as synchrotron radiation X-ray fluorescence (SR-XRF), X-ray absorption near-edge spectroscopy (XANES) and  $\mu$ -XRF have been performed to identify spatial distribution of P compounds and their association to other chemical elements in cells (Adams

et al., 2016; Rivas-Lamelo et al., 2017).

Using such techniques, Diaz et al. (2009) showed the presence of PolyP with diverse counterions at the sub-cellular level in *Chlamydomonas* sp. and *Chlorella* sp. cultures. In a study with microalgal cultures, (Adams et al., 2016) explain the important function of intracellular PolyP for copper internalization and detoxification using synchrotron radiation X-ray fluorescence (SR-XRF) and XANES.

### 3.1.1.3 Combination of techniques

Numerous scientific advances have been made concerning the detection and quantification of PolyP and PolyP accumulators. Several studies have combined the methods aforementioned in order to gather complementary information or obtain the validation of a protocol or novel results.

Techniques quantifying PolyP may be combined with visual techniques such as colorimetry or fluorescence (Majed et al., 2012). For example, extraction and digestion of PolyP was combined with DAPI fluorescence and the PolyP quantified by using a spectrofluorimeter (Martin and Van Mooy, 2013). FISH analyses in association with DAPI on the confocal can be used to assess the presence of PolyP with a specific bacterial strain (Wagner et al., 1994; Kawaharasaki et al., 1999; Crocetti et al., 2000). Also, the combination of  $\mu$ -XRF, SEM and TEM analyses made it possible to associate the hotspots of P detected by X-ray fluorescence in a sample with microorganisms hyperaccumulating PolyP (Rivas-Lamelo et al., 2017).

Combining a high throughput single-cell sorting such as flow cytometry (FC) with the fluorescent detection of PolyP is also possible. FC is a technique that provides rapid analysis and sorting, at the single-cell level, of the microorganisms based on optical and fluorescent properties (Lambrecht et al., 2018). The optical properties correspond to light scatter which can provide information on the cells size and granularity. The fluorescent properties correspond to either an autofluorescence or to cell bound fluorescent dyes. FC is a powerful technique which can be used to identify and quantify different subpopulations of microorganisms sequestering PolyP within a highly diverse bacterial community (Günther, 2011). The technique does not provide phylogenetic affiliation or information on functional genes but may subsequently be combined with the appropriate genomic analyses of the sorted P accumulating subpopulations. Only a few FC studies on PolyP intracellular inclusions exist. DAPI and/or Tc were used to either identify and quantify the subpopulations of PAO communities (Kawaharasaki et al., 2002; Günther et al., 2009; Günther, 2011; Terashima et al., 2020) or quantify PolyP concentrations (Schulz-Vogt et al., 2019).

### **3.1.2 Questions and strategy of the chapter**

In order to answer the questions raised at the beginning of this introduction, it is necessary to find a method to evaluate the heterogeneity of **MTBc** at the sub-cellular level, but also a technique to sort **MTBc** into different fractions according to the presence of **PolyP** or the size of their **PolyP** inclusions. **EM** combined with **XEDS** constitute the only technique allowing the simultaneous visualization of the different **MTBc PolyP** sequestration capabilities and the different magnetosome organizations. Therefore **TEM-XEDS** combined with the high vertical resolution sampling technique and multivariate statistics was used in this thesis to evaluate the **MTBc** heterogeneity as a function of the different environmental parameters. This part of the study was made on the exact same samples previously described and used for the evaluation of the **MTB** diversity in Chapter 2 of this thesis. **FC** in combination with a **PolyP** fluorescent staining is a high throughput cell-sorting method that can be used on heterogeneous and complex samples such as environmental samples. **FC** cell-sorting was thus chosen to sort the **MTBc** as a function of their **PolyP** sequestration capabilities, in order to later be able to identify them and characterize their metabolism through genomic approaches. **DAPI** and **Tc** constitute the two most used **PolyP** fluorescent dyes, but the colocalisation of the **iACC MTB** with the **MTBc** in the water column render the fluorescent dye **Tc** a source of bias. Indeed, as the ability of **Tc** to target the **PolyP** originates from its binding to divalent cations such as  $\text{Ca}^{2+}$ , it is most probable that **Tc** would bind to the **iACC MTB**. Therefore, **DAPI** was used as **PolyP** marker in **FC** and cell sorting.

This chapter first focuses on the P-sequestering Lake Pavin **MTBc** and aims to describe their heterogeneity and quantify the relative abundance of each **MTBc** morphotypes. The chapter also aims to characterize the specific environmental conditions in which the **MTBc** are accumulating **PolyP** thanks to microscopic, chemical and statistical analyses. Investigating any correlations in this dataset will help determine if the **MTBc PolyP** heterogeneity is specific to environmental parameters or to a morphotype and potentially a species. Another goal, and subject of the second part of this chapter, is to develop a protocol for an optimum **MTBc** cell-sorting with **FC**. Culture models were used to simplify the analyses and the interpretations, and develop an efficient protocol for **PolyP** sorting. Succeeding at optimizing the protocol to prepare the samples and the **FC** analyses will enable the characterization of the **MTBc** P accumulators and their metabolism via (meta-)genomic analyses.

## 3.2 Diversity and distribution of P-sequestering MTBc along the chemical gradients in the water column of Lake Pavin

### 3.2.1 Material and methods

#### 3.2.1.1 Water sampling strategy

For details about the sampling strategy and the physico-chemical and geochemical measurements see Chapter 2 part 2.4 material and methods 2.4.1.

#### 3.2.1.2 TEM grid deposition (optimization)

The conventional method for preparing TEM grids for MTB observation is presented in figure 3.4. This method consists in depositing a 2  $\mu\text{L}$  drop of magnetically concentrated MTB and attracting them to the edge of the drop by using their magnetotactic capabilities and a magnet on the grid's side. This method allows their aggregation on a "half-ring" shape at the edge of the drop onto the TEM grid but some dispersed MTB can still be observed in the center of the grid. The deposition of the sample on the grid lasts 15 min while MTB swim toward the edge of the drop to concentrate and aggregate. After a partial drying, the grid is subsequently washed twice with sterilized water and then left to dry completely. The high density of MTB on the grid allows their quick detection without searching for them extensively and the acquisition of a large number of MTB in a single image. This is thus very useful when one wants to quickly apprehend the different morphotypes present in a sample. This technique will be from now on called the "ring technique".

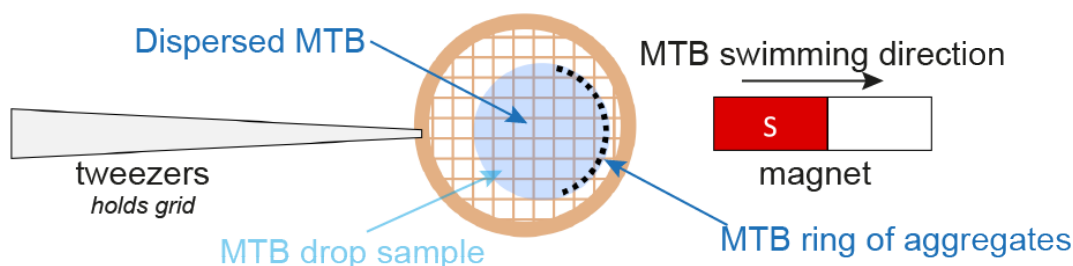


**Figure 3.4: Schematic view of the set up used for TEM grids preparation** Thanks to the magnetic field lines created by the magnet, MTB aggregate to the edge of the water droplet ensuring a higher concentration of observable bacteria.

However, the different preliminary observations on the TEM grids showed that the distribution of the different MTBc morphotypes was not homogeneous using this method. Indeed, it appeared that on the TEM grid squares related to the edge of the drop, PolyP bacteria were very few (see Fig. 3.5) whereas they were observed in higher quantities in the squares corresponding

### Chapter 3. Magnetotactic cocci in the water column of Lake Pavin: morphotype classification and sorting of P-sequestering cells

to a more central area of the drop. The PolyP-rich cells can be spotted in the cells thanks to their dark contrast in TEM-BF imaging mode (see Fig. 3.5B).

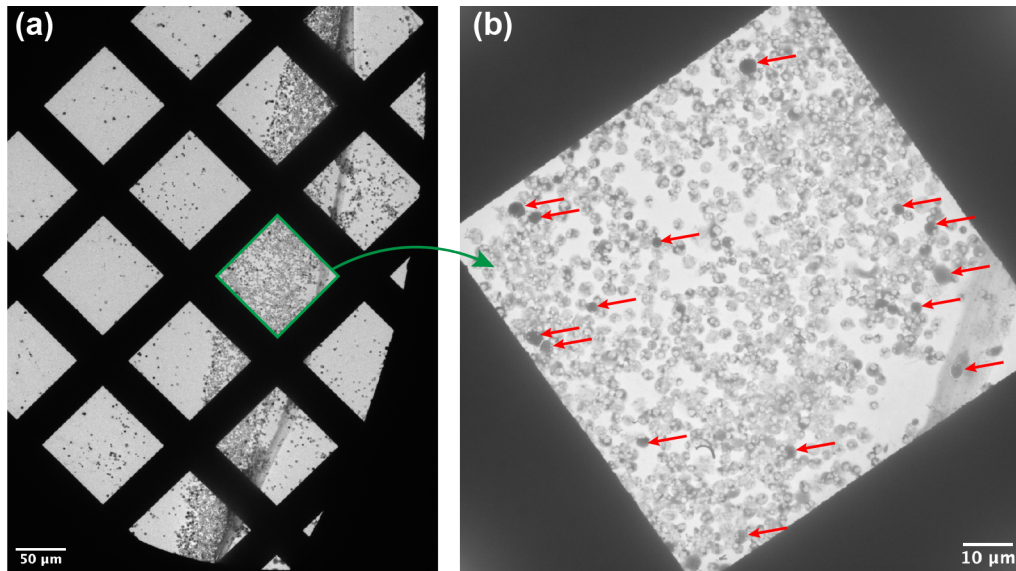


**Figure 3.5: TEM-BF observations of MTBc on a TEM grid prepared with the "ring technique" showing the segregation of the MTBc as a function of their PolyP accumulation capabilities.** (a) Low magnification image showing the high concentration of MTBc at the edge of the drop. The green square and arrow include and point out the square presented in (b) with a higher magnification. The square shows a low concentration of MTBc sequestering PolyP spotted by their dark contrast and indicated in majority by the red arrows.

This suggests that this technique segregates the MTBc accumulating P with respect to their accumulation capabilities. The reasons explaining this phenomenon are still unknown, but PolyP could play a role in weighing them down, thus slowing them in their movement and speed, or could provoke their quick deposition on the grid before they can reach the side of the drop.

In order to analyze statistically the MTBc as a function of their PolyP accumulation, and have counting duplicates (i.e. counts on several different squares on the grid), MTBc have to be homogeneously spread on the grid. Different methods have thus been tested to improve the MTB dispersion homogeneity and insure an unbiased analysis of the MTB populations.

The best results were obtained with a TEM grid ionized and poly-L-lysine-coated before the sample deposition (see Fig. 3.6). The ionization was done by using an EDwards ionizer which uses an Argon plasma to temporarily (~3 h) charge positively the surface of the grids, make it hydrophilic and favor the thin and homogeneous deposition of the poly-L-lysine on the grid. Poly-L-lysine is a positively charged polymer usually used to improve the cell adherence on sample holder for microscope observation. To coat the grid, 25  $\mu\text{L}$  of poly-L-lysine was deposited on parafilm and the TEM grids (carbon-side) placed on the top of the drop to incubate

### 3.2. Diversity and distribution of P-sequestering MTBc along the chemical gradients in the water column of Lake Pavin

for at least 30 min. The grid was then washed with filtered sterilized water by gently dipping it 2 to 3 times and let to dry on a Whatmann paper for few hours.

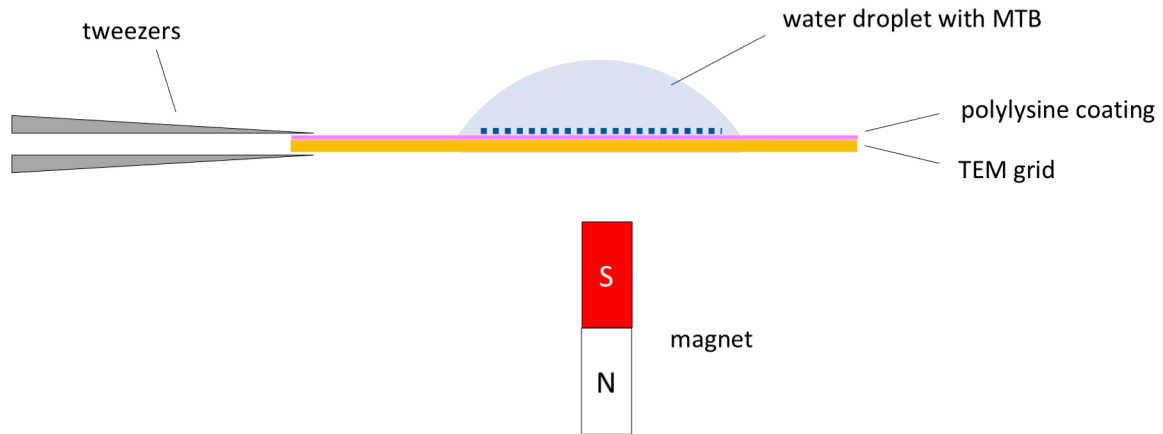


**Figure 3.6: Schematic view of the optimized TEM grid deposition with poly-L-lysine coating.** Subsequently to a magnetic sorting, the MTB sample is deposited on the TEM grid ionized and poly-L-lysine coated beforehand. The magnet is placed below the grid.

#### 3.2.1.3 Classification of the magnetotactic cocci according to the magnetosome organization and the relative size of PolyP granules

The phenotypic heterogeneity of the dominant MTBc morphotype, with respect to their ability to form PolyP granules of different sizes and different organization of magnetosomes, was investigated using STEM-HAADF and STEM-XEDS approaches. This was done using a JEOL 2100F, operating at 200 kV, and equipped with a JEOL XEDS detector. MTB from the water column were concentrated using a magnetic enrichment protocol. The magnetic enrichment, for each of the nine sampled depth (centered on the MTB maximum of abundance), consisted in placing the south pole of a stirring-magnet against the side and center of a 1 L bottle for 1h. These bottles corresponded to the ones used to determine the water column MTB diversity in the chapter 2 of this thesis in part 2.4. 15  $\mu$ L of MTB pellet was deposited, onto TEM grids coated with poly-L-lysine.

Each TEM grid was first observed at very low magnification to evaluate the bacteria abundance on the whole grid and to verify their distribution homogeneity. Following, several squares were randomly chosen and analyzed in details (i.e. for all the present bacteria on the squares; Fig. 3.7a). To allow statistical analyses, the number of cells observed and counted on the TEM grids averaged a few hundred to several hundreds of cells. This number was mainly dependent on the abundance of MTB on the grids. However, when the number of cells was low (i.e. less than a few hundred) all the cells present on the grid were counted. STEM-HAADF mode was favored with regard to its contrast enabling the better observation of the magnetosomes and the



diverse inclusions. **STEM-HAADF** mode did not allow to determine the nature of the inclusions (Fig. 3.7b-f).

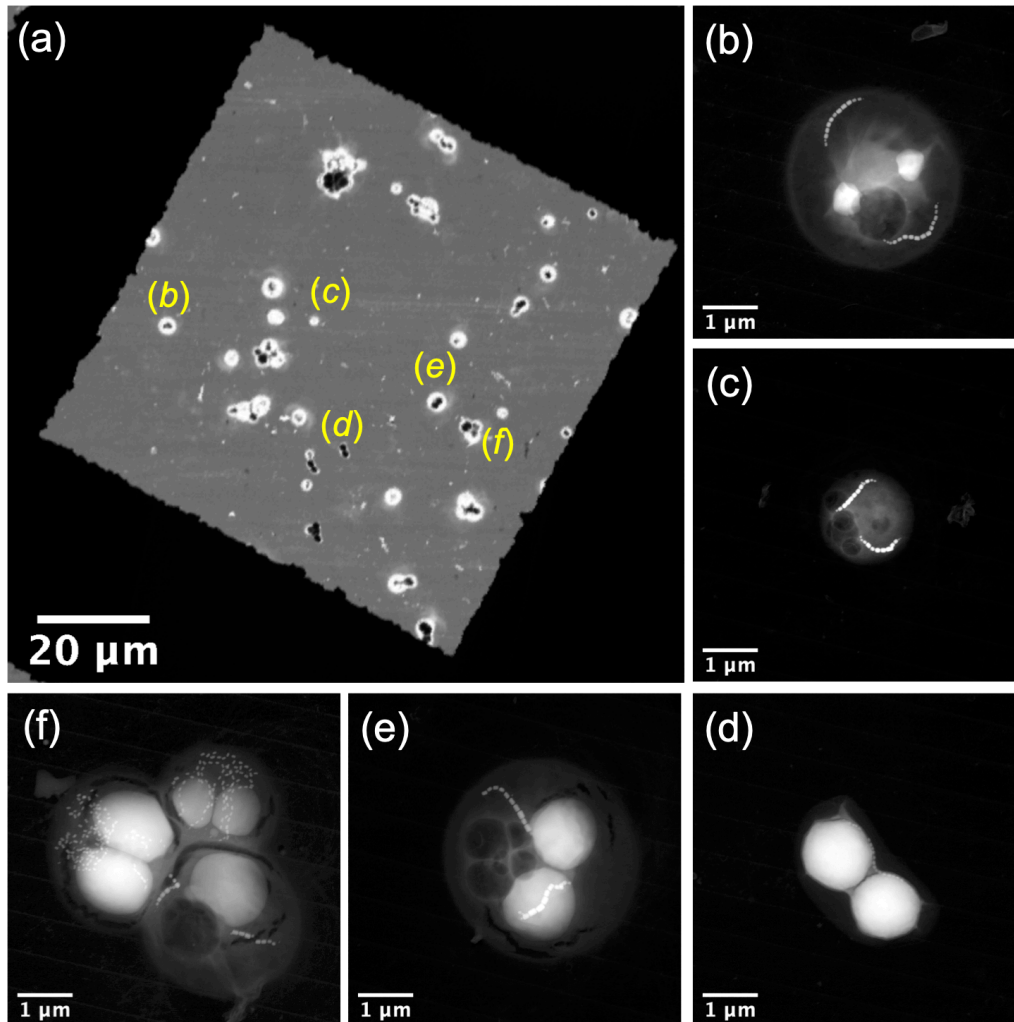


**Figure 3.7: STEM-HAADF observations of PolyP-accumulating MTBc and iACC-rods and their analyses on the TEM for statistical analysis.** (a) Low magnification image showing the dispersion of the different MTB observed on a square of a TEM grid. (b-f) Images at higher magnification detailing the different observed morphotypes. Three cells are visible on panel (f). Different magnetosomes organizations are highlighted: single chain (d), double chain (b,c,f,e), disorganized magnetosomes (f).

**STEM-XEDS** chemical maps allowed to remove the nature ambiguity of the inclusions by identifying the different chemical elements present in the cells thus detecting PolyP, sulfur and iACC granules (see Fig. 3.8). As a consequence a corpus of observations of the different morphotypes could be assembled (see in results in next section Fig. 3.9). On figure 3.7, the MTB could thus be linked to MTBc with PolyP granules (b,c,f,e) and to iACC MTB (d). These analyses enabled the relative quantification of each of the different MTBc morphotypes as a function of the overall MTBc and as a function of the environmental parameters.

### 3.2. Diversity and distribution of P-sequestering MTBc along the chemical gradients in the water column of Lake Pavin

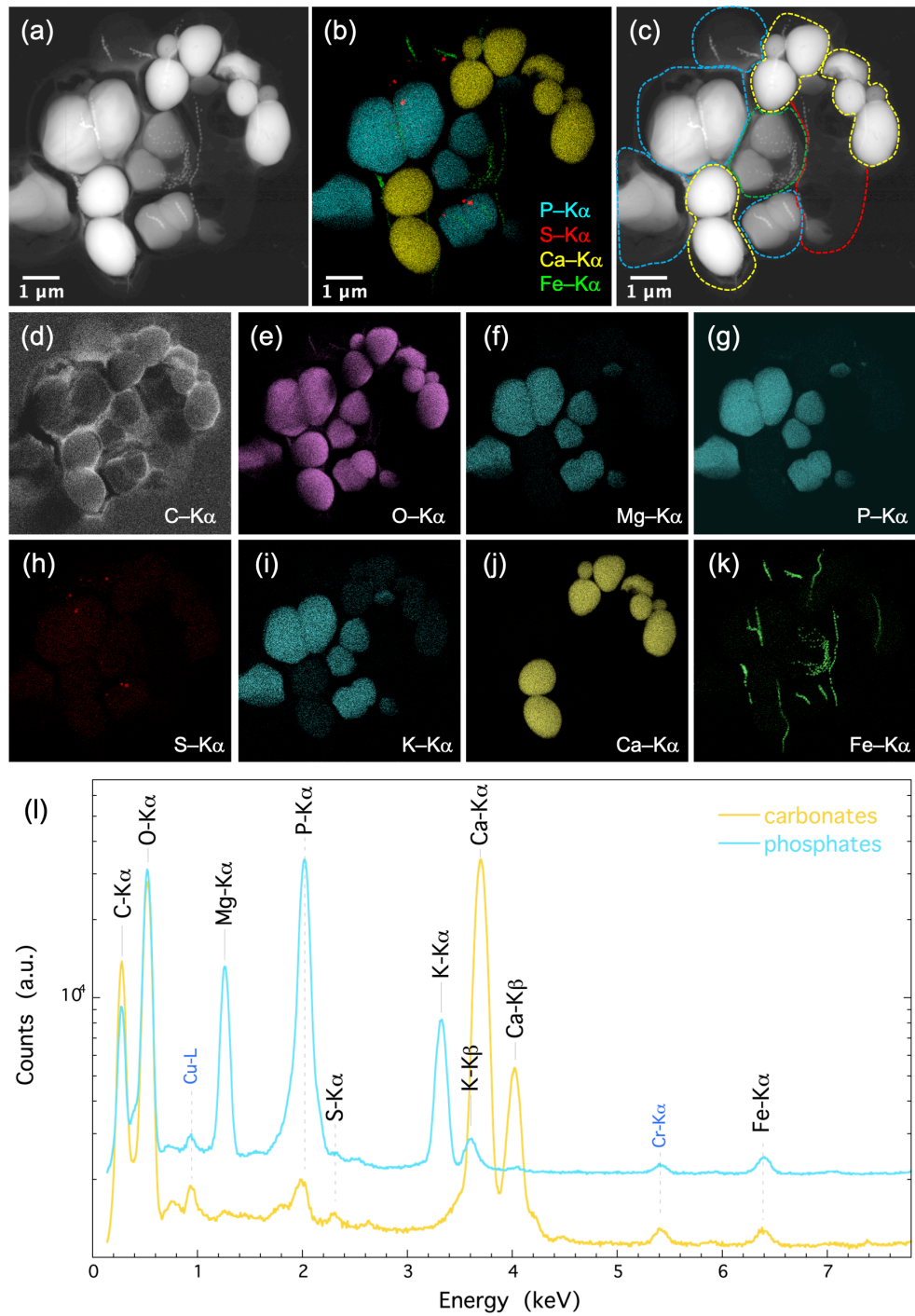


Figure 3.8: Caption on following page.

**Figure 3.8: Elemental mapping of MTB sequestering granules of PolyP, S or iACC.** (a) STEM-HAADF and (b) composite elemental image showing the coexistence of PolyP sequestering MTBc with double chains of magnetosomes (blue circle in (c)) or disorganized magnetosomes (green circle in (c)) and iACC-rods (yellow circle in (c)) MTB. Note also the coexistence of a MTB rod sequestering two small polar PolyP inclusions (red circle in (c)). (d-k) elemental STEM-XEDS mapping of major elements (X-ray lines are indicated). It has to be noticed that the images are not background corrected. For some images (Mg, P, S, K and Fe) apparent intensity may be due to Bremsstrahlung and is therefore not related to the actual presence of these elements. The Carbon C-K $\alpha$  map is affected by absorption process and shadowing effect because of the X-ray detector orientation. (l) X-ray fluorescence spectra related to respectively carbonates and phosphates (the second spectrum has been shifted for clarity). Intensity is plotted in logarithmic scale to emphasize the minor elements signal. Cu-L and Cr-K $\alpha$  peaks are spurious signals due to the sample holder.

### 3.2.1.4 Statistical analyses

Our dataset describing the MTB populations thriving at 9 depths in the water column (Table S1) consisted in the abundance of MTB cells, the two main MTB populations (MTBc and rods accumulating iACC, as counted by optical microscope with triplicates), and in the relative proportions of MTBc without PolyP, with small or big PolyP, double chains or disorganized magnetosomes MTBc (resulting from our TEM-based classification schema, with replicates at 4 water column depths).

Means of relative proportions were compared between pairs of samples with replicates, either by a paired Student's t-test or by a paired non-parametric Mann–Whitney U test if variables were not normally distributed. Differences were considered as significant when P-values were below 0.05.

Strength and direction of the pairwise linear or monotonous relationships between the biological and the environmental variables were evaluated by the Pearson's (when bivariate normality assumptions were satisfied) or Spearman's correlation coefficient, respectively. Water column depths without replicates were discarded. Correlations were considered as significant when the P value was lower than 0.05 (Bonferroni correction corresponding to a false positive error rate lower than 5% per test).

## 3.2.2 Results

### 3.2.2.1 The proportion of MTBc sequestering PolyP differs with depth in the water column

While rods forming iACC are phenotypically homogeneous, i.e., they all produce inclusions occupying the major part of their cytoplasm and exhibit the same magnetosome organization, MTBc include different populations according to their capability to accumulate PolyP or to have

### 3.2. Diversity and distribution of P-sequestering MTBc along the chemical gradients in the water column of Lake Pavin

different magnetosome organization (Fig. 3.9).

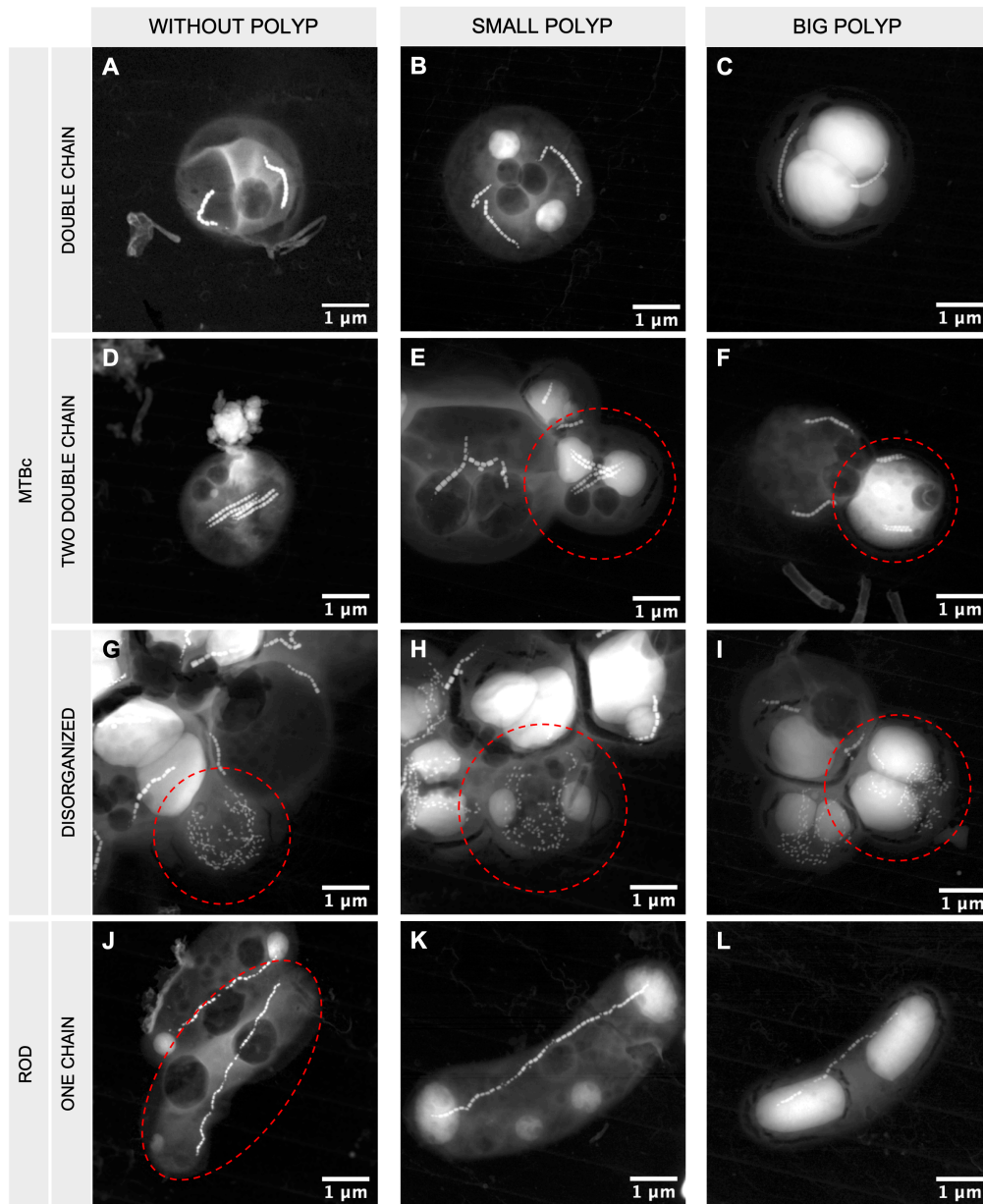


**Figure 3.9:** STEM-HAADF images showing different magnetosomes organizations and **PolyP** accumulation capacities of **MTBc** and **PolyP** accumulating rod-shaped **MTB**. **MTBc** with double chains (A - C), two double chains (D - F), disorganized magnetosomes (G - I) and rod-shaped **MTB** with one chain of magnetosomes (J - L). Column from left to right are presenting **MTB** without **PolyP**, small **PolyP** and large **PolyP**. The bacteria of interest are encircled in red.

The observation of a wide range of **PolyP** inclusions size suggests the presence of different populations of **MTBc** with different inclusions growth/hydrolysis stages that can be categorized in three groups: cells without **PolyP**, with small **PolyP** or with big **PolyP** inclusions; small and big referring to inclusions occupying less and more than half of the cell area, respectively (Fig. 3.9). The **MTBc** mineralize prismatic magnetosomes with 3 different spatial organization:

### Chapter 3. Magnetotactic cocci in the water column of Lake Pavin: morphotype classification and sorting of P-sequestering cells

most of them had one double chain (from 82% at 52 m and up to 100% at 53 and 53.5 m) and few had disorganized magnetosomes (from 0% at 50.5, 51, 53, 53.5 m and up to 17% at 52 m) (Fig. 3.11B and Table S1). Very rare MTBc with two double chains similar to those described in Zhang et al. (2017) and Liu et al. (2020) were also observed (Fig. 3.9D-F).

High resolution images and crystallographic analyses showed that the magnetosomes exhibited a prismatic shape with different aspect ratio for each of the three magnetosomes spatial distribution. Moreover, it appears that, for each of the chain configuration, the magnetosomes were aligned along the  $\langle 111 \rangle$  crystallographic direction (Fig. 3.10).

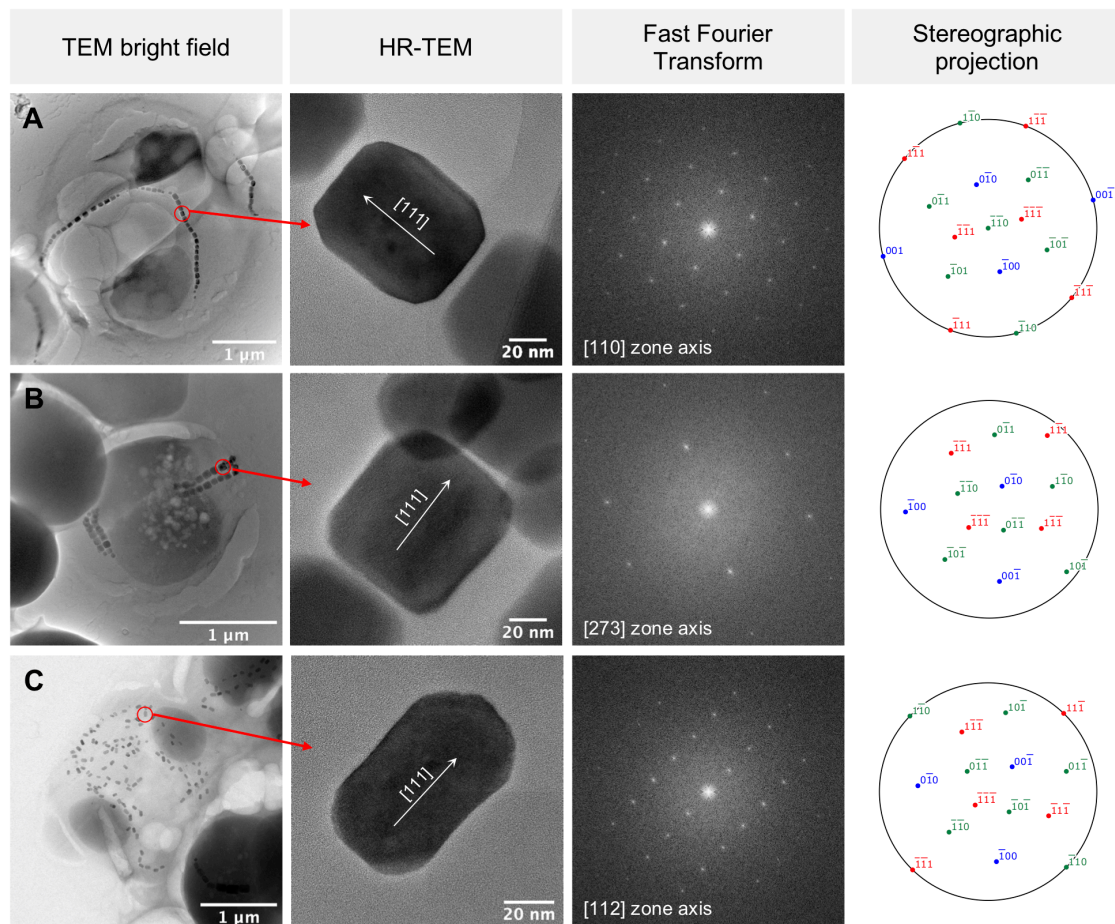


**Figure 3.10: Morphological analysis of prismatic magnetosomes in cocci with three different magnetosomes organizations.** (A) two single chains, (B) two double chains and (C) disorganized magnetosomes. Every cocci cell hosts prismatic shaped magnetosomes elongated along the  $[111]$  axis as demonstrated through HRTEM, FFT and crystallographic analysis.

Population sizes, i.e. number of cells classified in a given population, were too small on some TEM grids in order to provide counting replicates (see Methods for details). Considering all MTBc independently of their magnetosome organization, in case of the four water column depths with counting replicates (from 51.3 m to 52 m, Fig. 3.11), our data suggested that the relative proportion of MTBc forming big PolyP increases with depths reaching

### 3.2. Diversity and distribution of P-sequestering MTBc along the chemical gradients in the water column of Lake Pavin

a maximum at 52 m, while the opposite trend is observed for MTBc without PolyP (Fig. 3.11A).

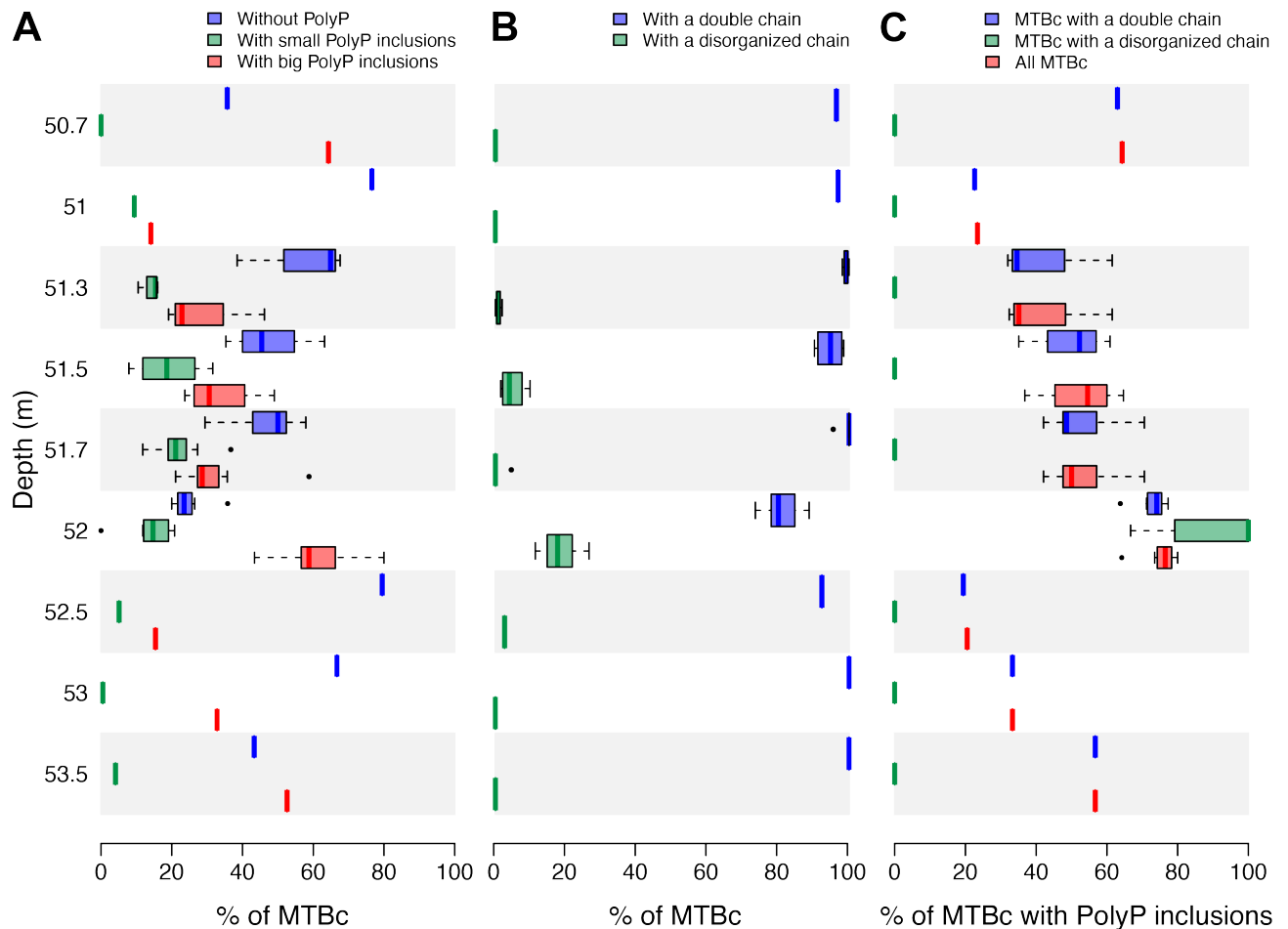


**Figure 3.11: Distribution of MTBc in the water column according to their ability to form different types of magnetosome chains and PolyP inclusions.** Boxplots showing (A) the frequency of MTBc without, with small or with big PolyP over the total amount of MTBc for each depth sampled, (B) the frequency of MTBc with double chains and disorganized chains independently of their capability to form PolyP and (C), the frequency of MTBc forming PolyP for each class of coccus (forming double chains and disorganized chains, or both). Boxplots could be obtained only for 4 depths from 51.3 m to 52 m. For the other depths, only one value is available because MTBc were not in sufficient number on the squares of the grid to get satisfactory statistics. The depth 52 m is the only one to differ significantly from the other depths for the MTBc without PolyP and the ones with big PolyP. This is supported by a student t-test (with  $p < 0.05$ ).

Although, MTBc with a double chain of magnetosomes represent the majority of cells in the four depths, MTBc with disorganized magnetosomes increase in proportion at the same depth where magnetotactic rods forming iACC are observed, i.e. at 52 m (Fig. 3.11B). When classifying MTBc according to their magnetosome chains, it has to be noticed that the frequency of PolyP accumulators is increasing with depth, for each class (Fig. 3.11C). The conditions

### Chapter 3. Magnetotactic cocci in the water column of Lake Pavin: morphotype classification and sorting of P-sequestering cells

---

observed at 52 m appear to be optimal for the formation of PolyP by MTBc but also for iACC by magnetotactic rods.

Despite the low number of usable observations ( $n = 4$ ), it has been possible to investigate links between PolyP accumulation and geochemistry. Relaxing the threshold up to 0.05, other frequencies are significantly anticorrelated with geochemical variables like concentration of dissolved boron, sulfate, particulate iron and barium (Appendices Fig. Fig. S3).

#### 3.2.3 Discussion

Two main populations of MTBc with different magnetosome organizations and a maximum of abundance at different depths were found along the water column of Lake Pavin. MTBc with two magnetosomes chains largely dominate the MTB abundance profile (> 57%). The maximum of abundance of this major morphotype was therefore located at the same depth than the maximum of MTB total abundance (51.3 m). The minor MTBc morphotype with disorganized magnetosomes analogous to those described by e.g. Koziyeva et al. (2019) and Liu et al. (2020) was most abundant at the same depth than the iACC rods (52 m). Both MTBc morphotypes were located in anoxic conditions. On average a minimum of ~30% and up to ~80% of these MTBc were able to accumulate intracellular PolyP. TEM analyses showed a significant increase of the proportion of MTBc capable of accumulating PolyP at 52 m, thus showing a propensity of MTBc to accumulate PolyP independently of their abundance. In addition, it is important to note that the PolyP sequestration capabilities was significantly higher at this depth for both morphotypes of MTBc (i.e. double chain and disorganized magnetosomes). This suggests that phosphorus hyperaccumulation capability is dependent on environmental conditions affecting both morphotypes.

The diversity of magnetosome intracellular organizations observed in MTBc suggests that there is more than one species of MTBc in the water column of Lake Pavin. This hypothesis, is based on a recent study which demonstrated that MTBc populations with magnetosomes differing in number, crystal size, axial ratio and chain configuration belong to different species (Liu et al., 2020). This hypothesis is also reinforced by previous phylogenetic analyses made on Lake Pavin MTBc, which based on 16S rRNA gene sequence, showed the presence of two different species (Rivas-Lamelo et al., 2017). One of these two species was shown to be more abundant than the other, potentially corresponding to MTBc with two magnetosome chains and disorganized magnetosomes, respectively.

A negative correlation with dissolved sulfate was evidenced with the propensity of MTBc cells to accumulate large PolyP (see appendices Fig. S3). Moreover, TEM characterization of intracellular inclusions of the major MTBc population (with two magnetosomes chains)

### 3.2. Diversity and distribution of P-sequestering MTBc along the chemical gradients in the water column of Lake Pavin

---

suggests that cells accumulating large PolyP inclusions harbor small sulfur globules (see appendices Fig. S4). This relationship could be due to intracellular space limitations or to the oxidation of the sulfur granules to gain energy for PolyP storage, the latter being previously evidenced by Kornberg (1995). While the observation of intracellular S granules suggests a sulfur-oxidation metabolism (Maki, 2013) such inclusions were only observed in ~20% cells of this morphotype. Only tiny sulfur granules are present in MTBc with disorganized magnetosomes, whatever the size of their PolyP inclusions. Only ~10% cells of this minor morphotype contain sulfur granules. It has been reported that P-hyperaccumulators found in the environment are sulfur-oxidizers (Möller et al., 2019; Brock and Schulz-Vogt, 2011), they can be found in different conditions, but always in the vicinity of the oxycline or within a gradient of sulfide. Bacteria belonging to the *Sulfurimonas* genus are situated in an euxinic zone (anoxic and  $> 0.1 \mu\text{M}$  of sulfide) of the water column of the Baltic Sea, where they need both nitrate and sulfide in order to gather energy and accumulate their PolyP (Möller et al., 2019). In contrast, MTB affiliated to the *Magnetococcaceae* family from the suboxic layer ( $< 0.1 \mu\text{M}$  oxygen and  $< 0.1 \mu\text{M}$  sulfide) in the water column of the Black Sea store PolyP near the oxygen disappearance and keep them in suboxic condition until they hydrolyze them upon reaching the sulfide-rich zone of the water column (Schulz-Vogt et al., 2019). These two situations come against part of the current paradigm based on *Beggiatoa* and *Thiomargarita* behavior for which PolyP are accumulated in oxic conditions but are hydrolysed in both anoxic and sulfide-rich conditions (Schulz and Schulz, 2005; Brock and Schulz-Vogt, 2011). Similarly to MTBc from the Black Sea and *Sulfurimonas* from the Baltic Sea, MTBc from Lake Pavin are also capable of keeping their PolyP in anoxic water. However, in contrast to the situation observed in the Black Sea, the Lake Pavin phosphorus accumulators do not seem to accumulate PolyP near the OATZ but rather deeper in the water column and closer to the sulfide increasing gradient. MTBc from Lake Pavin thus appear to have a closer metabolism to the *Sulfurimonas* from the Baltic Sea where sulfide is required to accumulate PolyP.

A large number of MTBc with empty vacuoles have been observed in samples at every depth. The exact nature and function of these empty vacuoles are undetermined. In the large sulfur-oxidizing *Beggiatoa*, *Thiomargarita* and *Thioploca*, empty vacuoles correspond to a nitrate-storing space for anoxic respiration and energy conservation (McHatton et al., 1996; Schulz, 1999; Zopfi et al., 2001). The closest relative to the Lake Pavin MTBc, the type strain *Magnetococcus marinus* MC-1 (Bazylynski et al., 2013b) have been shown to harbour the set of genes required for denitrification (Philippot, 2002). Such metabolic capability has also been hypothesized for MTBc from the Black Sea (Schulz-Vogt et al., 2019). Moreover, some MTB affiliated to the Nitrospirae phylum also presenting empty vacuoles were suggested to couple sulfur-oxidation with denitrification (Li et al., 2020a). Thus, MTBc of Lake Pavin could gain energy from their intracellular sulfur granules (i.e. sulfur-oxidation) and their potential



### Chapter 3. Magnetotactic cocci in the water column of Lake Pavin: morphotype classification and sorting of P-sequestering cells

---

intracellular nitrate (i.e. denitrification) for the accumulation of P as PolyP.

Previous studies of Lake Pavin showed a dissolved P (named SRP) concentration increase around the end of the MTB zone to reach up to  $\sim 300 \mu\text{M}$  deeper in the water column (Rivas-Lamelo et al., 2017). From our study, it appears that the SRP concentration starts to increase directly with increasing depth after the maximum PolyP accumulation capability of the MTBc. It has been shown that, after a time of P deprivation when P becomes available again, some organisms such as microalgae have the ability to store more P than necessary in case of future shortage (Solovchenko et al., 2019); this ability is called luxury uptake. In the water column of Lake Pavin, above the increase of SRP, the concentrations of SRP reach its minimum wherever MTBc are observed. It is possible that MTBc or local biomass are responsible for keeping this concentration at a minimum. Another possibility is that upon reaching waters with a higher P concentration, MTBc start accumulating PolyP to a greater extent in order to prepare for future deprivation. Another hypothesis could be that MTBc present a dynamic movement along the water column. They could swim downward to accumulate PolyP necessary for their metabolism, before swimming back upward, toward more optimum conditions at the depth where they are the most abundant and where they might hydrolyze their PolyP storage. It is interesting to note that the proportion of MTBc with big PolyP is lower at this depth. Whether the MTBc are hydrolyzing PolyP at this depth remain to be evaluated. In Li and Dittrich (2019), cyanobacteria were shown to accumulate PolyP in bigger amount during the lag phase due to an “overplus” uptake of P. However, the amount of PolyP was balanced during the exponential growth as a result of a competition between the P luxury uptake and its utilization for growth. MTBc could present lower amount of PolyP at their peak of abundance, due to an exponential phase, whereas hyperaccumulating PolyP deeper in the water column during their lag phase. This hypothesis would support the luxury uptake hypothesis in combination with their dynamic movement along the water column.

Particulate Mg and P were found significantly correlated to the MTBc abundance (fig. 2.3C). PolyP are composed of negatively charged molecules and are commonly associated with counter ions with either a valence of +1 or +2 (Peeverly et al., 1978; Kulaev et al., 2004). Our XEDS results showed that the PolyP are associated with magnesium and potassium, respectively of valence +2 and +1 (appendices Fig. S2), thus matching the correlation of particulate Mg with the MTBc. This association has already been reported in MTBc of Lake Pavin (Rivas-Lamelo et al., 2017). PolyP association with Mg has been also shown for the hyperaccumulators of P *Sulfurimonas* of the Baltic Sea (Möller et al., 2019) and the giant sulfur-oxidizing *Beggiatoa* (Brock et al., 2012). In addition to Mg as counter ion for PolyP in our samples, two other counter ions with a lower abundance were found to be associated with the PolyP, i.e. potassium and calcium. These two counter ions were shown to be significantly and positively correlated together.

Multivariate statistics revealed the significant correlation of particulate P with MTBc. In

### 3.2. Diversity and distribution of P-sequestering MTBc along the chemical gradients in the water column of Lake Pavin

---

Lake Pavin, particulate P has been previously linked to the turbidity peak and iron-phosphate particles (Cosmidis et al., 2014; Busigny et al., 2016). Moreover it has been shown that the particulate P of the MTBc and their PolyP represented only 1% of the total particulate P. In our study, the turbidity presents a broad increase around the peak of MTBc, it is thus likely that the particulate P correlation to MTBc originates from the co-localization in depth of MTBc and the current peak of iron phosphate. Around this depth, the systematic observation of incrustated cells with Fe-P minerals formerly suggested microbial interaction (Cosmidis et al., 2014; Miot et al., 2016; Berg et al., 2019). The contribution of the MTBc P metabolism to the phosphatogenesis, in particular PolyP hydrolysis, remains to be determined.

Our present observations evidenced in TEM the succession as a function of depth of MTBc with a double chain of magnetosomes, followed by MTBc with disorganized magnetosomes, then deeper the *Magnetococcaceae* rods accumulating PolyP. It may be asked if the succession of the three *Magnetococcaceae* morphotypes is due to competition or a difference of metabolism? The three of them have been shown to accumulate sulfur granules intracellularly suggesting they might all be SOB.

It appears from our results that magnetotaxis in MTBc of Lake Pavin would not function in conjunction with aerotaxis unlike for most known microaerophilic MTB that find efficiently their optimal oxygen concentration thanks to a magnetically assisted aerotaxis, the so-called magneto-aerotaxis (Frankel et al., 1997; Bennet et al., 2014; Lefèvre et al., 2014). MTBc would rather take advantage of their orientation with the Earth magnetic field to swim in one direction downward sulfur and phosphorus using the redox gradient to swim back and forth between their biotopes of interest. In MTBc, magnetosomes formation would thus represents a selective advantage to use magnetotaxis in conjunction with redox taxis, i.e., magnetically assisted redox taxis, or magneto-redox taxis, to efficiently migrate to and maintain position at their preferred redox (Fig. 3.12).

### Chapter 3. Magnetotactic cocci in the water column of Lake Pavin: morphotype classification and sorting of P-sequestering cells

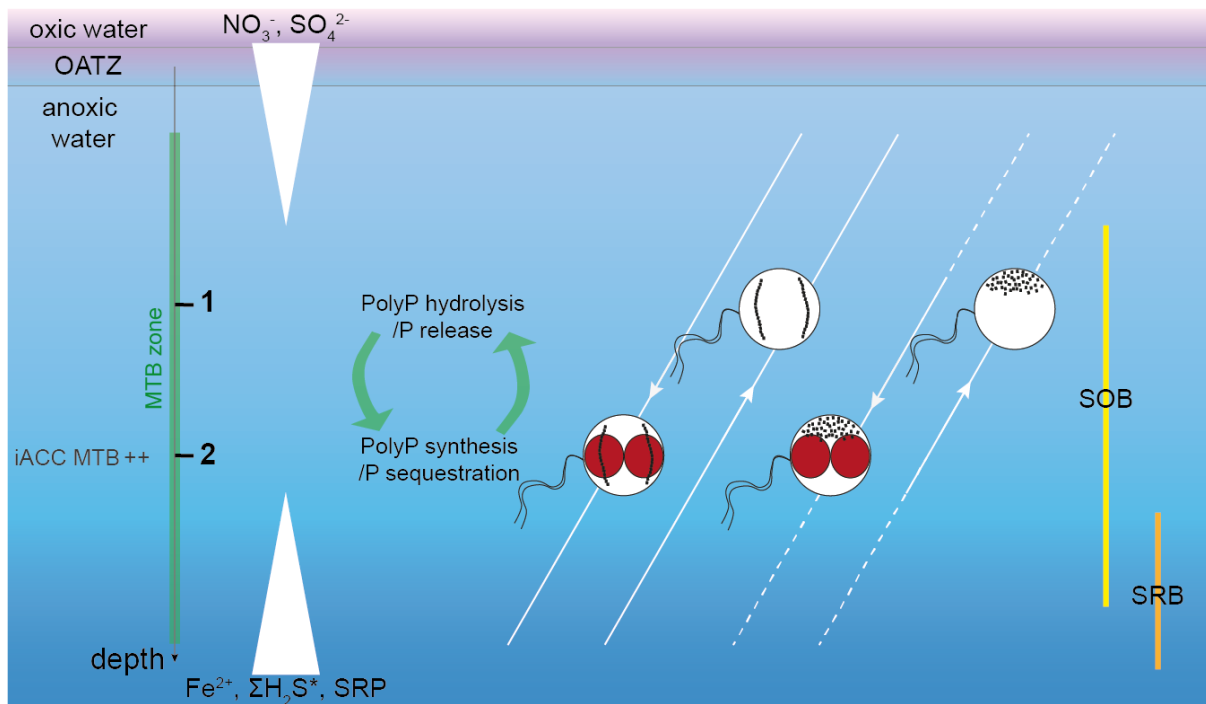


**Figure 3.12: Schematic illustration of the main MTBc morphotypes inhabiting the anoxic layer of the water column of Lake Pavin.** Six dominant morphotypes were defined according to TEM observations: with double chains or disorganized magnetosomes and without, with small PolyP or big PolyP (as presented in Fig. 3.9). For each magnetosome organization (double chains and disorganized magnetosomes), the majority MTBc morphotypes (without or with big PolyP) are represented as a function of the depth and the proportions presented in Fig. 3.11. Main geochemical gradients occurring along the water column are depicted by white triangles as follows. The concentration of dissolved nitrate begins at  $0 \mu\text{M}$  for about the first 20 m of the water column, then increases to reach a maximum around  $19 \mu\text{M}$  at the beginning of the MTB zone (50.7 m) and then decreases back down to the detection limit by the end of the MTB zone (Miot et al., 2016) (Table S1). Sulfate concentrations are nearly constant between the surface and the MTB zone, to then reach a maximum concentration ( $\sim 20 \mu\text{M}$ ) in the middle of the MTB zone (51.5 m) before decreasing importantly to reach  $0 \mu\text{M}$  with increasing depth for around 20 m (Miot et al., 2016) (Table S1 and Fig 2.3B). Dissolved Fe, P (SRP) and  $\text{H}_2\text{S}$  concentrations are stable around  $0 \mu\text{M}$  from the surface of the water column to the beginning of the MTB zone. These concentration then begin to increase in the MTB zone to reach respectively  $\sim 1200$ ,  $\sim 300$  and  $\sim 22 \mu\text{M}$  toward the bottom of the water column (Rivas-Lamelo et al., 2017) (Table S1). SOB and SRB are located as evidenced by Berg et al. (2019). Double chains and disorganized magnetosomes are represented by intracellular black dots. Intracellular PolyP granules are represented as (unscaled) red inclusions. MTBc with sulfur inclusions represented only a small fraction of the MTBc in the water column ( $<20\%$ ). The white lines represent the geomagnetic field lines, the white arrows indicating the direction and the dotted lines indicating depth where the MTBc concentrations were under the detection threshold.

### 3.3 Cell sorting of **MTBc** with large PolyP inclusions using flow cytometry: methodological developments and preliminary results

**TEM** analyses on the **MTBc** from Lake Pavin water column revealed a stratification of P accumulation capabilities. **FC** analyses in combination with a fluorescent PolyP dye offers the opportunity to single-cell sort the **MTB** as a function of their P accumulation capabilities.

**FC** measurements and sorting were done at Clermont-Auvergne University (France) in the Laboratoire Microorganismes: Génome Environnement (LMGE) with Anne-Catherine Lehours and Hermine Billard. Part of the results in this section were also obtained during the master internship of Clémentin Bouquet.

**DAPI**, in combination with a DNA marker, was tested on negative and positive bacterial controls presenting different PolyP accumulation capabilities and a similar size to the Lake Pavin bacteria ( $\sim 2 \mu\text{m}$ ). These bacterial models were used to delineate the PolyP fluorescent signal from the artificial fluorescent signal corresponding to the bacteria without PolyP. Different staining protocols were also tested in order to optimize the staining and the cell sorting as a function of the PolyP accumulation.

#### 3.3.1 Methodological strategy: samples and parameters

**Bacterial model choice.** During the first part of this study we focused on choosing bacterial models with or without PolyP. Three models were chosen for their PolyP accumulation capabilities. One was shown to accumulate PolyP in wide majority, the second one accumulated or not PolyP, and the last one did not accumulated PolyP (Fig. 3.13A).

**Dual staining to detect simultaneously live cells and PolyP.** To co-localize DNA in cells marked with **DAPI**, and thus delineate live from dead cells, a DNA marker is needed. The blue DNA **DAPI** signal and the green PolyP **DAPI** signal present a spectral interaction and are therefore not appropriate for a dual observation of the DNA and PolyP signal in **FC**. As a consequence, a DNA marker that did not present spectral interaction with the PolyP **DAPI** signal was chosen. The bacterial models were then observed in **FC** to test the DNA and PolyP dual staining. Both order of staining were tested (Fig. 3.13B).

**Bacterial model cell sorting.** Following the dual staining test, a cell sorting was made on a mix of the bacterial models to evaluate the dual staining and our capacities to sort the PolyP accumulators (Fig. 3.13C).

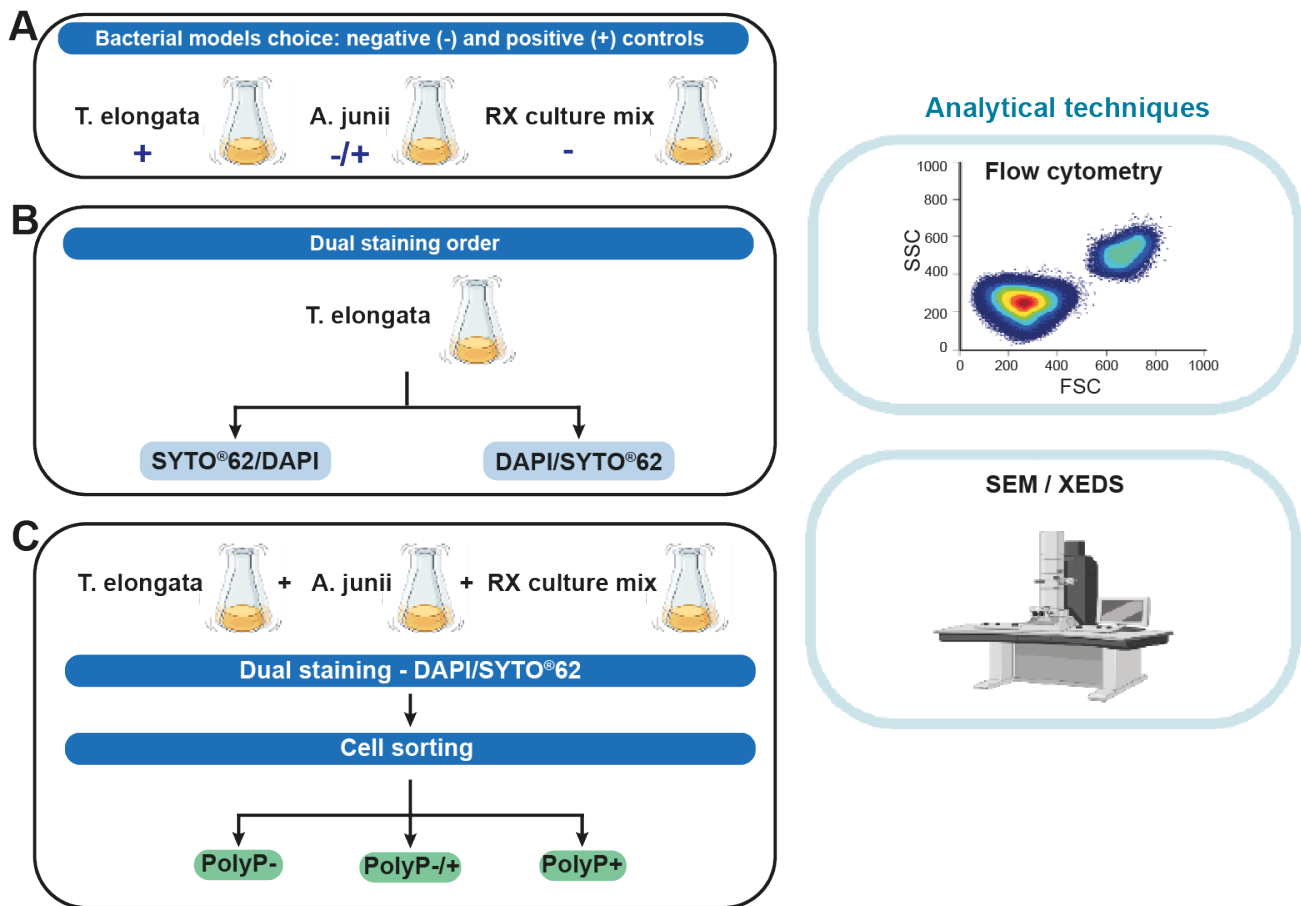


**Figure 3.13: Schematic representation of the experiments and analytical approaches used during the flow cytometry study.** SEM: scanning electron microscopy; XEDS: X-ray energy-dispersive spectrometry.

### 3.3.2 Material and methods

#### 3.3.2.1 Staining protocols

**DAPI staining.** The DAPI staining of MTB cells was prepared thanks to a stock solution of  $1 \text{ mg.mL}^{-1}$  of DAPI dihydrochloride (Sigma D9542;  $350.25 \text{ g/mol}$ ) kept at  $-20^{\circ}\text{C}$  in the dark. DAPI staining of the cells was made with a final DAPI concentration of  $10 \mu\text{g.mL}^{-1}$  and left to incubate for 30 min at room temperature (RT) in the dark. In the literature, diverse high concentrations of DAPI can be used for the visualization of the PolyP. At high concentration of DAPI the cell become permeant to the marker, but a too high concentration can induce a fluorescent background. In this work we chose the DAPI concentration used in studies for PolyP observations with FC in Günther et al. (2009) and with spectrofluorometry in Terashima et al. (2016).

The excitation laser  $405 \text{ nm}$  was used for the detection of the green PolyP DAPI signal and the emission signal was detected on a logarithmic scale with a filter combination of a  $595 \text{ nm}$

### 3.3. Cell sorting of **MTBc** with large **PolyP** inclusions using flow cytometry: methodological developments and preliminary results

---

longpass and 610/20 nm bandpass. At these emission wavelengths the **PolyP** signal is weaker but the **DAPI** DNA emission signal is avoided.

**DNA marker choice and staining protocol.** SYTO<sup>®</sup>62 Red Fluorescent Nucleic Acid Stain (S-11340; Thermo fisher) can evaluate the presence of live cells and thus separate the dead cells or particles found in a complex sample such as the sediments or the water column of Lake Pavin. In addition, this permeant marker possesses a maximum excitation and emission wavelength at respectively 650 nm and 681 nm and thus do not present spectral interaction with the **PolyP** **DAPI** fluorescence (maximum emission fluorescence 550 nm). This marker was thus chosen to stain the DNA in combination with **DAPI**.

A stock solution of 5 mM was kept at -20°C in the dark. The staining protocol consisted in a 1/5000 dilution to reach a final staining concentration of 1  $\mu$ M, then the mixture was left to incubate for at least 10 min. In **FC**, the excitation wavelength used was 640 nm and the emission signal was detected on a logarithmic scale with a filter combination of a 635 nm longpass and a 670/30 nm bandpass.

**Rinsing.** Rinsing of the samples before analyses in **FC** was not performed. Samples were left with the fixative (for the master internship) and/or staining solution throughout the experiments.

**Electron microscopy observations.** Cultures were checked for **PolyP** accumulation using **SEM**. Culture samples were filtered through polycarbonate GTTP 0.2  $\mu$ m filters in Swinnex filter holders, subsequently rinsed twice with 5 mL of Milli-Q<sup>®</sup> water and then let to dry. The filters were then placed on aluminum stubs using double-sided carbon tape and then carbon coated for the analyses. **SEM** was performed using a Zeiss ultra 55 field emission gun SEM, and images were acquired in SE2 or InLens mode at an accelerating voltage of 15 and 3 kV and a working distance of 7.5 and 4 mm respectively.

#### 3.3.2.2 Flow Cytometry set up

**FC** enables the detailed analysis of simple to complex populations. Samples are inserted into the flow cell (see Fig. 3.14A) where a sheath fluid (phosphate-buffer saline (**PBS**)) enables the cells in the sample to pass one by one through the interrogation point where the lasers intercepts the cells. This phenomenon is called hydrodynamic focusing. After the passage of the cells through the lasers the detectors receive the optic and fluorescent signals. The optics signals correspond to the scattering of light due to the interaction of the lasers with the cells (see Fig. 3.14B). Two detectors exist to detect this light, the forward scatter (**FSC**) and the side scatter (**SSC**) (Fig. 3.14A green dotted box). The signal these two detectors acquire is commonly stated to respectively give information on the relative cell size and its granularity.

### Chapter 3. Magnetotactic cocci in the water column of Lake Pavin: morphotype classification and sorting of P-sequestering cells

To obtain the **FSC** and the **SSC** signals the blue 488 nm laser is used. Fluorescence signals triggered by the lasers are acquired by the same detector as the **SSC**. The detected fluorescence corresponds to the autofluorescence of certain cell compounds for some organisms or to the fluorescence of a fluorescent markers applied to the cells beforehand (Fig. 3.14C). All of the signals acquired by the detectors can come from cells but also salt grains or particles present in the sample. Each signal detected is called an event and is represented as a dot in a 2D dot plot, afterward named cytogram (see Fig. 3.14D). **FC** can be coupled with fluorescence-activated cell sorting (FACS) and the events in the cytogram can be separated by using gates and thus selecting subpopulations that share light or fluorescent properties. After the passage of the cells through the lasers the sample is separated into droplets containing individual cells that have been selected by the gates placed on the cytogram (Fig. 3.14A). The rest of the events that are not included by the gates go to the waste. The droplets selected for the sorting are charged by an electrical charge in order to be deviated by the deflection plates toward the appropriate collection tubes.

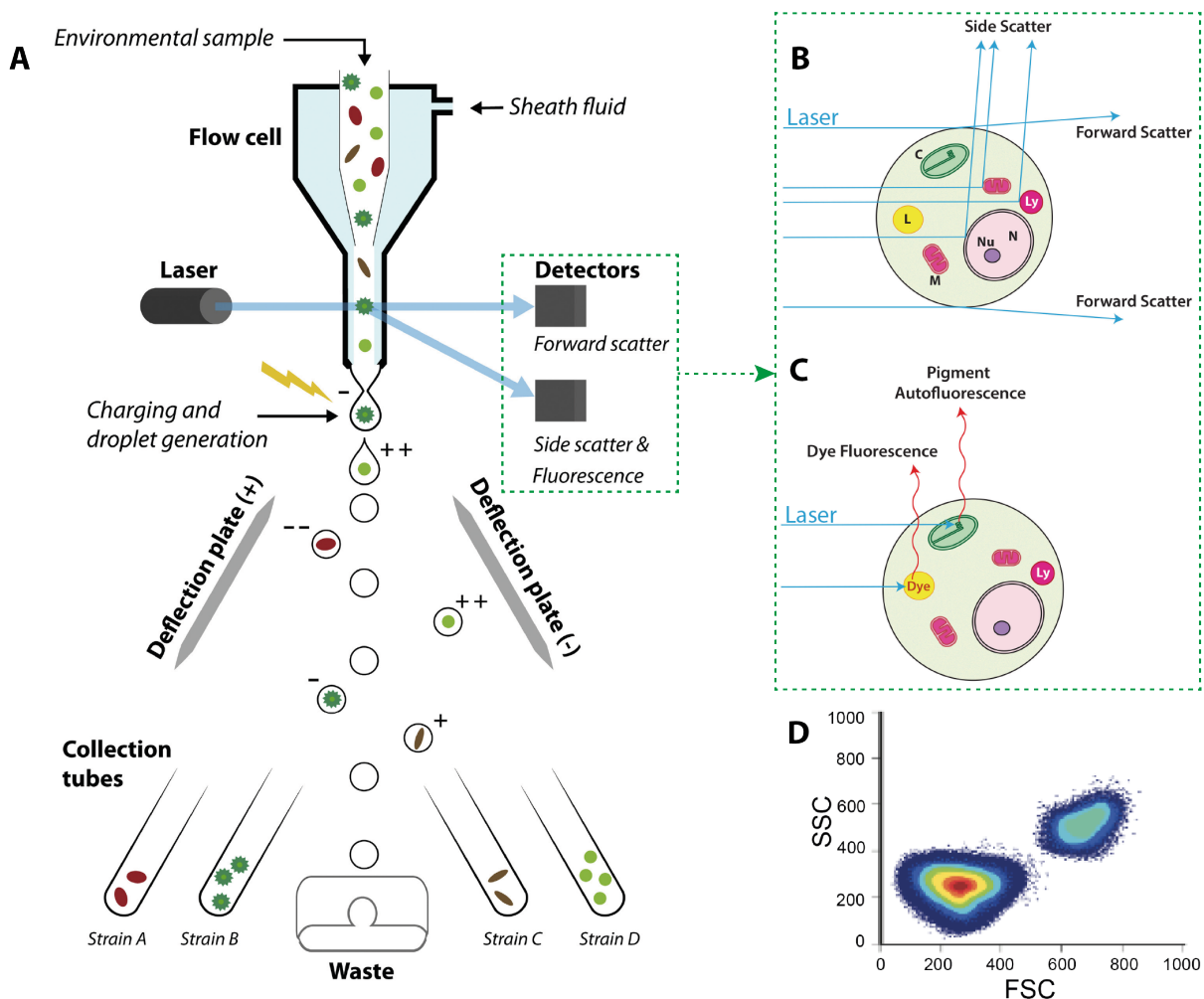


Figure 3.14: Caption on following page.

### 3.3. Cell sorting of MTBc with large PolyP inclusions using flow cytometry: methodological developments and preliminary results

---

**Figure 3.14: Schematic representation of the FC cell sorting of an environmental sample.** A/ Cells are confined to a narrow band by a liquid stream (sheath liquid) in the flow cell. Through high-speed vibration of the nozzle of the flow cell, the liquid is divided into droplets usually containing no more than one cell or particle, which is either positively or negatively charged. The cells are deviated into specific collection tubes by deflection plates according to the type and intensity of the electrical charge. B/ Light scattering and C/ fluorescence signal detected by FC (microalgae cell example) and D/ cytogram example presenting the FSC signal as a function of the SSC signal and showing an event distribution detected by FC. Figure adapted from Pereira et al. (2018).

The samples were analyzed with a flow cytometer BD FACS Aria<sup>TM</sup> Fusion SORP (Becton Dickinson, California, USA). The data were acquired at 25°C using the BD FACSDiva 8.0.3 software. Lasers alignment was achieved thanks to beads BD FACSDiva<sup>TM</sup> CS&T research (Becton Dickinson, Californie, USA) and the sample flow was adjusted as a function of the number of events per second and thus as a function of the nozzle used. The circles presented in the cytograms represent the events density. SSC signal was always used in the cytograms presenting a single marker staining. This was due to the fact that the SSC signal possesses a photomultiplier tubes (PMT) and thus get a more discriminant and precise signal than the FSC. For each experiments, cells were observed without fluorochromes to establish a negative signal threshold. Positive signals for each fluorescent marker were established as a function of the cells stained independently by each marker. Measurements replicates were done on each sample and the cell sorting was done in "purity" mode which constitute a compromise between the sorting mode yield which can get more sorting errors and the single-cell mode which is extremely stringent.

#### 3.3.3 Bacterial models: choice and conditions to obtain negative and positive controls

*Acinetobacter junii* (DSM 14184) is an ovoid bacterial strain of a few micrometer diameter isolated from a WWTP in Australia (Bouvet and Grimont, 1986). This bacterium was shown to accumulate PolyP intracellularly (Momba and Cloete, 1996). Its cultivation is done in tripticase soy broth or agar powder, respectively 30 g for aerobically liquid or 40 g in agar plate media (per liter).

The strain *Phycococcus elongatus* Lp2 or also called *Tetrasphaera elongata* Lp2 (DSM 14184) is a bacterium isolated from an activated sludge in Japan and known to accumulate intracellularly PolyP aerobically (Hanada et al., 2002). Several growth conditions were tested, rendering more or less aggregates. To lessen these aggregates, a medium called NM-1 which was showed to stop their motility, decrease their size and avoid clumps and spores (Hanada



### Chapter 3. Magnetotactic cocci in the water column of Lake Pavin: morphotype classification and sorting of P-sequestering cells

---

et al., 2002) was chosen. In this medium, the cells reached sizes of 0.7-1.0  $\mu\text{m}$  in diameter and 1.0-1.8  $\mu\text{m}$  long. This size is similar to the size of our Lake Pavin MTBc and thus this medium was kept for further experiments. The NM-1 medium contained (per liter): 0.5 g of glucose, peptone, monosodium glutamate and yeast extract, 0.44 g of  $\text{K}_2\text{HPO}_4$ , 0.1 g of  $(\text{NH}_4)_2\text{SO}_4$ , 0.1 g of  $\text{MgSO}_4 \cdot 7\text{H}_2\text{O}$  and 7.5 g of agar. In both media (830 or NM-1) *Tetrasphaera elongata* showed gliding growth on agar plates and showed more efficient growth in liquid media if inoculated from agar plates.

In Paris, both cultures were inoculated at 10 % vol/vol and were grown in liquid in 20 mL erlenmeyer flasks and kept in the dark at 30°C with a stirring of 120-150 rpm.

Surprisingly, *Acinetobacter junii* was found to generally not accumulate PolyP in the standard conditions of culture. Their sudden PolyP accumulation in only few cultures with the exact same conditions remains to be explained. As this strain was in great majority not sequestering PolyP this model was chosen as a versatile control for the future cell analyses and sorting in FC. *Tetrasphaera elongata* showed a strong accumulation of PolyP in the standard conditions of culture with two PolyP granules and one of each at each pole of the cell. This model was therefore chosen as positive control.

A culture mix of contaminant cells from an axenic culture obtained at the LMGE, containing unknown bacteria and named RX culture, was shown to accumulate very few PolyP and thus was used as a negative control. Cells were cultivated in PCA medium on agar plates at pH 7 and containing per liter: 5.0 g of tryptone; 2.5 g of yeast extract and 1.0 g of glucose. The medium was subsequently filtered under vacuum with 0.2  $\mu\text{m}$  Stericup after the auto-clave. The culture was inoculated at 10 % vol/vol and grown in oxic conditions in falcons with an hydrophobic 0.2  $\mu\text{m}$  membrane and kept in the dark at 28°C with an agitation of 100 rpm.

For the FC experiments, *Acinetobacter junii* and *Tetrasphaera elongata* were brought in agar plates to Clermont-Ferrand. The pre-cultures were grown during the day and the cultures for the analyses and the sorting were grown overnight in an incubator at 30°C and a stirring of 120 rpm.

#### 3.3.4 Dual staining on the positive control

DAPI, presenting affinities for DNA, may interact with the SYTO<sup>®</sup> 62 marker. Therefore, the dual staining was tested with either first the DAPI or the SYTO<sup>®</sup> 62. This dual staining was tested on both *Acinetobacter junii* and *Tetrasphaera elongata*. For the dual staining the cultures were subject to the two staining subsequently, each staining as stated in material and methods, and without intermediary rinsing.

Both results were similar, therefore only the results from *Tetrasphaera elongata* are presented

### 3.3. Cell sorting of **MTBc** with large PolyP inclusions using flow cytometry: methodological developments and preliminary results

here. Concerning the SYTO<sup>®</sup>62 signal, for both dual staining orders, both the fluorescence intensity and the population structure were similar to the single staining (see Fig. 3.15). The same results were observed for the DAPI signal of the single staining versus the signal from both dual staining orders.

This suggests that the markers are not interacting with each other in both conditions and that both staining order can be used for further experiments.

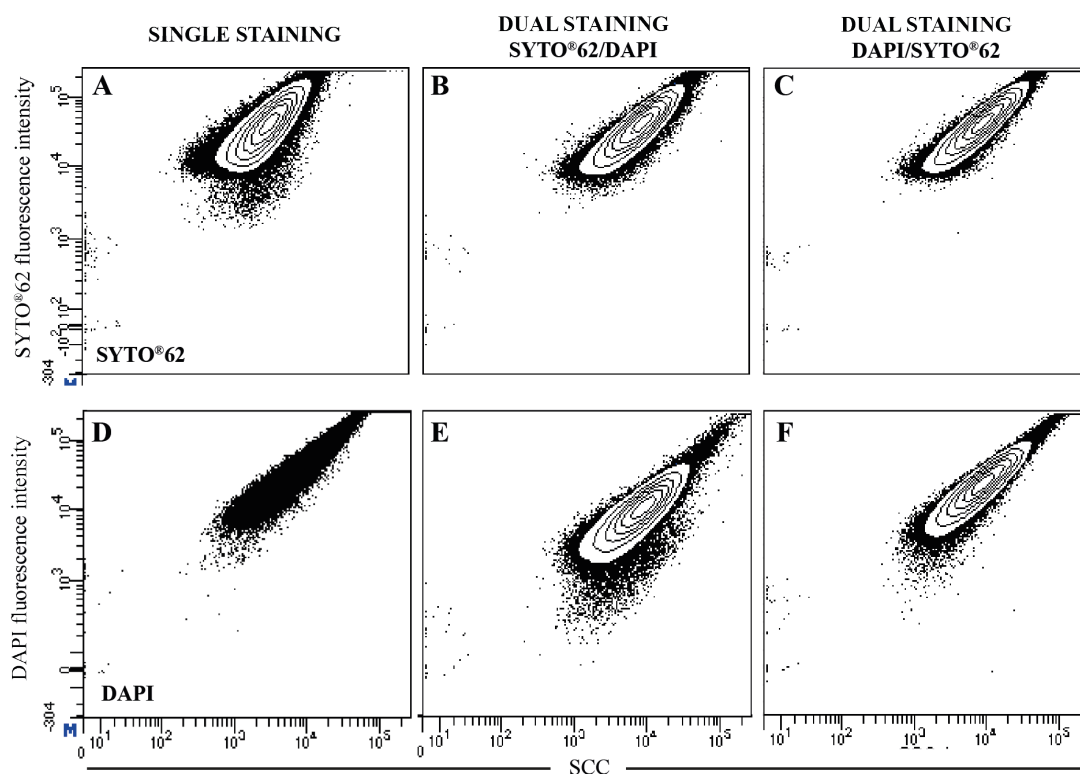


**Figure 3.15: Dual DAPI-SYTO<sup>®</sup>62 staining order comparison on the positive model control *Tetrasphaera elongata*.** Cytograms of both DAPI and SYTO<sup>®</sup>62 fluorescence intensity versus SSC. A and D correspond to respectively the DAPI and SYTO<sup>®</sup>62 single staining. B,E and C,F correspond respectively to the dual staining with SYTO<sup>®</sup>62 staining followed by DAPI and then in the inverse order. B and C correspond to both dual staining as a function of the fluorescence intensity detected with the SYTO<sup>®</sup>62 emission filters. E and F correspond to both dual staining as a function of the fluorescence intensity detected with the DAPI emission filters.

#### 3.3.5 Cell sorting on the bacterial models

Before sorting and after sorting the cultures were prepared for future SEM analyses back in Paris with the same protocol as described above in this section. After the DAPI/SYTO<sup>®</sup>62 dual staining, *Acinetobacter junii* and *Tetrasphaera elongata* cultures showed an overlap of their DAPI PolyP signal intensities (see Fig. 3.16). This suggested that some *Acinetobacter junii* were accumulating PolyP or that some of the *Tetrasphaera elongata* were not, or both.

### Chapter 3. Magnetotactic cocci in the water column of Lake Pavin: morphotype classification and sorting of P-sequestering cells

RX culture staining with DAPI and SYTO® 62 showed a DAPI fluorescence intensity distinct from the one of *Tetrasphaera elongata*. This suggested that RX culture did not accumulate intracellular PolyP.

To test the dual staining protocol and sort the cultures as a function of their PolyP accumulation, the three cultures were mixed equally in volumes and sorting gates were positioned on the resulting cytogram. A first gate included all the positive SYTO®62 fluorescence signal for the three cultures. Inside this gate, two other gates were placed to separate the events as a function of the DAPI fluorescence intensities with P5 and P6 respectively corresponding to a weaker and stronger DAPI fluorescence intensity (see Fig. 3.16). We then tried to respectively sort the three different cultures thanks to the gates P1 for RX, P2 for *Acinetobacter junii* and P4 for *Tetrasphaera elongata*. The position of these gates corresponded to their position in each of their individual cytograms (see Fig. 3.16).

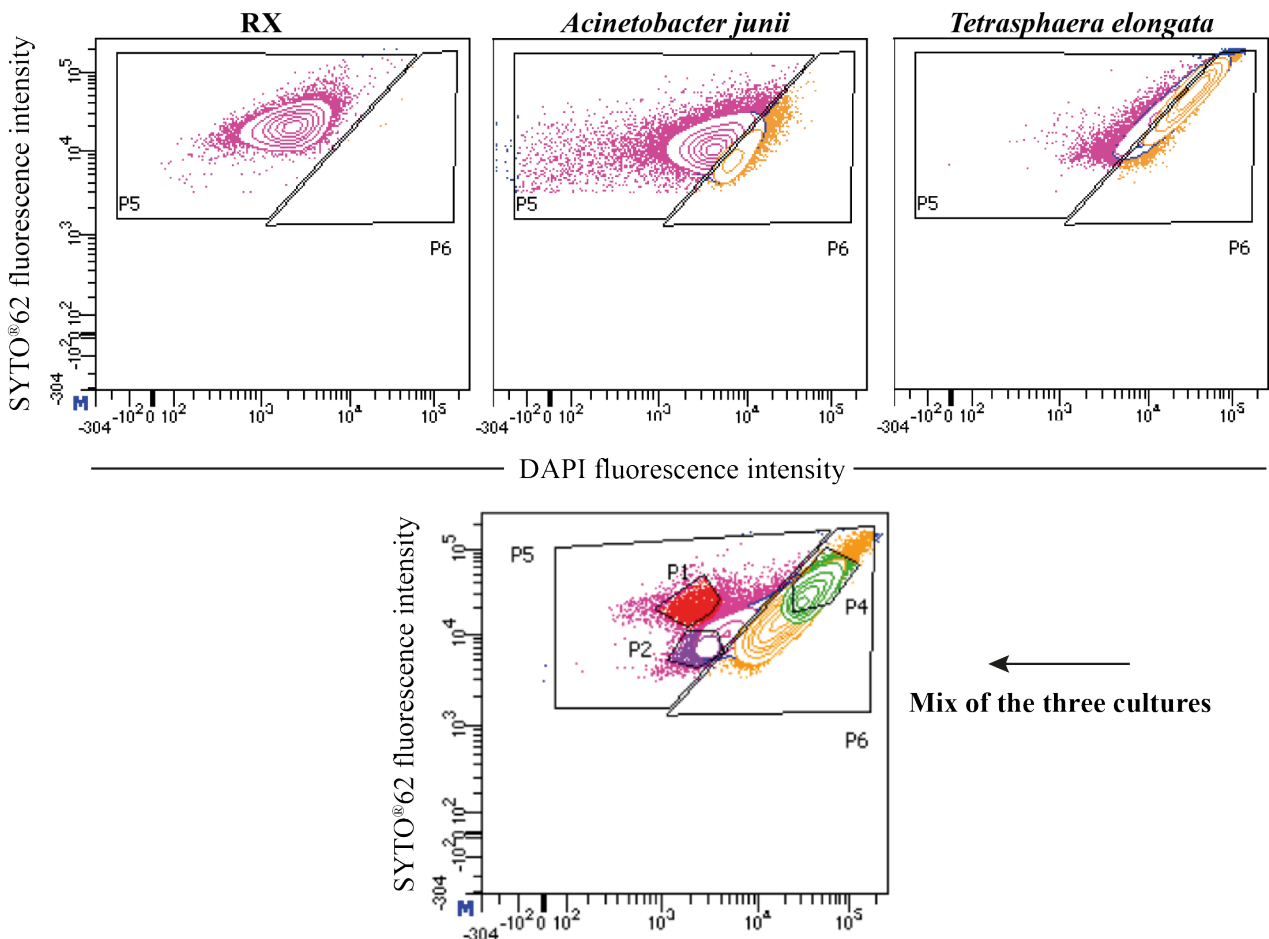


**Figure 3.16: Cytograms of the three culture models: RX culture, *Acinetobacter junii*, *Tetrasphaera elongata* and mixed of the three as a function of the fluorescence intensity of the PolyP DAPI and DNA SYTO® 62. P1, P2 and P4 gates correspond to the population sorted in purity mode.**

### 3.3. Cell sorting of **MTBc** with large PolyP inclusions using flow cytometry: methodological developments and preliminary results

A large number of cells was sorted for each of the sorted subpopulation and the three samples were prepared for **SEM-XEDS** analyses. The observation of the independent cultures, before sorting, in **SEM-XEDS** suggested that none of the two cultures, *Acinetobacter junii* and RX culture, stored intracellular **PolyP** inclusions (see Fig. 3.17). The RX culture showed the presence of cells with various sizes from  $\sim 2 \mu\text{m}$ , with a shape similar to *Acinetobacter junii*, to several  $\mu\text{m}$  long. The RX culture was difficult to distinguish in SE2 mode and was observed in InLens mode which possesses the highest spatial resolution. **XEDS** analysis exhibited the presence of **PolyP** associated to magnesium and potassium as counter-ions in every cells of *Tetrasphaera elongata* (see Fig. 3.17).

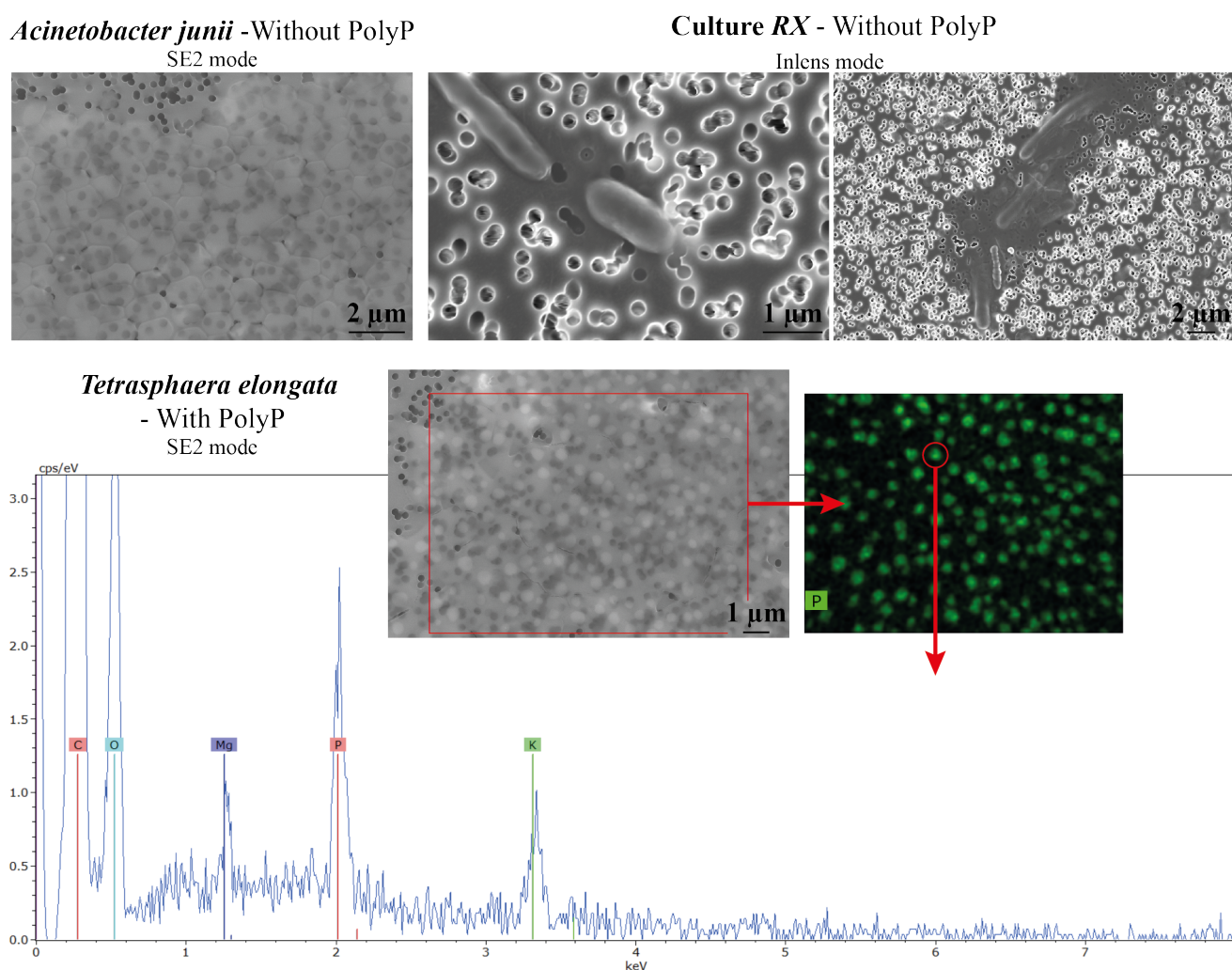


**Figure 3.17: SEM analyses coupled with XEDS of the three independent model cultures before sorting on the flow cytometer.** *Acinetobacter junii* and *Tetrasphaera elongata* were observed in SE2 mode whereas RX culture was observed in InLens mode. *Acinetobacter junii* and RX cultures did not show any **PolyP** intracellular inclusions. *Tetrasphaera elongata* observations with the **XEDS** revealed the presence of large amount of intracellular **PolyP**. The **XEDS** spectrum identify the elements constituting the **PolyP** granule in the red circle.

### Chapter 3. Magnetotactic cocci in the water column of Lake Pavin: morphotype classification and sorting of P-sequestering cells

The observations on the sorted populations revealed the presence of RX culture in both P1 and P2 (long cells of several  $\mu\text{m}$ ; see Fig. 3.18). Small size cells such as the ones shown for P1 in Fig. 3.18 were also observed in both populations. This cell shape and size resemble both *Acinetobacter junii* and RX culture, therefore they were not easily distinguishable from each other and the presence of *Acinetobacter junii* could not be confirmed. In the future it would be better to either choose *Acinetobacter junii* or RX culture as a negative model.

P4 sorted population exhibited the presence of small clusters of *Tetrasphaera elongata* with their two intracellular PolyP granules. Interestingly the XEDS analyze showed the presence of calcium as counter-ion for the PolyP (see Fig. 3.18) whereas, before sorting, the PolyP were associated with magnesium and potassium (see Fig. 3.17). Staining was done in Tris-EDTA (Tris hydrogen chloride and Ethylenediaminetetraacetic acid) (TE) and analyses and sorting in FC were done in PBS. In addition, the flow cytometer is systematically cleaned before and after each user. The reason for the counter-ions exchange thus remain to be found.

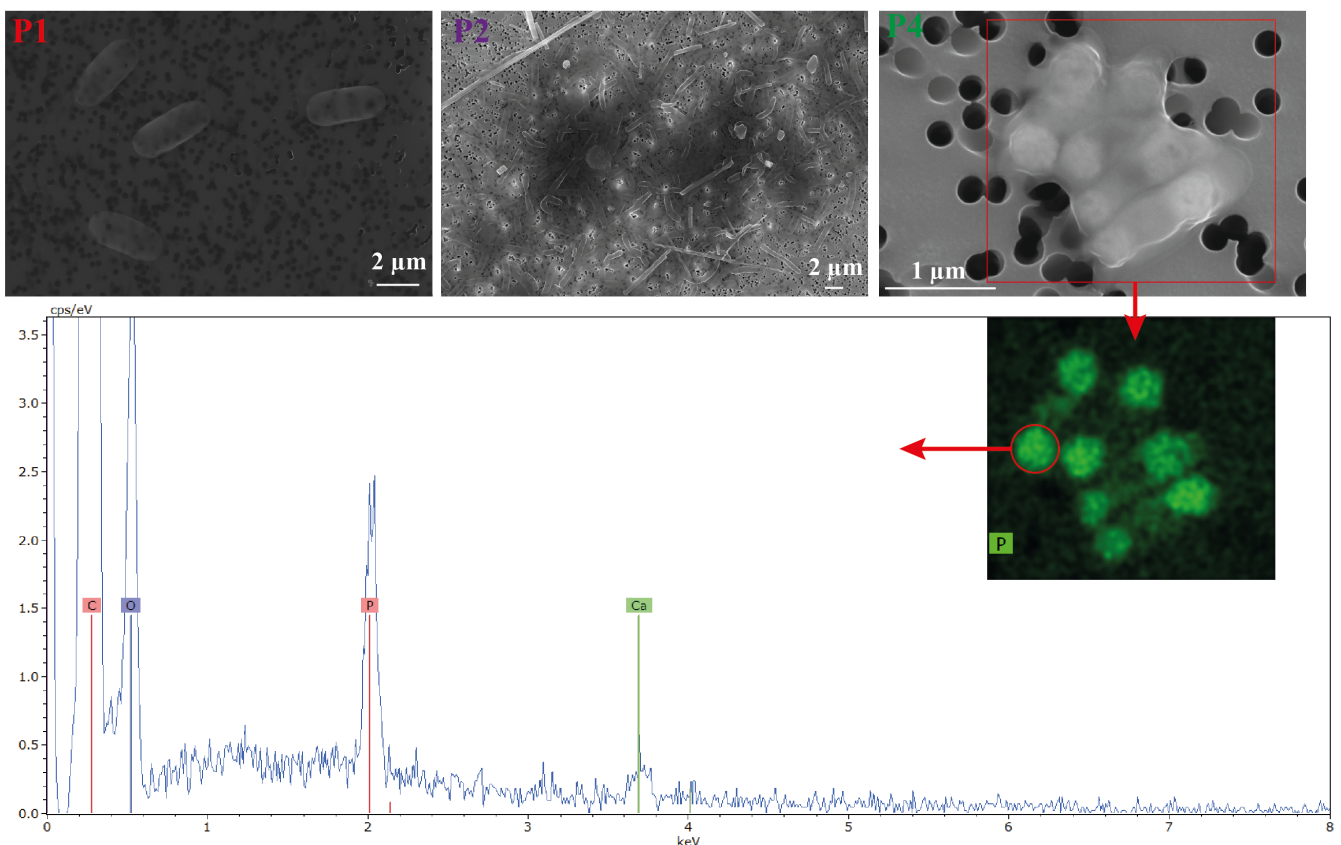


**Figure 3.18:** SEM analyses coupled with XEDS of the P1, P2 and P4 populations after sorting of the model culture mix on the flow cytometer. P1 and P2 only showed the presence of RX culture and did not show intracellular PolyP inclusions. P4 showed the presence of *Tetrasphaera elongata* with two electron dense granules at the cell poles. The XEDS spectrum identified the elements present in the intracellular granule in the red circle on the XEDS chemical map as P.

### 3.3. Cell sorting of **MTBc** with large **PolyP** inclusions using flow cytometry: methodological developments and preliminary results

---

To conclude, we could efficiently sort our positive control *Tetrasphaera elongata* as a function of its **PolyP** accumulation capabilities by using the **DAPI/SYTO**<sup>®</sup>62 dual staining. However, the negative and versatile control, RX and *Acinetobacter junii*, could not be distinguished in **SEM** as they share similar shape and size, thus the cell sorting of these models in particular could not be confirmed.

#### 3.3.6 Sample preparation optimization for flow cytometry analyses - M2 Internship - Clémentin Bouquet

In the literature, no consensus exists concerning the experimental preparation of the cells and the staining of **PolyP** by **DAPI**. Different solvents such as **PBS** or McIlvaine (Mukherjee et al., 2015); fixatives such as  $\text{BaCl}_2$  with  $\text{NiCl}_2$  with  $\text{NaN}_3$  (Günther, 2011), paraformaldehyde and glutaraldehyde (Schulz-Vogt et al., 2019); and permeant such as Tween-20 (Koch et al., 2013) or Triton X-100 can be used. During his M2 internship spanning from January to June 2021, Clémentin Bouquet evaluated the accuracy improvement of cell sorting provided by some experimental conditions (e.g., different solvents).

The accuracy was systematically estimated using epifluorescence or electronic microscopies. Thus, while the previous cell sorting on the models was only a qualitative analysis, the use of an epifluorescence microscope in the internship enabled a quantitative evaluation of the **FC** analyses and cell sorting. The cells from the same sample analyzed in **FC** were counted in epifluorescence as a function of their **PolyP** accumulation capabilities using **DAPI**. This quantification brought into light biases in certain protocol conditions or validated the **FC** analyses. **TEM-XEDS** analyses allowed a qualitative evaluation of the **FC** analyses and enabled the precise observation of the environmental and complex samples from Lake Pavin (particles, cells with or without **PolyP**, diatoms, etc...).

*Tetrasphaera elongata* was kept as the **PolyP** positive control and RX culture was kept as the negative control. **PolyP**- and **PolyP**+ will respectively qualify the fractions of cells considered, as a function of the **PolyP** fluorescence intensity, without and with **PolyP** in **FC**.

##### 3.3.6.1 Optimization of the dual staining protocol

Among the four different solvent tested for the **DAPI PolyP** staining of the bacteria models (**TE**, McIlvaine, 4-(2-hydroxyethyl)-1-piperazineethanesulfonic acid (**HEPES**), **PBS**), the **PBS** was the only solvent to not significantly impact the **DAPI** fluorescence signal or population structure. In our previous experiments, sample staining were carried out with the **TE** solvent. *Acinetobacter junii* were shown in **TEM** to not sequester intracellular **PolyP**, but **FC** analyses suggested the contrary for a fraction of the cells. **TE** responsibility in this result is possible

## Chapter 3. Magnetotactic cocci in the water column of Lake Pavin: morphotype classification and sorting of P-sequestering cells

but remain to be tested. Permeability with triton X-100 on the cells was revealed to decrease dramatically the number of cells in FC. For environmental samples which can not be analyzed immediately, 2% of formaldehyde at 4°C for up to 14 days was found to be the most optimum conditions to conserve the PolyP.

### 3.3.6.2 Cell sorting as a function of polyphosphate detection for a mix of both control cultures and for an environmental sample

Cell sorting was made on a mix of the cultures and on an environmental sample to compare the efficacy of our PolyP staining technique. The environmental sample corresponded to samples collected around the OATZ in the water column of Lake Pavin (Fig. 3.19a and b). The samples were collected in spring and were analyzed without preliminary magnetic sorting. TEM analyses revealed the presence of a large amount of detrital matter with the cells (Fig. 3.19c and d).

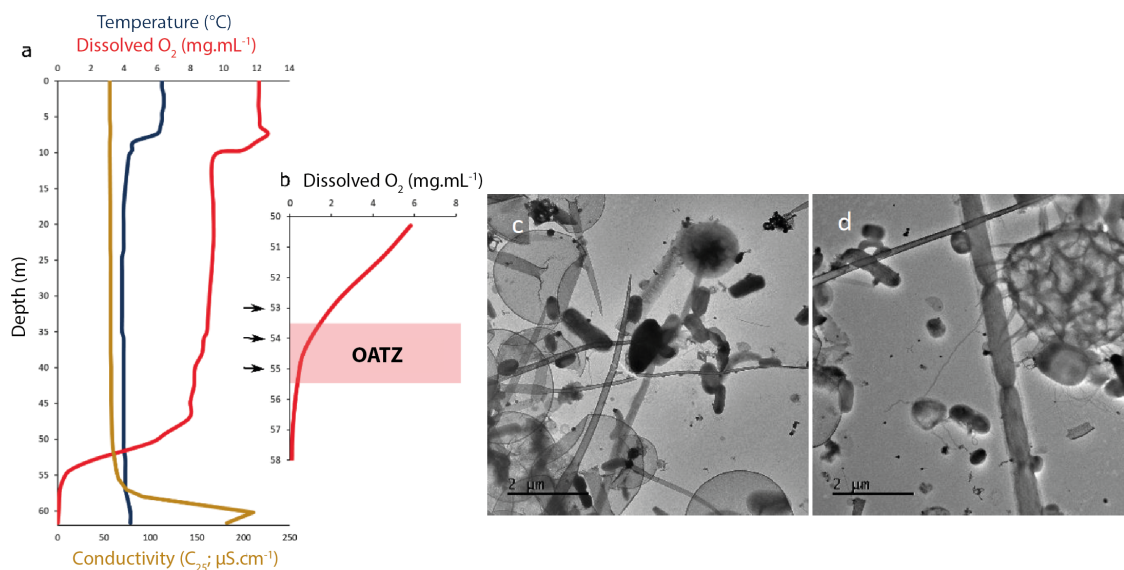


**Figure 3.19: Physico-chemical profiles of the temperature,  $O_2$  concentration and the conductivity in the water column of Lake Pavin (0-62 m) and TEM images of the samples collected at the OATZ for FC analyses. (a) Vertical profiles of the of the temperature,  $O_2$  concentration and the conductivity. (b) The three samples collected around the OATZ are indicated with the black arrows. (c and d) TEM images of the samples showing the presence of cells with a large amount of detrital matter.**

The cell sorting experiments were done with the improved staining of DAPI in PBS. The sorting gates (PolyP- and PolyP+) were placed as a function of the DAPI and SYTO<sup>®</sup>62 individual stained cultures analyses. The subsequent PolyP+ sorted sample exhibited a significant enrichment of PolyP+ with between 80 and 90 % of the events in the PolyP+ fraction (see Fig. 3.20A). This result was then confirmed by epifluorescence quantification

### 3.3. Cell sorting of **MTBc** with large **PolyP** inclusions using flow cytometry: methodological developments and preliminary results

(see Fig. 3.20B). The sorted **PolyP**- fraction showed the presence of some cells with **PolyP** but with a significant decrease of **PolyP**- compare to the mix of both cultures in **FC** (see Fig. 3.20A).

The environmental sample was stained with **DAPI** following the same protocol with **PBS** as with the mix of cultures. After the cell sorting the sorted **PolyP**+ fraction showed an increase of the **PolyP**+ cells (~ 50 %), but the sorting was not as efficient as with the axenic culture suggesting problems of specificity of the **DAPI** in a complex sample (see Fig. 3.20C).

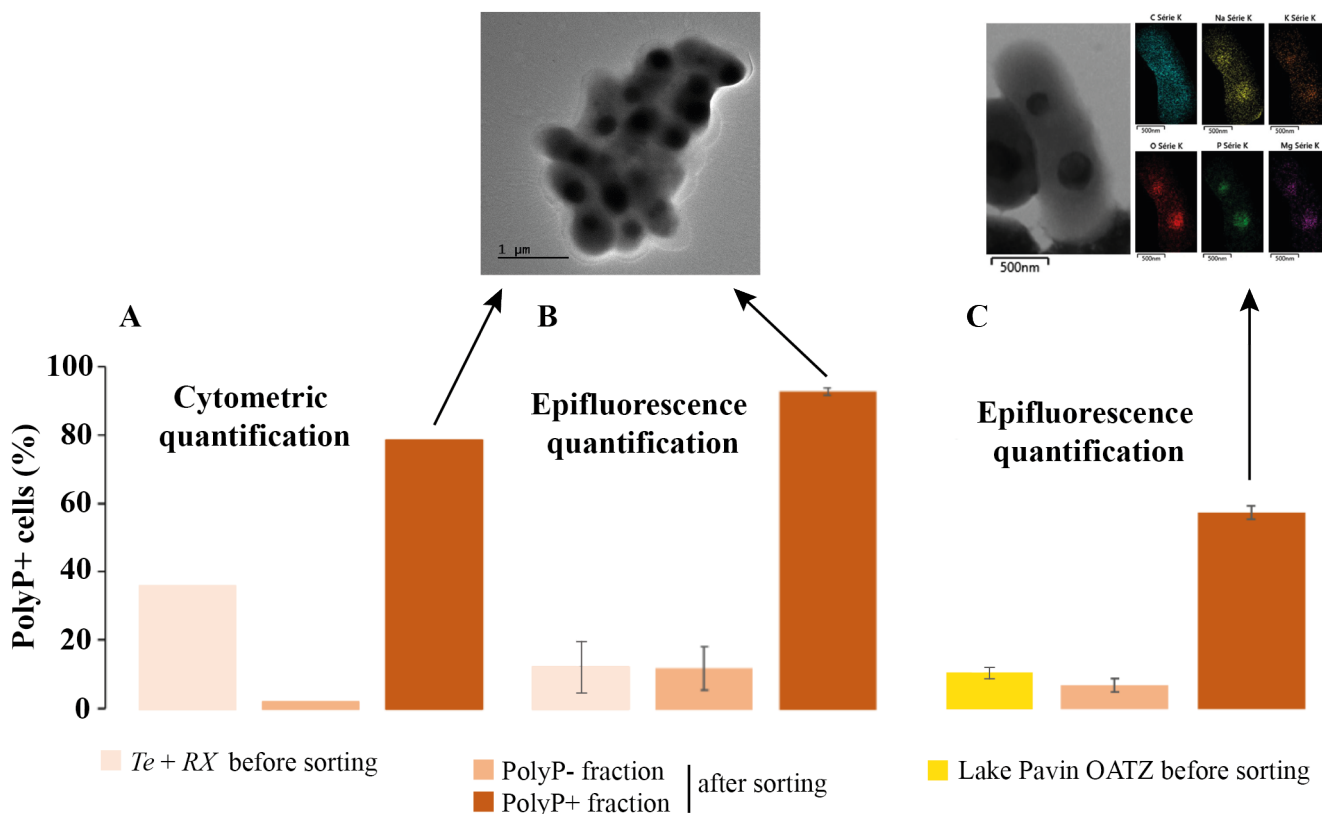


**Figure 3.20: **PolyP**+ cell proportions (%) for the culture mix *T. elongata* and *RX* and the environmental sample before sorting and in the **PolyP**- and **PolyP**+ collected fractions. A/ and B/ correspond to the proportions of **PolyP**+ cells counted in respectively **FC** and epifluorescence for the culture mix before sorting and for the two **PolyP**- and **PolyP**+ collected fractions after sorting. C/ correspond to the proportions of **PolyP**+ cells before sorting in a sample of the Lake Pavin water column **OATZ** and after sorting for the **PolyP**- and **PolyP**+ collected fractions in epifluorescence only.**

To conclude, the **PBS** is an adequate solvent for **PolyP** detection with **DAPI**. This improved protocol avoid additional step to permeate the cells, but also from a fixation in the case of culture analyses. For environmental samples which can not be analyzed immediately, the optimum conditions of fixation are 2% of formaldehyde at 4°C for up to 14 days. **FC** sorting on a mix of the axenic cultures and on an environmental sample allowed the significant enrichment



### **Chapter 3. Magnetotactic cocci in the water column of Lake Pavin: morphotype classification and sorting of P-sequestering cells**

---

of the PolyP<sup>+</sup> cell fraction, though with less efficacy for the environmental sample due to the unspecificity of the DAPI. This internship study put into light the diverse biases each of the conditions (e.g. type of solvent, fixative concentration) can bring to the fluorescence or population structure signals detected in FC. Overall, the cell sorting technique is highly efficient on bacterial culture with known accumulation of PolyP but less on the environmental samples.

### 3.4 Conclusions and Perspectives

In this chapter, the challenge was to obtain a homogeneous distribution of the cells on the TEM grid in order to only count a fraction of the cells and not all of them. If the distribution is not biased, then this fraction is representative of the whole population of cells on the grid. This bias was evaluated by using fraction replicates, corresponding to different squares on the TEM grid. These replicates enabled the classification and the comparison of the relative proportions of the different morphotypes of MTBc, as a function of their magnetosome organization and PolyP accumulation capabilities. Statistical analyses revealed a vertical distribution of the MTBc with respect to their magnetosome organization and their PolyP accumulation capabilities. MTBc harboring double chains of magnetosomes were shown to reach their peak of abundance at the MTB peak of abundance and where they constituted the main morphotype of MTB observed. However, the second main morphotype of MTBc, with disorganized magnetosomes, reached its peak of abundance at a different depth together with the iACC MTB. Both MTBc morphotypes were shown to accumulate from none to large granules of PolyP occupying most of the cell, and classified as without and with small or big PolyP. The depth corresponding to the maximum of abundance of the MTBc with disorganized magnetosomes exhibited the largest fraction of MTBc with PolyP and big PolyP for both MTBc (respectively ~ 80 % of MTBc with PolyP and 60 % MTBc with big PolyP). This suggests that the MTBc PolyP accumulation capabilities are not species-specific but rather specific to certain environmental conditions.

The different MTBc morphotypes relative proportions were compared to the different environmental conditions of Lake Pavin water column by using multivariate statistics. Dissolved sulfate, which was previously in the Chapter 2 found to be positively correlated to the overall MTBc, was found to be negatively correlated to the MTBc PolyP accumulation capabilities. This correlation reinforces the hypothesis that they possess a metabolism linked to the sulfur cycle and suggests its association to the MTBc PolyP metabolism.

Preliminary tests were made to develop a FC approach for the quantification and the cell sorting of microorganisms hyperaccumulating PolyP. Bacteria models, with different capabilities to accumulate PolyP, were chosen and used as PolyP negative and positive controls. A dual staining for simultaneously DNA and PolyP was tested and the combination of DAPI with SYTO<sup>®</sup>62 was chosen to avoid spectral interactions. The staining order between the two markers was tested and no significant interactions between the two markers could be observed. Cell sorting of the bacteria models with the dual staining successfully sorted the model with PolyP granules.

During a master internship, different sample preparations were tested and compared in order to improve our technique or reveal biases resulting from some conditions. The dual staining was shown to be the more optimum when achieved in PBS without permeant (triton X-100)

### **Chapter 3. Magnetotactic cocci in the water column of Lake Pavin: morphotype classification and sorting of P-sequestering cells**

---

and fixative (formaldehyde). However, for environmental samples which require to be fixed, preservation in 2 % formaldehyde at 4°C for up to 14 days was found to be the favored conditions. Cell sorting with the dual staining DAPI/SYTO<sup>®</sup> 62 was compared between the bacteria models and an environmental sample from Lake Pavin water column. DAPI was shown to be significantly more efficient in an homogeneous sample such as the bacteria culture models than in an heterogeneous sample such as Lake Pavin water column due to unspecific staining of the marker, with respectively 80% and 50% of PolyP enrichment.

#### **Perspectives:**

Further tests in Flow Cytometry to improve the sorting of environmental and complex samples. To avoid as much as possible DAPI unspecific staining but also autofluorescence from molecules such as chlorophyll, a low speed centrifugation could be used to remove the larger organic and mineral particles, but also a pre-treatment of the sample with an algicide inhibitor of photosynthesis (e.g. DCMU (3-(3,4-dichlorophenyl)-1,1-dimethylurea)) to reduce the autofluorescence. A magnetic sorting of the sample can also help concentrate the MTBc with PolyP and thus avoid as much as possible organic and detrital matter on which the DAPI can yield unspecific fluorescence.

JC markers were shown to be highly specific to PolyP in mammalian cells compare to DAPI, but also to be less toxic for the cells (Angelova et al., 2014). These markers were never tested on bacteria cells yet, but represent a promising alternative to DAPI especially in complex samples where DAPI was shown to loose specificity. It would therefore be interesting to compare cell sorting between DAPI and the JC markers to evaluate their respective specificity and efficiency on an heterogeneous and environmental sample.

#### MTBc taxonomic and metabolic diversity: clues to better constrain the drivers for MTBc PolyP accumulation.

In this chapter, the MTBc were characterized as a function of their morphologies and their PolyP accumulation capabilities. This characterization gave clues on the factors (i.e. environmental, taxonomic, metabolic) implicated in the MTBc PolyP accumulation but without certainty. Two distinct depths showing different PolyP accumulation capabilities were also characterized in this chapter, but whether these two depths correspond to depths where the MTBc are storing or hydrolyzing their PolyP storage remains to be known.

In order to gain better insights on MTBc PolyP storage dynamics, a gene expression profile of the genes whose expression correlates with P sequestration/hydrolysis using metatranscriptomics, would provide clues in this matter (Schulz-Vogt et al., 2019). The establishment of this profile would be particularly interesting at the two depths shown to respectively harbor a low and high fraction of cells with PolyP in Lake Pavin.

Metagenomic performed at the different depths structuring MTBc communities could also

help determine if the different morphotypes encountered in the water column correspond to different species and gain access to the functional repertoire of the *MTBc*. *FC* could be used on these two depths in order to sort, on magnetically sorted samples, the *MTB* fractions with or without *PolyP* by using *DAPI*, and then metagenomics on this sorted fractions to describe the infraspecific diversity of the *MTBc* (see Fig. 3.21). For the *MTB* sorted fraction without *PolyP*, a second sorting in *FC* is necessary in order to separate the *MTBc* without *PolyP* from all the different *MTB* without *PolyP*. To do so, the development of specific fluorescent probe for the *MTBc*, such as a *FISH* probe thanks to 16S rRNA sequencing, could help in this process. Once the two *MTBc* fractions with or without *PolyP* have been obtained DNA extraction, metagenome sequencing, binning and read assembly could then reveal the number of different genomes and thus taxonomic *MTBc* diversities present for each fractions and for each depths. Comparative metagenomics could then help highlight the similarities or differences between the genomes (e.g. gene families, functions, metabolic pathways) and thus give clues to explain the *MTBc* heterogeneity. The presence of the same genome in both fractions with and without *PolyP* at the same depth (e.g. genome A or F in Fig. 3.21) would then suggests that the *MTBc* strain do not accumulate *PolyP* systematically throughout its growth as it was shown to happen for cyanobacteria in *Li and Dittrich (2019)*. The same genome could also appear in the same *MTBc* fraction, with or without *PolyP*, at both depths with different geochemical conditions (e.g. genome B or D in Fig. 3.21). This situation would then suggests that the strain capability to sequester *PolyP* is not driven by environmental conditions but rather by its biological classification. Finally the same genome could be found in both *MTBc* fractions but at a different depth (e.g. genome C or E in Fig. 3.21). This configuration would then suggests that one or several environmental conditions met at these depth and which differ with depth can drive and impact the *PolyP* accumulation capability of the strain. Two or the three of these configurations could also happen simultaneously and thus suggest a combination of these different drivers.

This technique will be helpful in our case in the water column of Lake Pavin, to delineate whether the *MTBc* heterogeneity, with respect to their magnetosome morphology or *PolyP* accumulation capability, is driven by environmental conditions, their taxonomic affiliation, their growth stage or by a combination of two or the three.

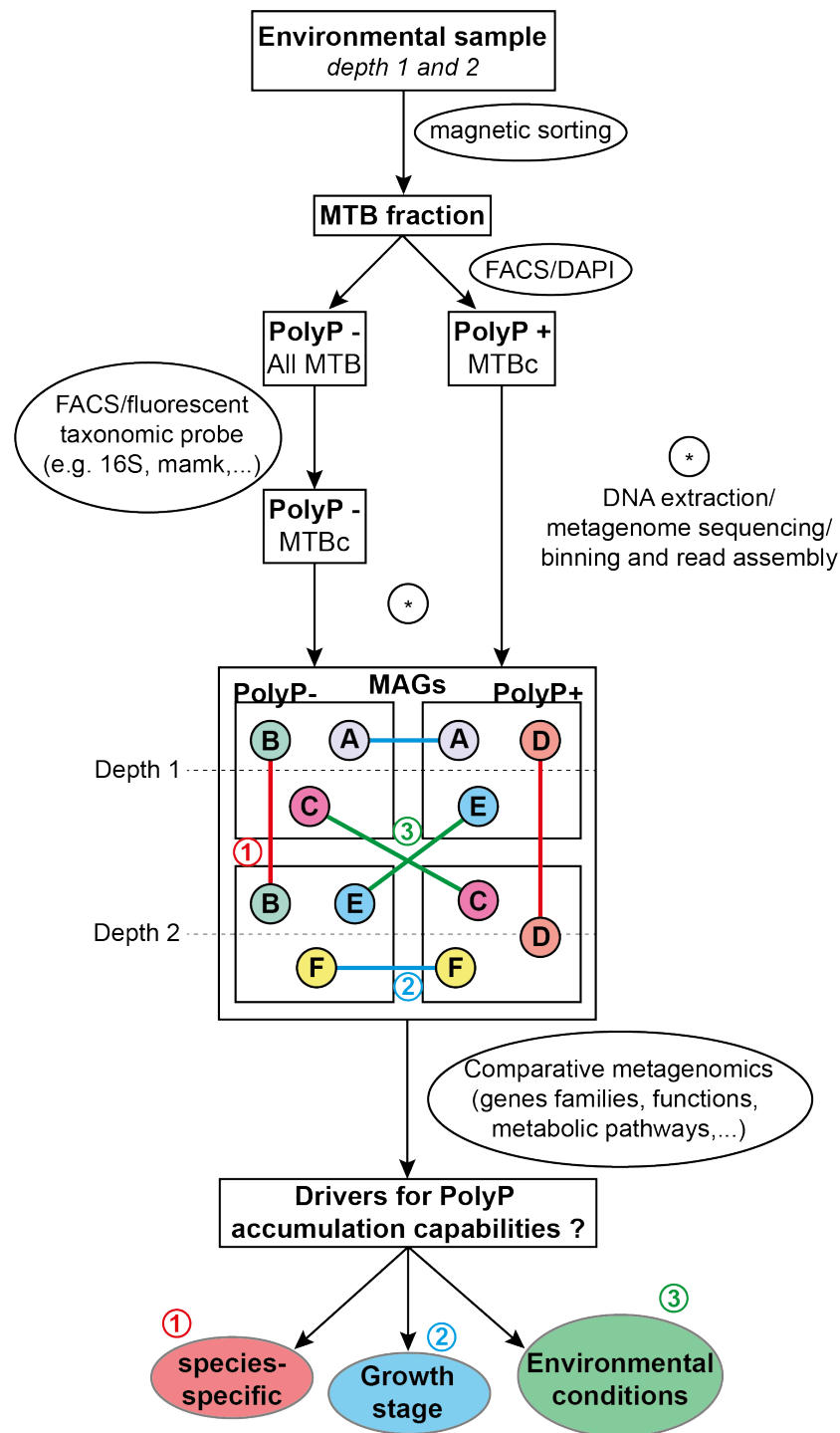


**Figure 3.21: Schematic of the methodology for the infraspecific diversity description of the MTBc as a function of their PolyP accumulation capabilities and the depth.** FACS: fluorescence-activated cell sorting. PolyP - and + respectively describe the sorted fractions in flow cytometry without and with PolyP as a function of the DAPI staining and its fluorescence intensity. MAGs: Metagenome-assembled genomes. The letters in the MAGs box represent different assembled genomes and thus different strains of MTBc. The lines between the assembled genomes represent the suggested drivers for PolyP accumulation capabilities.

#### Seasonality of the MTBc profile.

It would also be interesting to evaluate the seasonality of this high-resolution MTBc profile, especially knowing that the iACC MTB were shown in [Monteil et al. \(2021\)](#) to not be as abundant in spring compare to autumn when this profile was made. The iACC MTB being less abundant, would it be possible to see the MTBc with disorganized magnetosomes which are located at the same depth in higher concentration? If so, it could suggest that these MTB are in competition in the water column and that specific conditions impacting their abundances can change as a function of the season. The specific conditions driving the iACC MTB abundance were not found in this thesis, thus their study in spring with the same high resolution in combination with a precise geochemical profile could provide clues in this matter.



---

# Chapter 4. Conclusions and perspectives

---

## Contents

---

4.1	Conclusions	175
4.2	General perspectives	178

---

### 4.1 Conclusions

This thesis focused on magnetotactic cocci (MTBc) capable of storing P as large intracellular PolyP inclusions in the stratified water column of Lake Pavin. The study aimed at evaluating (i) the specificity of the habitat of the MTBc population and (ii) the heterogeneity of this population (e.g. proportion of cells with intracellular PolyP) along the geochemical gradients in the water column. One goal was also to identify, by using multivariate statistics, the biogeochemical parameters favouring P sequestration by MTBc in the water column of Lake Pavin. Another one was to attempt to cultivate MTBc and sort P-sequestering MTBc using flow cytometry. Overall, the ultimate goal was to understand the biological and environmental factors driving the accumulation of P in MTBc.

The following results were obtained:

- (i) MTBc belong to a diverse group of MTB and reach a maximum of abundance at a depth characterized by the local microbial biomass (correlation with wt% of C and N). Moreover, the MTBc are stratified in a biogeochemical niche linked to the sulfur cycle in Lake Pavin suggesting that they metabolize sulfur compounds.
- (ii) The MTBc PolyP accumulation capabilities do not seem to be species-dependent but instead seem to be impacted by environmental parameters such as sulfur availability.
- (iii) The development and optimization of a flow cytometry technique succeeded at sorting



**PolyP** accumulators with a varying efficiency depending on the complexity of the sample.

### **A specific biogeochemical niche for the MTBc**

The study of Lake Pavin **MTB** diversity led to the characterization of a new morphotype of **MTB** sequestering intracellular amorphous calcium carbonates (Monteil et al., 2021), named **iACC MTB**, and collocated with the **MTBc** in the water column. These **iACC MTB** were found to be abundant and thus were used as a means to statistically compare their respective distributions and their relative proportions. A new technique was used for the water column which enabled an inline sampling at high vertical resolution in parallel with *in situ* physico-chemical measurements (Busigny et al., 2021). Conductivity was found to be a good proxy to track the **MTB** maximum of abundance ( $65.8 \pm 1.4 \mu\text{S}\cdot\text{cm}^{-1}$ ). Using this method, nine samples were collected in the water column at different depths along the **MTB** habitat (zone with chemical gradients). Using electron microscopy, seven morphotypes of **MTB** were identified according to their cell shape and size and the type of their magnetosomes. Using optic microscopy, **MTBc** and **iACC MTB** appeared to be the most abundant **MTB** in the water column reaching up to 96%; however, distributions of **MTBc** and **iACC MTB** are different along the chemical gradients. Multivariate statistics revealed significant correlations between the geochemical parameters and the **MTBc** abundance, but not with the **iACC MTB** abundance. These results suggest that the vertical distribution of **MTBc** closely follows the distribution of microbial biomass. Moreover, a statistical association between the amount of dissolved sulfate and the **MTB** distribution suggests that they possess a metabolism linked to the sulfur cycle. Using these correlations, we designed isolation media with varying gradients of sulfur and oxygen in an attempt to mimic those found in the water column. The prepared media contained inverse gradients of oxygen and either hydrogen sulfide or thiosulfate. The media with hydrogen sulfide showed promising results and the isolation of magnetospirillum-like cells.

### **Stratification of the MTBc heterogeneity along the water column of Lake Pavin**

The homogeneous deposition of **MTB** on **TEM** grids, by using an improved protocol of deposition, enabled the quantification of the different relative proportions of the **MTBc** with respect to their magnetosome organization and their **PolyP** accumulation capabilities. Two main morphotypes of **MTBc** according to their magnetosome organization could be observed with respective distributions that did not correlate. The most abundant were **MTBc** having a double chain of magnetosomes with a maximum of abundance collocated with the peak of the total magnetotactic biomass. The second main morphotype of **MTBc** with disorganized magnetosomes showed a peak of abundance collocated with the one of the **iACC MTB**. Both morphotypes were observed with a similar range of **PolyP** accumulation with respect to the cell-scale. **TEM** allowed the classification of the different morphotypes of **MTBc** characterized based on **PolyP** presence and size. Statistical analyses revealed the same stratification of

**PolyP** accumulation capabilities for both morphotypes. At the depth where the **MTBc** with disorganized magnetosomes and the **iACC MTB** reach their maximum abundance, the **MTBc** fraction accumulating **PolyP** reaches ~ 80%, while at the depth of **MTBc** maximum abundance this fraction only reaches ~ 20%. This suggests that their accumulation capabilities are not species-specific but linked to environmental parameters. Multivariate statistics showed the significant and negative correlation of dissolved sulfate with the **MTBc PolyP** accumulation capabilities reinforcing the hypothesis that the **MTBc** possess a metabolism linked to the sulfur cycle which would be linked to their **PolyP** metabolism.

### **A dual PolyP and DNA staining for the quantification and cell sorting of the PolyP accumulators in flow cytometry**

In order to better know and understand when the optical (**FSC/SSC**) and fluorescence **PolyP** signals represent a cell of the size of our **MTBc** and with intracellular accumulation of **PolyP**, preliminary tests and optimization of the technique were made using a bacteria model (negative and positive controls) with a size close to **MTBc**.

A dual staining of the DNA and the **PolyP** was implemented in **FC** to sort both living from dead cells or particles and the **PolyP** accumulators. No significant interactions between the two fluorescent markers in both order of staining were observed. Additionally, the dual staining proved to be efficient at detecting and sorting the **PolyP** accumulators from the bacteria models. Optimizations of the protocol were made during a master's internship. This internship work showed that the choice of solvent for the staining is important and could induce significant biases and errors in the results as a function of the **PolyP** marker and the bacteria. Similarly, permeabilization and fixation of the cells can have a significant impact on the **FC** signals and must be tested beforehand. For environmental samples, fixation might be necessary before the analyses and sorting. This work determined that a fixation at 2% of formaldehyde conserved at 4°C up to 14 days did not interact with the **PolyP** fluorescence signal. Cell sorting with the dual staining **DAPI/SYTO<sup>®</sup>62** on both the bacteria models and an environmental sample (Lake Pavin water column at the **OATZ**) were compared. **DAPI** was found to sort efficiently the **PolyP** accumulators in a homogeneous sample such as cultures. **DAPI** was proved to be less specific, and thus less efficient in a heterogeneous and complex (composed of a mixture of cells, particles, organic matter,...) sample such as an environmental sample. The environmental cell sorting was nonetheless promising.

This thesis constitutes the first exploration of the diversity of **MTB** and of their **PolyP** accumulation heterogeneity in a ferruginous freshwater environment in the context of phosphatogenesis. Many methodological developments were carried out which helped characterize the **MTBc** P-sequestration capabilities as a function of their habitat but which also allowed the efficient cell sorting of P-sequestering microorganisms. Therefore, this study improves our

understanding of the key relationships between microbial diversity, environmental parameters and P cycling. Although the formation of PolyP has been repeatedly observed in MTB, the impact of these polymers on the biology of these bacteria and the relationships with magnetite biomineralization are poorly understood. This work not only paves the way for future studies on other MTB involved in the P biogeochemical cycle, but also for future studies on MTB diversity and how to study it as a function of diverse biological and environmental parameters. Finally, Lake Pavin represents a very promising natural laboratory to not only understand how PolyP are formed but also other types of biomineralization such as iACC or magnetosomes.

### 4.2 General perspectives

#### **Dynamics of the MTBc PolyP accumulation in controlled conditions in a growth medium**

Supposing the isolation of the MTBc in a growth medium is a success (see Chapter 3 part 2.4 for the preliminary test and the Chapter 3 perspectives for the propositions of future tests), it would be possible to study the MTBc metabolism and especially focus on their ability to sequester PolyP in response to varying controlled conditions. A culture of MTBc would allow for a precise investigation of the parameters involved in the sequestration and the hydrolysis of PolyP as well as the quantification the subsequent P uptake and release in the medium. Subjecting the MTBc to the conditions met in Lake Pavin could then help us evaluate the impact of the MTBc on the Lake Pavin water column P biogeochemical cycle and especially on the phosphogenesis occurring around the MTBc localization.

The MTBc PolyP metabolism could be different due to their taxonomic affiliation or impacted by the environmental conditions or even the growth stage in which we observe them. As done in Li and Dittrich (2019), PolyP dynamics (i.e. accumulation or hydrolysis) along the growth stage of the MTBc were assessed by monitoring the particulate and dissolved fractions of P, the expression of genes correlated with PolyP metabolism (e.g. alkaline phosphatase), and the MTBc PolyP content. It is possible that MTBc will grow in a semi solid medium, like many MTB (Bazylnski et al., 2013a) or other P hyperaccumulators (e.g. *Beggiatoa* (Brock and Schulz-Vogt, 2011) and *Sulfurimonas* (Möller et al., 2019)). Therefore, *in situ* measurements of the chemicals forming the gradients in combination with a vertical cell count of the MTBc along the chemical gradients could help determine their favored conditions (Möller et al., 2019). Measuring dissolved and particulate P along the chemical gradients could also provide constraints on the concentrations in which the MTB hydrolyze or sequester P (Brock and Schulz-Vogt, 2011).

#### **Study of other PolyP hyperaccumulators**

Numerous **MTB** are accumulating **PolyP**, among which the *Magnetococcaceae* family is particularly efficient (Cox et al., 2002; Eder et al., 2014; Chen et al., 2015; Schulz-Vogt et al., 2019; Li et al., 2020b). This ability to accumulate **PolyP** is further supported in this thesis for the Lake Pavin **MTBc**. Comparative metagenomics could be done between the Lake Pavin **MTBc** and other *Magnetococcaceae* models or other hyperaccumulators of **PolyP**. This comparison could bring further insights on the **PolyP** hyperaccumulators metabolisms and confirm or disprove the link between **PolyP** sequestration and a sulfur metabolism. Comparing their genomes could allow us to determine if the **PolyP** hyperaccumulators and the *Magnetococcaceae* share the same genes involved in the metabolism of **PolyP**, or if the *Magnetococcaceae* harbor specific genes whose expression prompt the hyperaccumulation of **PolyP**. In case of the confirmation of the second case, comparative metagenomics could be done on other cultivable and axenic **MTB** models accumulating **PolyP** in order to evaluate if these genes are shared by the **MTB** in general or if their presence is limited to the *Magnetococcaceae* family. The models could thus either be affiliated with the *Magnetococcaceae* family (e.g. the chemolithoautotroph oxidizing thiosulfate and sulfide MC-1; Bazylnski et al. (2013b)) or be metabolically similar to the **MTBc** but phylogenetically different from them (e.g. the chemolithoautotroph oxidizing thiosulfate and sulfide SS-5 from the *Gammaproteobacteria*; Lefèvre et al. (2012)).

Among the **MTB** characterized in this thesis on the Lake Pavin water column are rod-shaped **MTB** hyperaccumulating **PolyP**. This rod with a chain of prismatic magnetosomes has been previously affiliated with the *Magnetococcaceae* family (Monteil et al., 2021) and have been encountered as well in other marine and freshwater environments (Spring et al., 1995; Oestreicher et al., 2011; Kolinko et al., 2013). Thus the *Magnetococcaceae* do not only comprise **MTBc** but also rod-shaped **MTB**.

However, in the water column of Lake Pavin, this **MTB** morphotype was not abundant and thus any statistical comparison with the **MTBc**, the **iACC MTB** or the environmental parameters along the chemical gradients was not possible. Mass collection of the **MTB** in the water column could be done as developed in Busigny et al. (2021) so as to obtain a large number of this morphotype and perform statistical analyses. These statistical analyses, similarly to the ones made in Chapter 2 and 3, would compare the **MTB** relative abundances and distributions, find potential correlations with the environmental parameters and compare these results with the ones for the **MTBc**. The comparison between these two different *Magnetococcaceae* would then give us insight on whether this family of **MTB** accumulate in similar conditions and share a similar metabolism. Flow cytometry, similarly to the method discussed in 3 part 3.3, in combination with **TEM** could be used to further characterize the rod-shaped **MTB** hyperaccumulating **PolyP** taxonomically.

The mass collection in Busigny et al. (2021) involves the aerotactic behaviour of the **MTB** and thus their negative response toward increasing oxygen concentrations. As oxygen diffuses in

the recipient, in which they have been stored after sampling, they rapidly swim downward and away from the oxygen and concentrate at the bottom of the recipient. This technique, although proved efficient for the concentration of **MTB** from Lake Pavin water column, has not been evaluated in terms of **PolyP** conservation. It is possible that in that setup, as the **MTBc** or the rod-shaped **MTB** hyperaccumulating **PolyP** swim actively toward preferential conditions without oxygen, they use their **PolyP** for energy and to increase their motility (Seufferheld et al., 2008; Varela et al., 2010; Möller et al., 2019). If this is the case, then the estimation of the **MTB PolyP** accumulation capabilities would need to be corrected for a bias.

Finally, the mass collection of the **MTB** in Lake Pavin would not only allow the characterization of the rod-shaped **MTB** with **PolyP** as a function of the environmental parameters, but also the other four minority **MTB** described in this thesis in the water column of Lake Pavin (Chapter 2 part 2.4).

### **Study of **PolyP** hyperaccumulators in other meromictic lakes.**

Meromictic lakes contain distinct layers of water with different densities which promote the appearance of oxygenated and anoxic zones respectively on top and bottom of the lake that remain stable throughout the year (Zadereev et al., 2017). The transition between the upper (mixolimnion) and lower (monimolimnion) water layers is called the chemocline and constitutes a favorable environment to study with high vertical resolution the processes mediated by microorganisms along many different physico-chemical and geochemical gradients. Hyperaccumulators of **PolyP** and **MTB** being found in zones of redox gradients also means meromictic lakes are ideal sites to find more hyperaccumulators of **PolyP**.

Meromictic lakes are diverse in terms of size, geography, chemistry and origin (Zadereev et al., 2017). Hall and Northcote (2012) listed 177 meromictic lakes on the globe on five continents at the exception to South America. The chemical composition of meromictic lakes can vary greatly, in terms of dissolved concentrations of substances (e.g. ferrous iron, sulfate, hydrogen sulfide, ammonia, manganese,...), pH, and salinity as a function of the geolocalization of the lake, its origin, and history (Zadereev et al., 2017). Studying other meromictic lakes to find more potential **PolyP** hyperaccumulators could enrich our knowledge of these microorganisms, their metabolisms and the conditions, similar or not, in which they can accumulate or hydrolyze **PolyP**.

Lakes that are more or less concentrated in phosphorus, sulfur, or nitrogen compounds could potentially be of interest for the study of **PolyP** hyperaccumulators and their apparent link to the respective cycles of these elements. For example, the salty Lake Cadagno in the Swiss Alps is a sulfidogenic meromictic lake with high concentration of sulfur bacteria (Tonolla et al., 2017). In this thesis, distribution of **MTBc** hyperaccumulating **PolyP** was linked to the local biomass and most probably to the sulfur bacteria present at the same depths. Therefore, the study of this lake and of potential **PolyP** hyperaccumulators could help give insights onto this **PolyP**

hyperaccumulators and sulfur bacteria relationship.

Other meromictic lakes such as pit lakes, which originate from old mines and whose geochemical properties depends mainly on the material mined, could be interesting new environments to study. Meromictic pit lakes have been studied in former rock quarries, coalinite mines, sulphur mines, lignite mines, coal mines, and metal mines (Schultze et al., 2017). An example of pit lake is the lake Cueva de la Mora in Spain, the lake is acidic, mainly constituted of high concentration of iron, sulfate, metal, and metalloids, and also has a high concentration of P and nitrogen in its bottom layer. These high concentrations make this lake a strong candidate for observing PolyP accumulators and potentially accumulators that might use their PolyP to detoxify metals (Kulakovskaya et al., 2018).

Due to the increase of abandoned mines (Castendyk et al., 2009), which are more prone to become meromictic (Schultze et al., 2017), to human influence (water diversion, salt roads,...) and to climates changes (drought), the salinity of lakes can be significantly altered (Jeppesen et al., 2015; Sibert et al., 2015) meaning meromictic lakes likely to become more abundant around the globe. Their increased concentration could promote sites harboring microorganisms hyperaccumulating PolyP, and thus their study might become an even more important issue.



---

# Bibliography

---

- Abreu, F., Cantão, M. E., Nicolás, M. F., Barcellos, F. G., Morillo, V., Almeida, L. G., do Nascimento, F. F., Lefèvre, C. T., Bazylinski, D. A., R de Vasconcelos, A. T., and Lins, U. (2011). Common ancestry of iron oxide- and iron-sulfide-based biomineralization in magnetotactic bacteria. *The ISME Journal*, 5(10):1634–1640.
- Abreu, F., Carolina, A., Araujo, V., Leão, P., Silva, K. T., Carvalho, F. M. d., Cunha, O. d. L., Almeida, L. G., Geurink, C., Farina, M., Rodelli, D., Jovane, L., Pellizari, V. H., Vasconcelos, A. T. d., Bazylinski, D. A., and Lins, U. (2016). Culture-independent characterization of novel psychrophilic magnetotactic cocci from Antarctic marine sediments: Magnetotactic cocci in maritime Antarctica. *Environmental Microbiology*, 18(12):4426–4441.
- Adams, M. S., Dillon, C. T., Vogt, S., Lai, B., Stauber, J., and Jolley, D. F. (2016). Copper Uptake, Intracellular Localization, and Speciation in Marine Microalgae Measured by Synchrotron Radiation X-ray Fluorescence and Absorption Microspectroscopy. *Environmental Science & Technology*, 50(16):8827–8839.
- Ahlgren, J., De Brabandere, H., Reitzel, K., Rydin, E., Gogoll, A., and Waldebäck, M. (2007). Sediment Phosphorus Extractants for Phosphorus-31 Nuclear Magnetic Resonance Analysis: A Quantitative Evaluation. *Journal of Environmental Quality*, 36(3):892–898.
- Ahn, K. and Kornberg, A. (1990). Polyphosphate kinase from *Escherichia coli*. Purification and demonstration of a phosphoenzyme intermediate. *Journal of Biological Chemistry*, 265(20):11734–11739.
- Albi, T. and Serrano, A. (2016). Inorganic polyphosphate in the microbial world. Emerging roles for a multifaceted biopolymer. *World Journal of Microbiology and Biotechnology*, 32(2):27.
- Almeida, F. P., Viana, N. B., Lins, U., Farina, M., and Keim, C. N. (2013). Swimming behaviour of the multicellular magnetotactic prokaryote ‘*Candidatus Magnetoglobus multicellularis*’ under applied magnetic fields and ultraviolet light. *Antonie van Leeuwenhoek*, 103(4):845–857.



## Bibliography

---

- Amann, R., Peplies, J., and Schüler, D. (2007). Diversity and Taxonomy of Magnetotactic Bacteria. In Schüler, D., editor, *Magnetoreception and Magnetosomes in Bacteria*, volume 3, pages 25–36. Springer Berlin Heidelberg. Series Title: Microbiology Monographs.
- Angelova, P. R., Agrawalla, B. K., Elustondo, P. A., Gordon, J., Shiba, T., Abramov, A. Y., Chang, Y.-T., and Pavlov, E. V. (2014). *In Situ* Investigation of Mammalian Inorganic Polyphosphate Localization Using Novel Selective Fluorescent Probes JC-D7 and JC-D8. *ACS Chemical Biology*, 9(9):2101–2110.
- Angelova, P. R., Iversen, K. Z., Teschemacher, A. G., Kasparov, S., Gourine, A. V., and Abramov, A. Y. (2018). Signal transduction in astrocytes: Localization and release of inorganic polyphosphate. *Glia*, 66(10):2126–2136.
- Aschar-Sobbi, R., Abramov, A. Y., Diao, C., Kargacin, M. E., Kargacin, G. J., French, R. J., and Pavlov, E. (2008). High Sensitivity, Quantitative Measurements of Polyphosphate Using a New DAPI-Based Approach. *Journal of Fluorescence*, 18(5):859–866.
- Ault-Riché, D., Fraley, C. D., Tzeng, C. M., and Kornberg, A. (1998). Novel assay reveals multiple pathways regulating stress-induced accumulations of inorganic polyphosphate in *Escherichia coli*. *Journal of Bacteriology*, 180(7):1841–1847.
- Baba, Y., Yosa, N., and Ohashi, S. (1984). Simultaneous determination of phosphate and phosphonate by flow injection analysis with a parallel detection system. *Journal of Chromatography A*, 295:153–160.
- Bahaj, A. S., James, P. A. B., Ellwood, D. C., and Watson, J. H. P. (1993). Characterization and growth of magnetotactic bacteria: Implications of clean up of environmental pollution. *Journal of Applied Physics*, 73(10):5394–5396.
- Bahaj, A. S., James, P. A. B., and Moeschler, F. D. (2002). EFFICIENCY ENHANCEMENTS THROUGH THE USE OF MAGNETIC FIELD GRADIENT IN ORIENTATION MAGNETIC SEPARATION FOR THE REMOVAL OF POLLUTANTS BY MAGNETOTACTIC BACTERIA. *Separation Science and Technology*, 37(16):3661–3671.
- Balaban, R. S. (1984). The application of nuclear magnetic resonance to the study of cellular physiology. *American Journal of Physiology-Cell Physiology*, 246(1):C10–C19.
- Banik, S. and Dey, B. (1983). Phosphate-Solubilizing Potentiality of the Microorganisms Capable of Utilizing Aluminium Phosphate as a Sole Phosphate Source. *Zentralblatt für Mikrobiologie*, 138(1):17–23.
- Barkley, A. E., Prospero, J. M., Mahowald, N., Hamilton, D. S., Pependorf, K. J., Oehlert, A. M., Pourmand, A., Gatineau, A., Panechou-Pulcherie, K., Blackwelder, P., and Gaston, C. J. (2019). African biomass burning is a substantial source of phosphorus deposition to the Amazon, Tropical Atlantic Ocean, and Southern Ocean. *Proceedings of the National Academy of Sciences*, 116(33):16216–16221.

- Bazylinski, D. A., Dean, A. J., Schuler, D., Phillips, E. J. P., and Lovley, D. R. (2000). N<sub>2</sub>-dependent growth and nitrogenase activity in the metal-metabolizing bacteria, *Geobacter* and *Magnetospirillum* species. *Environmental Microbiology*, 2(3):266–273.
- Bazylinski, D. A., Dean, A. J., Williams, T. J., Long, L. K., Middleton, S. L., and Dubbels, B. L. (2004). Chemolithoautotrophy in the marine, magnetotactic bacterial strains MV-1 and MV-2. *Archives of Microbiology*, 182(5):373–387.
- Bazylinski, D. A. and Frankel, R. B. (2004). Magnetosome formation in prokaryotes. *Nature Reviews Microbiology*, 2(3):217–230.
- Bazylinski, D. A., Lefèvre, C. T., and Schüler, D. (2013a). *Part 12: Magnetotactic Bacteria*. Springer-Verlag Berlin Heidelberg.
- Bazylinski, D. A. and Williams, T. J. (2007). Ecophysiology of Magnetotactic Bacteria. In Schüler, D., editor, *Magnetoreception and Magnetosomes in Bacteria*, volume 3, pages 37–75. Springer Berlin Heidelberg. Series Title: Microbiology Monographs.
- Bazylinski, D. A., Williams, T. J., Lefevre, C. T., Berg, R. J., Zhang, C. L., Bowser, S. S., Dean, A. J., and Beveridge, T. J. (2013b). *Magnetococcus marinus* gen. nov., sp. nov., a marine, magnetotactic bacterium that represents a novel lineage (Magnetococcaceae fam. nov., Magnetococcales ord. nov.) at the base of the Alphaproteobacteria. *INTERNATIONAL JOURNAL OF SYSTEMATIC AND EVOLUTIONARY MICROBIOLOGY*, 63(Pt 3):801–808.
- Bennet, M., McCarthy, A., Fix, D., Edwards, M. R., Repp, F., Vach, P., Dunlop, J. W. C., Sitti, M., Buller, G. S., Klumpp, S., and Faivre, D. (2014). Influence of Magnetic Fields on Magneto-Aerotaxis. *PLoS ONE*, 9(7):e101150.
- Bennett, E. M., Carpenter, S. R., and Caraco, N. F. (2001). Human Impact on Erodeable Phosphorus and Eutrophication: A Global Perspective. *BioScience*, 51(3):227.
- Benzerara, K., Miot, J., Morin, G., Ona-Nguema, G., Skouri-Panet, F., and Féraud, C. (2011). Significance, mechanisms and environmental implications of microbial biomineralization. *Comptes Rendus Geoscience*, 343(2-3):160–167.
- Berg, J. S., Jézéquel, D., Duverger, A., Lamy, D., Laberty-Robert, C., and Miot, J. (2019). Microbial diversity involved in iron and cryptic sulfur cycling in the ferruginous, low-sulfate waters of Lake Pavin. *PLOS ONE*, 14(2):e0212787.
- Bidre-Petit, C., Jézéquel, D., Dugat-Bony, E., Lopes, F., Kuever, J., Borrel, G., Viollier, E., Fonty, G., and Peyret, P. (2011). Identification of microbial communities involved in the methane cycle of a freshwater meromictic lake: Methane cycle in a stratified freshwater ecosystem. *FEMS Microbiology Ecology*, 77(3):533–545.

## Bibliography

---

- Bidierre-Petit, C., Taib, N., Gardon, H., Hochart, C., and Debroas, D. (2019). New insights into the pelagic microorganisms involved in the methane cycle in the meromictic Lake Pavin through metagenomics. *FEMS Microbiology Ecology*, 95(3).
- Bigio, L. and Angert, A. (2018). Isotopic signature of atmospheric phosphate in airborne tree pollen. *Atmospheric Environment*, 194:1–6.
- Bigio, L. and Angert, A. (2019). Oxygen Isotope Signatures of Phosphate in Wildfire Ash. *ACS Earth and Space Chemistry*, 3(5):760–769.
- Blakemore, R. (1975). Magnetotactic bacteria. *Science*, 190(4212):377–379.
- Blakemore, R. P., Frankel, R. B., and Kalmijn, A. J. (1980). South-seeking magnetotactic bacteria in the Southern Hemisphere. *Nature*, 286(5771):384–385.
- Blum, E., Py, B., Carpousis, A. J., and Higgins, C. F. (1997). Polyphosphate kinase is a component of the *Escherichia coli* RNA degradosome. *Molecular Microbiology*, 26(2):387–398.
- Bode, G., Mauch, F., Ditschuneit, H., and Malfertheiner, P. (1993). Identification of structures containing polyphosphate in *Helicobacter pylori*. *Journal of General Microbiology*, 139(12):3029–3033.
- Bonhomme, C., Jézéquel, D., Poulin, M., Saad, M., Vinçon-Leite, B., and Tassin, B. (2016). Lake Pavin Mixing: New Insights from High Resolution Continuous Measurements. In Boivin, P., Sime- Ngando, T., Chapron, E., Jezequel, D., and Meybeck, M., editors, *Lake Pavin*, pages 177–184. Springer International Publishing, Cham.
- Bonting, C. F., Kortstee, G. J., and Zehnder, A. J. (1991). Properties of polyphosphate: AMP phosphotransferase of *Acinetobacter* strain 210A. *Journal of Bacteriology*, 173(20):6484–6488.
- Boswell, C. D., Dick, R. E., and Macaskie, L. E. (1999). The effect of heavy metals and other environmental conditions on the anaerobic phosphate metabolism of *Acinetobacter johnsonii*. *Microbiology*, 145(7):1711–1720.
- Bouvet, P. J. M. and Grimont, P. A. D. (1986). Taxonomy of the Genus *Acinetobacter* with the Recognition of *Acinetobacter baumannii* sp. nov., *Acinetobacter haemolyticus* sp. nov., *Acinetobacter johnsonii* sp. nov., and *Acinetobacter junii* sp. nov. and Emended Descriptions of *Acinetobacter calcoaceticus* and *Acinetobacter lwoffii*. *International Journal of Systematic Bacteriology*, 36(2):228–240.
- Bowlin, M. Q. and Gray, M. J. (2021). Inorganic Polyphosphate in Host and Microbe Biology. *Trends in Microbiology*, page S0966842X21000366.
- Brock, J., Rhiel, E., Beutler, M., Salman, V., and Schulz-Vogt, H. N. (2012). Unusual polyphosphate inclusions observed in a marine *Beggiatoa* strain. *Antonie van Leeuwenhoek*, 101(2):347–357.
- Brock, J. and Schulz-Vogt, H. N. (2011). Sulfide induces phosphate release from polyphosphate in cultures of a marine *Beggiatoa* strain. *The ISME Journal*, 5(3):497–506.

- Bunce, J. T., Ndam, E., Ofiteru, I. D., Moore, A., and Graham, D. W. (2018). A Review of Phosphorus Removal Technologies and Their Applicability to Small-Scale Domestic Wastewater Treatment Systems. *Frontiers in Environmental Science*, 6:8.
- Bura-Nakić, E., Viollier, E., Jézéquel, D., Thiam, A., and Ciglencčki, I. (2009). Reduced sulfur and iron species in anoxic water column of meromictic crater Lake Pavin (Massif Central, France). *Chemical Geology*, 266(3-4):311–317.
- Busigny, V., Jézéquel, D., Cosmidis, J., Viollier, E., Benzerara, K., Planavsky, N. J., Albéric, P., Lebeau, O., Sarazin, G., and Michard, G. (2016). The Iron Wheel in Lac Pavin: Interaction with Phosphorus Cycle. In Sime-Ngando, T., Boivin, P., Chapron, E., Jezequel, D., and Meybeck, M., editors, *Lake Pavin*, pages 205–220. Springer International Publishing, Cham.
- Busigny, V., Mathon, F. P., Jézéquel, D., Bidaud, C. C., Viollier, E., Bardoux, G., Bourrand, J., Benzerara, K., Duprat, E., Menguy, N., Monteil, C. L., and Lefevre, C. T. (2021). Mass collection of magnetotactic bacteria from the permanently stratified ferruginous Lake Pavin, France. *Environmental Microbiology*, pages 1462–2920.15458.
- Busigny, V., Planavsky, N. J., Jézéquel, D., Crowe, S., Louvat, P., Moureau, J., Viollier, E., and Lyons, T. W. (2014). Iron isotopes in an Archean ocean analogue. *Geochimica et Cosmochimica Acta*, 133:443–462.
- Cade-Menun, B. J. and Preston, C. M. (1996). A comparison of soil extraction procedures for  $^{31}\text{P}$  NMR spectroscopy. *Soil Science*, 161(11):770–785.
- Castendyk, D. N., Eary, L. E., and Society for Mining, Metallurgy, a. E. U., editors (2009). *Mine pit lakes: characteristics, predictive modeling, and sustainability*. Number v. 3 in Management technologies for metal mining influenced water. Society for Mining, Metallurgy & Exploration, Littleton, Colo.
- Chariaou, M., Rahn-Lee, L., Kind, J., García-Rubio, I., Komeili, A., and Gehring, A. (2015). Anisotropy of Bullet-Shaped Magnetite Nanoparticles in the Magnetotactic Bacteria *Desulfovibrio magneticus* sp. Strain RS-1. *Biophysical Journal*, 108(5):1268–1274.
- Chaudhry, V. and Nautiyal, C. S. (2011). A high throughput method and culture medium for rapid screening of phosphate accumulating microorganisms. *Bioresource Technology*, 102(17):8057–8062.
- Chen, H., Li, J., Xing, X., Du, Z., and Chen, G. (2015). Unexpected Diversity of Magnetococci in Intertidal Sediments of Xiaoshi Island in the North Yellow Sea. *Journal of Nanomaterials*, 2015:1–11.
- Choi, B. K., Hercules, D. M., and Houalla, M. (2000). Characterization of Polyphosphates by Electro-spray Mass Spectrometry. *Analytical Chemistry*, 72(20):5087–5091.
- Clark, J. E., Beegen, H., and Wood, H. G. (1986). Isolation of intact chains of polyphosphate from "Propionibacterium shermanii" grown on glucose or lactate. *Journal of Bacteriology*, 168(3):1212–1219.

## Bibliography

---

- Clark, J. E. and Wood, H. G. (1987). Preparation of standards and determination of sizes of long-chain polyphosphates by gel electrophoresis. *Analytical Biochemistry*, 161(2):280–290.
- Cosmidis, J., Benzerara, K., Morin, G., Busigny, V., Lebeau, O., Jézéquel, D., Noël, V., Dublet, G., and Othmane, G. (2014). Biomineralization of iron-phosphates in the water column of Lake Pavin (Massif Central, France). *Geochimica et Cosmochimica Acta*, 126:78–96.
- Cotel, A. J. (1999). A trigger mechanism for the Lake Nyos disaster. *Journal of Volcanology and Geothermal Research*, 88(4):343–347.
- Couradeau, E., Benzerara, K., Gerard, E., Moreira, D., Bernard, S., Brown, G. E., and Lopez-Garcia, P. (2012). An Early-Branching Microbialite Cyanobacterium Forms Intracellular Carbonates. *Science*, 336(6080):459–462.
- Cox, B. L., Popa, R., Bazylinski, D. A., Lanoil, B., Douglas, S., Belz, A., Engler, D. L., and Neelson, K. H. (2002). Organization and Elemental Analysis of P-, S-, and Fe-rich Inclusions in a Population of Freshwater Magnetococci. *Geomicrobiology Journal*, 19(4):387–406.
- Crocetti, G. R., Hugenholtz, P., Bond, P. L., Schuler, A., Keller, J., Jenkins, D., and Blackall, L. L. (2000). Identification of Polyphosphate-Accumulating Organisms and Design of 16S rRNA-Directed Probes for Their Detection and Quantitation. *Applied and Environmental Microbiology*, 66(3):1175–1182.
- Crosby, C. H. and Bailey, J. V. (2012). The role of microbes in the formation of modern and ancient phosphatic mineral deposits. *Frontiers in Microbiology*, 3.
- Descamps, E. C., Monteil, C. L., Menguy, N., Ginet, N., Pignol, D., Bazylinski, D. A., and Lefèvre, C. T. (2017). *Desulfamplus magnetovallimortis* gen. nov., sp. nov., a magnetotactic bacterium from a brackish desert spring able to biomineralize greigite and magnetite, that represents a novel lineage in the Desulfobacteraceae. *Systematic and Applied Microbiology*, 40(5):280–289.
- Diaz, J., Ingall, E., Vogt, S., de Jonge, M. D., Paterson, D., Rau, C., and Brandes, J. A. (2009). Characterization of phosphorus, calcium, iron, and other elements in organisms at sub-micron resolution using X-ray fluorescence spectromicroscopy: X-ray spectromicroscopy of organisms. *Limnology and Oceanography: Methods*, 7(1):42–51.
- Diaz, J. M., Björkman, K. M., Haley, S. T., Ingall, E. D., Karl, D. M., Longo, A. F., and Dyhrman, S. T. (2016). Polyphosphate dynamics at Station ALOHA, North Pacific subtropical gyre: Polyphosphate at Station ALOHA. *Limnology and Oceanography*, 61(1):227–239.
- Diaz, J. M. and Ingall, E. D. (2010). Fluorometric Quantification of Natural Inorganic Polyphosphate. *Environmental Science & Technology*, 44(12):4665–4671.
- Diaz, R. J. and Rosenberg, R. (2008). Spreading Dead Zones and Consequences for Marine Ecosystems. *Science*, 321(5891):926–929.

- Dieing, T., Hollricher, O., and Toporski, J., editors (2010). *Confocal Raman microscopy*. Number 158 in Springer series in optical sciences. Springer, Heidelberg [Germany] ; New York. OCLC: ocn639165073.
- Du, E., de Vries, W., Han, W., Liu, X., Yan, Z., and Jiang, Y. (2016). Imbalanced phosphorus and nitrogen deposition in China's forests. *Atmospheric Chemistry and Physics*, 16(13):8571–8579.
- Dyhrman, S. T., Benitez-Nelson, C. R., Orchard, E. D., Haley, S. T., and Pellechia, P. J. (2009). A microbial source of phosphonates in oligotrophic marine systems. *Nature Geoscience*, 2(10):696–699.
- Eder, S. H. K., Gigler, A. M., Hanzlik, M., and Winklhofer, M. (2014). Sub-Micrometer-Scale Mapping of Magnetite Crystals and Sulfur Globules in Magnetotactic Bacteria Using Confocal Raman Micro-Spectrometry. *PLoS ONE*, 9(9):e107356.
- Ehrlich, H. L., Newman, D. K., and Kappler, A., editors (2015). *Ehrlich's Geomicrobiology*. CRC Press, 6th edition.
- Elser, J. and Bennett, E. (2011). A broken biogeochemical cycle. *Nature*, 478(7367):29–31.
- Fernandez, E. J. and Clark, D. S. (1987). N.m.r. spectroscopy: A non-invasive tool for studying intracellular processes. *Enzyme and Microbial Technology*, 9(5):259–271.
- Ferris, F. G. and Beveridge, T. J. (1985). Functions of Bacterial Cell Surface Structures. *BioScience*, 35(3):172–177.
- Frankel, R., Bazylinski, D., Johnson, M., and Taylor, B. (1997). Magneto-aerotaxis in marine coccoid bacteria. *Biophysical Journal*, 73(2):994–1000.
- Froelich, P. N., Bender, M. L., Luedtke, N. A., Heath, G. R., and DeVries, T. (1982). The marine phosphorus cycle. *American Journal of Science*, 282(4):474–511.
- Geelhoed, J. S., Kleerebezem, R., Sorokin, D. Y., Stams, A. J. M., and Van Loosdrecht, M. C. M. (2010). Reduced inorganic sulfur oxidation supports autotrophic and mixotrophic growth of *Magnetospirillum* strain J10 and *Magnetospirillum gryphiswaldense*: Reduced sulfur utilization by *Magnetospirillum* spp. *Environmental Microbiology*, 12(4):1031–1040.
- Gilbert, N. (2009). Environment: The disappearing nutrient. *Nature*, 461(7265):716–718.
- Glasauer, S., Weidler, P. G., Langley, S., and Beveridge, T. J. (2003). Controls on Fe reduction and mineral formation by a subsurface bacterium. *Geochimica et Cosmochimica Acta*, 67(7):1277–1288.
- Goldhammer, T., Brüchert, V., Ferdelman, T. G., and Zabel, M. (2010). Microbial sequestration of phosphorus in anoxic upwelling sediments. *Nature Geoscience*, 3(8):557–561.

## Bibliography

---

- Gross, A., Nishri, A., and Angert, A. (2013). Use of Phosphate Oxygen Isotopes for Identifying Atmospheric-P Sources: A Case Study at Lake Kinneret. *Environmental Science & Technology*, 47(6):2721–2727.
- Gross, A., Turner, B. L., Goren, T., Berry, A., and Angert, A. (2016). Tracing the Sources of Atmospheric Phosphorus Deposition to a Tropical Rain Forest in Panama Using Stable Oxygen Isotopes. *Environmental Science & Technology*, 50(3):1147–1156.
- Gross, J. H. (2017). Electrospray Ionization. In *Mass Spectrometry*, pages 721–778. Springer International Publishing, Cham.
- Gächter, R. and Meyer, J. S. (1993). The role of microorganisms in mobilization and fixation of phosphorus in sediments. *Hydrobiologia*, 253(1-3):103–121.
- Günther, S. (2011). *Population structure and dynamics of polyphosphate accumulating organisms in a communal wastewater treatment plant*. PhD thesis.
- Günther, S., Trutnau, M., Kleinstaub, S., Hause, G., Bley, T., Roske, I., Harms, H., and Müller, S. (2009). Dynamics of Polyphosphate-Accumulating Bacteria in Wastewater Treatment Plant Microbial Communities Detected via DAPI (4',6'-Diamidino-2-Phenylindole) and Tetracycline Labeling. *Applied and Environmental Microbiology*, 75(7):2111–2121.
- Hall, K. and Northcote, T. (2012). Meromictic Lake. In Bengtsson, L., Herschy, R., and Fairbridge, R., editors, *Encyclopedia of lakes and reservoirs*, pages 519–524. Springer, Dordrecht.
- Hallett, M., Schneider, A. S., and Carbone, E. (1972). Tetracycline fluorescence as calcium-probe for nerve membrane with some model studies using erythrocyte ghosts. *The Journal of Membrane Biology*, 10(1):31–44.
- Hanada, S., Liu, W.-T., Shintani, T., Kamagata, Y., and Nakamura, K. (2002). *Tetrasphaera elongata* sp. nov., a polyphosphate-accumulating bacterium isolated from activated sludge. *International Journal of Systematic and Evolutionary Microbiology*, 52(3):883–887.
- He, S. and McMahon, K. D. (2011). Microbiology of 'Candidatus Accumulibacter' in activated sludge: Microbiology of 'Candidatus Accumulibacter'. *Microbial Biotechnology*, 4(5):603–619.
- Head, I. M., Gray, N. D., Clarke, K. J., Pickup, R. W., and Jones, J. G. (1996). The phylogenetic position and ultrastructure of the uncultured bacterium *Achromatium oxaliferum*. *Microbiology*, 142(9):2341–2354.
- Hilderbrand, R. L. (2018). *The role of phosphonates in living systems*. OCLC: 1020690889.
- Hongve, D. (1997). Cycling of iron, manganese, and phosphate in a meromictic lake. *Limnology and Oceanography*, 42(4):635–647.

- Hupfer, M., Gloess, S., and Grossart, H. (2007). Polyphosphate-accumulating microorganisms in aquatic sediments. *Aquatic Microbial Ecology*, 47:299–311.
- Hupfer, M., Glöss, S., Schmieder, P., and Grossart, H.-P. (2008). Methods for detection and quantification of polyphosphate and polyphosphate accumulating microorganisms in aquatic sediments. *International Review of Hydrobiology*, 93:1–30.
- Isambert, A., Menguy, N., Larquet, E., Guyot, F., and Valet, J.-P. (2007). Transmission electron microscopy study of magnetites in a freshwater population of magnetotactic bacteria. *American Mineralogist*, 92(4):621–630.
- Jendrossek, D. (2020). Polyphosphate Granules and Acidocalcisomes. In Jendrossek, D., editor, *Bacterial Organelles and Organelle-like Inclusions*, volume 34, pages 1–17. Springer International Publishing, Cham. Series Title: Microbiology Monographs.
- Jeppesen, E., Brucet, S., Naselli-Flores, L., Papastergiadou, E., Stefanidis, K., Nöges, T., Nöges, P., Attayde, J. L., Zohary, T., Coppens, J., Bucak, T., Menezes, R. F., Freitas, F. R. S., Kernan, M., Søndergaard, M., and Beklioglu, M. (2015). Ecological impacts of global warming and water abstraction on lakes and reservoirs due to changes in water level and related changes in salinity. *Hydrobiologia*, 750(1):201–227.
- Ji, B., Zhang, S.-D., Zhang, W.-J., Rouy, Z., Alberto, F., Santini, C.-L., Mangenot, S., Gagnot, S., Philippe, N., Pradel, N., Zhang, L., Tempel, S., Li, Y., Médigue, C., Henrissat, B., Coutinho, P. M., Barbe, V., Talla, E., and Wu, L.-F. (2017). The chimeric nature of the genomes of marine magnetotactic coccoid-ovoid bacteria defines a novel group of *P roteobacteria*: Genome of marine magnetotactic strain MO-1. *Environmental Microbiology*, 19(3):1103–1119.
- Jogler, C., Wanner, G., Kolinko, S., Niebler, M., Amann, R., Petersen, N., Kube, M., Reinhardt, R., and Schuler, D. (2011). Conservation of proteobacterial magnetosome genes and structures in an uncultivated member of the deep-branching Nitrospira phylum. *Proceedings of the National Academy of Sciences*, 108(3):1134–1139.
- Jones, D. S., Flood, B. E., and Bailey, J. V. (2016). Metatranscriptomic insights into polyphosphate metabolism in marine sediments. *The ISME Journal*, 10(4):1015–1019.
- Jupp, A. R., Beijer, S., Narain, G. C., Schipper, W., and Slootweg, J. C. (2021). Phosphorus recovery and recycling – closing the loop. *Chemical Society Reviews*, 50(1):87–101.
- Kampinga, H. (2014). Chaperoned by Prebiotic Inorganic Polyphosphate Molecules: An Ancient Transcription-Independent Mechanism to Restore Protein Homeostasis. *Molecular Cell*, 53(5):685–687.
- Karl, D. M. and Björkman, K. M. (2015). Dynamics of Dissolved Organic Phosphorus (Chapter 5). In Hansell, D. A. and Carlson, C. A., editors, *Biogeochemistry of Marine Dissolved Organic Matter*, pages 233–334. Academic Press, second edition edition.



## Bibliography

---

- Kawaharasaki, M., Manome, A., Kanagawa, T., and Nakamura, K. (2002). Flow cytometric sorting and RFLP analysis of phosphate accumulating bacteria in an enhanced biological phosphorus removal system. *Water Science and Technology*, 46(1-2):139–144.
- Kawaharasaki, M., Tanaka, H., Kanagawa, T., and Nakamura, K. (1999). In situ identification of polyphosphate-accumulating bacteria in activated sludge by dual staining with rRNA-targeted oligonucleotide probes and 4',6-diamidino-2-phenylindol (DAPI) at a polyphosphate-probing concentration. *Water Research*, 33(1):257–265.
- Kawakoshi, A., Nakazawa, H., Fukada, J., Sasagawa, M., Katano, Y., Nakamura, S., Hosoyama, A., Sasaki, H., Ichikawa, N., Hanada, S., Kamagata, Y., Nakamura, K., Yamazaki, S., and Fujita, N. (2012). Deciphering the Genome of Polyphosphate Accumulating Actinobacterium *Micrococcus phosphovorus*. *DNA Research*, 19(5):383–394.
- Keim, C. N., Lopes Martins, J., Lins de Barros, H., Lins, U., and Farina, M. (2006). Structure, Behavior, Ecology and Diversity of Multicellular Magnetotactic Prokaryotes. In Schüler, D., editor, *Magnetoreception and Magnetosomes in Bacteria*, volume 3, pages 103–132. Springer Berlin Heidelberg. Series Title: Microbiology Monographs.
- Koch, C., Günther, S., Desta, A. F., Hübschmann, T., and Müller, S. (2013). Cytometric fingerprinting for analyzing microbial intracommunity structure variation and identifying subcommunity function. *Nature Protocols*, 8(1):190–202.
- Koda, S., Kawakami, T., and Nomura, H. (1994). Raman Spectroscopic Studies on the Interaction between Counterions and Polyphosphate Ion. *Polymer Journal*, 26(4):473–477.
- Kolinko, S., Jogler, C., Katzmann, E., Wanner, G., Peplies, J., and Schüler, D. (2012). Single-cell analysis reveals a novel uncultivated magnetotactic bacterium within the candidate division OP3: Uncultivated MTB in candidate division OP3. *Environmental Microbiology*, 14(7):1709–1721.
- Kolinko, S., Wanner, G., Katzmann, E., Kiemer, F., M. Fuchs, B., and Schüler, D. (2013). Clone libraries and single cell genome amplification reveal extended diversity of uncultivated magnetotactic bacteria from marine and freshwater environments: Undiscovered phylogeny of magnetotactic bacteria. *Environmental Microbiology*, 15(5):1290–1301.
- Komeili, A. (2012). Molecular mechanisms of compartmentalization and biomineralization in magnetotactic bacteria. *FEMS Microbiology Reviews*, 36(1):232–255.
- Konhauser, K. O. (1998). Diversity of bacterial iron mineralization. *Earth-Science Reviews*, 43(3-4):91–121.
- Konhauser, K. O., Fyfe, W. S., Schultze-Lam, S., Ferris, F. G., and Beveridge, T. J. (1994). Iron phosphate precipitation by epilithic microbial biofilms in Arctic Canada. *Canadian Journal of Earth Sciences*, 31(8):1320–1324.

- Kornberg, A. (1995). Inorganic polyphosphate: toward making a forgotten polymer unforgettable. *Journal of bacteriology*, 177(3):491–496.
- Kornberg, A., Rao, N. N., and Ault-Riché, D. (1999). Inorganic polyphosphate: a molecule of many functions. In *Inorganic Polyphosphates*, volume 68, pages 89–125. Springer Berlin Heidelberg. Annual Review of Biochemistry.
- Koziaeva, V., Dziuba, M., Leão, P., Uzun, M., Krutkina, M., and Grouzdev, D. (2019). Genome-Based Metabolic Reconstruction of a Novel Uncultivated Freshwater Magnetotactic coccus “Ca. Magnetaquicoccus inordinatus” UR-1, and Proposal of a Candidate Family “Ca. Magnetaquicocaceae”. *Frontiers in Microbiology*, 10.
- Koziaeva, V. V., Alekseeva, L. M., Uzun, M. M., Leão, P., Sukhacheva, M. V., Patutina, E. O., Kolganova, T. V., and Grouzdev, D. S. (2020). Biodiversity of Magnetotactic Bacteria in the Freshwater Lake Beloe Bordukovskoe, Russia. *Microbiology*, 89(3):348–358.
- Kristiansen, R., Nguyen, H. T. T., Saunders, A. M., Nielsen, J. L., Wimmer, R., Le, V. Q., McIlroy, S. J., Petrovski, S., Seviour, R. J., Calteau, A., Nielsen, K. L., and Nielsen, P. H. (2013). A metabolic model for members of the genus *Tetrasphaera* involved in enhanced biological phosphorus removal. *The ISME Journal*, 7(3):543–554.
- Kulaev, I. and Kulakovskaya, T. (2000). Polyphosphate and Phosphate Pump. *Annual Review of Microbiology*, 54(1):709–734.
- Kulaev, I. S. (1975). Biochemistry of inorganic polyphosphates. In Adrian, R. H., Helmreich, E., Holzer, H., Jung, R., Krayner, O., Linden, R. J., Lynen, F., Miescher, P. A., Piiper, J., Rasmussen, H., Renold, A. E., Trendelenburg, U., Ullrich, K., Vogt, W., and Weber, A., editors, *Reviews of Physiology, Biochemistry and Pharmacology, Volume 86*, volume 86, pages 131–158. Springer Berlin Heidelberg, Berlin, Heidelberg. Series Title: Reviews of Physiology, Biochemistry and Pharmacology.
- Kulaev, I. S. and Vagabov, V. M. (1983). Polyphosphate Metabolism in Micro-Organisms. In *Advances in Microbial Physiology*, volume 24, pages 83–171. Elsevier.
- Kulaev, I. S., Vagabov, V. M., and Kulakovskaya, T. V. (2004). *The biochemistry of inorganic polyphosphates - 2nd edition*. J. Wiley, Chichester, West Sussex ; Hoboken, NJ, 2nd ed edition.
- Kulakovskaya, T., Ryazanova, L., Zvonarev, A., Khokhlova, G., Ostroumov, V., and Vainshtein, M. (2018). The biosorption of cadmium and cobalt and iron ions by yeast *Cryptococcus humicola* at nitrogen starvation. *Folia Microbiologica*, 63(4):507–510.
- Kulakovskaya, T. V., Vagabov, V. M., and Kulaev, I. S. (2012). Inorganic polyphosphate in industry, agriculture and medicine: Modern state and outlook. *Process Biochemistry*, 47(1):1–10.
- Labry, C., Youenou, A., Delmas, D., and Michelon, P. (2013). Addressing the measurement of particulate organic and inorganic phosphorus in estuarine and coastal waters. *Continental Shelf Research*, 60:28–37.

## Bibliography

---

- Lambrecht, J., Schattenberg, F., Harms, H., and Mueller, S. (2018). Characterizing Microbiome Dynamics - Flow Cytometry Based Workflows from Pure Cultures to Natural Communities. *Journal of Visualized Experiments*, (137).
- Lechaire, J.-P., Shillito, B., Frébourg, G., and Gaill, F. (2002). Elemental characterization of microorganism granules by EFTEM in the tube wall of a deep-sea vent invertebrate. *Biology of the Cell*, 94(4-5):243–249.
- Lee, T. C., Mohsin, S., Taylor, D., Parkesh, R., Gunnlaugsson, T., O'Brien, F. J., Giehl, M., and Gowin, W. (2003). Detecting microdamage in bone. *Journal of Anatomy*, 203(2):161–172.
- Lefevre, C. T., Abreu, F., Schmidt, M. L., Lins, U., Frankel, R. B., Hedlund, B. P., and Bazylinski, D. A. (2010). Moderately Thermophilic Magnetotactic Bacteria from Hot Springs in Nevada. *Applied and Environmental Microbiology*, 76(11):3740–3743.
- Lefevre, C. T. and Bazylinski, D. A. (2013). Ecology, Diversity, and Evolution of Magnetotactic Bacteria. *Microbiology and Molecular Biology Reviews*, 77(3):497–526.
- Lefevre, C. T., Menguy, N., Abreu, F., Lins, U., Posfai, M., Prozorov, T., Pignol, D., Frankel, R. B., and Bazylinski, D. A. (2011). A Cultured Greigite-Producing Magnetotactic Bacterium in a Novel Group of Sulfate-Reducing Bacteria. *Science*, 334(6063):1720–1723.
- Lefèvre, C., Bennet, M., Landau, L., Vach, P., Pignol, D., Bazylinski, D., Frankel, R., Klumpp, S., and Faivre, D. (2014). Diversity of Magneto-Aerotactic Behaviors and Oxygen Sensing Mechanisms in Cultured Magnetotactic Bacteria. *Biophysical Journal*, 107(2):527–538.
- Lefèvre, C. T., Bernadac, A., Yu-Zhang, K., Pradel, N., and Wu, L.-F. (2009). Isolation and characterization of a magnetotactic bacterial culture from the Mediterranean Sea. *Environmental Microbiology*, 11(7):1646–1657.
- Lefèvre, C. T., Frankel, R. B., Pósfai, M., Prozorov, T., and Bazylinski, D. A. (2011a). Isolation of obligately alkaliphilic magnetotactic bacteria from extremely alkaline environments: Obligately alkaliphilic magnetotactic bacteria. *Environmental Microbiology*, 13(8):2342–2350.
- Lefèvre, C. T., Pósfai, M., Abreu, F., Lins, U., Frankel, R. B., and Bazylinski, D. A. (2011b). Morphological features of elongated-anisotropic magnetosome crystals in magnetotactic bacteria of the Nitrospirae phylum and the Deltaproteobacteria class. *Earth and Planetary Science Letters*, 312(1-2):194–200.
- Lefèvre, C. T., Trubitsyn, D., Abreu, F., Kolinko, S., de Almeida, L. G. P., de Vasconcelos, A. T. R., Lins, U., Schüler, D., Ginet, N., Pignol, D., and Bazylinski, D. A. (2013a). Monophyletic origin of magnetotaxis and the first magnetosomes: Monophyletic origin of magnetotaxis. *Environmental Microbiology*, 15(8):2267–2274.

- Lefèvre, C. T., Trubitsyn, D., Abreu, F., Kolinko, S., Jogler, C., de Almeida, L. G. P., de Vasconcelos, A. T. R., Kube, M., Reinhardt, R., Lins, U., Pignol, D., Schüler, D., Bazylinski, D. A., and Ginet, N. (2013b). Comparative genomic analysis of magnetotactic bacteria from the *Deltaproteobacteria* provides new insights into magnetite and greigite magnetosome genes required for magnetotaxis: New insights in genes required for magnetotaxis. *Environmental Microbiology*, pages n/a–n/a.
- Lefèvre, C. T., Vilorio, N., Schmidt, M. L., Pósfai, M., Frankel, R. B., and Bazylinski, D. A. (2012). Novel magnetite-producing magnetotactic bacteria belonging to the Gammaproteobacteria. *The ISME Journal*, 6(2):440–450.
- Lehours, A.-C., Bardot, C., Thenot, A., Debroas, D., and Fonty, G. (2005). Anaerobic Microbial Communities in Lake Pavin, a Unique Meromictic Lake in France. *Applied and Environmental Microbiology*, 71(11):7389–7400.
- Lehours, A.-C., Evans, P., Bardot, C., Joblin, K., and Gérard, F. (2007). Phylogenetic Diversity of Archaea and Bacteria in the Anoxic Zone of a Meromictic Lake (Lake Pavin, France). *Applied and Environmental Microbiology*, 73(6):2016–2019.
- Lepère, C., Domaizon, I., Hugoni, M., Vellet, A., and Debroas, D. (2016). Diversity and Dynamics of Active Small Microbial Eukaryotes in the Anoxic Zone of a Freshwater Meromictic Lake (Pavin, France). *Frontiers in Microbiology*, 7.
- Leão, P., Le Nagard, L., Yuan, H., Cypriano, J., Da Silva Neto, I., Bazylinski, D. A., Acosta-Avalos, D., Barros, H. L., Hitchcock, A. P., Lins, U., and Abreu, F. (2020). Magnetosome magnetite biomineralization in a flagellated protist: evidence for an early evolutionary origin for magnetoreception in eukaryotes. *Environmental Microbiology*, 22(4):1495–1506.
- Li, J. and Dittrich, M. (2019). Dynamic polyphosphate metabolism in cyanobacteria responding to phosphorus availability: Polyphosphate in cyanobacteria. *Environmental Microbiology*, 21(2):572–583.
- Li, J., Liu, P., Wang, J., Roberts, A. P., and Pan, Y. (2020a). Magnetotaxis as an adaptation to enable bacterial shuttling of microbial sulfur and sulfur cycling across aquatic oxic–anoxic interfaces. *Journal of Geophysical Research: Biogeosciences*.
- Li, J., Menguy, N., Gatel, C., Boureau, V., Snoeck, E., Patriarche, G., Leroy, E., and Pan, Y. (2015). Crystal growth of bullet-shaped magnetite in magnetotactic bacteria of the *Nitrospirae* phylum. *Journal of The Royal Society Interface*, 12(103):20141288.
- Li, J., Menguy, N., Leroy, E., Roberts, A. P., Liu, P., and Pan, Y. (2020b). Biomineralization and magnetism of uncultured magnetotactic coccus strain THC-1 with non-chained magnetosomal magnetite nanoparticles. *Journal of Geophysical Research: Solid Earth*.
- Li, J., Zhang, H., Menguy, N., Benzerara, K., Wang, F., Lin, X., Chen, Z., and Pan, Y. (2017). Single-Cell Resolution of Uncultured Magnetotactic Bacteria via Fluorescence-Coupled Electron Microscopy. *Applied and Environmental Microbiology*, 83(12).

## Bibliography

---

- Lin, W., Li, J., and Pan, Y. (2012a). Newly Isolated but Uncultivated Magnetotactic Bacterium of the Phylum Nitrospirae from Beijing, China. *Applied and Environmental Microbiology*, 78(3):668–675.
- Lin, W. and Pan, Y. (2010). Temporal variation of magnetotactic bacterial communities in two freshwater sediment microcosms. *FEMS Microbiology Letters*, 302(1):85–92.
- Lin, W., Pan, Y., and Bazylinski, D. A. (2017). Diversity and ecology of and biomineralization by magnetotactic bacteria: Diversity of magnetotactic bacteria. *Environmental Microbiology Reports*, 9(4):345–356.
- Lin, W., Wang, Y., Gorby, Y., Neelson, K., and Pan, Y. (2013). Integrating niche-based process and spatial process in biogeography of magnetotactic bacteria. *Scientific Reports*, 3(1):1643.
- Lin, W., Wang, Y., and Pan, Y. (2012b). Short-term effects of temperature on the abundance and diversity of magnetotactic cocci. *MicrobiologyOpen*, 1(1):53–63.
- Lin, W., Zhang, W., Paterson, G. A., Zhu, Q., Zhao, X., Knight, R., Bazylinski, D. A., Roberts, A. P., and Pan, Y. (2020). Expanding magnetic organelle biogenesis in the domain Bacteria. *Microbiome*, 8(1):152.
- Liu, P., Liu, Y., Zhao, X., Roberts, A. P., Zhang, H., Zheng, Y., Wang, F., Wang, L., Menguy, N., Pan, Y., and Li, J. (2020). Diverse phylogeny and morphology of magnetite biomineralized by magnetotactic cocci. *Environmental Microbiology*, pages 1462–2920.15254.
- Lorenz, B. and Schröder, H. C. (1999). Methods for Investigation of Inorganic Polyphosphates and Polyphosphate-Metabolizing Enzymes. In Jeanteur, P., Kostovic, I., Kuchino, Y., Müller, W. E. G., Macieira-Coelho, A., Rhoads, R. E., Schröder, H. C., and Müller, W. E. G., editors, *Inorganic Polyphosphates*, volume 23, pages 217–239. Springer Berlin Heidelberg, Berlin, Heidelberg. Series Title: Progress in Molecular and Subcellular Biology.
- Lovley, D. R., Holmes, D. E., and Nevin, K. P. (2004). Dissimilatory Fe(III) and Mn(IV) Reduction. In *Advances in Microbial Physiology*, volume 49, pages 219–286. Elsevier.
- Lundberg, P., Harmsen, E., Ho, C., and Vogel, H. J. (1990). Nuclear magnetic resonance studies of cellular metabolism. *Analytical Biochemistry*, 191(2):193–222.
- Majed, N. and Gu, A. Z. (2010). Application of Raman Microscopy for Simultaneous and Quantitative Evaluation of Multiple Intracellular Polymers Dynamics Functionally Relevant to Enhanced Biological Phosphorus Removal Processes. *Environmental Science & Technology*, 44(22):8601–8608.
- Majed, N., Li, Y., and Gu, A. Z. (2012). Advances in techniques for phosphorus analysis in biological sources. *Current Opinion in Biotechnology*, 23(6):852–859.
- Maki, J. S. (2013). Bacterial Intracellular Sulfur Globules: Structure and Function. *Journal of Molecular Microbiology and Biotechnology*, 23(4-5):270–280.

- Mandala, V. S., Loh, D. M., Shepard, S. M., Geeson, M. B., Sergeev, I. V., Nocera, D. G., Cummins, C. C., and Hong, M. (2020). Bacterial Phosphate Granules Contain Cyclic Polyphosphates: Evidence from  $^{31}\text{P}$  Solid-State NMR. *Journal of the American Chemical Society*, 142(43):18407–18421.
- Mao, X., Egli, R., Petersen, N., Hanzlik, M., and Liu, X. (2014). Magneto-Chemotaxis in Sediment: First Insights. *PLoS ONE*, 9(7):e102810.
- Martin, P., Dyhrman, S. T., Lomas, M. W., Poulton, N. J., and Van Mooy, B. A. S. (2014). Accumulation and enhanced cycling of polyphosphate by Sargasso Sea plankton in response to low phosphorus. *Proceedings of the National Academy of Sciences*, 111(22):8089–8094.
- Martin, P. and Van Mooy, B. A. S. (2013). Fluorometric Quantification of Polyphosphate in Environmental Plankton Samples: Extraction Protocols, Matrix Effects, and Nucleic Acid Interference. *Applied and Environmental Microbiology*, 79(1):273–281.
- Martín, H. G., Ivanova, N., Kunin, V., Warnecke, F., Barry, K. W., McHardy, A. C., Yeates, C., He, S., Salamov, A. A., Szeto, E., Dalin, E., Putnam, N. H., Shapiro, H. J., Pangilinan, J. L., Rigoutsos, I., Kyrpides, N. C., Blackall, L. L., McMahon, K. D., and Hugenholtz, P. (2006). Metagenomic analysis of two enhanced biological phosphorus removal (EBPR) sludge communities. *Nature Biotechnology*, 24(10):1263–1269.
- McHatton, S. C., Barry, J. P., Jannasch, H. W., and Nelson, D. C. (1996). High Nitrate Concentrations in Vacuolate, Autotrophic Marine Beggiatoa spp. *Applied and Environmental Microbiology*, 62(3):954–958.
- Meldrum, F. C., Mann, S., Heywood, B. R., Frankel, R. B., and Bazylinski, D. A. (1993). Electron Microscopy Study of Magnetosomes in a Cultured Coccoid Magnetotactic Bacterium. *Proceedings: Biological Sciences*, 251(1332):231–236.
- Meybeck, M. (2016). Dragons, Fairies, Miracles and Worship at Pavin and Other European Maar-Lakes. In Sime-Ngando, T., Boivin, P., Chapron, E., Jezequel, D., and Meybeck, M., editors, *Lake Pavin*, pages 53–79. Springer International Publishing, Cham.
- Michard, G., Viollier, E., Jézéquel, D., and Sarazin, G. (1994). Geochemical study of a crater lake: Pavin Lake, France — Identification, location and quantification of the chemical reactions in the lake. *Chemical Geology*, 115(1-2):103–115.
- Miot, J., Jézéquel, D., Benzerara, K., Cordier, L., Rivas-Lamelo, S., Skouri-Panet, F., Férard, C., Poinot, M., and Duprat, E. (2016). Mineralogical Diversity in Lake Pavin: Connections with Water Column Chemistry and Biomineralization Processes. *Minerals*, 6(2):24.
- Momba, M. and Cloete, T. (1996). The relationship of biomass to phosphate uptake by *Acinetobacter junii* in activated sludge mixed liquor. *Water Research*, 30(2):364–370.

## Bibliography

---

- Monteil, C. L., Benzerara, K., Menguy, N., Bidaud, C. C., Michot-Achdjian, E., Bolzoni, R., Mathon, F. P., Coutaud, M., Alonso, B., Garau, C., Jézéquel, D., Viollier, E., Ginet, N., Floriani, M., Swaraj, S., Sachse, M., Busigny, V., Duprat, E., Guyot, F., and Lefevre, C. T. (2021). Intracellular amorphous Ca-carbonate and magnetite biomineralization by a magnetotactic bacterium affiliated to the Alphaproteobacteria. *The ISME Journal*, 15(1):1–18.
- Monteil, C. L. and Lefevre, C. T. (2020). Magnetoreception in Microorganisms. *Trends in Microbiology*, 28(4):266–275.
- Monteil, C. L., Vallenet, D., Menguy, N., Benzerara, K., Barbe, V., Fouteau, S., Cruaud, C., Floriani, M., Viollier, E., Adryanczyk, G., Leonhardt, N., Faivre, D., Pignol, D., López-García, P., Weld, R. J., and Lefevre, C. T. (2019). Ectosymbiotic bacteria at the origin of magnetoreception in a marine protist. *Nature Microbiology*, 4(7):1088–1095.
- Moore, C. M., Mills, M. M., Arrigo, K. R., Berman-Frank, I., Bopp, L., Boyd, P. W., Galbraith, E. D., Geider, R. J., Guieu, C., Jaccard, S. L., Jickells, T. D., La Roche, J., Lenton, T. M., Mahowald, N. M., Marañón, E., Marinov, I., Moore, J. K., Nakatsuka, T., Oschlies, A., Saito, M. A., Thingstad, T. F., Tsuda, A., and Ulloa, O. (2013). Processes and patterns of oceanic nutrient limitation. *Nature Geoscience*, 6(9):701–710.
- Morillo, V., Abreu, F., Araujo, A. C., de Almeida, L. G. P., Enrich-Prast, A., Farina, M., de Vasconcelos, A. T. R., Bazylinski, D. A., and Lins, U. (2014). Isolation, cultivation and genomic analysis of magnetosome biomineralization genes of a new genus of South-seeking magnetotactic cocci within the Alphaproteobacteria. *Frontiers in Microbiology*, 5.
- Moskowitz, B. M., Bazylinski, D. A., Egli, R., Frankel, R. B., and Edwards, K. J. (2008). Magnetic properties of marine magnetotactic bacteria in a seasonally stratified coastal pond (Salt Pond, MA, USA). *Geophysical Journal International*, 174(1):75–92.
- Moudříková, □., Ivanov, I. N., Vítová, M., Nedbal, L., Zachleder, V., Mojžeš, P., and Bišová, K. (2021). Comparing Biochemical and Raman Microscopy Analyses of Starch, Lipids, Polyphosphate, and Guanine Pools during the Cell Cycle of *Desmodesmus quadricauda*. *Cells*, 10(1):62.
- Moudříková, □., Sadowsky, A., Metzger, S., Nedbal, L., Mettler-Altmann, T., and Mojžeš, P. (2017). Quantification of Polyphosphate in Microalgae by Raman Microscopy and by a Reference Enzymatic Assay. *Analytical Chemistry*, 89(22):12006–12013.
- Mukherjee, C., Mukherjee, C., and Ray, K. (2015). An improved DAPI staining procedure for visualization of polyphosphate granules in cyanobacterial and microalgal cells. *Protocol Exchange*.
- Murat, D., Quinlan, A., Vali, H., and Komeili, A. (2010). Comprehensive genetic dissection of the magnetosome gene island reveals the step-wise assembly of a prokaryotic organelle. *Proceedings of the National Academy of Sciences*, 107(12):5593–5598.

- Mußmann, M., Hu, F. Z., Richter, M., de Beer, D., Preisler, A., Jørgensen, B. B., Huntemann, M., Glöckner, F. O., Amann, R., Koopman, W. J. H., Lasken, R. S., Janto, B., Hogg, J., Stoodley, P., Boissy, R., and Ehrlich, G. D. (2007). Insights into the Genome of Large Sulfur Bacteria Revealed by Analysis of Single Filaments. *PLoS Biology*, 5(9):e230.
- Mänd, K., Kirsimäe, K., Lepland, A., Crosby, C. H., Bailey, J. V., Konhauser, K. O., Wirth, R., Schreiber, A., and Lumiste, K. (2018). Authigenesis of biomorphic apatite particles from Benguela upwelling zone sediments off Namibia: The role of organic matter in sedimentary apatite nucleation and growth. *Geobiology*, 16(6):640–658.
- Möller, L., Laas, P., Rogge, A., Goetz, F., Bahlo, R., Leipe, T., and Labrenz, M. (2019). Sulfurimonas subgroup GD17 cells accumulate polyphosphate under fluctuating redox conditions in the Baltic Sea: possible implications for their ecology. *The ISME Journal*, 13(2):482–493.
- Nakazawa, H., Arakaki, A., Narita-Yamada, S., Yashiro, I., Jinno, K., Aoki, N., Tsuruyama, A., Okamura, Y., Tanikawa, S., Fujita, N., Takeyama, H., and Matsunaga, T. (2009). Whole genome sequence of *Desulfovibrio magneticus* strain RS-1 revealed common gene clusters in magnetotactic bacteria. *Genome Research*, 19(10):1801–1808.
- Nausch, M., Achterberg, E. P., Bach, L. T., Brussaard, C. P. D., Crawford, K. J., Fabian, J., Riebesell, U., Stühr, A., Unger, J., and Wannicke, N. (2018). Concentrations and Uptake of Dissolved Organic Phosphorus Compounds in the Baltic Sea. *Frontiers in Marine Science*, 5:386.
- Nelson, D. C. and Jannasch, H. W. (1983). Chemoautotrophic growth of a marine *Beggiatoa* in sulfide-gradient cultures. *Archives of Microbiology*, 136(4):262–269.
- Newsome, L., Morris, K., and Lloyd, J. R. (2014). The biogeochemistry and bioremediation of uranium and other priority radionuclides. *Chemical Geology*, 363:164–184.
- Nguyen, H. T. T., Nielsen, J. L., and Nielsen, P. H. (2012). *Candidatus Halomonas phosphatis*, a novel polyphosphate-accumulating organism in full-scale enhanced biological phosphorus removal plants: Polyphosphate-accumulating uncultured *Halomonas*. *Environmental Microbiology*, 14(10):2826–2837.
- Oestreicher, Z., Lower, S., and Lower, B. (2011). Magnetotactic Bacteria Containing Phosphorus-Rich Inclusion Bodies. *Microscopy and Microanalysis*, 17(S2):140–141.
- Ohtomo, R., Sekiguchi, Y., Kojima, T., and Saito, M. (2008). Different chain length specificity among three polyphosphate quantification methods. *Analytical Biochemistry*, 383(2):210–216.
- Oyserman, B. O., Moya, F., Lawson, C. E., Garcia, A. L., Vogt, M., Heffernan, M., Noguera, D. R., and McMahon, K. D. (2016). Ancestral genome reconstruction identifies the evolutionary basis for trait acquisition in polyphosphate accumulating bacteria. *The ISME Journal*, 10(12):2931–2945.



## Bibliography

---

- Pan, Y., Lin, W., Li, J., Wu, W., Tian, L., Deng, C., Liu, Q., Zhu, R., Winklhofer, M., and Petersen, N. (2009). Reduced Efficiency of Magnetotaxis in Magnetotactic Coccoid Bacteria in Higher than Geomagnetic Fields. *Biophysical Journal*, 97(4):986–991.
- Pan, Y., Liu, B., Cao, J., Liu, J., Tian, S., and Du, E. (2021). Enhanced atmospheric phosphorus deposition in Asia and Europe in the past two decades. *Atmospheric and Oceanic Science Letters*, page 100051.
- Pasek, M. A. (2008). Rethinking early Earth phosphorus geochemistry. *Proceedings of the National Academy of Sciences*, 105(3):853–858.
- Paytan, A. and McLaughlin, K. (2007). The Oceanic Phosphorus Cycle. *ChemInform*, 38(20).
- Pereira, H., Schulze, P. S., Schüler, L. M., Santos, T., Barreira, L., and Varela, J. (2018). Fluorescence activated cell-sorting principles and applications in microalgal biotechnology. *Algal Research*, 30:113–120.
- Peretyazhko, T., Zachara, J., Kennedy, D., Fredrickson, J., Arey, B., McKinley, J., Wang, C., Dohnalkova, A., and Xia, Y. (2010). Ferrous phosphate surface precipitates resulting from the reduction of intragrain 6-line ferrihydrite by *Shewanella oneidensis* MR-1. *Geochimica et Cosmochimica Acta*, 74(13):3751–3767.
- Petermann, H. and Bleil, U. (1993). Detection of live magnetotactic bacteria in South Atlantic deep-sea sediments. *Earth and Planetary Science Letters*, 117(1-2):223–228.
- Peverly, J. H., Adamec, J., and Parthasarathy, M. V. (1978). Association of Potassium and Some Other Monovalent Cations with Occurrence of Polyphosphate Bodies in *Chlorella pyrenoidosa*. *Plant Physiology*, 62(1):120–126.
- Philippot, L. (2002). Denitrifying genes in bacterial and Archaeal genomes. *Biochimica et Biophysica Acta (BBA) - Gene Structure and Expression*, 1577(3):355–376.
- Pick, U., Bental, M., Chitlaru, E., and Weiss, M. (1990). Polyphosphate-hydrolysis - a protective mechanism against alkaline stress? *FEBS Letters*, 274(1-2):15–18.
- Piper, D. Z. and Codispoti, L. A. (1975). Marine Phosphorite Deposits and the Nitrogen Cycle. *Science*, 188(4183):15–18.
- Postec, A., Tapia, N., Bernadac, A., Joseph, M., Davidson, S., Wu, L.-F., Ollivier, B., and Pradel, N. (2012). Magnetotactic Bacteria in Microcosms Originating from the French Mediterranean Coast Subjected to Oil Industry Activities. *Microbial Ecology*, 63(1):1–11.
- Pósfai, M., Moskowitz, B. M., Arató, B., Schüler, D., Flies, C., Bazylinski, D. A., and Frankel, R. B. (2006). Properties of intracellular magnetite crystals produced by *Desulfovibrio magneticus* strain RS-1. *Earth and Planetary Science Letters*, 249(3-4):444–455.

- Qian, X., Santini, C., Kosta, A., Menguy, N., Le Guenno, H., Zhang, W., Li, J., Chen, Y., Liu, J., Alberto, F., Espinosa, L., Xiao, T., and Wu, L. (2020). Juxtaposed membranes underpin cellular adhesion and display unilateral cell division of multicellular magnetotactic prokaryotes. *Environmental Microbiology*, 22(4):1481–1494.
- Quinn, J. P., Kulakova, A. N., Cooley, N. A., and McGrath, J. W. (2007). New ways to break an old bond: the bacterial carbon?phosphorus hydrolases and their role in biogeochemical phosphorus cycling. *Environmental Microbiology*, 9(10):2392–2400.
- Ramamoorthy, P., Karthikeyan, M., and Nirubana, V. (2020). Role of phosphate solubilizing microorganisms in Agriculture. *Agri Mirror: Future India*, 1(7).
- Rao, N. N., Liu, S., and Kornberg, A. (1998). Inorganic polyphosphate in *Escherichia coli*: the phosphate regulon and the stringent response. *Journal of Bacteriology*, 180(8):2186–2193.
- Rao, N. N. and Torriani, A. (1988). Utilization by *Escherichia coli* of a high-molecular-weight, linear polyphosphate: roles of phosphatases and pore proteins. *Journal of Bacteriology*, 170(11):5216–5223.
- Ritz, K. (2007). The Plate Debate: Cultivable communities have no utility in contemporary environmental microbial ecology: The plate debate. *FEMS Microbiology Ecology*, 60(3):358–362.
- Rivas-Lamelo, S., Benzerara, K., Lefèvre, C., Monteil, C., Jézéquel, D., Menguy, N., Viollier, E., Guyot, F., Féraud, C., Poinot, M., Skouri-Panet, F., Trcera, N., Miot, J., and Duprat, E. (2017). Magnetotactic bacteria as a new model for P sequestration in the ferruginous Lake Pavin. *Geochemical Perspectives Letters*, pages 35–41.
- Roberts, J. K. and Jardetzky, O. (1981). Monitoring of cellular metabolism by NMR. *Biochimica et Biophysica Acta (BBA) - Reviews on Bioenergetics*, 639(1):53–76.
- Roden, E. E. and Edmonds, J. W. (1997). Phosphate mobilization in iron-rich anaerobic sediments: microbial Fe (III) oxide reduction versus iron-sulfide formation. *Archiv für Hydrobiologie*, 139(3):347–378.
- Rodríguez, H. and Fraga, R. (1999). Phosphate solubilizing bacteria and their role in plant growth promotion. *Biotechnology Advances*, 17(4-5):319–339.
- Rugnini, L., Costa, G., Congestri, R., and Bruno, L. (2017). Testing of two different strains of green microalgae for Cu and Ni removal from aqueous media. *Science of The Total Environment*, 601-602:959–967.
- Ruttenberg, K. (2003). The Global Phosphorus Cycle. In *Treatise on Geochemistry*, pages 585–643. Elsevier.
- Ruttenberg, K. (2019). Phosphorus Cycle. In *Encyclopedia of Ocean Sciences*, pages 447–460. Elsevier.

## Bibliography

---

- Sannigrahi, P. and Ingall, E. (2005). Polyphosphates as a source of enhanced P fluxes in marine sediments overlain by anoxic waters: Evidence from  $^{31}\text{P}$  NMR. *Geochemical Transactions*, 6(3).
- Santos, M. M., Lemos, P. C., Reis, M. A., and Santos, H. (1999). Glucose metabolism and kinetics of phosphorus removal by the fermentative bacterium *Micrococcus phosphovorans*. *Applied and Environmental Microbiology*, 65(9):3920–3928.
- Schewiakoff, W. (1893). Über einen neuen bacterienähnlichen Organismus des Süßwassers. *Heidelb Habilit.*, pages 1–38.
- Schoumans, O. F., Bouraoui, F., Kabbe, C., Oenema, O., and van Dijk, K. C. (2015). Phosphorus management in Europe in a changing world. *AMBIO*, 44(S2):180–192.
- Schultze, M., Boehrer, B., Wendt-Potthoff, K., Sánchez-España, J., and Castendyk, D. (2017). Meromictic Pit Lakes: Case Studies from Spain, Germany and Canada and General Aspects of Management and Modelling. In Gulati, R. D., Zadereev, E. S., and Degermendzhi, A. G., editors, *Ecology of Meromictic Lakes*, volume 228, pages 235–275. Springer International Publishing, Cham. Series Title: Ecological Studies.
- Schulz, H. N. (1999). Dense Populations of a Giant Sulfur Bacterium in Namibian Shelf Sediments. *Science*, 284(5413):493–495.
- Schulz, H. N. and Schulz, H. D. (2005). Large Sulfur Bacteria and the Formation of Phosphorite. *Science*, 307(5708):416–418.
- Schulz-Vogt, H. N., Pollehne, F., Jürgens, K., Arz, H. W., Beier, S., Bahlo, R., Dellwig, O., Henkel, J. V., Herlemann, D. P. R., Krüger, S., Leipe, T., and Schott, T. (2019). Effect of large magnetotactic bacteria with polyphosphate inclusions on the phosphate profile of the suboxic zone in the Black Sea. *The ISME Journal*, 13(5):1198–1208.
- Schuster, K., Urlaub, E., and Gapes, J. (2000). Single-cell analysis of bacteria by Raman microscopy: spectral information on the chemical composition of cells and on the heterogeneity in a culture. *Journal of Microbiological Methods*, 42(1):29–38.
- Schüler, D. (2002). The biomineralization of magnetosomes in *Magnetospirillum gryphiswaldense*. *International Microbiology*, 5(4):209–214.
- Schüler, D. (2008). Genetics and cell biology of magnetosome formation in magnetotactic bacteria. *FEMS Microbiology Reviews*, 32(4):654–672.
- Schüler, D. and Müller, F. D. (2020). Biosynthesis and Intracellular Organization of Magnetosomes in Magnetotactic Bacteria. In Jendrossek, D., editor, *Bacterial Organelles and Organelle-like Inclusions*, volume 34, pages 53–70. Springer International Publishing, Cham. Series Title: Microbiology Monographs.

- Schüler, D., Spring, S., and Bazylinski, D. A. (1999). Improved Technique for the Isolation of Magnetotactic *Spirilla* from a Freshwater Sediment and their Phylogenetic Characterization. *Systematic and Applied Microbiology*, 22(3):466–471.
- Serafim, L. S., Lemos, P. C., Levantesi, C., Tandoi, V., Santos, H., and Reis, M. A. (2002). Methods for detection and visualization of intracellular polymers stored by polyphosphate-accumulating microorganisms. *Journal of Microbiological Methods*, 51(1):1–18.
- Seufferheld, M. J., Alvarez, H. M., and Farias, M. E. (2008). Role of Polyphosphates in Microbial Adaptation to Extreme Environments. *Applied and Environmental Microbiology*, 74(19):5867–5874.
- Shapiro, O. H., Hatzenpichler, R., Buckley, D. H., Zinder, S. H., and Orphan, V. J. (2011). Multicellular photo-magnetotactic bacteria: Multicellular photo-magnetotactic bacteria. *Environmental Microbiology Reports*, 3(2):233–238.
- Shimoshige, H., Kobayashi, H., Shimamura, S., Mizuki, T., Inoue, A., and Maekawa, T. (2021). Isolation and cultivation of a novel sulfate-reducing magnetotactic bacterium belonging to the genus *Desulfovibrio*. *PLOS ONE*, 16(3):e0248313.
- Sibert, R. J., Koretsky, C. M., and Wyman, D. A. (2015). Cultural meromixis: Effects of road salt on the chemical stratification of an urban kettle lake. *Chemical Geology*, 395:126–137.
- Sime-Ngando, T., Boivin, P., Chapron, E., Jezequel, D., and Meybeck, M., editors (2016). *Lake Pavin*. Springer International Publishing, Cham.
- Simmons, S. L., Bazylinski, D. A., and Edwards, K. J. (2006). South-Seeking Magnetotactic Bacteria in the Northern Hemisphere. *Science*, 311(5759):371–374.
- Simmons, S. L., Sievert, S. M., Frankel, R. B., Bazylinski, D. A., and Edwards, K. J. (2004). Spatiotemporal Distribution of Marine Magnetotactic Bacteria in a Seasonally Stratified Coastal Salt Pond. *Applied and Environmental Microbiology*, 70(10):6230–6239.
- Solovchenko, A., Khozin-Goldberg, I., Selyakh, I., Semenova, L., Ismagulova, T., Lukyanov, A., Mamedov, I., Vinogradova, E., Karpova, O., Konyukhov, I., Vasileva, S., Mojzes, P., Dijkema, C., Vecher-skaya, M., Zvyagin, I., Nedbal, L., and Gorelova, O. (2019). Phosphorus starvation and luxury uptake in green microalgae revisited. *Algal Research*, 43:101651.
- Spring, S., Amann, R., Ludwig, W., Schleifer, K.-H., Schüler, D., Poralla, K., and Petersen, N. (1995). Phylogenetic Analysis of Uncultured Magnetotactic Bacteria from the Alpha-Subclass of Proteobacteria. *Systematic and Applied Microbiology*, 17(4):501–508.
- Spring, S., Amann, R., Ludwig, W., Schleifer, K. H., van Gemerden, H., and Petersen, N. (1993). Dominating role of an unusual magnetotactic bacterium in the microaerobic zone of a freshwater sediment. *Applied and Environmental Microbiology*, 59(8):2397–2403.

## Bibliography

---

- Spring, S., Lins, U., Amann, R., Schleifer, K.-H., Ferreira, L. C. S., Esquivel, D. M. S., and Farina, M. (1998). Phylogenetic affiliation and ultrastructure of uncultured magnetic bacteria with unusually large magnetosomes. *Archives of Microbiology*, 169(2):136–147.
- Stokholm-Bjerregaard, M., McIlroy, S. J., Nierychlo, M., Karst, S. M., Albertsen, M., and Nielsen, P. H. (2017). A Critical Assessment of the Microorganisms Proposed to be Important to Enhanced Biological Phosphorus Removal in Full-Scale Wastewater Treatment Systems. *Frontiers in Microbiology*, 8.
- Stramma, L., Johnson, G. C., Sprintall, J., and Mohrholz, V. (2008). Expanding Oxygen-Minimum Zones in the Tropical Oceans. *Science*, 320(5876):655–658.
- Streichan, M., Golecki, J. R., and SchÄ¶n, G. (1990). Polyphosphate-accumulating bacteria from sewage plants with different processes for biological phosphorus removal. *FEMS Microbiology Letters*, 73(2):113–124.
- Syers, J. K., Johnston, A. E., and Curtin, D. (2008). *Efficiency of soil and fertilizer phosphorus use: reconciling changing concepts of soil phosphorus behaviour with agronomic information*. Number 18 in FAO fertilizer and plant nutrition bulletin. Food and Agriculture Organization of the United Nations, Rome. OCLC: ocn231748259.
- Tarafdar, J. and Claassen, N. (1988). Organic phosphorus compounds as a phosphorus source for higher plants through the activity of phosphatases produced by plant roots and microorganisms. *Biology and Fertility of Soils*, 5(4).
- Tarayre, C., Nguyen, H.-T., Brognaux, A., Delepierre, A., De Clercq, L., Charlier, R., Michels, E., Meers, E., and Delvigne, F. (2016). Characterisation of Phosphate Accumulating Organisms and Techniques for Polyphosphate Detection: A Review. *Sensors*, 16(6):797.
- Tatsuhiko, E., Sally E., S., and F., A. S. (2001). Differentiation of polyphosphate metabolism between the extra□ and intraradical hyphae of arbuscular mycorrhizal fungi. *New Phytologist*, 149(3):555–563.
- Terashima, M., Kamagata, Y., and Kato, S. (2020). Rapid Enrichment and Isolation of Polyphosphate-Accumulating Organisms Through 4′6-Diamidino-2-Phenylindole (DAPI) Staining With Fluorescence-Activated Cell Sorting (FACS). *Frontiers in Microbiology*, 11:793.
- Terashima, M., Yama, A., Sato, M., Yumoto, I., Kamagata, Y., and Kato, S. (2016). Culture-Dependent and -Independent Identification of Polyphosphate-Accumulating *Dechloromonas* spp. Predominating in a Full-Scale Oxidation Ditch Wastewater Treatment Plant. *Microbes and Environments*.
- Tinsley, C. R. and Gotschlich, E. C. (1995). Cloning and characterization of the meningococcal polyphosphate kinase gene: production of polyphosphate synthesis mutants. *Infection and immunity*, 63(5):1624–1630.
- Tinsley, C. R., Manjula, B. N., and Gotschlich, E. C. (1993). Purification and characterization of polyphosphate kinase from *Neisseria meningitidis*. *Infection and Immunity*, 61(9):3703–3710.

- Tipping, E., Benham, S., Boyle, J. F., Crow, P., Davies, J., Fischer, U., Guyatt, H., Helliwell, R., Jackson-Blake, L., Lawlor, A. J., Monteith, D. T., Rowe, E. C., and Toberman, H. (2014). Atmospheric deposition of phosphorus to land and freshwater. *Environ. Sci.: Processes Impacts*, 16(7):1608–1617.
- Tonolla, M., Storelli, N., Danza, F., Ravasi, D., Peduzzi, S., Posth, N. R., Cox, R. P., Jørgensen, M. F., Gregersen, L. H., Daugbjerg, N., and Frigaard, N.-U. (2017). Lake Cadagno: Microbial Life in Crenogenic Meromixis. In Gulati, R. D., Zadereev, E. S., and Degermendzhi, A. G., editors, *Ecology of Meromictic Lakes*, volume 228, pages 155–186. Springer International Publishing, Cham. Series Title: Ecological Studies.
- Turner, B. L. (2008). Soil organic phosphorus in tropical forests: an assessment of the NaOH–EDTA extraction procedure for quantitative analysis by solution  $^{31}\text{P}$  NMR spectroscopy. *European Journal of Soil Science*, 59(3):453–466.
- Tyrrell, T. (1999). The relative influences of nitrogen and phosphorus on oceanic primary production. *Nature*, 400(6744):525–531.
- Tyrrell, T. (2001). Redfield Ratio. In *Encyclopedia of Ocean Sciences*, pages 2377–2387. Elsevier.
- Varela, C., Mauriaca, C., Paradela, A., Albar, J. P., Jerez, C. A., and Chávez, F. P. (2010). New structural and functional defects in polyphosphate deficient bacteria: A cellular and proteomic study. *BMC Microbiology*, 10(1):7.
- Vliet, D. M., Meijenfeldt, F. B., Dutilh, B. E., Villanueva, L., Sinninghe Damsté, J. S., Stams, A. J., and Sánchez-Andrea, I. (2020). The bacterial sulfur cycle in expanding dysoxic and euxinic marine waters. *Environmental Microbiology*, pages 1462–2920.15265.
- Wagner, M., Erhart, R., Manz, W., Amann, R., Lemmer, H., Wedi, D., and Schleifer, K. H. (1994). Development of an rRNA-targeted oligonucleotide probe specific for the genus *Acinetobacter* and its application for in situ monitoring in activated sludge. *Applied and Environmental Microbiology*, 60(3):792–800.
- Wang, L., Yan, J., Wise, M. J., Liu, Q., Asenso, J., Huang, Y., Dai, S., Liu, Z., Du, Y., and Tang, D. (2018). Distribution Patterns of Polyphosphate Metabolism Pathway and Its Relationships With Bacterial Durability and Virulence. *Frontiers in Microbiology*, 9:782.
- Wang, X., Li, Y., Zhao, J., Yao, H., Chu, S., Song, Z., He, Z., and Zhang, W. (2020). Magnetotactic bacteria: Characteristics and environmental applications. *Frontiers of Environmental Science & Engineering*, 14(4):56.
- Wang, X. K., Ma, Q. F., Jiang, W., Lv, J., Pan, W. D., Song, T., and Wu, L.-F. (2008). Effects of Hypomagnetic Field on Magnetosome Formation of *Magnetospirillum Magneticum* AMB-1. *Geomicrobiology Journal*, 25(6):296–303.
- Wang, Y., Lin, W., Li, J., and Pan, Y. (2013). High Diversity of Magnetotactic Deltaproteobacteria in a Freshwater Niche. *Applied and Environmental Microbiology*, 79(8):2813–2817.

## Bibliography

---

- Watson, S. J., Needoba, J. A., and Peterson, T. D. (2019). Widespread detection of *Candidatus Accumulibacter phosphatis*, a polyphosphate-accumulating organism, in sediments of the Columbia River estuary. *Environmental Microbiology*, 21(4):1369–1382.
- Weber, K. A., Achenbach, L. A., and Coates, J. D. (2006). Microorganisms pumping iron: anaerobic microbial iron oxidation and reduction. *Nature Reviews Microbiology*, 4(10):752–764.
- Weinberger, R., Weiner, T., and Angert, A. (2016). Isotopic signature of atmospheric phosphate emitted from coal combustion. *Atmospheric Environment*, 136:22–30.
- Wenter, R., Wanner, G., Schüler, D., and Overmann, J. (2009). Ultrastructure, tactic behaviour and potential for sulfate reduction of a novel multicellular magnetotactic prokaryote from North Sea sediments. *Environmental Microbiology*, 11(6):1493–1505.
- Westheimer, F. (1987). Why nature chose phosphates. *Science*, 235(4793):1173–1178.
- Wetzel, R. G. (2001). *Limnology: lake and river ecosystems*. Academic Press, San Diego, 3rd ed edition.
- Widdel, F., Schnell, S., Heising, S., Ehrenreich, A., Assmus, B., and Schink, B. (1993). Ferrous iron oxidation by anoxygenic phototrophic bacteria. *Nature*, 362(6423):834–836.
- Williams, T. J., Zhang, C. L., Scott, J. H., and Bazylinski, D. A. (2006). Evidence for Autotrophy via the Reverse Tricarboxylic Acid Cycle in the Marine Magnetotactic Coccus Strain MC-1. *Applied and Environmental Microbiology*, 72(2):1322–1329.
- Wolfe, R., Thauer, R., and Pfennig, N. (1987). A ‘capillary racetrack’ method for isolation of magnetotactic bacteria. *FEMS Microbiology Letters*, 45(1):31–35.
- Wolin, E., Wolin, M., and Wolfe, R. (1963). Formation of Methane by Bacterial Extracts. *Journal of Biological Chemistry*, 238(8):2882–2886.
- Yoshimura, T., Nishioka, J., Saito, H., Takeda, S., Tsuda, A., and Wells, M. L. (2007). Distributions of particulate and dissolved organic and inorganic phosphorus in North Pacific surface waters. *Marine Chemistry*, 103(1-2):112–121.
- Youssef, M. I. (1965). Genesis of bedded phosphates. *Economic Geology*, 60(3):590–600.
- Yuan, Z., Pratt, S., and Batstone, D. J. (2012). Phosphorus recovery from wastewater through microbial processes. *Current Opinion in Biotechnology*, 23(6):878–883.
- Zachara, J. M., Fredrickson, J. K., Li, S.-M., Kennedy, D. W., Smith, S. C., and Gassman, P. L. (1998). Bacterial reduction of crystalline Fe (super 3+) oxides in single phase suspensions and subsurface materials. *American Mineralogist*, 83(11-12 Part 2):1426–1443.

- Zadereev, E. S., Boehrer, B., and Gulati, R. D. (2017). Introduction: Meromictic Lakes, Their Terminology and Geographic Distribution. In Gulati, R. D., Zadereev, E. S., and Degermendzhi, A. G., editors, *Ecology of Meromictic Lakes*, volume 228, pages 1–11. Springer International Publishing, Cham. Series Title: Ecological Studies.
- Zapata, F. and Roy, R. (2004). Use of phosphate rocks for sustainable agriculture. *FAO Fertilizer and Plant Nutrition Bulletin*, 35(38):1–148.
- Zhang, H., Ishige, K., and Kornberg, A. (2002). A polyphosphate kinase (PPK2) widely conserved in bacteria. *Proceedings of the National Academy of Sciences*, 99(26):16678–16683.
- Zhang, H., Menguy, N., Wang, F., Benzerara, K., Leroy, E., Liu, P., Liu, W., Wang, C., Pan, Y., Chen, Z., and Li, J. (2017). Magnetotactic Coccus Strain SHHC-1 Affiliated to Alphaproteobacteria Forms Octahedral Magnetite Magnetosomes. *Frontiers in Microbiology*, 8.
- Zhang, H., Sekiguchi, Y., Hanada, S., Hugenholtz, P., Kim, H., Kamagata, Y., and Nakamura, K. (2003). *Gemmatimonas aurantiaca* gen. nov., sp. nov., a Gram-negative, aerobic, polyphosphate-accumulating micro-organism, the first cultured representative of the new bacterial phylum Gemmatimonadetes phyl. nov. *International Journal of Systematic and Evolutionary Microbiology*, 53(4):1155–1163.
- Zhang, W.-y., Zhang, S.-d., Xiao, T., Pan, Y.-x., and Wu, L.-f. (2010). Geographical distribution of magnetotactic bacteria. *Huan Jing Ke Xue = Huanjing Kexue*, 31(2):450–458.
- Zhu, J., Loubéry, S., Broger, L., Zhang, Y., Lorenzo-Orts, L., Utz-Pugin, A., Fernie, A. R., Young-Tae, C., and Hothorn, M. (2020). A genetically validated approach for detecting inorganic polyphosphates in plants. *The Plant Journal*, 102(3):507–516.
- Zopfi, J., Kjær, T., Nielsen, L. P., and Jørgensen, B. B. (2001). Ecology of *Thioploca* spp.: Nitrate and Sulfur Storage in Relation to Chemical Microgradients and Influence of *Thioploca* spp. on the Sedimentary Nitrogen Cycle. *Applied and Environmental Microbiology*, 67(12):5530–5537.



## **Bibliography**

---

# **Appendices**



---

## Wolfe's mineral solution

in Bazylnski et al. (2000) modified from Wolin et al. (1963)

<b>Ingredients for 1 L</b>	<b>Amount</b>
Nitrilotriacetic acid (NTA)	1.5 g
MgCl <sub>2</sub> .7H <sub>2</sub> O	3.0 g
MnSO <sub>4</sub> .H <sub>2</sub> O	0.5 g
NaCl	1.0 g
FeSO <sub>4</sub> .7H <sub>2</sub> O	0.1 g
CoCl <sub>2</sub> .6H <sub>2</sub> O or CoSO <sub>4</sub> .7H <sub>2</sub> O	0.1 g
CaCl <sub>2</sub> .2H <sub>2</sub> O	0.1 g
ZnSO <sub>4</sub> .7H <sub>2</sub> O	0.1 g
CuSO <sub>4</sub> .5H <sub>2</sub> O	0.025 g
AlK(SO <sub>4</sub> ) <sub>2</sub> .12H <sub>2</sub> O	0.01 g
H <sub>3</sub> BO <sub>3</sub> (Boric acid)	0.01 g
Na <sub>2</sub> MoO <sub>4</sub> .2H <sub>2</sub> O	0.4 g
NiCl <sub>2</sub> .6H <sub>2</sub> O	0.01 g

Add NTA (caution - carcinogenic!) to 500 mL distilled water. Adjust pH to 6.5 with saturated KOH with constant stirring. NTA will dissolved as pH rises. Once the NTA is completely dissolved and the pH at 6.5, add each mineral salt in order given, letting each dissolve before adding the next. Then bring volume up to 1 L with distilled water. Autoclave and store at 4°C.

---

## Vitamin Elixir

in Frankel et al. (1997)

<b>Ingredients for 100 mL:</b>	<b>Stock concentration</b>	<b>Amount</b>
Thiamin (hydrochloride)	-	90 mg
Inositol (myo-inositol)	-	40 mg
D-, L-Ca <sup>2+</sup> pantothenate	2 mg/mL	4 mL
Para amino benzoic acid	2 mg/mL	2.5 mL
B <sub>12</sub> Vitamin	1 mg/mL	5 mL
Pyridoxine (hydrochloride, vitamin B <sub>6</sub> )	1 mg/mL	4 mL
Niacin (Nicotinic acid)	-	-
Niacin (Nicotinic acid)	1 mg/mL	4 mL
Biotin*	0.1 mg/mL	1 mL
Folic acid**	0.1 mg/mL	0.4 mL

Add Thiamin and Iositol to approximately 50 mL distilled deionized water, then add the stocks solutions of vitamins and bring up the volume to 100 mL.

\*Biotin stock need to be warmed to about 50°C to get it into solution.

\*\*Folic acid stock is more like a suspension than a solution; mix well before taking an aliquot. It will dissolve in final solution.

## SUPPLEMENTARY INFORMATION

Intracellular amorphous Ca-carbonate and magnetite biomineralization by a magnetotactic bacterium affiliated to the Alphaproteobacteria

Caroline L. Monteil<sup>1,2\*</sup>, Karim Benzerara<sup>2\*</sup>, Nicolas Menguy<sup>2\*</sup>, Cécile C. Bidaud<sup>1,2</sup>, Emmanuel Michot--Achdjian<sup>1</sup>, Romain Bolzoni<sup>1,2</sup>, François P. Mathon<sup>1,3</sup>, Margot Coutaud<sup>2</sup>, Béatrice Alonso<sup>1</sup>, Camille Garau<sup>1</sup>, Didier Jézéquel<sup>3</sup>, Eric Viollier<sup>3</sup>, Nicolas Ginet<sup>4</sup>, Magali Floriani<sup>5</sup>, Sufal Swaraj<sup>6</sup>, Martin Sachse<sup>7</sup>, Vincent Busigny<sup>3</sup>, Elodie Duprat<sup>2</sup>, François Guyot<sup>2</sup> & Christopher T. Lefevre<sup>1</sup>

<sup>1</sup>Aix-Marseille University, CNRS, CEA, UMR7265 Institute of Biosciences and Biotechnologies of Aix-Marseille, CEA Cadarache, F-13108 Saint-Paul-lez-Durance, France

<sup>2</sup>Sorbonne Université, Muséum National d'Histoire Naturelle, UMR CNRS 7590, IRD. Institut de Minéralogie, de Physique des Matériaux et de Cosmochimie (IMPMC), 4 Place Jussieu, 75005 Paris, France.

<sup>3</sup>Université de Paris, Institut de Physique du Globe de Paris, CNRS, F-75005, Paris, France

<sup>4</sup>Laboratoire de Chimie Bactérienne, UMR 7283 CNRS, Aix-Marseille Université, Institut de Microbiologie de la Méditerranée, 13402 Marseille, France

<sup>5</sup>Institut de Radioprotection et de Sûreté Nucléaire (IRSN), PRP-ENV/SERIS/LECO, Cadarache, Saint-Paul-lez-Durance 13115, France.

<sup>6</sup>Synchrotron SOLEIL, L'Orme des Merisiers, Saint-Aubin-BP 48, 91192 Gif-sur-YVETTE Cedex, France.

<sup>7</sup>Ultrastructural Bioimaging unit, Institut Pasteur, 24-28 rue du Docteur-Roux, 75015 Paris, France.

\*These authors contributed equally to this work

For correspondence. E-mail [christopher.lefevre@cea.fr](mailto:christopher.lefevre@cea.fr); Tel. +33 4 42 25 32 93

# Supplementary Figure and Figure Legends

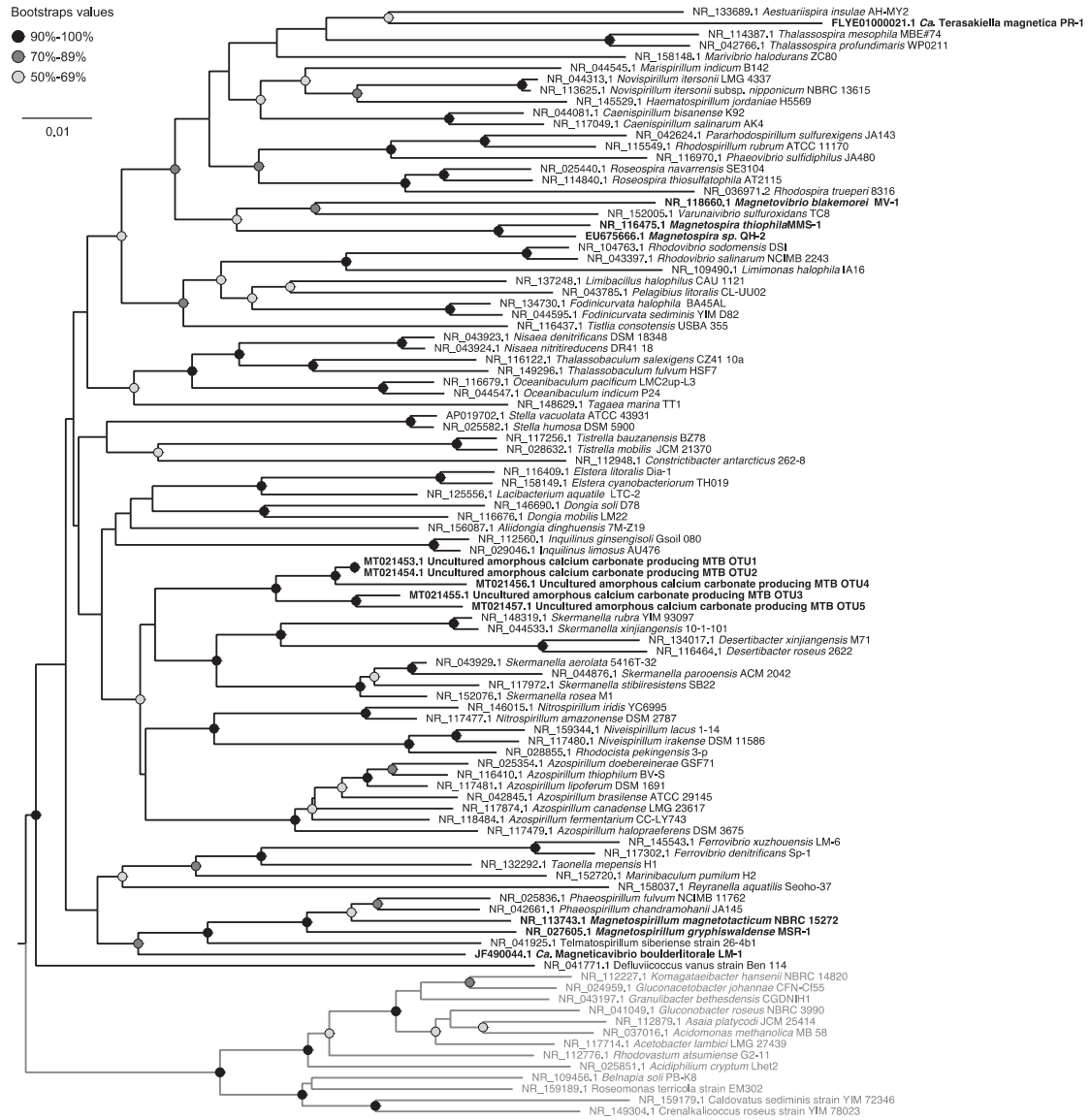


Figure S1. Neighbor-joining tree of the Rhodospirillaceae family (NCBI taxonomy) based on 16S rRNA gene sequences and rooted with representative members of the Acetobacteraceae (grey) using a Jukes-Cantor matrix for describing nucleotide evolution. Branch length represents the number of substitutions per site. Bootstrap values were estimated with a non-parametric bootstrap approach and 200 replicates. Representative MTB species are in bold.

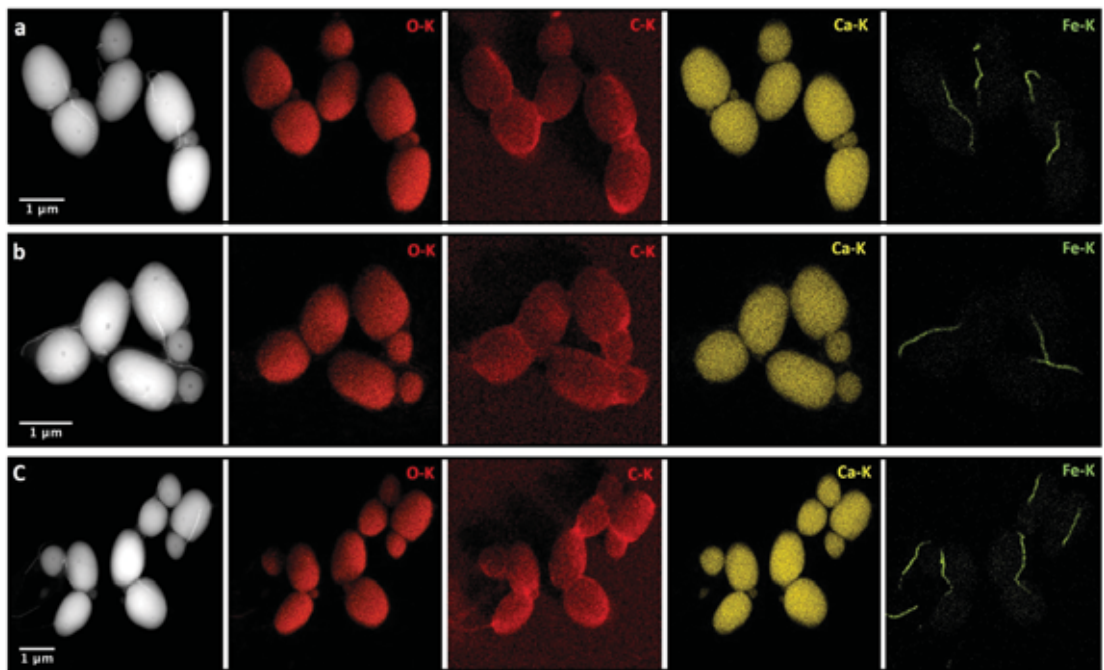


Figure S2. XEDS elemental maps showing newly formed ACC in dividing or recently divided cells isolated from a Lake Pavin sediment sample. Oxygen, carbon, calcium and iron elemental maps showing ACC-producing MTB at different growth stages.



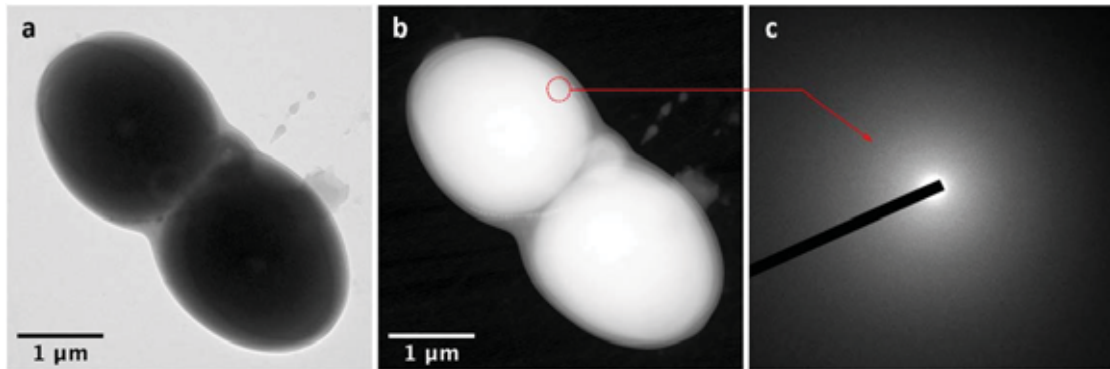


Figure S3. Electron microscope analysis to decipher the crystallinity of these large inclusions. a and b TEM bright-field and STEM-HAADF images, respectively, of a magnetotactic bacterium producing two large inclusions, isolated from a sediment sample. c Selected area electron diffraction (SAED) pattern of the edge of an inclusion shown by the dashed red circle in panel b. The absence of diffraction spots and the presence of diffuse scattering is indicative of the amorphous structure of the inclusions.

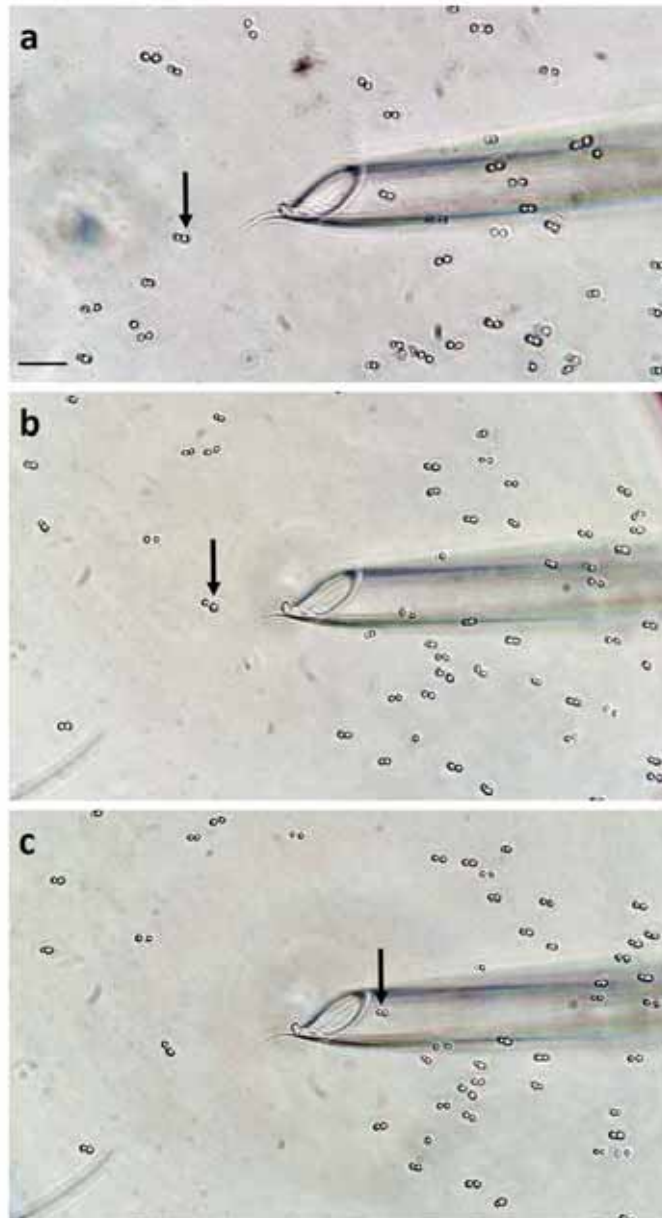


Figure S4. Single-cell sorting of an ACC-producing magnetotactic bacterium using a micromanipulator under the light microscope. Light microscopy images a to c represent the progressive aspiration of a cell (shown with arrows) into the microcapillary before its transfer in a sterile drop of 4  $\mu$ L of phosphate buffer saline to carry whole genome amplification. Note that the majority of the cells are aligned in the same direction due to the magnetic field applied close to the cell's suspension. Scale bar represents 5  $\mu$ m.

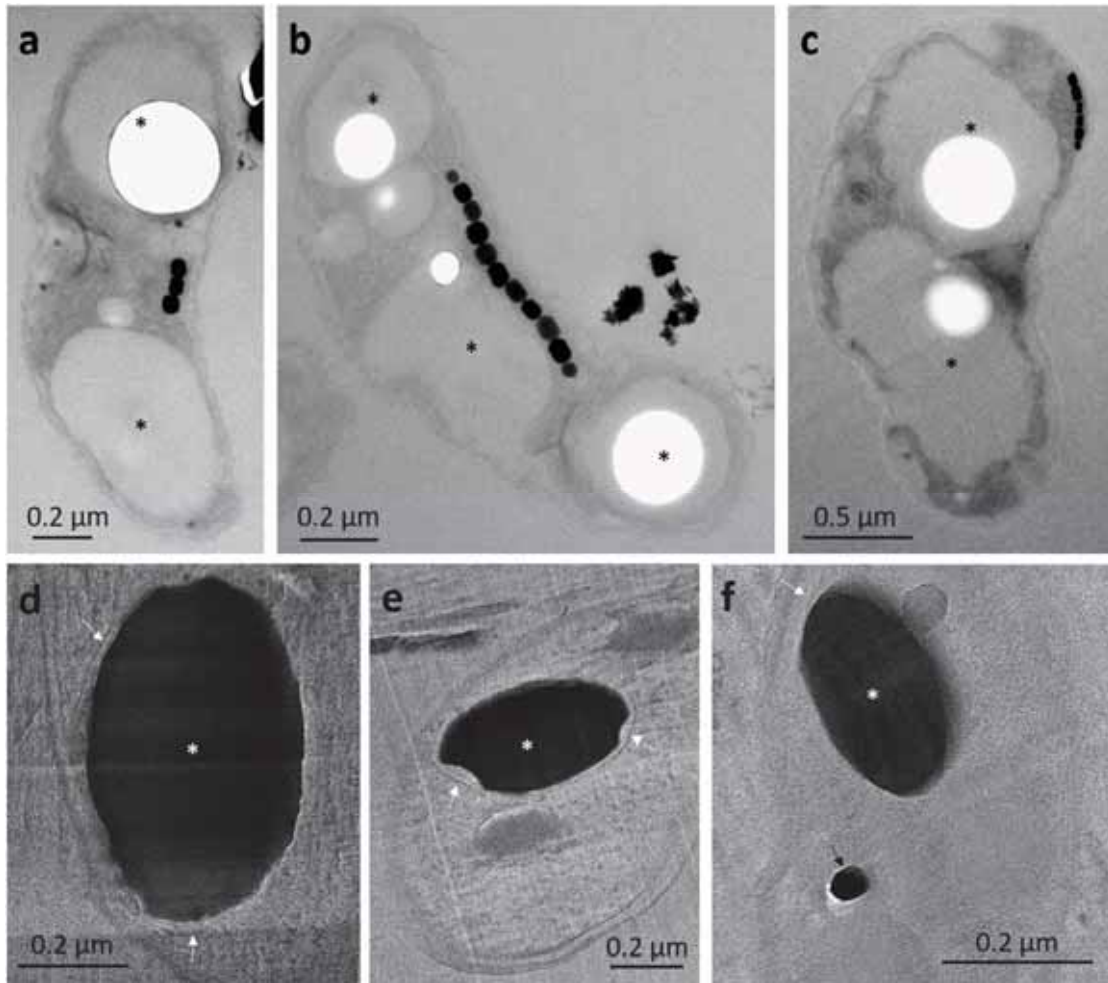


Figure S5. Bright-field TEM observations of conventional and cryo thin-sections of ACC-producing MTB from sediment samples. a to c Images of thin-sections obtained using a conventional protocol. The large ACC inclusions, shown with black stars, were lost during the preparation. d to f Images of thin-sections obtained by CEMOVIS. The large ACC inclusions, shown with white stars, were preserved. Note the presence of a membrane, shown with white arrows, surrounding the inclusions. In panel f, a magnetosome is shown by the black arrow.

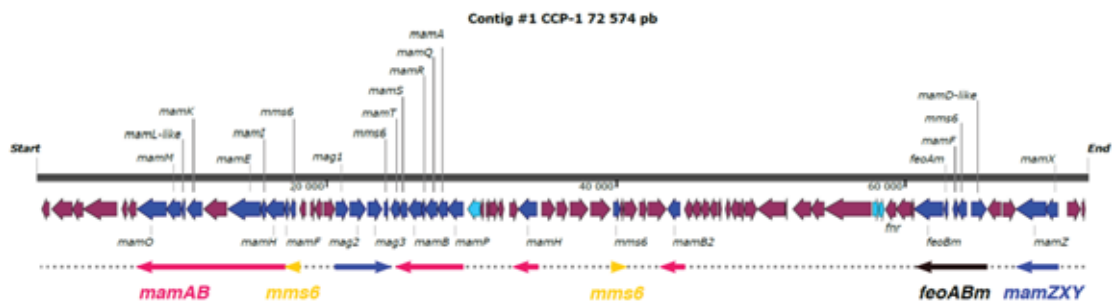


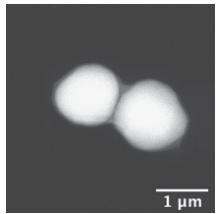
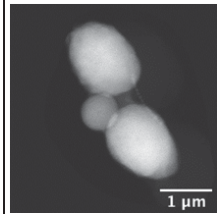
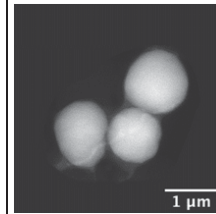
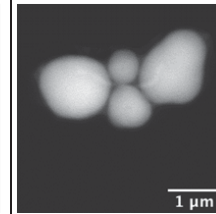
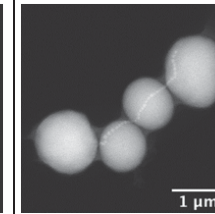
Figure S6. Magnetosome gene cluster (MGC) organization of the ACC-producing MTB clone CCP-1 representing OTU1. All genes homologous to any known magnetosome gene is coloured in dark blue. Any gene with unknown function conserved in the vicinity of other MGCs is highlighted in light blue. The map of the contig was drawn to scale and its sequences can be retrieved under the Genbank accession number MT411893. Main operons organisation described in *Magnetospirillum* species [5] are symbolized with arrows below the map.

## Supplementary Table Legend

Table S1. List of putative Mam homologs detected in CCP1 (Genbank accession number MT411893) detected using the BLASTP algorithm and annotated reference proteomes of magnetotactic Alphaproteobacteria.

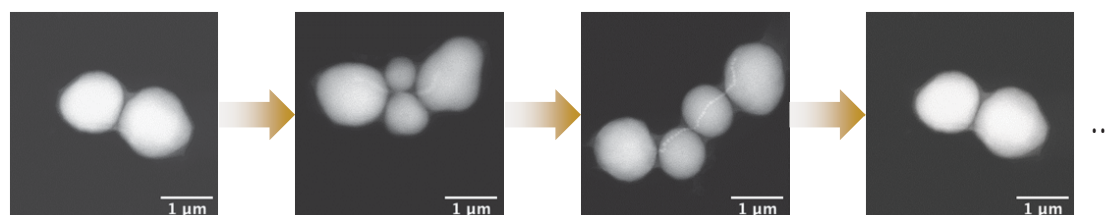
## Supplementary Information on cell division

To give some insights into the fate of carbonate inclusions during cell division, 186 cells were observed using STEM-HAADF imaging, proven to be efficient for electron dense inclusion visualization. For these bacteria, ACC inclusion with a size between ~100 nm and up to 1  $\mu\text{m}$  were observed. Based on morphological criteria (*i.e.* ACC inclusion size, number and position relative to cell polarity; magnetosomes chain continuity), all bacteria morphotypes could be classified into one out of 5 morphotype categories as follows:

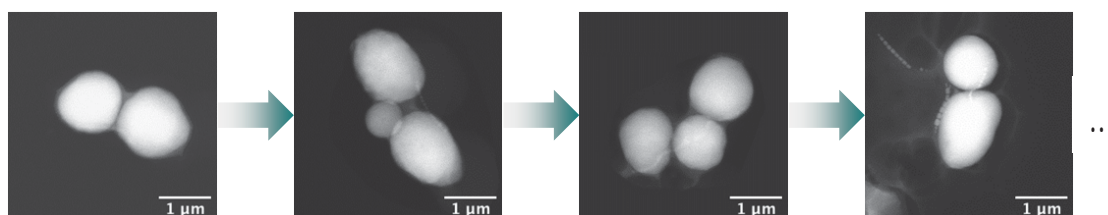
2 large inclusions	2 large inclusions + 1 smaller	2 large inclusions + 1 smaller	2 large inclusions + 2 smaller	2 large inclusions + 2 smaller
				
50 % (93)	17 % (31)	8 % (14)	21 % (39)	5 % (9)

Assuming that the inclusion size is related to the growth step, two cell division mechanisms regarding the ACC inclusion formation are proposed:

**Mechanism #1:** (i) two small inclusions form at the septum, (ii) the new inclusions grow and (iii) after cell division, the two daughter cells contain 2 inclusions (*i.e.* one mature and a new one).

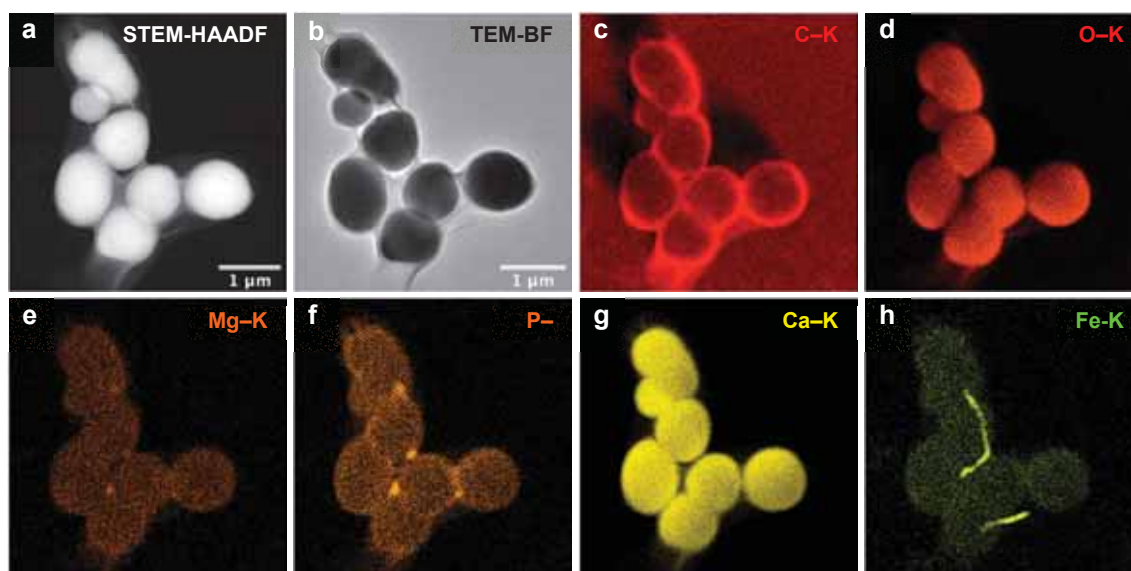


**Mechanism #2:** (i) only one small inclusion forms at the septum (ii) the new single inclusion grows and (iii) after cell division, only one daughter cell contains 2 inclusions (*i.e.* one mature and a new one). Some isolated ACC inclusions that may correspond to the second daughter cell in this mechanism have been observed but are not straightforwardly distinguishable from damaged cells.

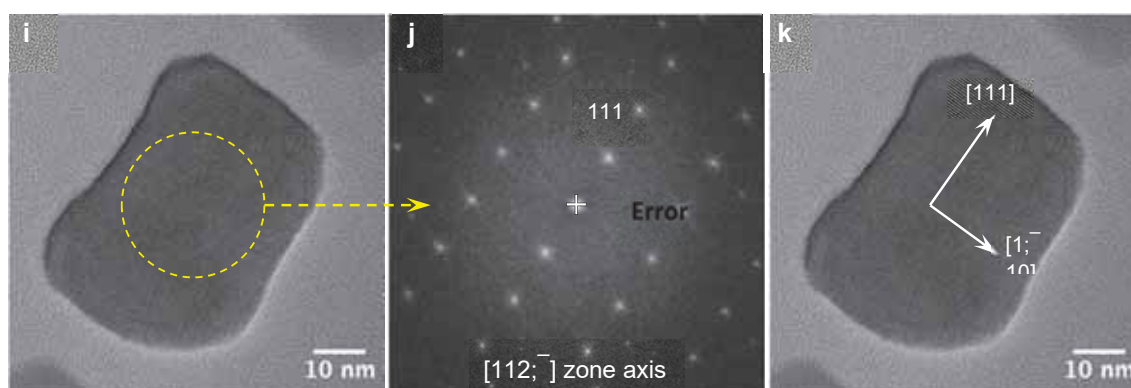


## Supplementary Information to figure 3

Here, we give additional information on the chemical and shape identification of the mineral phases for bacteria producing large Ca-rich inclusions described in figure 3.

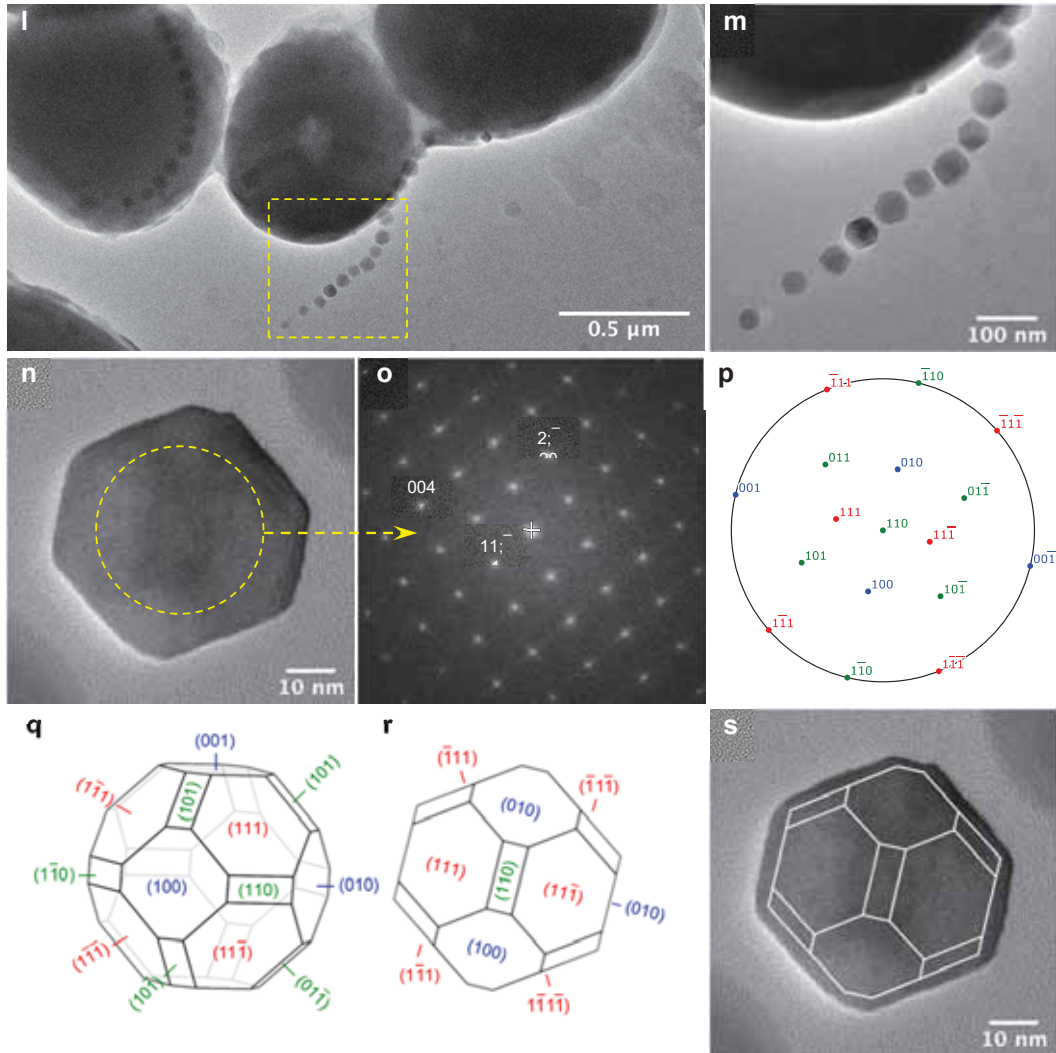


**Mineral composition:** Panels a and b represent STEM-HAADF and TEM-BF images respectively, while panels c-h show raw STEM-XEDS elemental maps of carbon, oxygen, magnesium, phosphorus, calcium and iron, respectively. Electron dense inclusions coincide spatially with high concentration of carbon, oxygen and calcium. Intensity variations observed on carbon and oxygen elemental maps are due to (i) absorption effect (stronger for light element such as carbon) and (ii) shadowing effect owing to the low take-off angle of the X-ray detector.



**Prismatic magnetosome crystallography:** i HR-TEM image of a prismatic magnetosome corresponding to figure 3c. The yellow dashed circle defines the area analyzed by fast Fourier transform (FFT) using ImageJ software. j FFT pattern indexed with the magnetite structure

(spacegroup  $Fm\bar{3}m$ ,  $a = 8.04 \text{ \AA}$ ). k same HRTEM image as in panel i with crystallographic directions shown by white arrows.



**Cuboctahedral magnetosome crystallography:** Panel l represents the TEM-BF image of a bacterium with large ACC inclusions and cuboctahedral shaped magnetosomes, while the panel m zooms on the area defined by the dashed yellow square in panel l. n HR-TEM image of a cuboctahedral magnetosome corresponding to figure 3f. The yellow dashed circle in panel n defines the area analyzed by FFT. o FFT pattern indexed with the magnetite structure (spacegroup  $Fm\bar{3}m$ ,  $a = 8.04 \text{ \AA}$ ). p The stereographic projection is oriented with respect to the orientation inferred from n using SingleCrystal software. q Following the procedure previously described in [1], the cuboctahedron with small  $\{110\}$  faces was chosen among the different possible isotropic morphologies with  $m\bar{3}m$  point group symmetry. r Cuboctahedron oriented with respect to the stereographic projection. s The cuboctahedron outline is superimposed to the image of the actual crystal with an acceptable match.



## References

1. Faivre D, Menguy N, Pósfai M, Schüler D. Environmental parameters affect the physical properties of fast-growing magnetosomes. *Am Miner* 2008; **93**: 463–469.

# 1 **Supporting Information**

2

## 3 **Mass collection of magnetotactic bacteria from the permanently stratified ferruginous** 4 **Lake Pavin, France**

5

6 Vincent Busigny<sup>1,2,\*</sup>, François P. Mathon<sup>1,3</sup>, Didier Jézéquel<sup>1,4</sup>, Cécile C. Bidaud<sup>5</sup>, Eric  
7 Viollier<sup>1</sup>, Gérard Bardoux<sup>1</sup>, Jean-Jacques Bourrand<sup>1</sup>, Karim Benzerara<sup>5</sup>, Elodie Duprat<sup>5</sup>,  
8 Nicolas Menguy<sup>5</sup>, Caroline L. Monteil<sup>3</sup>, Christopher T. Lefevre<sup>3,\*</sup>

9

10

11 <sup>1</sup>Université de Paris, Institut de Physique du Globe de Paris, CNRS, F-75005, Paris, France

12

13 <sup>2</sup>Institut Universitaire de France, 75005 Paris, France

14

15 <sup>3</sup>Aix-Marseille University, CNRS, CEA, UMR7265 Institute of Biosciences and  
16 Biotechnologies of Aix-Marseille, CEA Cadarache, F-13108 Saint-Paul-lez-Durance, France

17

18 <sup>4</sup>INRAE & Université Savoie Mont Blanc, UMR CARTELE, 74200 Thonon-les-Bains, France

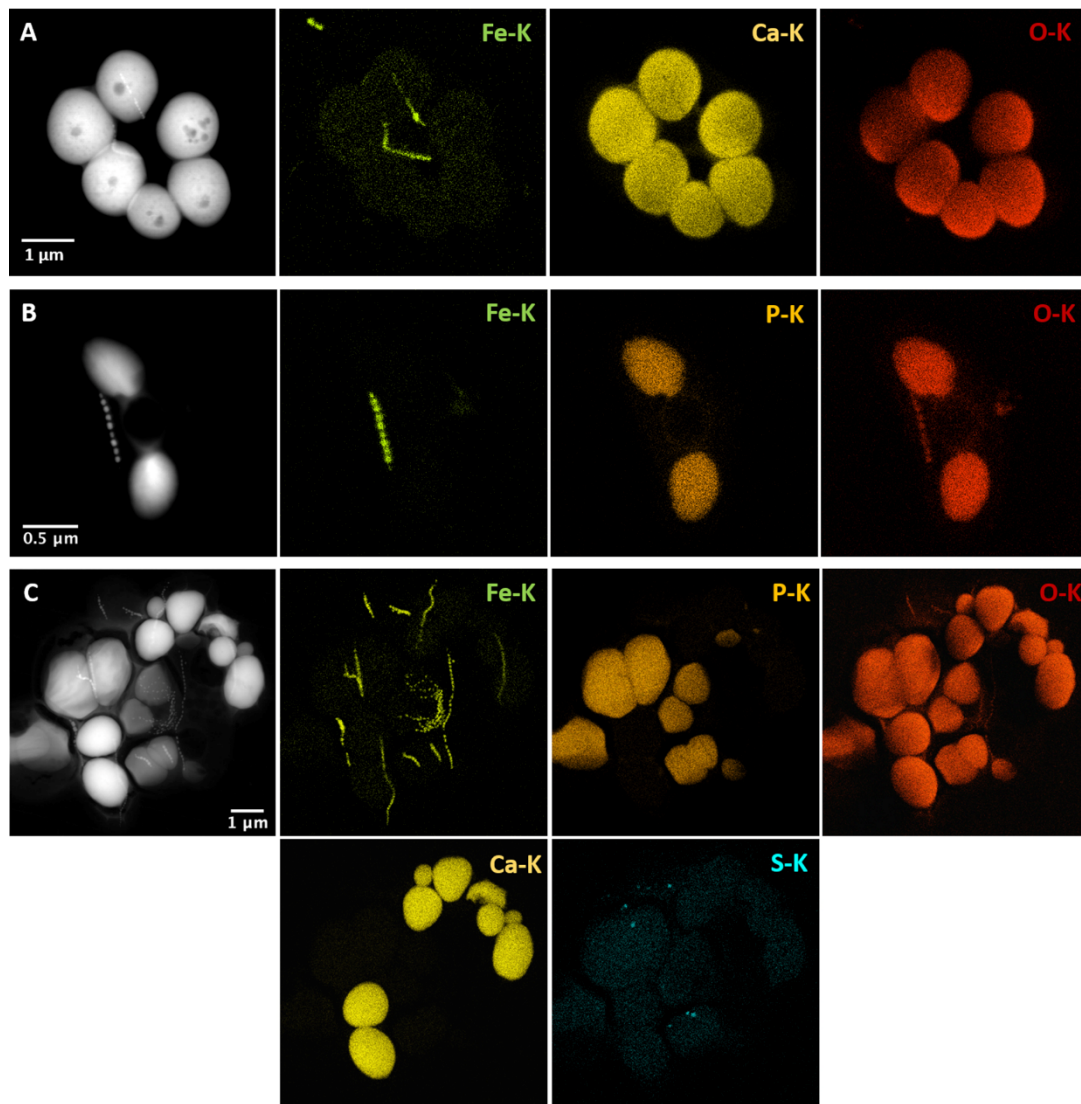
19

20 <sup>5</sup>Sorbonne Université, Muséum National d'Histoire Naturelle, UMR CNRS 7590, IRD. Institut  
21 de Minéralogie, de Physique des Matériaux et de Cosmochimie (IMPMC), Paris, France.

22

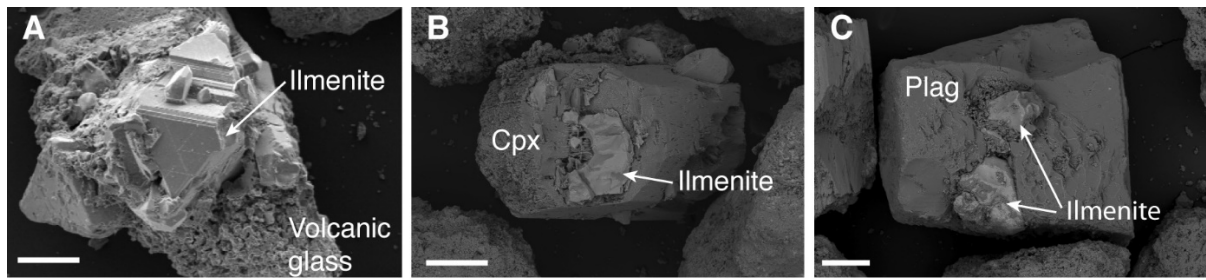
23

24 \*For correspondence. E-mails: busigny@ipgp.fr, christopher.lefevre@cea.fr



26

27 **Fig. S1.** Z-contrast imaging in the high-angle annular dark field (STEM-HAADF) mode, and  
 28 elemental mapping by X-ray energy-dispersive spectrometry (XEDS) showing the chemical  
 29 composition of inclusions formed by magnetotactic bacteria present in the sediments (A and  
 30 B) and in the water column (C) of Lake Pavin.



31

32 **Fig. S2.** Scanning electron microscope images of ilmenite inclusions in volcanic glass (A), and

33 clinopyroxene (Cpx) (B) and plagioclase (Plag) (C) crystals. This illustrates the volcanic origin

34 of ilmenite from Lake Pavin sediments. Scale bars represent 100  $\mu\text{m}$ .

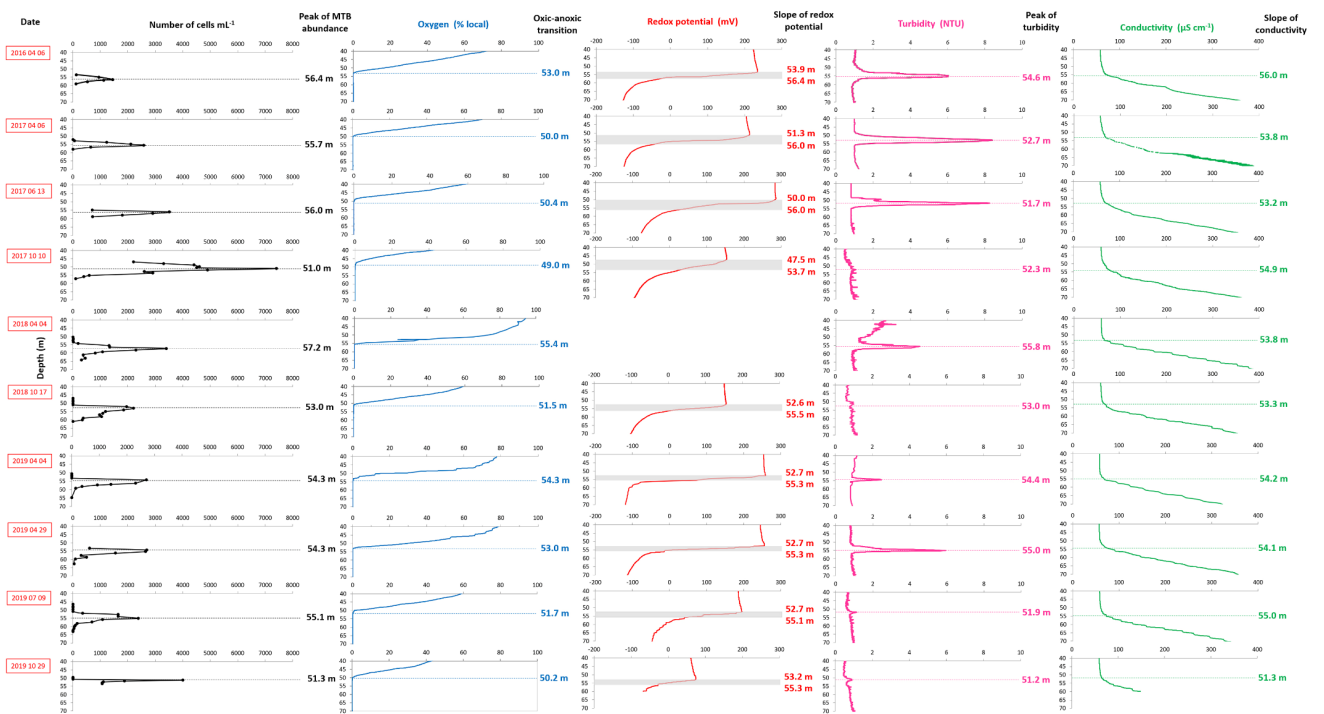
35



36

37 **Fig. S3.** Picture of the migration track system. Edges of the drop exposed to a magnetic field

38 generated by the two disc magnets are shown by arrows. The scale is shown by a ruler.



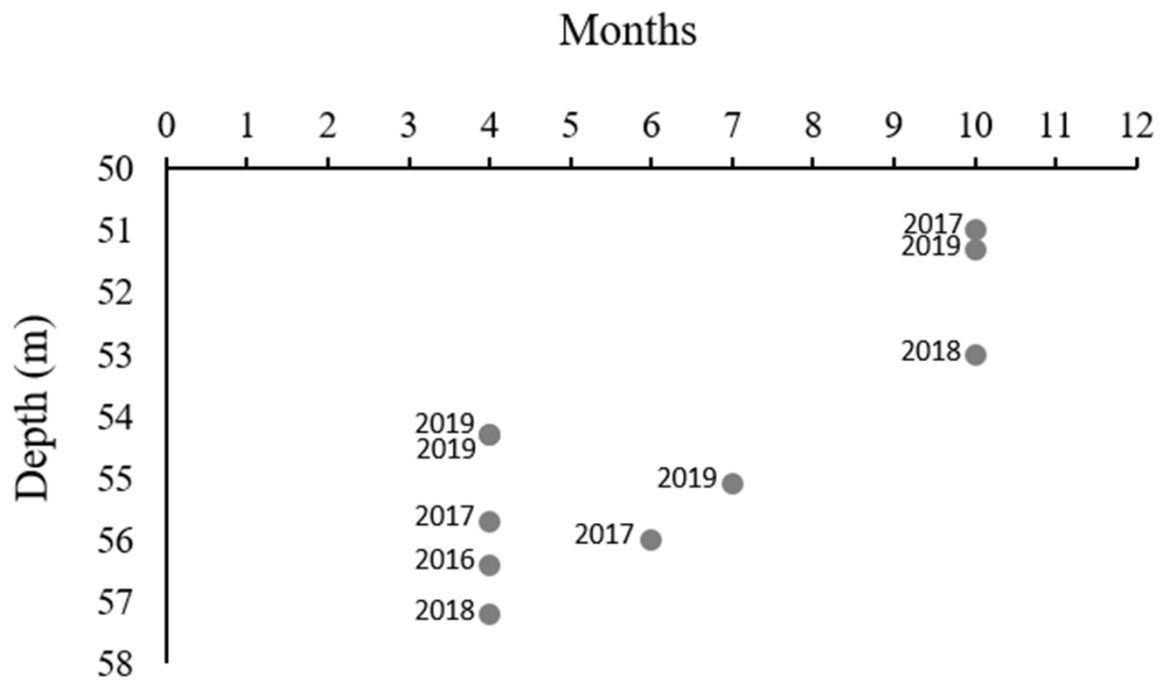
39

40

41 **Fig. S4.** Vertical profiles of magnetotactic cells abundance (A), dissolved oxygen concentration (B), redox potential (C), turbidity (D) and  
42 conductivity ( $C_{25}$ ) (E) through the water column. Sampling campaigns were carried out at ten different dates between April 2016 and October 2019.  
43 Note that measurements extend through the oxic-anoxic interface and the deeper regions of the anaerobic zone of the water column. Samples used  
44 for magnetotactic cells counting were collected using a Niskin bottle. All other parameters correspond to continuous profiles measured using *in situ*  
45 probes.

46

47



48

49 **Fig. S5.** Depth of the maximum abundance of MTB counted in the water column of Lake Pavin  
 50 as a function of the month. It illustrates that MTB are generally located shallower in the water  
 51 column in autumn compared to spring and summer.

52



Supplementary Information October 2019 field trip

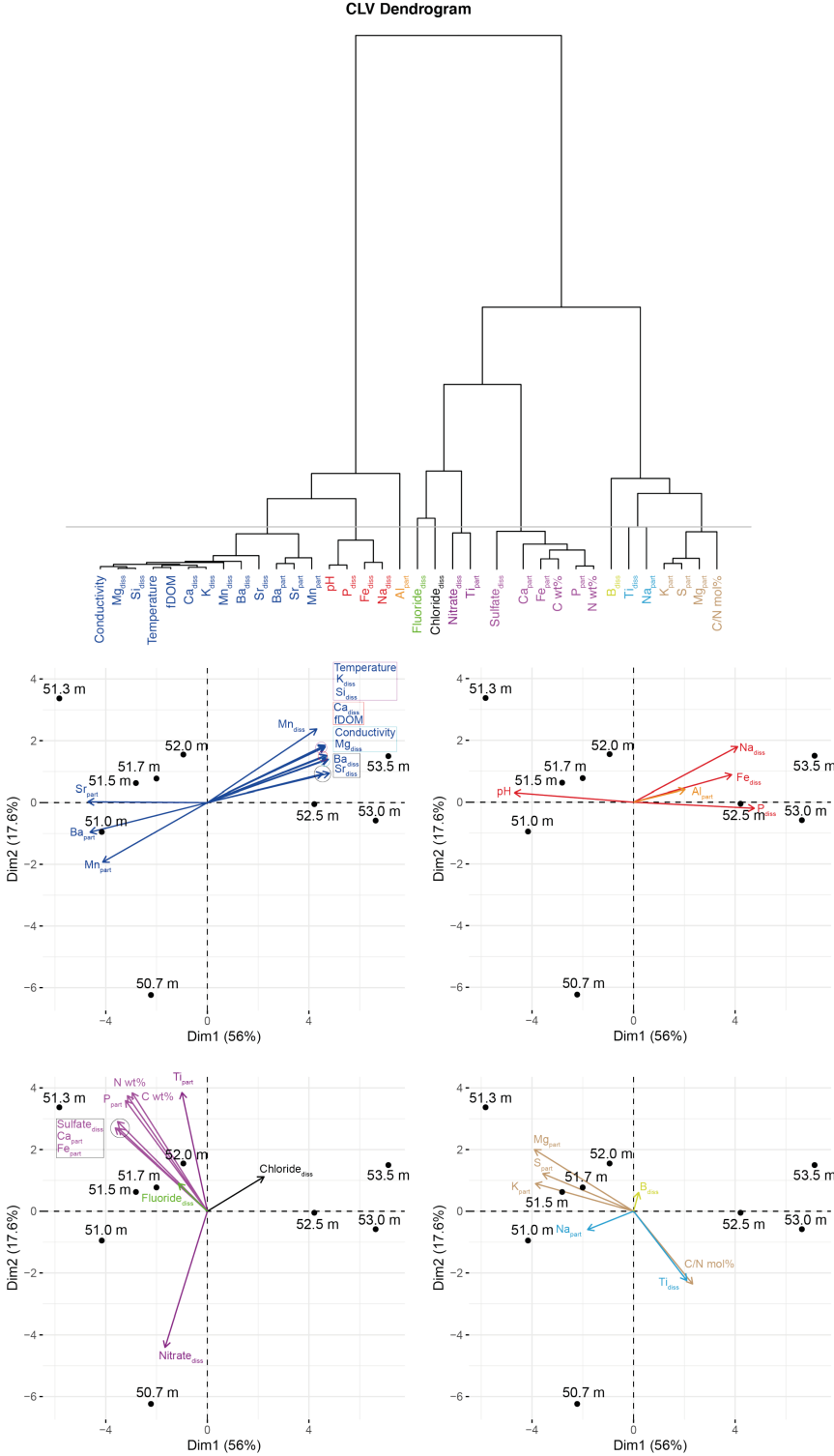
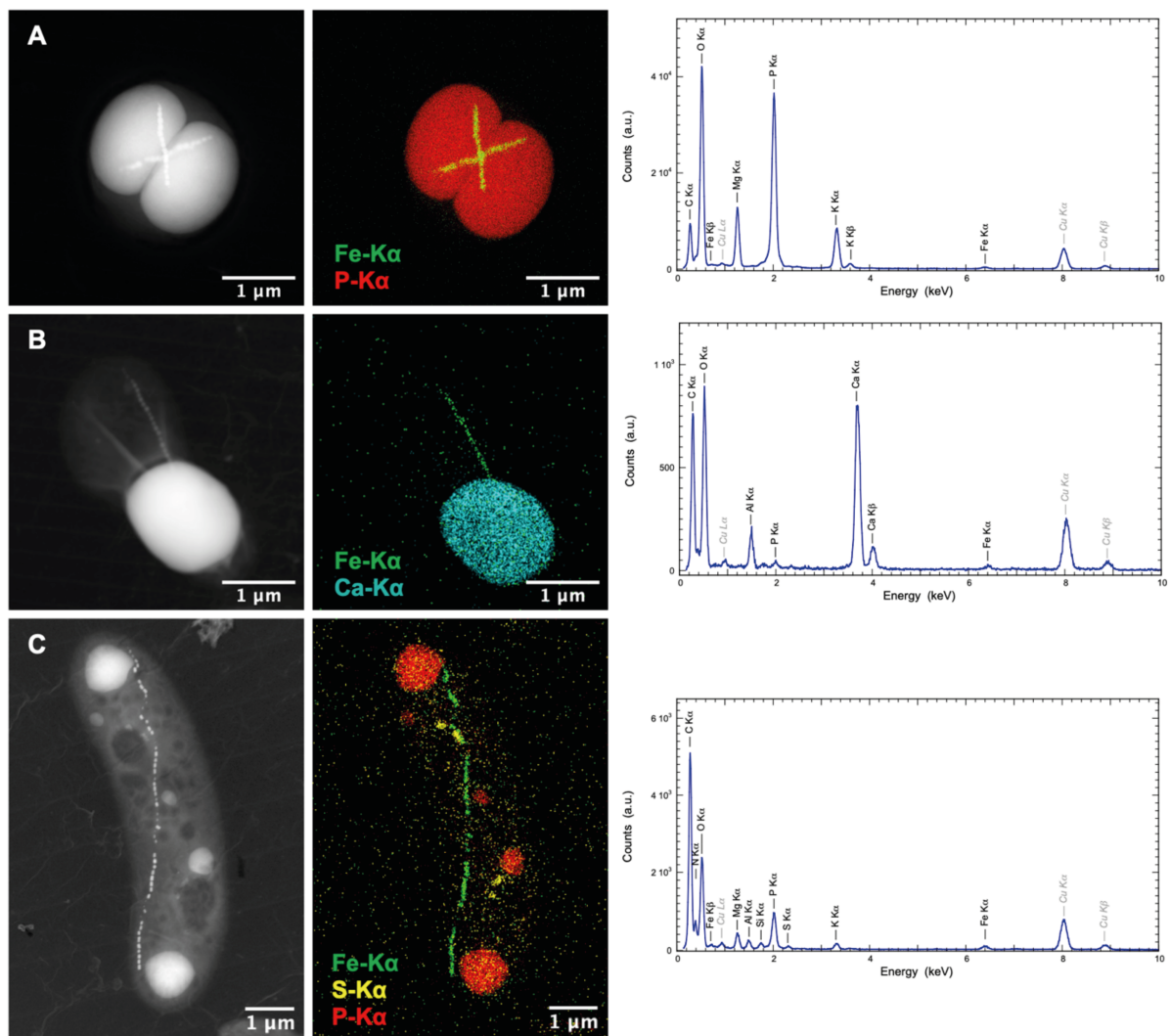
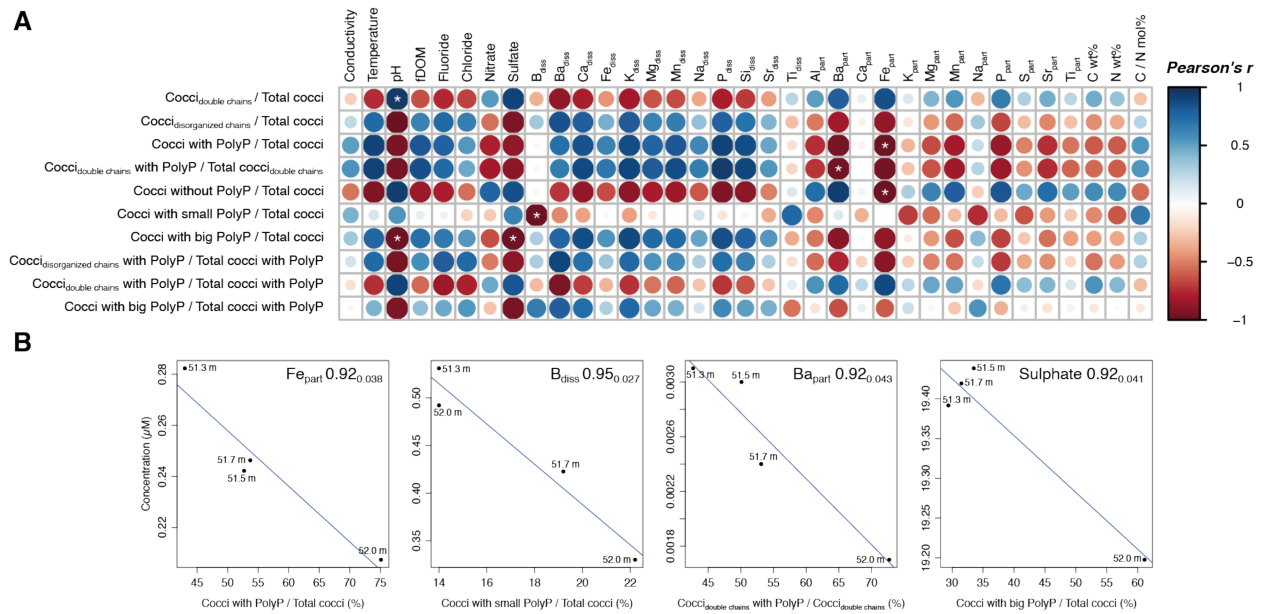


Fig. S1. Dendrogram representing the ten directional groups of physicochemical and geochemical parameters, with in addition their detailed PCA separated for a better visibility.



**Fig. S2. Chemical identification alongside their respective spectrum of the intracellular inclusions as well as the magnetosomes in the cocci, CCP and rod-shaped MTB of fig. 3. (A) cocci MTB accumulating large inclusions of PolyP. (B) CCP MTB accumulating calcium carbonate inclusions. (C) Rod-shaped MTB (Fig. 3C) accumulating PolyP.**



**Fig. S3. Linear regression modelling the relationships of geochemical variables with the frequency of cocci ability to form different types of magnetosome chains and PolyP inclusions. (A)** The plot shows the Pearson's correlation matrix. The size and the colour of the circles are related to the correlation coefficient value, meaning that: the bigger and the darker the circle, the better the correlation. Blue and red circles refer positive and negative correlations respectively. The white stars indicate correlations statistically significantly upon the p-value of 0.05 for the Pearson's test. **(B)** Biplots of the most significant correlations. All statistics are given in Supplementary Table S2.

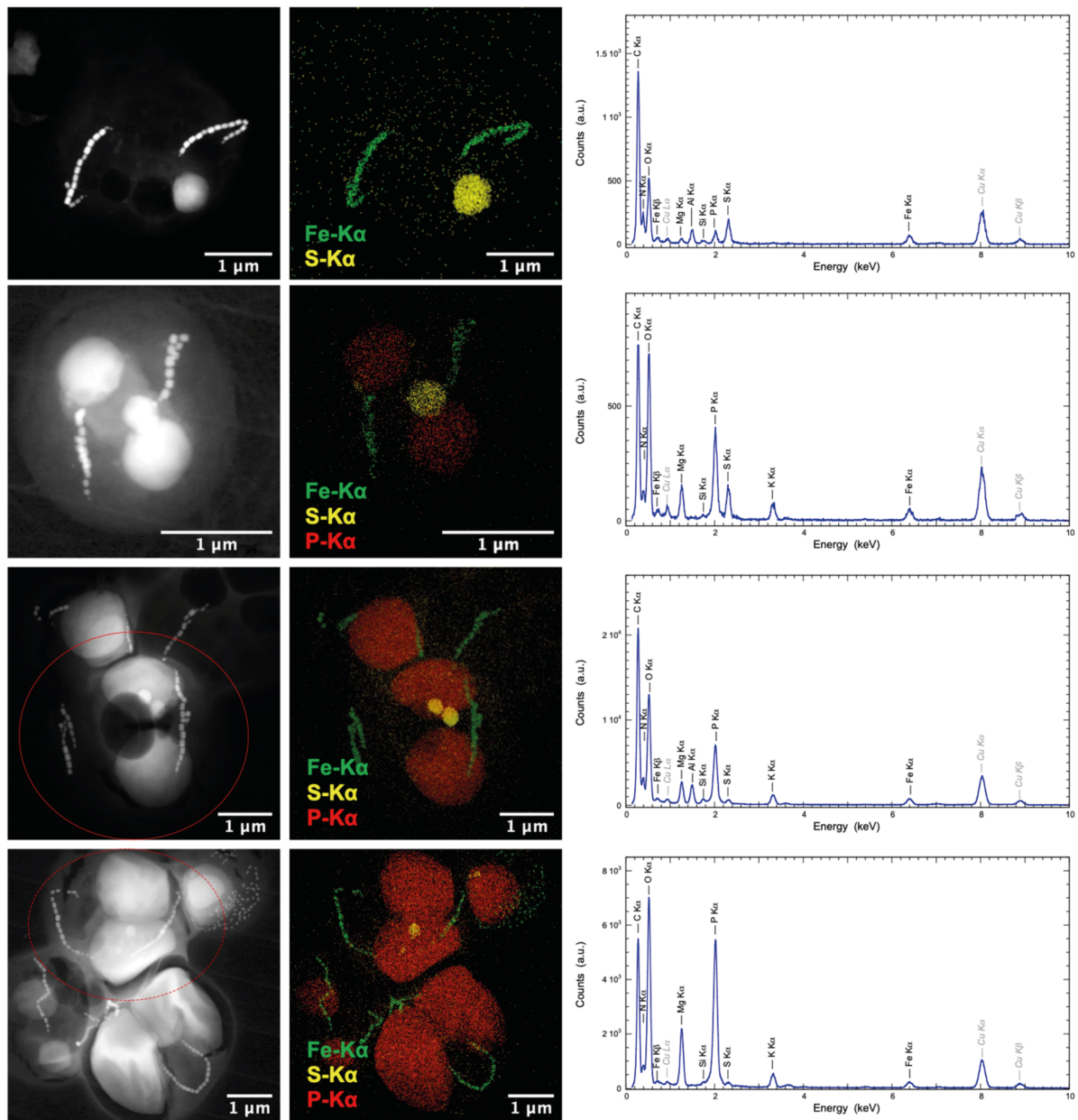


**Fig. S4. Chemical analyses of P and S intracellular inclusions with their respective spectrum in cocci MTB. The images show a negative correlation of the sulphur inclusions size over the PolyP inclusions size.**

---

## Hyperlinks for Table S1 and S2

Table S1:

<https://dropsu.sorbonne-universite.fr/s/aZSLsAg5fnZr3pB>

Table S2:

<https://dropsu.sorbonne-universite.fr/s/yqLXRpGcpQbc8BL>





Université de Paris

## **Phosphorus sequestration by magnetotactic bacteria in the stratified water column of Lake Pavin**

by

**Cécile BIDAUD**

### **Summary**

Phosphorus (P) is essential for life but limited or pollutant in some environments. Few microorganisms known to accumulate P as polyphosphates (PolyP) in oxic conditions, at marine water-sediment interface or in wastewater treatment plants, provide a promising strategy for P resource management.

This thesis stems on the recent discovery of a group of magnetotactic bacteria (MTB) affiliated to the Magnetococcaceae family (MTBc), sequestering PolyP in the anoxic layer of the water column of Lake Pavin. Both biological and environmental drivers of this process remain unknown. First, this thesis aimed at describing the vertical distributions of MTB populations along chemical gradients of the lake water column and the relative abundance of MTBc. By combining *in situ* monitoring of physicochemical parameters, bulk geochemistry, optical and electron microscopies and multivariate statistics, my work contributed to (i) describe a unique morphotype capable to form intracellular calcium carbonates, (ii) develop a water sampling strategy with high vertical resolution and (iii) identify the biogeochemical niche of MTBc whose parameters were further used to design a promising isolation medium.

The second part of this thesis focused on MTBc heterogeneity according to their P sequestration capabilities. My work contributed to (i) develop a cell classification scheme based on ultrastructural description of their inclusions, (ii) identify a stratification of MTBc along the chemical gradients of the water column confirming the relationship between P and S metabolisms and (iii) optimize sample preparation and staining for specific sorting of PolyP-sequestering cells by flow cytometry.

Keywords: magnetotactic bacteria, polyphosphates, Lake Pavin, biogeochemical niches, chemical gradients, electron microscopy, intracellular inclusions, biomineralization, flow cytometry.

### **Résumé**

Le phosphore (P) est essentiel à la vie mais limité ou polluant dans certains environnements. Quelques microorganismes connus pour accumuler le P sous forme de polyphosphates (PolyP) en oxygène, à l'interface marine eau-sédiments ou en stations d'épuration, offrent une stratégie prometteuse pour la gestion des ressources de P.

Cette thèse fait suite à la récente découverte de bactéries magnétotactiques (MTB) affiliées à la famille Magnetococcaceae (MTBc) séquestrant des PolyP en zone anoxique de la colonne d'eau du Lac Pavin. Les facteurs biologiques et environnementaux de ces processus restent inconnus.

Cette thèse a eu pour objectif de décrire les distributions verticales des MTB le long des gradients chimiques de la colonne d'eau et l'abondance relative des MTBc. En alliant les mesures *in situ* des paramètres physicochimiques, la géochimie des eaux, la microscopie optique et électronique et des statistiques multivariées, mon travail a permis de (i) décrire un morphotype formant des carbonates de calcium intracellulaires, (ii) développer une méthode d'échantillonnage à haute résolution et (iii) identifier la niche biogéochimique des MTBc dont les données ont servi à créer un milieu d'isolement prometteur.

La thèse s'est aussi centrée sur l'hétérogénéité de séquestration du P des MTBc. Mon travail a permis de (i) créer une classification cellulaire basée sur la description ultrastructurale des inclusions, (ii) identifier une stratification des MTBc le long des gradients chimiques de la colonne d'eau confirmant la relation entre les métabolismes du P et du S et (iii) optimiser la préparation et le marquage des échantillons pour le tri de cellules séquestrant du P par cytométrie en flux.

Mots-clés: bactéries magnétotactiques, polyphosphates, Lac Pavin, niches biogéochimiques, gradients chimiques, microscopie électronique, inclusions intracellulaires, biominéralisation, cytométrie de flux.

